Remodelling of the cardiac caveolar domain in heart failure and its putative influence on beta adrenergic signalling

Ruth Anne Astley Norman

Submitted in accordance with the requirements for the degree of
Doctor of Philosophy

University of Leeds
Faculty of Biological Sciences
School of Biomedical Sciences
Multidisciplinary Cardiovascular Research Centre

November, 2016

The candidate confirms that the work submitted is her own and that appropriate credit has been given where reference has been made to the work of others.

Acknowledgements

There are many people I have to thank who have helped and shaped my PhD at Leeds. . Firstly I would like to thank my supervisor Sarah Calaghan who introduced me to the importance of specialised lipid rafts (the ones that form small membrane invaginations) and allowed me to work on the project. Sarah has been a huge help and source of encouragement during the project as well as giving great guidance when exploring my own ideas in research. The copious amount of home baked goods provided throughout the 4 years has also helped fuel me through my PhD, all of which I have thoroughly enjoyed!

My co-supervisor Ed White has provided much knowledge and insight on the MCT model, and has been a great help throughout my project. I am very grateful for the opportunity Ed presented, allowing me to travel to Auckland University for a laboratory visit that helped broaden my skills, meet new people and visit an amazing country.

David MacDougall took me under his science wing when I first joined the group and showed me the way of Western blotting. He encouraged me to question experimental design and showed me that science was 'cool'. As well as enjoying strong coffee and getting me to explore vegan baking, he also tried his best to improve my grammar. I am grateful to both Rachel and Matt who were involved in teaching me new techniques when I first started my PhD and I have very much enjoyed working with them both.

I was fortunate to have the opportunity to work with a number of different groups from around the UK and across the world, from the Fuller Lab in the Molecular and Cellular Medicine Department at the University of Dundee, to the Ward Lab in the Cardiac Physiology Group *down under* in Auckland University. Both of these groups were hugely welcoming and helpful during my time there. Chris and Amelia were extremely patient in helping me learn new skills and techniques. I am grateful to the groups in Manchester University and Liverpool University, with whom I have collaborated who have helped further my work within this thesis. I have John Colyer to thank for establishing the project with Liverpool University and seeing it through.

I would not have this PhD if it were not for the funding through the Anatomy Demonstrator Studentship, which I am exceedingly grateful for. During these 4 years of teaching anatomy at Leeds I have had the pleasure to work with some great people and make some really good friends including Katie, Aaron, Nick, James, Tom and Lauren.

I have been lucky enough to have worked with an amazing bunch of people in the Cellular Cardiology Group and have made some great friends including Emma, Ewan and Sabine, who have all made excellent companions in the pub. Ewan has been a huge help with a lot of the MCT work as well as providing stimulating discussions about science and unrelated topics over coffee and pub trips. He has also helped keep me active through many triathlon/cycling adventures. Sabine, my Western blotting companion, was perenially helpful with almost all possible Western blotting troubles and well as teaching me some key French words. Emma is always a smiling face in the group and has the patience of a saint; she has happily listened to many of my experiments that didn't quite work out. Emma has also been a great comrade while writing up and helped keep me sane in the process.

While being at Leeds I have also made some wonderful friends from many different groups across the Faculty, including Jess, Claudia, Andrew, Tony and Roger who have helped provide much enjoyment during my time. Helen, who I met on the first day of starting my PhD has put up with living with me for two years, and has always been a help and support outside of science as well as being a great gym buddy. Lorena and Anna have also endured living with me for two years, I have thoroughly enjoyed many walks and runs around Yorkshire with them. A special thank you to James for the endless supportive hugs and for just being there for me, you always know how to make me smile.

Finally, thanks you to my ever-supporting family for believing in me. Even if I am all the way 'up north', you have never failed to let me know how proud you are of me, which has helped keep me going.

Author publications

ZHANG, H. M. B. CANNELL, S. J. KIM, J. J. WATSON, **R. NORMAN**, S. C. CALAGHAN, C. H. ORCHARD and A. F. JAMES. 2016. Cellular Hypertrophy and Increased Susceptibility to Spontaneous Calcium-Release of Rat Left Atrial Myocytes Due to Elevated Afterload. *PLoS ONE,* **10**(12), pe0144309.

Published abstracts:

NORMAN, R., M. HARDY, E. FOWLER, E. WHITE and S. CALAGHAN. 2013. Remodelling of the caveolar domain in right ventricular failure in rats*.: 37th Congress of IUPS,* Birmingham, UK. p.PCB044

NORMAN, R., M. DRINKHILL, J. DEUCHARS and S. CALAGHAN. 2014. Altered Glycosylation and distribution of the β2 adrenoceptor in heart failure *Heart,* **100**(Suppl 4), pA22.

NORMAN, R., E. FOWLER, R. STONES, E. WHITE and S. CALAGHAN. 2015. Reverse-remodelling of cardiac β-adrenergic responsiveness in metoprolol-treated pulmonary hypertensive rats *: Physiology 2015,* Cardiff, UK. p.PC019

FOWLER ED., **R. NORMAN**, E. STEER, E.PERVOLARAKI, R. STONES, M. DRINKHILL, SC. CALAGHAN, DS. STEELE & E. WHITE. 2015. The β1 adrenergic receptor blocker metoprolol improves survival and partially restores Ca2+ handling abnormalities in rat pulmonary artery hypertension*: Physiology 2015,* Cardiff, UK. p.PC03

NORMAN, R., E. FOWLER, E. WHITE and S. CALAGHAN. 2016. Metoprolol Reverses β2;-Adrenergic Remodeling in the Failing Right Ventricle of Pulmonary Artery Hypertensive (PAH) Rats. *Biophysical Journal,* **110**(3), pp.89a-90a.

Abstract

Over 500,000 people in the UK have heart failure (HF). After an initial insult to the heart, sympathetic drive increases which leads to detrimental remodelling of cardiac β-adrenergic receptors (βAR) and further cardiac dysfunction. The main βAR expressed in the heart are the β_1AR and β_2AR. In heart failure, remodelling is characterised by reduced β_1AR density, desensitisation of the remaining β_1AR and aberrations of normal βAR signal compartmentalisation.

Caveolae, flask-shaped lipid rafts, are present in most cells including cardiac myocytes and are characterised by the presence of caveolin and cavin proteins. Caveolar proteins create distinct micro-domains within the membrane and play a key role in compartmentalisation of signalling from both the β_1AR and β_2AR. Isolated reports of changes in caveolar structure and proteins in HF have implications for β-AR signalling, however the full array of caveolar protein changes in HF has not previously been assessed. Here we establish how the expression and membrane location of β-AR cascade and caveolar proteins changes in rat models of right ventricular (RV) and left ventricular (LV) failure induced by monocrotaline and aortic banding, respectively. For the RV model, we examined changes in β-AR responsiveness, and tested the potential for reversing functional and caveolar remodelling using a common LV therapy (the β-blocker metoprolol). Quantitative analyses of caveolar protein expression in myocyte and myocardial samples was also carried out using custom-designed calibrating peptides (CavCATs).

Both HF models showed a reduction in caveolar protein expression, with protein redistribution also found in the RV model. Decreased expression of β-AR signalling proteins (β_1AR, adenylyl cyclase) accompanied by increased expression of inhibitory proteins (Gαi, GRK2) was also observed in both models, with some remodelling of membrane distribution. β-blocker treatment in RV failure partially recovered expression of caveolar and β-AR cascade proteins. Cardiac β_1AR responsiveness was reduced in RV failure and again, this was partially recovered by β-blocker treatment. Quantitative work highlights the importance of studying non muscle-specific caveolar protein isoforms in the cardiac myocyte given e.g. similar expression of Cav 3 and Cav 1 in these cells.

Caveolae are dynamic membrane compartments which change in HF. This work suggests that caveolar changes affect β-AR signalling protein membrane location, which contributes to aberrations of signalling which (in the case of RV failure) can be reversed by β blockers.

Contents

Figures

Chapter 1

Chapter 2

Chapter 3

Chapter 4

Chapter 5

Chapter 6

Chapter 7

Chapter 8

Chapter 9

Tables

Chapter 1

Main Abbreviations and Agents

$[Ca^{2+}]_i$	Intracellular Ca^{2+} concentration
AB	Aortic banded animals
AC	Adenylyl cyclase
AKAP	A-kinase anchoring proteins
AP	Action potential
ATP	Adenosine triphosphate
AVN	Atrioventricular node
BIN1	Bridging integrator 1
bisoprolol	β1 adrenoceptor-specific antagonist
CamKII	Ca-Calmodulin dependent protein kinase
cAMP	Cyclic adenosine 3′,5′-monophosphate
carvedilol	Non-selective α1/β1/β2 adrenoceptor antagonist
Cav 1	Caveolin 1
Cav 2	Caveolin 2
Cav 3	Caveolin 3
cGMP	Cyclic guanosine monophosphate
CICR	Ca^{2+} induced Ca^{2+} release
cMyBP-C	Cardiac myosin-binding protein C
CON	Control (saline treated rats)
CSD	Caveolin-scaffolding domain
DHPR	dihydropyridine receptor
EC coupling	Excitation-contraction coupling
ECM	Extra cellular matrix
EF	Ejection fraction
E_m	Membrane potential
EM	Electron microscopy
eNOS	Endothelial nitric oxide synthase
FABP	Fatty acid binding proteins
FKBP	FK-506 binding protein
FRET	Förster resonance energy transfer
GPCR	G-protein coupled receptors
GRK	G-protein regulated kinase

HEPES	4-(2-hydroxyethyl)-1-piperazineethanesulfonic acid, pH buffer
$I_{Ca,L}$	L-type Ca^{2+} current
ICYP	[125I]iodocyanopindolol
I_{Na}	Na^{+} current
JPH2	Junctophilin 2
KO	Knock-out
LV	Left ventricle
LVADs	Left ventricular assist devices
MBCD	methyl-beta-cyclodextrin
MCT	Monocrotaline
MCT+BB	monocrotaline rats treated with metoprolol
metoprolol	β1 adrenoceptor-specific antagonist
mmHg	
MURC	Muscle-restricted coiled-coil protein
NCX	Na^{+}/Ca^{2+} exchange
NO	Nitric oxide
OXPHOS	Oxidative phosphorylation
PDE	phosphodiesterase
PDH	Pyruvate dehydrogenase
PKA	Protein kinase A
PLB	Phospholamban
PP	Protein phosphate
PTRF	Polymerase 1 and transcript release factor
RV	Right ventricle
RyR	Ryanodine receptor
SAN	Sinoatrial node
SDR	Serum deprivation response protein
SERCA	Sarcoplasmic reticulum Ca^{2+}-ATPase
Sham	Sham operated animals
SR	sarcoplasmic reticulum
SRBC	Serum deprivation response factor-related gene product that binds to C-kinase
TCA	Tricarboxylic acid
TnC	Troponin C
TnI	Troponin I

TnT	Troponin T
Trabeculae	Trabeculae carneae
t-tubules	Transverse tubules
β-AR	β-adrenergic receptors

Chapter 1. Introduction

1.1. General introduction

Heart failure is a multicausal disease with poor survival rates; after being admitted to hospital the majority of patients die within 5 years (Nieminen et al., 2006). Approximately 26 million people are living with heart failure worldwide (Xie et al., 2012), resulting in a large burden on the health services and society. Heart failure is a chronic disease with most treatments only relieving symptoms and not specifically treating the failing heart. When heart failure becomes severe, mechanical devices or heart transplant become the only options.

An initial insult to the heart, such as a myocardial infarction, causes the body to compensate in order to maintain cardiac output, typically by increasing sympathetic drive to the heart. When this compensation is prolonged the adaptive responses of the heart, such as hypertrophy, then become maladaptive. The heart can no longer maintain sufficient output for the body's metabolism and clinical symptoms of heart failure follow. The heart typically becomes desensitised to increased sympathetic drive in addition to muscle mechanical failure. A better understanding is needed of the changes in the myocardium when this de-compensatory/failure stage is reached. By understanding the basic changes which underlie dysfunction and remodelling within the myocyte, novel pharmacological targets could be identified. In particular our interests lie in the changes to β-adrenergic receptors (βAR) and their signalling proteins at the membrane, and the way that their organisation via caveolae is altered.

1.2. The heart

1.2.1. Human embryological development

The heart is formed from the cardiogenic field, which starts to develop around the third week after fertilisation. The steps of heart development are depicted in Figure 1-1. Initially the heart is a primitive tube enlarging within the newly formed pericardial cavity, made up of three layers: endocardium, myocardium and epicardium (Sadler and Langman, 2014). The coronary arteries are formed from the epicardium layer. By day 23, the heart tube begins to bend and form the cardiac loop, the primitive atrium and major vessels at the

caudal end of the tube shift dorsally and rostrally while the primitive ventricle bends ventrally, caudally and to the right. All the while the heart tube continues to enlarge. By the end of the formation of the heart loop, trabeculae carneae begin to form in the primitive ventricle while most of the bulbus cordis remains smooth (Sadler and Langman, 2014). The proximal third of the bulbus cordis also becomes trabeculated and forms the primitive right ventricle, while the primitive ventricle mostly forms the primitive left ventricle (Kramer, 1942). By the fourth week of development the heart receives an umbilical blood supply via the sinus venosus, a common chamber which receives blood before entering the primative atria. The sinus venosus and part of the right sinus horn leading into the sinus venosus will eventually form part of the right atria (Larsen et al., 2001). The major septa of the heart are formed between week 4 and 6. The foramen ovale within the atrial septum remains open until birth. The atrioventricular junction, which originally flowed only into the primitive left ventricle, enlarges to the right allowing blood to pass into the primitive right ventricle as well. The atrioventricular valves are formed from dense mesenchymal tissue on the surrounding atrioventricular orifice (Schoenwolf et al., 2015). The division of the ventricular outflow tract is formed by three conotruncal ridges which twist around each other to form the aortic pulmonary septum. The interventricular septum forms from two parts, a muscular and a membranous part, which fuse together (Kramer, 1942). The pacemaker cells of the heart originate in the sinus venous which is incorporated into the right atria forming the sinoatrial node (SAN). The atrioventricular node (AVN) and the bundle of His are formed from the cells from the sinus venosus and the atrioventricular canal. By week 8, the heart is a functional four chambered vessel resembling that in post-natal life enabling blood circulation for the embryo.

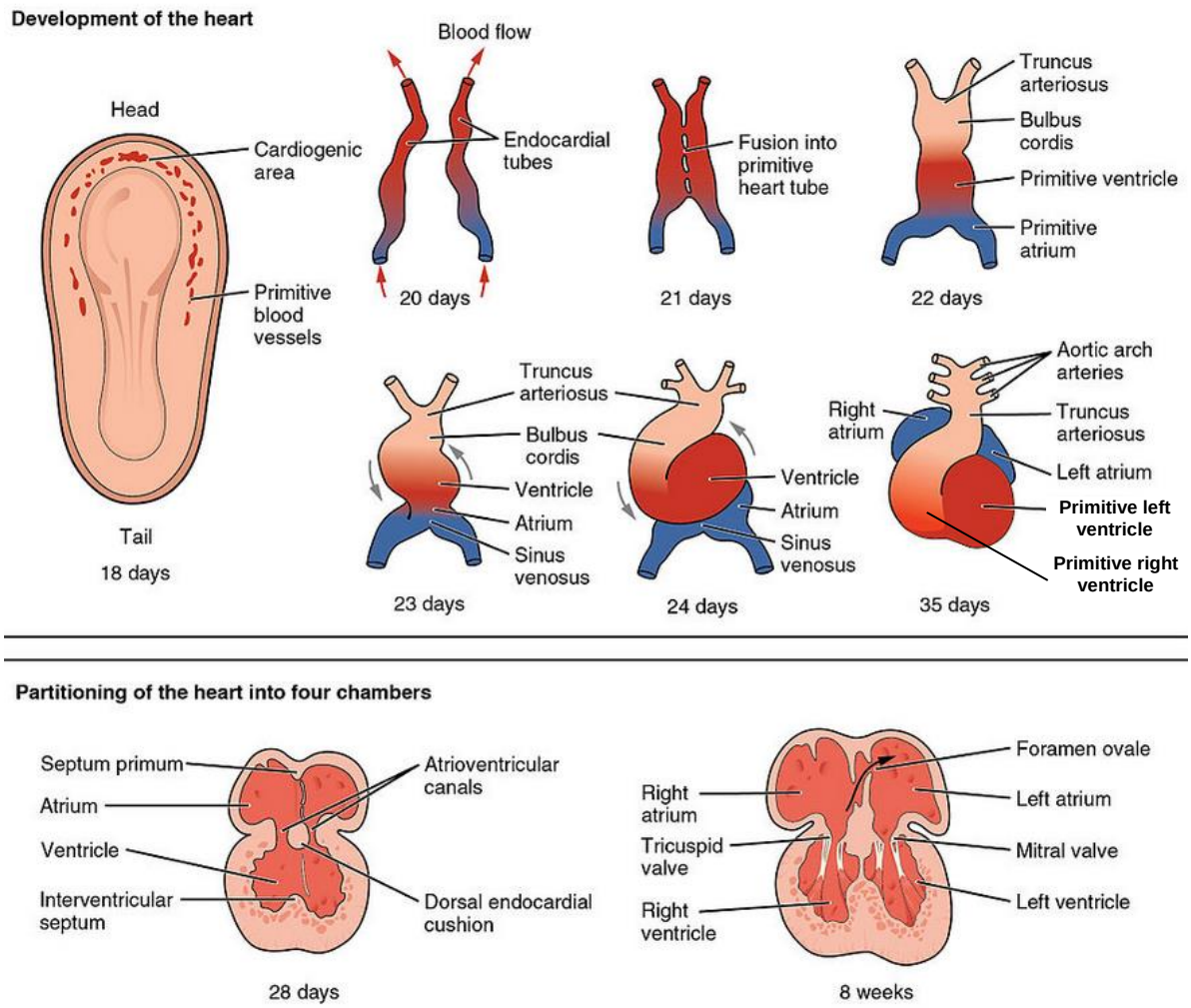

Figure 1-1 Embryological development of the human heart

Figure modified from (Touchnet, 2016), shows the formation of the primitive heart tube, and the stages in folding to form the 4 chambers of the heart. Formation of the septum and valves is shown in the bottom of the diagram. Time post fertilisation is listed under each stage.

1.2.2. Anatomy

After birth the foramen ovale closes, pressure within the pulmonary vessels drops and the circulation changes to its adult course. This change in pressure within the ventricles also causes a change in function within the different chambers and leads to rapid thickening of the left ventricular wall and the thinning of the right ventricle within the first postnatal month (Keen, 1955). From the second postnatal month, both ventricles go through a progressive increase in size as the heart grows during development.

In an adult human the right ventricular free wall is an average of 4-5 mm in thickness, while the left ventricular free wall is around 10-15 mm in thickness (Traill et al., 1978). Sitting within the chest cavity within the pericardial sac the right ventricle makes up most of the inferior border of the heart. The left ventricle makes up the right border of the heart and the most inferior and ventral aspect known as the apex. The right atria, receiving blood from the inferior and supervisor vena cava, makes up the right border and the left atria makes up the base of the heart at its most dorsal aspect (Noble, 2005). The right ventricle receives blood from the right atria through the tricuspid valve and pumps blood to the lungs through the pulmonary truck which splits into the right and left pulmonary arteries running towards the right and left lung (mean pulmonary artery pressure 10-20 mmHg)(LiDCO Group). The left atria receives blood from four pulmonary veins, and pumps blood to the left ventricle through the mitral valve which then circulates the oxygenated blood round the systemic circulation (mean arterial pressure 70-105 mmHg)(LiDCO Group). The cardiac output of the right ventricle is equal to that of the left ventricle, but due to the reduced pressure within the pulmonary vasculature does so with ~ a fifth of the energy cost (Friedberg and Redington, 2014).

1.2.3. The conducting system

From around week 6 of development the heart begins to beat and does so until the end of life (Schoenwolf et al., 2015). There are specialised myocytes within the heart which are self-excitable, called pacemaker cells. Only 1% of the developing cells within the heart represent this phenotype; these are located within the SAN and AVN and within the bundle of His. Each has its own intrinsic rhythm; SAN 60-100 beats/min, AVN 40-55 beats/min and the bundle of His 25-40 beats/min (Noble et al., 2013). The branches of the vagus nerve and branches from the sympathetic chain form cardiac plexuses on the heart and innervate the SAN controlling its excitation rate. The balance between sympathetic and parasympathetic

nervous innervation is controlled by the cardiovascular centre within the brain and regulates the beating rate of the heart.

Cardiac excitation normally begins in the SAN located on the crista terminalis, the junction between the primitive atria and the sinus venosus in development. The electrical signal is then propagated through the atrial cardiac myocytes till its reaches the AVN, where the signal is delayed. This delay in signal propagation serves to allow the ventricles to fill after atrial contraction. From the AVN, the signal travels down the bundle of His into the right and left bundle branches within the interventricular septum towards the apex of the heart. Excitation of the ventricular muscle is then initiated starting at the apex with the electrical signals propagated towards the base of the heart (Noble et al., 2013). Purkinje fibers allow rapid conduction of the action potential within the ventricle and help synchronous contraction. Purkinje fibres also aid in initiating contraction within the papillary muscles, which are attached to the atrioventricular value via chordae tendineae, and help prevent regurgitation of blood back into the atria.

1.2.4. Extracellular matrix

The cardiac myocyte is not the only cell type present within the heart; there are many other cell types including, fibroblasts, endothelial cells and vascular smooth muscle cells, as well as the extra cellular matrix (ECM). The ECM forms a scaffold within the heart providing strength and support for the cells and allowing for distribution of mechanical forces. It is comprised mainly of collagen types I and III, but also contains other collagen types as well as glycoproteins and fibronectin. Fibroblasts are the key cell within the heart which maintain the ECM (Eghbali, 1992).

1.3. Cardiac myocyte

1.3.1. Basic structure

In humans the average size of an individual myocyte is around 50-100 μm in length and about 10-20 μm in diameter. An example of the cardiac myocyte cellular structure is depicted in Figure 1-2. Cardiac cells are multinucleated and contain a high proportion of mitochondria due to the cells' high metabolic demand. The plasma membrane forms a number of long protrusions into the cell called transverse tubules (t-tubules). The sarcoplasmic reticulum (SR) is a store of Ca^{2+} within the cell which is essential for

contraction. Within mammalian physiology there are three types of muscle; cardiac muscle, skeletal muscle and smooth muscle. The cardiac myocyte is the contractile cell of cardiac muscle, which contracts from pre-natal life till death. The contractile unit within the cardiac myocyte is the sarcomere (~2 μm length). These are bordered at each end by the Z-line which is formed from the α-actinin protein. F-actin attaches to the Z-lines and forms the thin filaments made of G-actin monomers and tropomyosin joined in a helical shape. Running in-between these parallel thin filaments are strands of myosin protein forming thick filaments. Where the thick and thin filaments overlay, cross-bridges can be formed (Noble et al., 2013). Multiple sarcomeres are joined end to end and run in parallel to make up a myofibril, making up the majority of the cellular volume. Cardiac myocytes form connections with other cardiac myocytes through specialised junctions called intercalated discs, which contain gap junctions (connexons) allowing electrical communication, and desmosomes which provide strength to the junction.

1.3.2. Plasma membrane

The plasma membrane is a lipid bilayer surrounding the cell which in mammalian cardiac myocytes can be defined as two distinct areas: the surface sarcolemma and the t-tubules. T-tubules are long invaginations of the cell which generally line up with the z-line of the sarcomere and are key for synchronous contraction of the cell. The surface sarcolemma and t-tubules are continuous with one another, with the t-tubules calculated to comprise 21% to 64% of the membrane (Bers, 2001; Page, 1978; Page et al., 1971).

The plasma membrane serves to control movement in and out of the cardiac cell and communicates with the extracellular matrix and other cells within the heart. The lipid bilayer is a fluid and dynamic structure which is highly changeable. The mobility of the membrane is variable depending upon its lipid composition. Membrane lipid bilayers are asymmetrical and enriched in phospholipids and sphingolipds (Allan, 1996; Meder and Simons, 2006). The outer leaflet is enriched in sphingolipids such as sphingomyelin and glycosphingolipids while the inner leaflet is mainly comprised of phosphatidylethanolamines and phosphatidylserine. Cholesterol is present in both the outer and inner leaflets of the lipid bilayer (Meder and Simons, 2006). Within the plasma membrane co-clusters of lipids exist known as lipid rafts. Some specialised lipid rafts form small invaginations within the membrane called caveolae which are discussed later (Section 1.4).

A

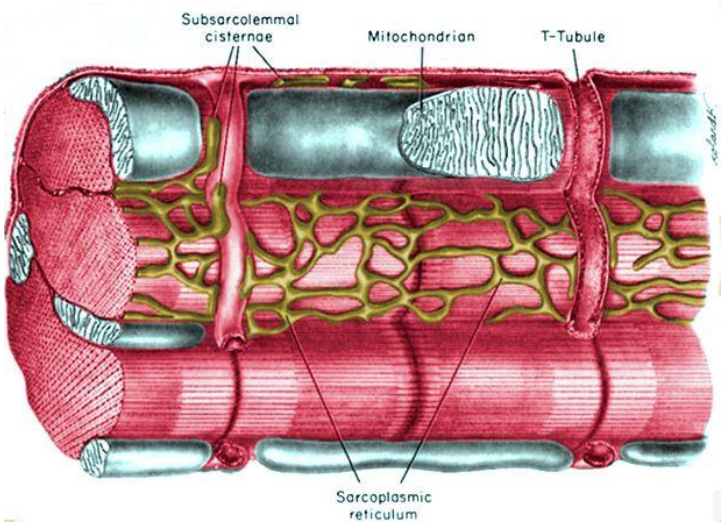

B

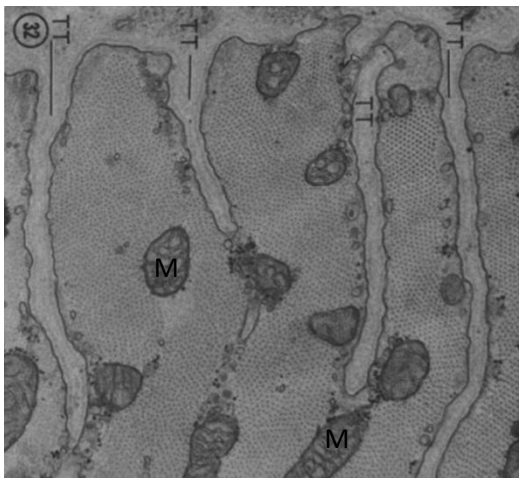

Figure 1-2 Structure of a cardiac myocyte

A. Drawing of a cat cardiac myocyte adapted from (Fawcett and McNutt, 1969) showing the t-tubules, sub-sarcolemmal mitochondria, sarcomeres (made up of contractile myofilaments), and sarcoplasmic reticulum (SR). The surface sarcolemma is invaginated into two t-tubules with the SR forming close connections to this and the surface sarcolemma **B.** Electron micrograph (EM) of a transverse section of a cat cardiac muscle from (Fawcett and McNutt, 1969). EM shows four T tubules (TT) extending inward into the body of the myocyte. Mitochondria (M) can also be visualised within this section. In the paper this is stated as a rare image, due to the fact that the plane of a thin section seldom coincides with one of the rows of T tubules opening onto the surface. X 32,000.

1.3.3. T-tubules

T-tubules are not present in neonatal cardiac myocytes (Sedarat et al., 2000), and are not as prevalent in atrial cells from some small mammals as in adult ventricular myocytes (Richards et al., 2011). The increase in cardiac myocyte size in development means that Ca^{2+} diffusion from the sarcolemma is no longer sufficiently rapid to synchronously activate Ca^{2+} induced Ca^{2+} release (CICR)(further detail in section 1.3.7.2) within the cell. In a study of rabbit development, the percentage of couplon (paired L-type Ca^{2+} channels and ryanodine receptors (Section 1.3.7.2)) events at the surface reduce from 80% in 3 day-old rabbits to 20% at day 20 (Sedarat et al., 2000). The precise mechanisms for t-tubule formation are not understood but scaffolding proteins help stabilise the structure throughout the normal cardiac cycle (Kostin et al., 1998). Caveolin 3 (Cav 3), junctophilin 2 (JPH2) and bridging integrator 1 (BIN1) are all implicated in assisting the structure and organisation of t-tubule (Galbiati et al., 2001; Beavers et al., 2014; Lee et al., 2002). In the adult mammalian cardiac myocyte t-tubules are regularly spaced, occurring around every 2 μm and contain longitudinal and axial components (Page, 1978; Brette and Orchard, 2003). Thanks to advances in super resolution imaging and new electron microscopy (EM) techniques, the finer details and structure of t-tubules, such as variation in t-tubule diameter, are beginning to be discovered (Jayasinghe et al., 2015; Rog-Zielinska et al., 2016; Pinali et al., 2013). In the adult cardiac myocyte, the t-tubules are the location of the majority of couplons, as well as many important ion channels and other proteins that modulate function within the cardiac myocyte, including cAMP-dependent protein kinase (Brette and Orchard, 2003; Chen-Izu et al., 2006). Using the technique of detubulation, which functionally uncouples the t-tubules from the cell by osmotic shock, it was shown that 80% of the L-type Ca^{2+} current ($I_{Ca,L}$) and 63% of the Na^{+}/Ca^{2+} exchanger (NCX) current is located within the t-tubules (Brette et al., 2004; Despa et al., 2003).

1.3.4. Mitochondria

Mitochondria take up around 35% of the volume of the cardiac myocyte in mammals (Page, 1978). They contain an outer membrane and a folded inner membrane (cristae). The cardiac myocyte has a high demand for energy in the form of ATP. The main source of ATP in the cell is from oxidative phosphorylation (OXPHOS) which takes place in the mitochondria. ATP from fatty acid β-oxidation accounting for the majority of mitochondrial ATP production (60% - 90% contribution), while glucose oxidation contributes to a smaller percentage (10% - 30%) (Neely and Morgan, 1974). Fatty acid binding proteins (FABP) transport fatty acid into the cell after which fatty acyl CoA synthase adds a CoA group

allowing long-chain fatty acids into the mitochondria (Lopaschuk et al., 2010). These are then converted to acetyl CoA by fatty acid β-oxidation. Pyruvate is formed by glycolysis of glucose within the cell which, when coupled with glucose oxidation, allows pyruvate to enter the mitochondria (Stanley et al., 2005). Pyruvate is then converted into acetyl CoA by pyruvate dehydrogenase (PDH) (Fillmore and Lopaschuk, 2013; Herzig et al., 2012). Acetyl CoA enters the tricarboxylic acid (TCA) cycle which produces NADH and $FADH_2$, two high energy intermediates which enter the electron transport chain. The electron transport chain then uses the NADH and $FADH_2$ to drive H^+ ions across the internal membrane of the mitochondria and synthesises ATP from ADP (Scheffler, 2007). Mitochondria are also involved in buffering the cytosolic Ca^+. The Ca^+ exchange in the mitochondria is slow compared to the beat-to-beat regulation by the SR, but the cumulative effect of Ca^+ entering the mitochondria enhances ATP production (Bers, 2008).

1.3.5. Sarcoplasmic reticulum

The sarcoplasmic reticulum (SR) is a form of specialised endoplasmic reticulum which is the main Ca^{2+} store within the cardiac myocyte. A 3D reconstruction of the SR within the sheep cardiac myocyte shows the SR to be a continuous interlinking network within the cell (Pinali et al., 2013). The SR forms close connections with the t-tubules and surface sarcolemma known as dyadic clefts (10-20 nm). The SR have "feet" (ryanodine receptors, see Section 1.3.7.2) at these points of close connection with t-tubules and the surface sarcolemma (Franzini-Armstrong, 1975).

The sarcoplasmic reticulum Ca^{2+}-ATPase (SERCA) is the main protein involved in Ca^{2+} uptake into the SR. Different forms of SERCA are present in different cell types, and SERCA2a is the isoform expressed within the cardiac myocyte (Brandl et al., 1987). The SERCA pump initially opens to the cytosol which allows two Ca^{2+} ions to enter, then with the hydrolysis of ATP the channel is momentarily occluded. SERCA is then phosphorylated by ATP causing the channel to change state allowing for the Ca^{2+} to enter the SR lumen in exchange for two H^+ ions pumped out into the cytosol (MacLennan, 1970; Clarke et al., 1989). Post-translational modifications of the SERCA pump, including phosphorylation and oxidation, modulates its activity. Phospholamban (PLB) interacts with SERCA2a and reversibly inhibits the pump by decreasing Ca^{2+} transport (Fujii et al., 1987; Tada and Katz, 1982). PLB can also be phosphorylated, which lowers its affinity with SERCA2a thereby increasing the Ca^{2+} pump rate (MacLennan and Kranias, 2003).

The ryanodine receptor (RyR) is responsible for release of Ca^{2+} from the SR. RyR type 2 (RyR2) is the main isoform expressed in cardiac myocytes. RyR2 is made up of four subunits containing a large cytosolic domain and α-helical membrane domain. Ca^{2+} binds to the RyR2 causing Ca^{2+} release from the SR. The cytosolic RyR2 domain has a number of other binding sites, as revealed by the crystal structure, for calmodulin (RyR2 stabilizer) and FK-506 binding protein (FKBP) (Wagenknecht et al., 1997); both of which tightly regulate the open/closed state of the channel and reduce open probability (Hwang et al., 2014; Guo et al., 2006; Xu and Meissner, 2004). Like SERCA, RyR2 can be phosphorylated at multiple sites by protein kinase A (PKA) or Ca^{2+}-Calmodulin dependent protein kinase (CaMKII) which also changes the activity of the channel, increasing the open probability (Valdivia et al., 1995; Witcher et al., 1991; Bers, 2016).

1.3.6. The contractile units of the myocyte

The contractile unit of the cardiac myocyte, as mentioned above, is the sarcomere. Contraction occurs through movement between the thick and thin filaments. The thick filament contains ~300 myosin molecules along with titin and cardiac myosin-binding protein C (cMyBP-C) (Bers, 2001). Each myosin molecule is composed of two myosin heavy chains and two myosin light chains associated with each heavy chain. The myosin heavy chains consist of an α-helical tail, which coil together to form the body of the thick filament, and a globular head which interacts with the thin filament to form the crossbridge (Bers, 2001). The light chains on each myosin consist of an essential light chain and a regulatory light chain. cMyBP-C is associated with the thick filament and aids in modulation of contraction by regulating cross-bridge formation probability, phosphorylation of cMyBP-C alters its binding to myosin and increases the rate of force development (Moss, 2016).

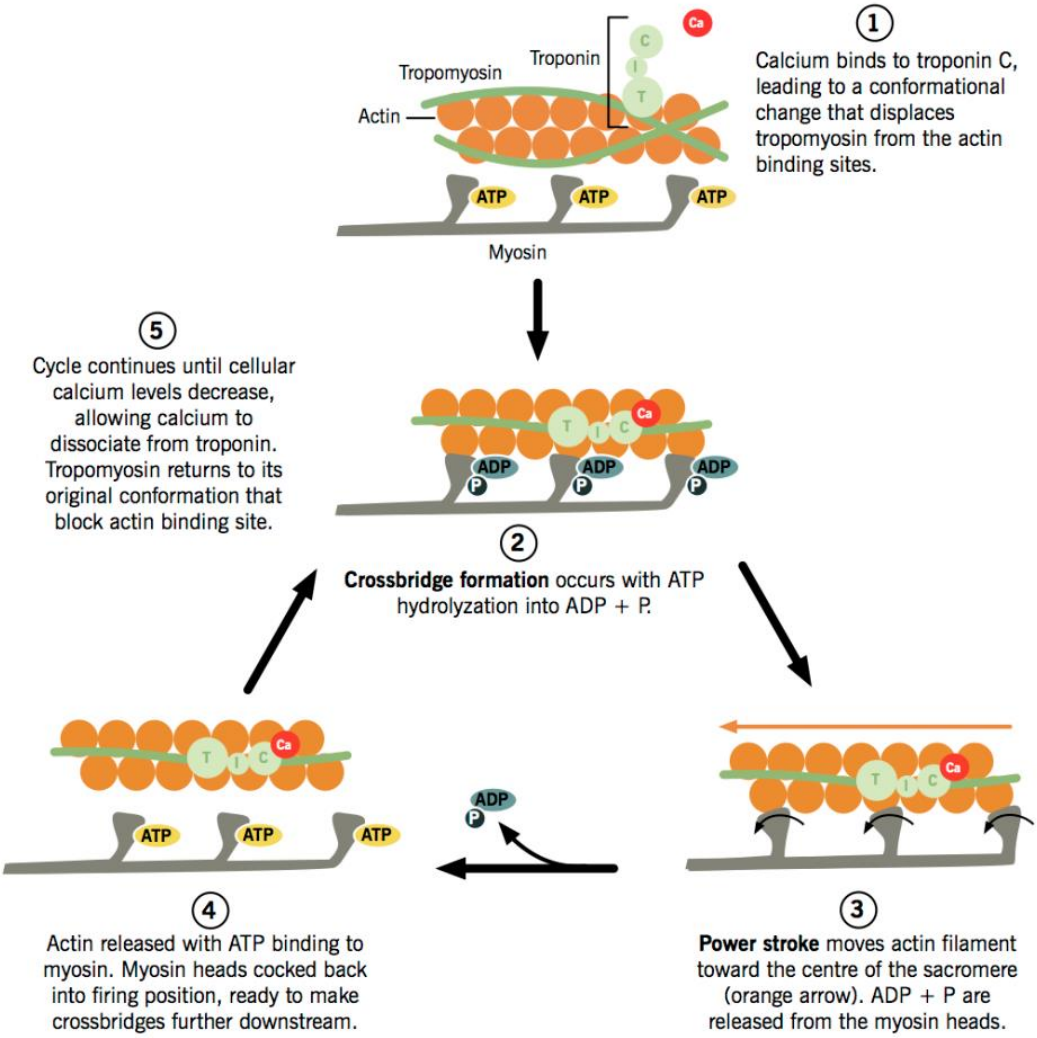

Figure 1-3 Cardiac myocyte contraction cycle

Modified from (Ikonnikov and Yelle, 2016). Flow diagram demonstrates the process of contraction. When $[Ca^{2+}]_i$ is low tropomyosin inhibits the formation of crossbridges. When $[Ca^{2+}]_i$ rises after CICR the depicted crossbridge cycling is activated.

The thin filament consists of helical ropes of globular actin molecules with tropomyosin lying in the grove between these. The individual tropomyosin molecules link together and overlap by 5-10 amino acids with the next tropomyosin (Lehrer et al., 1997). The troponin complex, which is composed of three subunits (troponin T (TnT), troponin C (TnC), and troponin I (TnI)), is attached to the tropomyosin strand every seventh actin. The TnT molecule lies along the tropomyosin and spans three actin molecules, while TnI binds to both TnT and TnC, as well as directly to actin to inhibit myosin binding. TnC contains three Ca^{2+} binding sites, and binding of Ca^{2+} to the Ca^{2+}-specific site on TnC causes an increase in strength of interaction between TnC and TnI destabilising the TnI interaction with actin. This allows the myosin head to form a crossbridge with actin (Gordon et al., 2000). The actin filament is then moved over the myosin causing a small contraction from the rotation of the myosin head (Huxley and Simmons, 1971; Tyska et al., 1999). Ca^{2+} is also essential for the myosin ATPase to hydrolyze ATP which alters the conformation of the myosin head. At rest myosin is bound to ATP, but with a rise in Ca^{2+} the phosphate is released and the myosin bound ADP interacts with actin (Goldman and Brenner, 1987). The actin-myosin bond is dissociated when ATP binds to myosin again. In this manner the myosin head walks along the actin filament until either Ca^{2+} or ATP is depleted (Figure 1-3).

The Frank-Starling mechanism, discovered by Otto Frank (1895) and Ernest Starling (1914), describes the situation whereby the resting length of the muscle in diastole determines the work performed during systole. This occurs partly through increased crossbridge formation (via changes in myofilament overlap) but mainly by increased Ca^{2+} sensitivity of the myofilaments (Fuchs and Smith, 2001).

1.3.7. Cardiac excitation contraction coupling

The process of excitation-contraction coupling (EC coupling) begins with the electrical stimulation of the cell and results in mechanical contraction as first described by Sandow (Sandow, 1952). Ca^{2+} enters the cardiac cell through voltage gated Ca^{2+} channels, activated by depolarisation of the cell membrane, which causes the further release of Ca^{2+} from the intracellular stores (SR) resulting in an increase in intracellular Ca^{2+} concentration ($[Ca^{2+}]_i$) and contraction (Bers, 2002). To terminate contraction, and to allow for relaxation, the Ca^{2+} is either sequestered back into the SR (and mitochondria), or extruded from the cell via ion pumps or exchangers. This is summarised in Figure 1-4

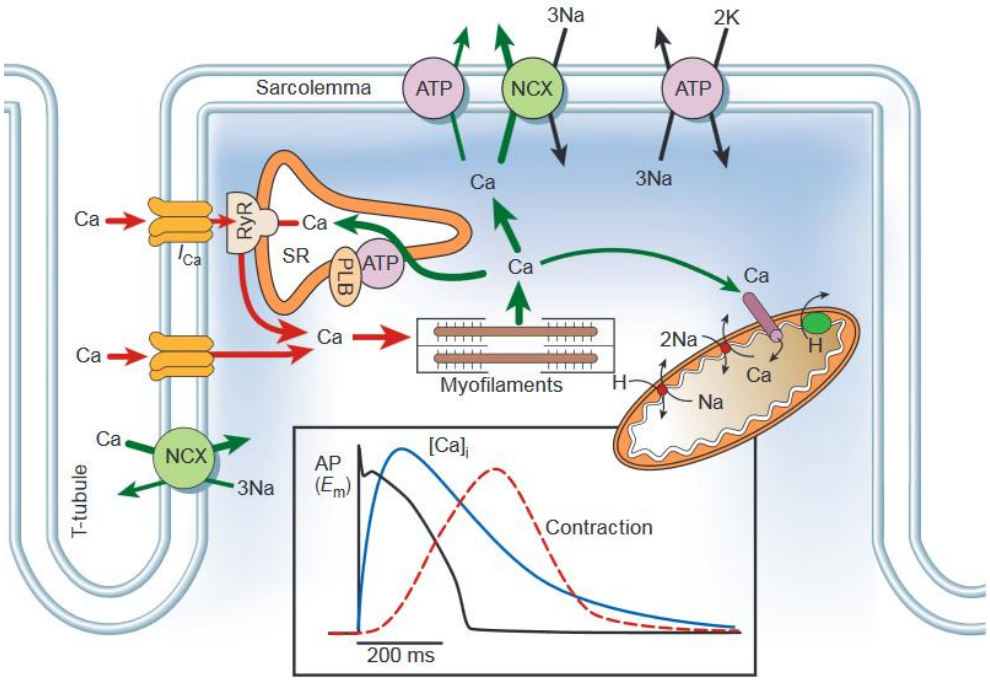

Figure 1-4 Excitation contraction coupling in a cardiac myocyte

Figure from (Bers, 2002). Ca^{2+} channels are activated in response to electrical activation. Figure depicts the main ion channels and exchangers involved in cardiac excitation contraction coupling (EC coupling). Inset depicts action potential (AP), the intracellular Ca^{2+} concentration $[Ca^{2+}]_i$, changes during contraction of a rabbit ventricular myocyte.

The force of the contraction is graded by the $[Ca^{2+}]_i$, the higher the $[Ca^{2+}]_i$ the more actin-myosin crossbridges form.

1.3.7.1. Action potential

EC coupling is initiated within the cardiac myocyte by an action potential (AP). The action potentials of different myocytes within the heart vary according to their location and function (Figure 1-5A). An AP represents the change in membrane potential of the cell as a result of the co-ordinated opening and closing of ion channels. An AP can be recorded with a sharp microelectrode inserted into the cardiac myocyte, and the membrane potential (E_m) measured as the potential difference across the membrane. A summary of the ventricular action potential and the ion channels involved is depicted in Figure 1-5B. The ventricular myocyte AP can be summarised in 4 phases; the rapid upstroke is designated as phase 0, there is then a brief period of repolarisation which is classed as phase 1, following this is a plateau of sustained depolarisation (phase 2), followed by a repolarisations back to the resting membrane potential which is much slower than the depolarisation in phase 0. There is then a lag phase, classed as phase 4, before the next action potential starts (Bers, 2001). At rest the intracellular K^+ concentration greatly exceeds that in the extracellular fluid, which is controlled by K^+ channels. The opposite is true for Na^+, as the extracellular Na^+ concentration greatly exceeds the intracellular concentration. The resting potential of the ventricular cells is around -85 mV, which is maintained by the Na^+/K^+ ATPase.

During the action potential, there is an initial rise in E_m through electrical coupling with neighboring cells, via gap junctions, which triggers the opening of the voltage gated Na^+ channels. This results in an inward current of Na^+ (I_{Na}), causing the E_m to rise to between +20 and +30 mV. The Na^+ channels are rapidly inactivated by this increase in membrane potential and remain closed for the duration of the AP. The brief initial repolarisation in phase 1 is due to rapid activation of the transient outward K current (I_{to}). I_{to} consists of a fast and a slow inactivation channels (Nerbonne, 2000). Both K^+ and Ca^{2+} channels are activated by the depolarisation of the cell, which forms phase 2, with Ca^{2+} entering the cell through L-type Ca^{2+} channels and K^+ leaving through a number of different K^+ channels. Delayed K^+ rectifying currents (I_{Kr}, I_{Ks}, I_{Kur}) are activated towards the end of phase 0, but take considerably longer time to become active compared to some of the other channels (Sanguinetti and Jurkiewicz, 1990).

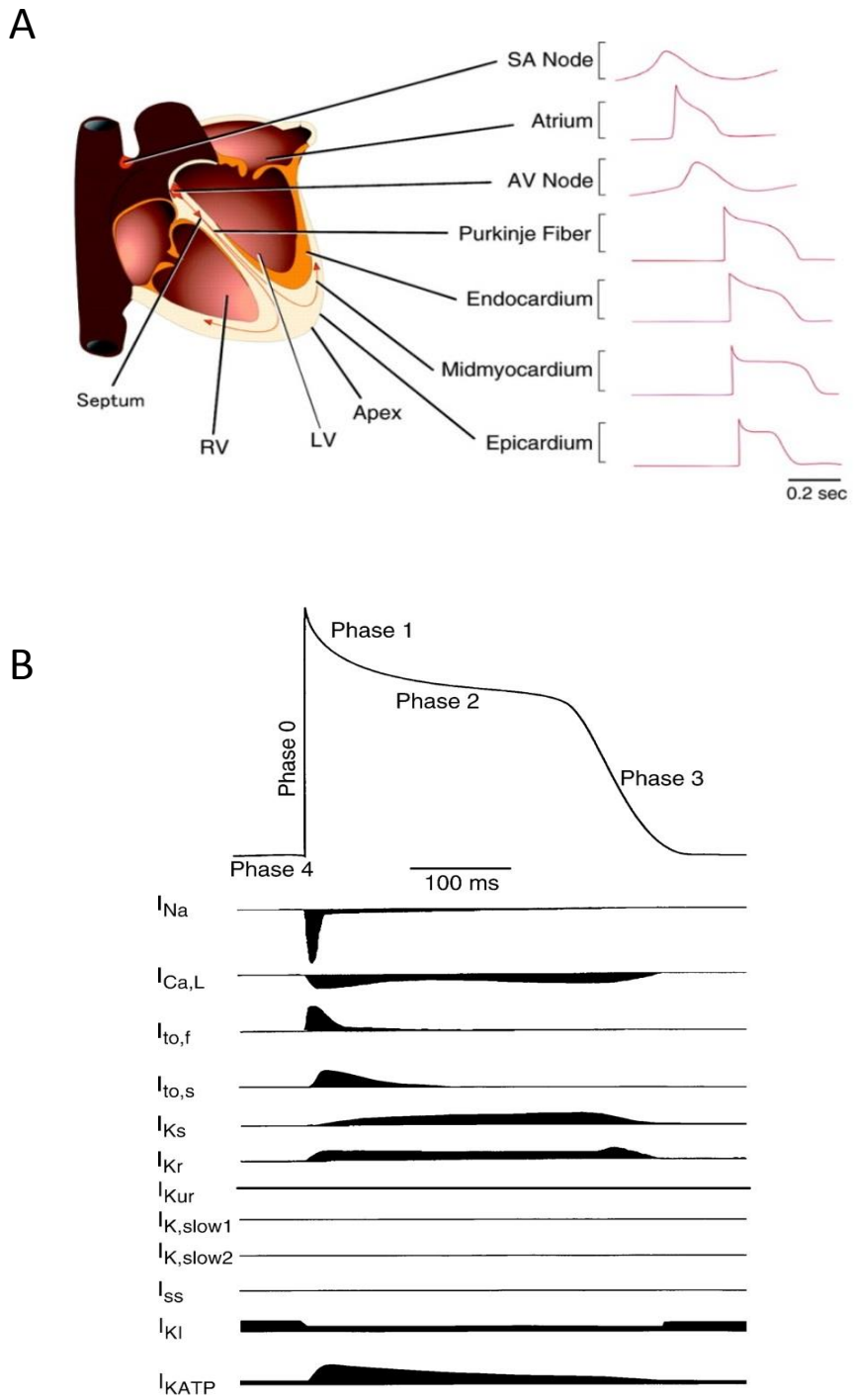

Figure 1-5 Cardiac action potential

A. Modified from (Nerbonne and Kass, 2005) shows the variations in the cardiac action potential in different areas on the heart. **B.** A single cardiac action potential time course demonstrating inward (downward deflections) and outward (upward deflections) currents activated in a single action potential in a human ventricular myocyte.

During phase 3, the efflux of K^+ exceeds the influx of Ca^{2+}, and this brings the cell back to its resting E_m. Restoration of the Na^+ and K^+ concentrations is driven by Na^+/K^+ ATPase in phase 4. An AP in rat ventricular myocytes lack the extended lag phase (phase 2) during repolarisation, due to low or absent I_{Kr} and I_{Ks} channels, allowing for a faster resting heart rate (380-480 beats per minute)

1.3.7.2. Ca^{2+} induced Ca^{2+} release

Ca^{2+} induced Ca^{2+} release (CICR) is the widely accepted mechanism of Ca^{2+} activated SR Ca^{2+} release, first described in cardiac myocytes by Fabiato and Fabiato (Fabiato and Fabiato, 1975). When the cell membrane is depolarised at the beginning of the action potential the L-type Ca^{2+} channel is activated allowing a small influx of Ca^{2+} into the cell. The L-type Ca^{2+} channel (dihydropyridine receptor; DHPR) exhibits Ca^{2+} dependent inactivation by calmodulin which limits the amount of Ca^{2+} entry into the myocyte (Peterson et al., 1999). The DHPR is composed of six membrane-spanning domains and is found concentrated (10-25 channels) around the dyadic junction in association with the "feet" of the SR which contains around 100-200 RyRs. A collection of DHPRs coupled with RyRs at the dyad are known as a couplon and these form the functional Ca^{2+} release unit. The initial influx of Ca^{2+} activates the RyR2 and allows the release of Ca^{2+} from the SR store (Bers, 2008). A single L-type Ca^{2+} channel opening can cause a Ca^{2+} release event, but usually several channels in a cluster (10-25 DHPRs) open during rhythmic contraction of the cell (Bers, 2001). This raises the $[Ca^{2+}]_i$ within the dyadic clef to 200-400 μM, from where the Ca^{2+} diffuses into the cytosol (Bers, 2001). For synchronous contraction of the cell to occur all couplons must be activated simultaneously.

The Na^+/Ca^{2+} exchanger (NCX) is a reversible antiporter which extrudes one Ca^{2+} in exchange for three Na^+ ions (an inward $I_{Na/Ca}$) (Fujioka et al., 2000). This can be reversed to bring Ca^{2+} ions into the cell in exchange for Na^+ (outward $I_{Na/Ca}$), by a positive membrane potential and high $[Na^+]_i$ (Bers, 2001). The NCX may contribute to the influx of Ca^{2+} at the beginning of the action potential, but until recently this was not thought to be the main mechanism for CICR. However, renewed interest in the role of the NCX in CICR has come about with the advances in spatial resolution within the dyad offered by super resolution microscopy. Computer models of the NCX using this new information predict that the NCX may have more of an influential role in Ca^{2+} entry into the dyad during the depolarisation stage of the action potential, as outward $I_{Na/Ca}$ was predicted to precede the activation of L-type Ca^{2+} channels and RyR2 (Chu et al., 2016). The mechanisms which terminate Ca^{2+}

release events from the SR are not clear, but the luminal SR [Ca^{2+}] content is thought to play a role by favouring the closed state of the RyR (Bers, 2008).

$[Ca^{2+}]_i$ is then extruded from the cytsol via the NCX which uses the electrochemical Na^+ gradient to drive inward $I_{Na/Ca}$, and by pumping of Ca^{2+} back into the SR via the SERCA pump, allowing for relaxation of the muscle (Bers, 2002). In a steady state of contraction, during each beat the amount of Ca^{2+} extruded from the cell is equal to that which entered at the beginning of the action potential (Eisner et al., 2000).

1.4. Caveolae

Caveolae are small flask-shaped invaginations of the cell membrane, typically 50-100 nm in size. They are a type of lipid raft, enriched in cholesterol and sphingolipids, but their lipid composition differs from other lipid rafts (Yao et al., 2009). Caveolae were first visualised by electron microscopy (EM) in the 1950s by Palade (Palade, 1953). Since then caveolae have been found to be present within most mammalian cells and are particularly abundant in endothelial and adipose cells (Hibbs et al., 1958; Parton, 2003). Caveolae are defined by the presence of caveolin proteins, required for caveolae formation, whose molecular identity was confirmed in the 1990s (Monier et al., 1995; Fra et al., 1995; Rothberg et al., 1992). These consist of caveolin 1 (Cav 1), caveolin 2 (Cav 2) and the muscle specific caveolin 3 (Cav 3). Typically ~ 144 caveolin molecules are suggested to be integrated into a single caveolae (Pelkmans and Zerial, 2005).

Caveolae have multiple functions and are proposed to act as mechanosesonsors and membrane reservoirs, aid in regulation of lipid transport, form scaffolds for signalling proteins and act as endocytosis vesicles (Komarova and Malik, 2010; Sinha et al., 2011; Siddiqui et al., 2011; Pilch and Liu, 2011; Kozera et al., 2009). The importance and function of caveolae within the cell has been extensively studied (Cheng and Nichols, 2016), but there is still much which is unknown about these functional units of the plasma membrane. This is, in part, related to difficulties in imaging caveolae due to their size which is below the diffraction limit of normal light microscopy. This means that visualisation of these membrane domains to date has been through EM. New imaging techniques being developed are beginning to overcome some of the problems and are revealing new information about caveolae.

1.4.1. Caveolins

Cav 1, and Cav 3 in muscle cells, is vital for formation of caveolae within the plasma membrane (Park et al., 2002). The tissue distribution of Cav 2 is similar to that of Cav 1 but it is not required for caveolae formation, as knock out (KO) of Cav 2 only causes a reduction in Cav 1 expression and no change to the morphologically defined caveolae, measured in endothelial and adipose cells (Razani et al., 2002). Interestingly Cav 1 and Cav 3 knock-out mice are viable and fertile but display a number of different phenotypes including dyslipidemia and cardiac dysfunction (Woodman et al., 2002; Park et al., 2002).

Monomeric caveolin proteins (18-22 kDa) insert in the membrane in a hairpin formation with both the N and C termini facing the cytosol (Dupree et al., 1993)(Figure 1-6). Caveolin oligomerise after synthesis within the Golgi and within the plasma membrane. Amino acid residues 97-135 of human Cav 1 (and equivalent sequences in Cav 2 and 3) have been demonstrated to form a "horseshoe" shape which is suggested to form a "wedge" in the membrane aiding in deformation and forming the characteristic caveolar shape (Yang et al., 2014). The three caveolin isoforms contain a conserved region towards the N-terminus called the caveolin-scaffolding domain (CSD) which can bind to proteins containing a complementary caveolar binding motif, a sequence rich in aromatic residues (Φ*X*Φ*XXXX*Φ, Φ*XXXX*Φ*XX*Φ, or Φ*X*Φ*XXXX*Φ*XX*Φ (Couet et al., 1997) (Figure 1-6 inset). For many years it was accepted that the CSD interacts with a number of different signalling proteins through the caveolar binding motif, however this concept has more recently been questioned as many of the binding motifs are buried deep in the 3D structure of proteins and are unavailable for interaction (Byrne et al., 2012). The CSD, as well as the intramembrane domain (amino acids 102-135) have also been shown to be important for caveolar formation (Ariotti et al., 2015).

Caveolin can have either direct positive or negative effects on its binding partners. Negative regulation is the most common, as illustrated by effects on endothelial nitric oxide synthase (eNOS) (García-Cardeña et al., 1997). Caveolin binding constitutively inhibits eNOS and loss of Cav 1 results in persistent eNOS activation and an increase in nitric oxide (NO) generation within the cell (Yu et al., 2006).

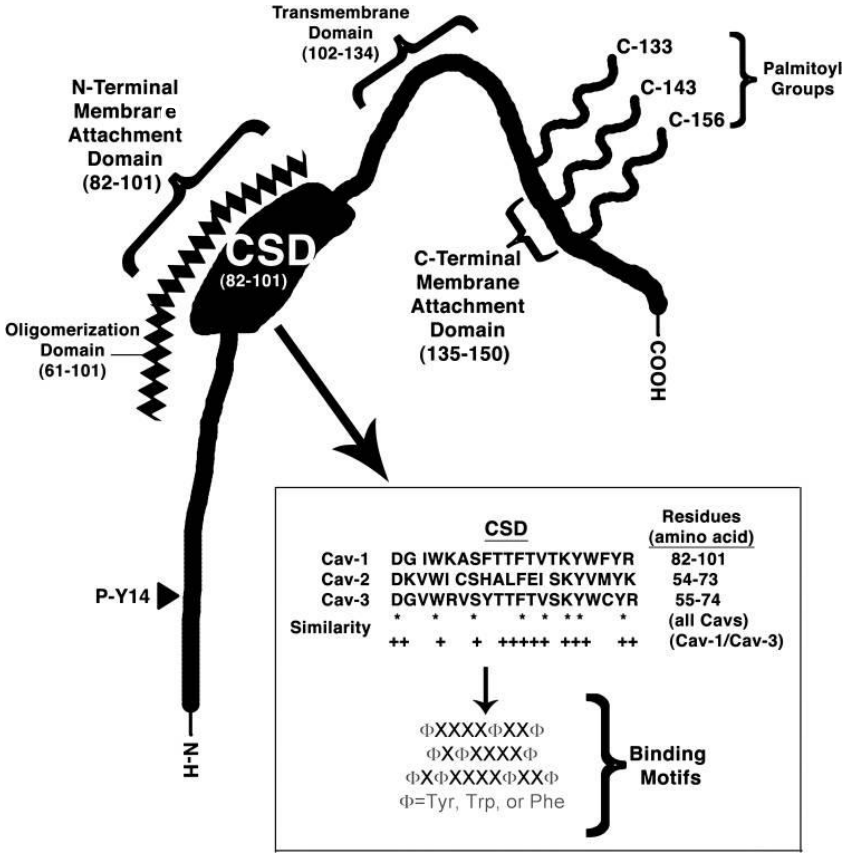

Figure 1-6 Caveolin shape and components

Modified from (Patel and Insel, 2009) shows the typical shape of a caveolin protein hairpin insertion into the plasma membrane. Inset details the sequences of the caveolar scaffolding domain (CSD) in the different caveolin proteins and the corresponding caveolin binding motif.

On the other hand caveolin binding to insulin receptors increases activity (Yamamoto et al., 1998). Caveolin proteins can also have an indirect effect on signalling and cellular function via recruitment of additional proteins to aid in signalling control (Balycheva et al., 2015). Cav 1 and Cav 3 are subject to a number of post-translational modifications, including palmitoylation (at multiple sites) which may affect additional protein binding and location within the membrane (Kim et al., 2014; Wypijewski et al., 2015). Other post-translation modifications include SUMOylation in Cav 3, which alters β_2-adrenergic receptors expression (Fuhs and Insel, 2011), and phosphorylation of Cav 1, which is required for caveolar dependent endocytosis (Parton and Simons, 2007).

1.4.2. Cavins

Within the last decade, a new class of protein, the cavins, have been discovered to play a role in caveolae formation and function within the cell (Briand et al., 2011; Hill et al., 2008). The cavin proteins were not originally considered as caveolar proteins (Jansa et al., 1998), hence the dual naming of this family: cavin 1 (PTRF - polymerase 1 and transcript release factor), cavin-2 (SDR - serum deprivation response protein), cavin-3 (SRBC -serum deprivation response factor-related gene product that binds to C-kinase) and cavin-4 (MURC -muscle-restricted coiled-coil protein). Cavins do not aid in the formation of caveolae but are recruited to the membrane after caveolin formation, and help stabilise the caveolae shape. Cavin 1 has been shown to have a crucial role in stabilisation of caveolae, with KO of cavin in mouse models showing a dramatic reduction and almost complete loss of caveolae in all cell types studied, including lung, intestine and muscle (Liu et al., 2008; Hill et al., 2008; Hill et al., 2012). Cavin 2 aids in regulation of the caveolae shape and morphology and has been shown to bind to cavin 1 and promote its recruitment to caveolae (Hansen et al., 2009). Cavin 3 aids in trafficking and internalisation of the caveolae, as demonstrated by partial impairment of intracellular Cav 1-mediated trafficking when cavin 3 expression is reduced (McMahon et al., 2009). Cavin 4, like the Cav 3 protein, is a muscle specific caveolar protein. The percentage similarities between cavin isoforms is show in Figure 1-7. The cavin proteins share a number of PEST (proline, glutamic acid, serine, and threonine-rich) domains (see Figure 1-7). These PEST domains have been suggested to play an important role in regulation of homeostasis and function of the cavin proteins through proteolysis (Bastiani et al., 2009; Kovtun et al., 2015).

A

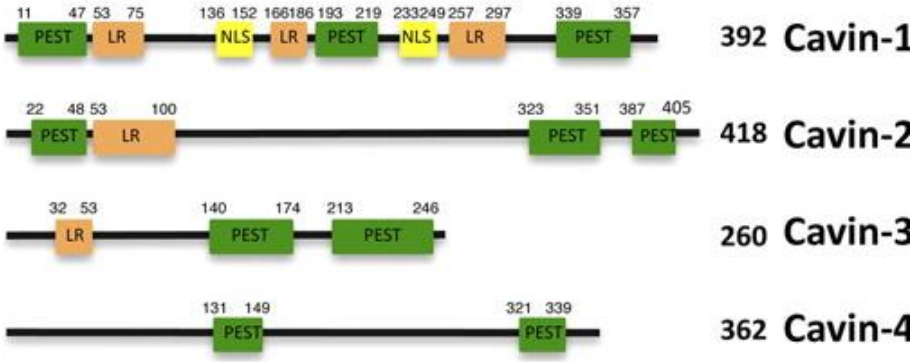

B

	Cavin-1	Cavin-2	Cavin-3	Cavin-4
Cavin-1	100			
Cavin-2	35/53	100		
Cavin-3	22/37	28/41	100	
Cavin-4	29/49	24/42	20/39	100

Figure 1-7 Cavin proteins basic sequence and homology

A. Figure from (Bastiani et al., 2009) shows cavin protein sequence with common proline, glutamic acid, serine, and threonine-rich (PEST) domains, leucine-rich regions (LR) and nuclear localization sequences (NLS) sights (mouse) **B.** Percentage similarity in cavin proteins (murine)

Cavin 1 is phosphorylated at multiple sites, with phosphorylation at Ser36 and Ser40 thought to be important for membrane location (Bai et al., 2011), while insulin-dependent phosphorylation of cavin 1 in adipocytes triggers movement of cavin 1 from the plasma membrane (Aboulaich et al., 2011). Cavin 1 has been shown to have little or no direct interaction with the caveolin proteins (Liu and Pilch, 2008).

1.4.3. Caveolar coat complex

The exact organisation of the caveolar proteins within caveolae is not fully understood, but the shape of the caveolae is thought to play a role in its function. As mentioned previously, the size of caveolae causes limitations in imaging techniques available and impeded detailed investigation. New EM techniques and labelling has vastly improved within the last 5 years which, paired with computer technology, has enabled the 3D reconstruction of caveolae and caveolar proteins (Ludwig et al., 2013). Oligomerisation of caveolin is thought to be crucial for the formation of caveolae which initially happens in the trans-Golgi network and is cholesterol dependent (Hayer et al., 2010). This results in an 8S complex of caveolin molecules (Monier et al., 1996). The cavin monomer forms rod shaped homotrimers, or heterotrimers with either cavin 2 or cavin 3 (Gambin et al., 2014), and around 18-20 trimers are then thought to be involved in the caveolar coat complex forming a "nano-net" (Stoeber et al., 2016). Cavin 2 and cavin 3 appear to compete for binding sites within the caveolar coat complex (Ludwig et al., 2013). The final caveolar coat complex is an 80S caveolin complex with cavins forming a network mesh lining. Two recent cryo-EM studies of the caveolar coat complex have both come to the conclusion that the membrane forms a polyhedral structure with an edge length predicted at 31.6 nm and 30-40 nm (Stoeber et al., 2016; Ludwig et al., 2016) (Figure 1-8).

1.4.4. Caveolae in the cardiac myocyte

Caveolae are found within the plasma membrane of the cardiac myocytes, although the exact extent of the membrane composed of caveolae or the location of caveolae (surface/t-tubules) have remained controversial. Cav 3 is the muscle specific caveolin protein which is highly abundant in the myocyte cell, as visualised with immunocytochemistry (Figure 1-9). The Cav 3 protein can be located within caveolae and on non-caveolar sarcolemmal membranes, as Cav 3 expression is seen in both buoyant (cholesterol-rich) and heavy (non-lipid raft membranes) fractions in sucrose gradient fractionations, however the presence of caveolae within the t-tubules is much debated, see (Wright et al., 2014).

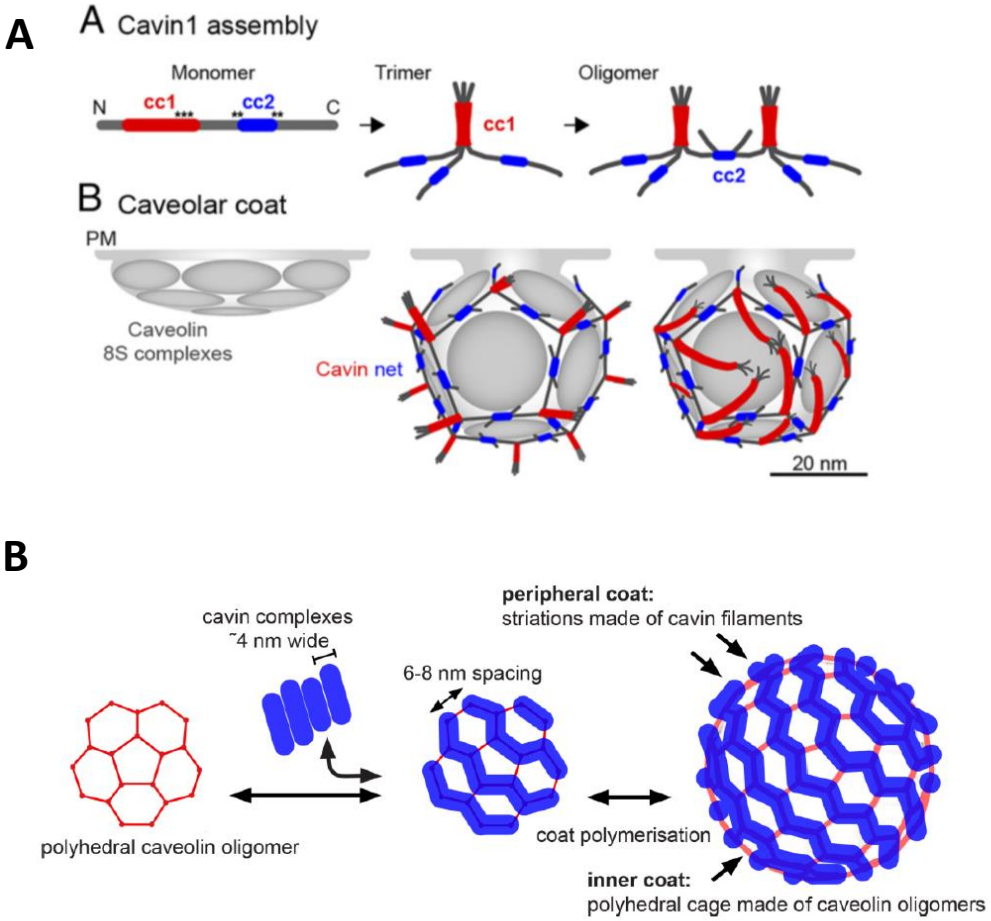

Figure 1-8 Model and theory of assembly of the caveolar coat complex

Modified from (Stoeber et al., 2016; Ludwig et al., 2016) shows two recent papers which have used EM to visualise and reconstruct the possible structure of the caveolar coat complex. **Model A.** Cavin 1 monomers form trimers which then interconnect to form oligomers. The cc1 domains (red) form a parallel trimeric coiled-coil creating a stiff rod shaped structure 17-nm-long. The 12 faces of the dodecahedron are predicted to be occupied by disc-shaped caveolin oligomers. Addition of cavin 2 and cavin 3 may induce breaks in the polyhedron as they do not contain the c22 domain. (Stoeber et al., 2016) **Model B.** Caveolin oligomerises in a polyhedral shape and then further oligomerise into a polyhedral cage. Cavin oligomers associate with the edge of the polyhedral shapes (Ludwig et al., 2016)

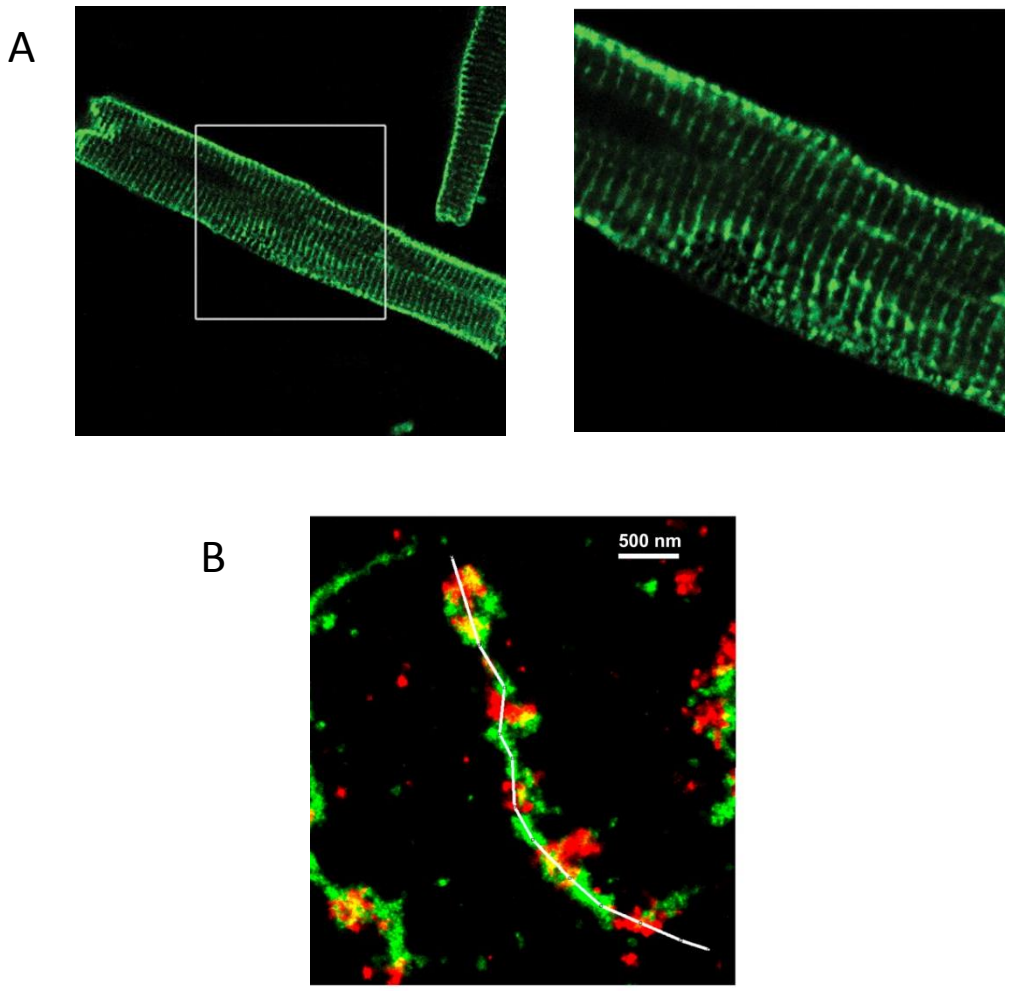

Figure 1-9 Immunocytochemistry of caveolin 3 staining in a cardiac myocyte

Images from (Garg et al., 2009) and (Wong et al., 2013) **A.** (right) Confocal image of adult rat cardiac myocyte stained with Cav 3 antibody (green), white box represents the enlarged area shown to the right. (right) Close up highlighting staining along the z-lines (Garg et al., 2009). **B.** Super resolution image of cardiac myocyte stained with Cav 3 (green) and RyR2 (red) antibodies. White trace shows t-tubules (Wong et al., 2013)

With EM, caveolae are imaged routinely within the surface sarcolemma (Wright et al., 2014) but due to the difficulty in sectioning t-tubules along their length, there are few reports of caveolae in the t-tubular membrane, see (Levin and Page, 1980). However this may soon change with new imaging techniques, highlighting the role of caveolae and caveolar proteins within the t-tubules. Super resolution microscopy has placed a larger percentage of the RyR2 than was previously thought co-localised with caveolin 3 within the t-tubules (Wong et al., 2013).

Loss or mutation of the caveolar proteins (cavin 1 and Cav 3) produces a range of different effects on the heart including reduced ejection fraction, increased cardiac fibrosis and long-QT syndrome (Taniguchi et al., 2016; Vatta et al., 2006). By contrast, over-expression of Cav 3 has been shown to be cardio protective (Markandeya et al., 2015). Caveolae and/or Cav 3 have been implicated numerous times in regulation of the β-adrenergic signalling within the heart (Calaghan et al., 2008; Rybin et al., 2000; Head et al., 2005; Insel et al., 2005), as discussed in the next section.

1.5. β-adrenergic receptors

Regulation of the rate and force of contraction of the heart is important for homeostasis and is controlled through sympathetic and parasympathetic innervation of the heart and circulating hormones (e.g. adrenaline). During periods of increased metabolism within the body, such as during exercise, there is a reduction in parasympathetic output and an increase in sympathetic stimulation of the heart resulting in an increased heart rate and cardiac output. This is achieved through the β-ARs located in the cardiac myocyte membrane.

The β-ARs are part of a large family of G-protein coupled receptors (GPCR)(Table 1-1). They have 7 transmembrane α-helical domains and are coupled with a trimeric (αβγ) G-protein on the intracellular side. Of the GPCR family, muscarinic and adrenergic receptors play key roles in the regulation of cardiac function (Rockman et al., 2002). Other GPCRs in the heart include prostanoid and histamine receptors (Salazar et al., 2007). The adrenergic receptor family tissue distribution and signalling pathways are outlined in Figure (Table 1-1).

Receptor	β_1	β_2	β_3	$\alpha_{1/A/B/D}/AT_1/ET$	α_2	M_2
Primary G protein	G_s	G_s/G_i	G_s/G_i	G_q/G_{11}	G_i	G_i
Tissue distribution	Heart	Heart, lungs, vessels, kidney	Adipose, heart	Heart, vessels, smooth muscle	Coronary vessels, CNS, pancreas, platelets	Heart
Primary effector in heart tissue	AC, L-type Ca^{2+} channel	AC, L-type Ca^{2+} channel	AC	PLC-β	AC	AC, K^+ channels
Signals	↑ cAMP/PKA	↑ cAMP/PKA, MAPK	↑ cAMP/PKA	↑ DAG/$InsP_3$, PKC, MAPK	↓ cAMP/PKA	↓cAMP/PKA ↑PI(3)K
Endogenous agonist	NA, A	NA, A	NA, A	NA, A, angiotensin II, endothelin	NA, A	ACh

Table 1-1 Seven transmembrane-spanning domain receptors in the heart

α, α-adrenergic receptor subtypes 1,2 ; β, β-adrenergic receptor subtypes 1, 2, 3; AC, adenylyl cyclase; ACh, acetylcholine; A, adrenaline; AT_{II}, angiotensin-II receptor subtype 2; cAMP, adenosine 3',5' monophosphate; DAG, diacylglycerol; ET, endothelin receptor; $InsP_3$, inositol 1,4,5 triphosphate, M_2, muscarinic cholinergic receptor subtype 2; MAPK, mitogen-activated protein kinase; NA noradrenaline; PKA, protein kinase A; PKC, protein kinase C; PLC-β, phospholipase C-β. Modified from (Rockman et al., 2002)

Binding of an extracellular ligand drives a conformational change in the GPCR and subsequently causes a switch from GDP to GTP binding to the α subunit of the associated G-protein. This results in a dissociation of the Gα subunit from the GPCR which initiates downstream signalling events (Telser, 2002).

In the cardiac myocyte there are three subtypes of βARs, β_1AR, β_2AR and β_3AR, with β_1AR being the predominant. β_3AR expression is very low compared to β_1AR and β_2AR, although expression has been shown to increase in some forms of heart disease (Belge et al., 2014). β_3AR acts through the secondary messenger cyclic guanosine monophosphate (cGMP), through NO mediated signalling and inhibits cardiac contraction (Gauthier et al., 1998). However much is still not understood about this receptor which has shown to produce both positive and negative contractile effects on the heart (Napp et al., 2009; Bundgaard et al., 2010). β_1AR and β_2AR both act through cyclic adenosine 3′,5′-monophosphate (cAMP) as a secondary messenger, although the downstream targets and signalling response are distinctly different. One of the main differences between these two receptors is that β_2AR couples with both the α_i (inhibitory) and the α_s(stimulatory) G protein subunit, while β_1AR only couples with α_s. The α_s subunit activates adenylyl cyclase (AC) stimulating production of cAMP from adenosine triphosphate (ATP), cAMP then binds the regulatory subunit of cAMP-dependent protein kinase (PKA) which in turn phosphorylates a number of target proteins (Xiang and Kobilka, 2003). By contrast, the α_i subunit inhibits AC activity. Stimulation of the β_1AR produces a robust global cAMP response causing an increased inotropic (contraction), chronotropic (heart rate) and lusitropic (rate of relaxation) effect; while β_2AR stimulation only produces a small localized cAMP response and a modest inotropic effect (Nikolaev et al., 2006).

1.5.1. Regulation of contraction

The β_1AR make up around 70-80% of the total β-AR population within the heart and couple solely with the $G\alpha_s$ subunit. Upon stimulation of the β_1AR the $G\alpha_s$ increases cAMP production through AC 5 and 6, which are the main cardiac isoforms (Defer et al., 2000), this in turn activates PKA. PKA has many targets involved in EC coupling which cause a positive ionotropic response. These include the L-type Ca^{2+} channel, RyR2 and PLB (Rapundalo, 1998; Bers, 2008). PLB is phosphorylated at Ser16 which decreases its infinity

for SERCA inhibition and causes an increase in the rate and amount of Ca^{2+} taken back into the SR via the SERCA pump (MacLennan and Kranias, 2003). This in turn generates a larger release of Ca^{2+} during CICR producing a larger force of contraction (Luo et al., 1994). L-type Ca^{2+} channel phosphorylation enhances the I_{CaL} by increasing open probability (van der Heyden et al., 2005). PKA also has targets within the contractile proteins including cMyBP-C and TnI. TnI is phosphorylated at Ser23/24 and this decreases the Ca^{2+} sensitivity of the myofilaments and speeds the rate of relaxation (Kobayashi and Solaro, 2005).

Although the secondary messenger cAMP is common to both β_1AR and β_2AR signalling pathways, selective stimulation of these two receptors produces distinctly different results. Stimulation of the β_2AR does not cause phosphorylation of proteins of the SR (PLB) or myofilaments (TnI) (Calaghan et al., 2008; Nikolaev et al., 2006). The different responses to stimulation of these two βARs are thought to arise as a result of compartmentalisation.

1.5.2. Compartmentalisation of signalling

Following β-AR stimulation, cAMP-dependent PKA activates proteins which contribute to compartmentalisation of the signal. These proteins include phosphodiesterases (PDE) and protein phosphates (PP)(Conti and Beavo, 2007).

PDEs hydrolyse cAMP and tightly control the cAMP-dependent signalling. They consist of a larger family of 11 proteins; PDE4 and PDE8A specifically hydrolyse cAMP while PDE1, PDE2 and PDE3 can hydrolyse cAMP or another common secondary messenger cGMP (Beavo, 1995; Conti et al., 2003; Patrucco et al., 2010). PDE2 and PDE3 are thought to compartmentalise the cAMP signal of EC coupling proteins under basal conditions, but upon β-AR stimulation PDE4 is recruited and contributes to compartmentalisation (Mika et al., 2013). In rat ventricular myocytes PDE3 and PDE4 are the predominant PDEs responsible for hydrolysis of cAMP, and play an important role in controlling SR Ca^{2+} load (Leroy et al., 2008; Mika et al., 2013). PDEs are directly activated by PKA and act as a negative feedback loop. PDE2 has been specifically implicated in modulation of $I_{Ca,L}$ when β-AR are stimulated (Verde et al., 1999).

The two main PPs PP1 and PP2A contribute to more than 90% of the PP activity within the mammalian heart (Macdougall et al., 1991). PP1 inhibitor-1 (I-1) is phosphorylated by PKA and inhibits PP1 activity, in turn enhancing PLB phosphorylation promoting re-uptake back into the SR and producing a positive feedback loop (Braz et al., 2004). PPs play an important

role in de-phosphorylating various EC coupling proteins, including myofilament proteins and L-type Ca^{2+} channels, during the cardiac cycle (duBell et al., 2002).

Spatial compartmentalisation and physical distribution of signalling proteins is another way in which the β-AR signalling is compartmentalised. In a recently created computer model of β-AR signalling in the cardiac myocyte, PDEs alone (at a physiological concentration) were not enough to produce the compartmentalisation of the cAMP signal seen in cardiac myocytes, instead it was suggested that physical diffusion barriers and scaffolding of proteins also played a role (Yang et al., 2016). A-kinase anchoring proteins (AKAPs) are a family of scaffolding proteins which bind to PKA and localize it to the targeted phosphorylation sites. In particular AKAP5 has been shown to play an important role in sympathetic regulation (Nichols et al., 2010). Nichols et al. showed that AKAP5 formed complexes with Cav 3, AC5/6, β-AR, PKA, PP2B and the L-type Ca^{2+} channel. Using KO animals it was seen that AC 5/6 and PP2B were dependent on AKAP5 for their association with the Cav 3 complex. Selective stimulation of the βARs revealed an essential role of AKAP5 in targeting PKA to the RyR2 and PLB (Nichols et al., 2010), two proteins which are major players in the inotropic and lusitropic response to βAR stimulation.

1.5.2.1. Caveolae compartmentalisation

Caveolae and the caveolar proteins are another form of scaffold within the cardiac myocyte which aid in β-AR signalling compartmentalisation. The Cav 3 CSD sequence contains a binding site for both AC 5 and PDE 4 which acts to restrict the cAMP being produced (Timofeyev et al., 2013). The CSD has also been found to bind the G-protein α subunit, G-protein regulated kinase (GRK)2 and PKA. GRK2 phosphorylates the βAR and causes internalization, and desensitization of the receptor (Freedman et al., 1995). Cav 3 as mentioned previously is an important structural protein for the t-tubules, and can be located within caveolae or on the non-caveolar sarcolemma. Many of the β-AR signalling proteins, such as β-AR, AC 5/6, G_α etc. have found to be located within the caveolae and lipid rafts (Head et al., 2006; Rybin et al., 2000; MacDougall et al., 2012). It is currently unclear to what extent caveolae play a role in compartmentalisation of the β_1AR signalling pathway, although β_1AR has been detected in lipid rafts and cholesterol depletions significantly increases isolated cardiac myocytes response to low levels of isoprenaline estimation (Agarwal et al., 2011). Selective stimulation of the β_1AR also causes an increase in the percentage of cavin 1 located within the caveolar domain (Wypijewski et al., 2015). Both of these results suggest a dynamic regulation of the β_1AR, It is more widely accepted that

caveolae play an important role in compartmentalisation of the β_2AR (Calaghan and White, 2006; MacDougall et al., 2012; Wright et al., 2014). Both disruption to membrane cholesterol and the Cav 3 protein cause an increase in the signalling response recorded after β_2AR stimulation in the cardiac myocyte (Wright et al., 2014; MacDougall et al., 2012). Translocation of the β_2AR from lipid rich/caveolar membranes to non-caveolar membranes (Rybin et al., 2000), and an increase in cavin 1 located within the caveolar domain after isoprenaline stimulation of cardiac myocytes again suggest a dynamic regulation of the β_2AR by caveolae (Wypijewski et al., 2015).

1.5.3. β_2-adrenergic receptor

The β_2AR does not produce as large a cAMP signal as the β_1AR, and only produces a small inotropic response to stimulation (Xiao et al., 1999b). In part this is due to the compartmentalisation of the β_2AR signal, but the ability of the receptor to couple to both $G\alpha_s$ and $G\alpha_i$ also contributes to the diminutive response (Xiao, 2001). The coupling of β_2AR to $G\alpha_i$ aids in preventing overstimulation of the cAMP pathway and also promotes anti-apoptotic signalling through the phosphatidylinositol 3-kinase (PI-3K) signalling pathway (Chesley et al., 2000). The primary location of the β_2AR has been contested, some groups claim that it is predominantly located within the t-tubules in non-caveolar sarcolemma (Nikolaev et al., 2010), with an additional small functional role in caveolar at the surface sarcolemma (Wright et al., 2014), while other find the main population of β_2AR within caveolae (Rybin et al., 2000). In the experimental setting, stimulation of the β_2AR in the cardiac myocyte produces varied responses which, in part, can be ascribed to the use of different combinations of antagonist/agonist. A new three state receptor model has been proposed for the β_2AR, with different agonists showing differential activity on the receptor. Some agonists were shown to stabilise the active state of the β_2AR, while others which stabilise the active state can simultaneously destabilise the inactive state (Staus et al., 2016).

1.5.4. Down regulation of the β-adrenergic receptor

Stimulation of the β-AR results in agonist desensitisation, which can happen in a non-specific manner through direct phosphorylation of the β-AR via PKA or PKC resulting in a conformational change which prevents the receptor's interaction with G-protein subunits (Lefkowitz, 1998). This type of desensitisation does not discriminate between stimulated and unstimulated receptors. Agonist-specific desensitisation occurs through the G-protein receptor kinase family, with GRK2 and GRK5 being the most abundant isoforms expressed in the heart (Penela et al., 2006). GRK phosphorylation of the β-AR promotes arrestin

binding to the receptor preventing further stimulation. KO of GRK2 in mice causes fatality at day 12-15 of embryonic life due to severe underdevelopment of the heart and heart failure (Jaber et al., 1996). Phosphorylation of the β_2AR via PKA and GRK also causes the shift in coupling with $G\alpha_s$ to $G\alpha_i$ coupling (Zamah et al., 2002; Wang et al., 2008).

1.6. Heart failure

Heart failure is defined as the inability of the heart to reach the cardiac output needed to meet the body's metabolic demands. It is a serious problem affecting nearly 1 million people in the UK today and incurs substantial costs to the National Health Service every year. The causes of heart failure can vary from genetic mutations, which are inherited, to coronary artery disease or hypertension. Heart failure usually starts with a primary insult, such as myocardial infarction (MI) or mechanical overload, which then results in necrosis of tissue, remodelling and impaired contractility of the heart. In response to the primary insult to the heart which results in decreased cardiac output, there is an increase in sympathetic stimulation to the heart to increase output to normal levels. In heart failure patients there is typically a sympathetic hyperactivity and attenuated parasympathetic activity (Triposkiadis et al., 2009). Remodelling describes the many different cellular changes which the heart adopts to try to adapt to the initial insult (Swynghedauw, 1999); this occurs during the progression to heart failure. Initially remodelling is a compensatory mechanism, but this quickly becomes detrimental to the heart. To maintain sufficient cardiac output the heart often has to work harder. The majority of mitochondrial ATP is produced through fatty acid oxidation (see Section 1.3.1), but excessive β-AR stimulation drives excessive mobilisation of free fatty acids and fatty acid oxidation which has been linked with oxygen waste (Opie and Knuuti, 2009). Towards the end stages of heart failure there is a down regulation of fatty acid oxidation and glucose oxidation is unregulated, with mitochondrial dysfunction and OXPHOS inefficiency (Dávila-Román et al., 2002; Park et al., 2016). Short term and long term stimulation of the β_2AR has been linked with increased glucose uptake into the cell and altered energy metabolism (Ciccarelli et al., 2013).

Structural remodelling of the cell and the ECM has also been noted in heart failure. In both human patients and animal models of heart failure, a remodelling of the t-tubular system has been reported, characterised by super resolution microscopy and confocal microscopy (Crossman et al., 2015; Kostin et al., 1998; Dibb et al., 2009). Loss of t-tubules in heart failure

results in dis-synchrony of CICR and EC coupling, and redistribution of many of the proteins involved in regulation of contraction (Guo et al., 2013).

The idea of 'reverse remodelling' (a reversal of the detrimental remodelling seen in the progression of heart failure) is becoming a popular strategy for treatment of heart failure (Koitabashi and Kass, 2012). One example of this is in the use of β-blockers which have been shown to re-sensitise the βAR (Reiken et al., 2003) and increase exercise tolerance. Although the exact mechanisms by which the β-blockers work is not fully understood, the principle of reversing the destructive changes in heart disease is what many new drug targets and therapies aim to achieve. An alternative means of reverse remodelling is the use of left ventricular assist devices (LVADs) which unload the failing ventricle. Clinical studies have looked at the differences in myocytes before and after the insertion of an LVAD and shown that there is a restoration of both β_1AR density and AC activity (Kassner et al., 2012). Mechanically aiding the heart in this way helps improve cell compliance and function.

1.6.1. β-adrenergic changes in heart failure

One characteristic of cardiac remodelling in heart failure is a reduction in β_1AR and desensitisation of β-AR signalling (Bristow et al., 1982). Desensitization can come about from chronic stimulation of the β-AR leading to an increase in GRK2 expression as reported in patients with heart failure (Ungerer et al., 1993a). Necrosis has also been seen to increase with the chronic stimulation of the βAR (Teerlink et al., 1994). The normal positive ionotropic response in human hearts is diminished (Colucci et al., 1988), resulting in exercise intolerance and fatigue. Reduced expression of the β_1AR at both the mRNA and protein level has been shown in human patients and animal models of heart failure (Engelhardt et al., 1996; Steinfath et al., 1992). Uncoupling of the $G\alpha_s$ subunit from the βAR and hypophosphorylation of PLB, TnI and cMyBP-C have been reported within the failing human heart (Bartel et al., 1996; Messer et al., 2007). On the other hand hyperphosphorylation of the RyR2 (Marx et al., 2000), and increased L-type Ca^{2+} channel open probability has been detected in myocytes isolated from heart failure transplant patients (Schröder et al., 1998). Chronic β-AR stimulation induced phosphorylation of RyR2 mediated through CamKII and increased RyR Ca^{2+} (Grimm et al., 2015). These changes in phosphorylation state have all been suggested to be linked with the changes in β-AR signalling in heart failure.

Desensitisation of the β-AR is considered to be a protective mechanism which prevents aberrations in myocyte function through arrhythmias, energy deletion and apoptosis

(Eschenhagen, 2008). Desensitisation is primarily mediated through GRK2 phosphorylation of the β-AR, and consequent β-arrestin binding which targets the receptor for internalisation. From this point, the receptor can then either be recycled through de-phosphorylation via PP2A, or degraded. However chronic β-AR stimulation appears to push the β_1AR towards the degradation pathway (Ungerer et al., 1993a). β_2AR signalling changes in various heart failure models. One influential hypothesis is that β_2ARs are relocated from t-tubules to the crest (surface) sarcolemma where they produce a more robust cAMP response similar to that seen with the β_1AR, due to loss of normal t-tubule-based compartmentalisation mechanisms (Nikolaev et al., 2010).

1.6.2. Caveolar changes in heart failure

Caveolae are essential regulators of cardiac function and it is no surprise that changes in these structures and their proteins have been reported in a number of cardiac diseases including heart failure. Changes in Cav 1 and Cav 3 protein and mRNA expression have been reported in both animal models of heart failure and human patients (Ratajczak et al., 2003; Feiner et al., 2011), as well as a reduction in caveolae density as imaged by EM (Wright et al., 2014). In a rat model of myocardial infarction both Cav 1 and Cav 3 were shown to dissociate from caveolae to non-caveolar sarcolemma, as measured by sucrose gradient fractionation (Ratajczak et al., 2003). Together, these support the idea the caveolae are disrupted in heart failure. Cav 3 is found to be co-located with key proteins involved in contraction, as measured with immune-precipitation (Insel et al., 2005). Disruption to Cav 3 may results in disorganisation of these contractile proteins. Mutations of Cav 3 seen in patients results in disrupted electrical activity and cardiomyopathies. Congenital long-QT syndrome patients were found to have a genetic mutation in CAV3 (Vatta et al., 2006). A mutation in the Cav 3 protein has also been found within familial hypertrophic cardiomyopathy patients (Hayashi et al., 2004). Disruption to caveolae in heart failure has also been linked with changes in β-AR signalling (Nikolaev et al., 2010), resulting in dysregulation of downstream signalling. Mechanically unloading the heart has shown to increase cardiac function and β-AR density (Uray et al., 2003; Heerdt et al., 2000). Tissue from patients with left ventricular aided devices (used as a bridge to heart transplant) were taken before and after the device was inserted. Protein expression and mRNA levels increased for all of the caveolin proteins, and this was linked to the reverse remodelling of the βAR signalling cascade (Uray et al., 2003).

The cavin proteins were only discovered 11 years ago and their potential role in cardiovascular disease is just beginning to be studied (Williams and Palmer, 2014). A genetic mutation in cavin 1 was found in patients with enlarge but weak muscles, and has been shown to cause cardiac arrhythmias and long-QT syndrome (Rajab et al., 2010).

1.6.3. Right and left ventricular heart failure

The right and left ventricle develop from different embryological origins, and in adult life are subjected to distinctly different environments. Early in post-natal development the ventricles go through very different remodelling phases to enable the LV to cope with high pressure and for the RV to become a compliant chamber. In humans the RV does not have the same capacity to respond to an acute increase in afterload as that of the LV (MacNee, 1994), and is incapable of generating pressures higher than 40 mmHg. In comparison the LV can respond to a wide range of afterload pressures with very little change in output. In mouse, trabeculae from the right and left ventricle produce almost opposite responses to α_1-adrenergic receptor (α_1-AR) stimulation (Wang et al., 2006). In a canine model, the RV myocytes have an enhanced response to non-selective β-AR stimulation with isoprenaline compared with those from the LV, and this is thought to be shaped by different PDE3 and PDE4 compartmentalisation between the ventricles (Molina et al., 2014). Interestingly in Eisenmenger syndrome, which is caused by a congenital defect most often within the septum, the RV does not thin during the post-natal development phase and RV and LV thickness are similar in the adult. These patients have a higher systemic cardiac index ($L/min/m^2$) and lower mortality rates than those with other causes of pulmonary artery hypertension (Hopkins et al., 1996). In Eisenmenger syndrome, the RV appears to hold the potential to adequately adapt to increased afterload on the heart. The RV and LV show a different patterns of change in gene expression in response to increased afterload (Bogaard et al., 2009). Friedberg and Redington have summarised the similarities and differences of RV and LV adaptation to pressure overload and failure, along with RV and LV interactions. They concluded that although there are known differences between the ventricles they still share many common maladaptations in failure with the ventricular-ventricular interaction playing an important role (Friedberg and Redington, 2014). However clinical treatment of RV or LV heart failure have remained distinctly different due to different reactions produced; drugs used for RV treatment show little or no effect in LV failure (Anand et al., 2004). These differences should be taken into consideration when studying different models of heart failure. To date there is no information within the literature of differences between the LV and RV in relation to caveolae.

1.7. The study of β-AR and caveolae in heart failure

Caveolin and β-AR protein expression within myocytes and ventricular homogenates have been studied through Western blotting in a number of different animal models of heart failure. Caveolae can be visualised with EM (Kozera et al., 2009), and are starting to be visualised with super-resolution microscopy (Platonova et al., 2015). However antibodies targeting the β-AR are limited and not often used to visualise the β-AR. Instead the study of the β-AR focuses on radioligand binding assays ([125I]iodocyanopindolol (ICYP) -binding), measurements of cAMP by FRET-based cAMP sensors and the functional response as indexed by $[Ca^{2+}]_i$ transients and/or contraction/shortening. These approaches examine very different aspects of the β-AR signalling cascade. The radio ligand binding assay assesses β-AR density on the plasma membrane, whereas FRET-based cAMP sensors measure the cAMP produced in response to β-AR stimulation. Neither of these give a direct measurement of function, which can be measured at the cellular level in the cardiac myocyte, at the multicellular level in trabeculae carnae or in whole heart preparations.

1.7.1. Caveolar protein knock-out and mutation models

KO or genetic mutation of the caveolin and cavin proteins has been used to replicate a number of different phenotypes observed within heart failure. KO of Cav 1 causes cardiac hypertrophy, pulmonary hypertension and cardiac dysfunction (Zhao et al., 2002; Wunderlich et al., 2006), however it is not clear whether this is due to loss of caveolin in the myocytes or in the other cells within the heart (fibroblast or endothelial cells) (Fridolfsson and Patel, 2013). KO of Cav 3 similarly causes cardiac hypertrophy and dysfunction, as well as t-tubule abnormalities within the cardiac myocyte (Galbiati et al., 2001; Woodman et al., 2002). Mutation of Cav 3 to form a dominant negative from, which lacks three amino acids in the CSD and causes a reduction in caveolae, has been used to mimic the phenotype of cardiac cells seen in heart failure, which is then rectified when Cav 3 is re-introduced (Wright et al., 2014; Barbagallo et al., 2016). Cavin 1 KOshave also been studied in relation to mimic cardiovascular diseases (Taniguchi et al., 2016).

1.7.2. Membrane distribution

Caveolae are rich in cholesterol and sphingolipids, which can be exploited in two common methods to study caveolae and their protein composition. Centrifugation of samples on a

discontinuous sucrose density gradient fractionation can separate membrane fractions based upon their buoyancy (cholesterol content). Some groups use detergents such as Triton-X, as caveolae fractions are thought to be detergent-resistant and this removes the need for sonication, however others have seen disruptions in caveolae-associated proteins using detergent (Yao et al., 2009). Sucrose density gradient fractionation allows the study of protein distribution in the membrane and how this changes with disease. The other is through cholesterol depletions by methyl-beta-cyclodextrin (MBCD) (Ilangumaran and Hoessli, 1998), and has shown to markedly reduce the number of caveolae in the cardiac myocyte (Kozera et al., 2009). Employing this approach has revealed redistribution of multiple caveolar proteins in cardiac myocytes and consequent changes in β_2AR signalling (MacDougall et al., 2012; Wypijewski et al., 2015). The use of a CSD peptide, which is a complementary sequence for the CSD and completes for binding on this site, has been used to complement cholesterol-depletion methods (MacDougall et al., 2012).

1.8. Aims of the study

This study aims to test the hypothesis that in heart failure there are changes to an array of caveolar proteins/caveole which have an effect on β-AR signalling. There are isolated reports of remodelling of caveolae and caveolar proteins in the failing heart which have also been linked with changes in β-AR signalling within the heart. However Cav 3 has been the main focus of all previous studies linking changes in caveolae/caveolar proteins with changes in β-AR signalling. To date caveolar and cavin protein changes have not been studied together in relation to β-AR signalling in any animal model of heart failure. Here we aim to test the hypothesis by using two models of LV and RV heart failure with the specific study aims being:

- Characterising the LV heart failure model, this has already been done in the RV model, by measuring hemodynamic changes and remodelling of the failing heart

- Assessing the impact of heart failure on the β-AR function by measuring isolated cardiac myocyte and multicellular preparations response to selective β_1AR and β_2AR stimulation in isolated cardiac myocytes and multicellular preparations

- Assessing the impact of heart failure on the expression of the caveolar and β-AR signalling proteins within the myocyte and their distribution across the membrane

- To determine the relative importance of Cav 1 and Cav 3 expression in the cardiac myocyte. One by testing how Cav 1 effects the membrane distribution of other caveolar and β-AR signaling proteins. Then further measuring protein levels of caveolar proteins in a quantitative manner.

Collating these data could help improve our knowledge of caveolae and the changes to the caveolar proteins in heart failure and present possible implications and links with aberrant β-AR signalling within the failing heart.

Chapter 2. Methods

2.1. Heart Failure Models:

All UK based animal experiments were carried out in accordance with the Animal (scientific procedures) EU **Directive 2010/63/EU** and conformed to the Guiding Principles in the Care and Use of Animals with UK Home Office and local ethical approval. All animal experiments in New Zealand were carried out in accordance with the Animal Welfare Act 1999 and were approved by the University of Auckland Animal Ethics Committee (AEC 1232). Animals were housed in 50% humidity with a 12h light/dark cycle.

2.1.1. Left Ventricular failure model

Left ventricular (LV) failure was induced by banding of the transverse limb of the arc of the aorta (AB), performed by Dr Sarah Calaghan and Prof Jim Deuchars. Male Wistar rats, bred by the University of Leeds, target weight 80 ± 20 g were anaesthetised in a chamber ventilated with 5% isoflurane (IsoFlo, Abbott Laboratories, IL) mixed with medical O_2. Animals were transferred to a sterile surgical table and maintained under anaesthesia on a ventilator ~3-5% isoflurane. Partial thoracotomy (2 or 3 ribs) was performed and the thymus tissue around the aorta was cleared with blunt dissection. Initially, silk suture was used to apply constriction around the aorta at a set gauge (silk suture applied around a 23 gauge needle (O.D 0.6414 mm)). Due to concerns over the appropriate constriction being applied and the variability in initial weights of the animals on the day of surgery, a titanium hemoclip (Weck) was later adopted to apply constriction around the aorta which varied slightly depending on animal weight (for animals <85 g, the internal diameter of clip was 0.6 mm, whereas for animals >85 g clip size was increased to ≈0.7 mm). Constriction was placed after the innominate artery of the aorta. Ribs, muscle and skin were sutured separately. Sham animals underwent the same surgery minus clip/silk suture. An intra-muscular injection of an analgesic agent (buprenorphine, 0.03mL of 0.3 mg/mL solution) was injected post-surgery. Animals were checked 3-4 h later for signs of pain, if needed an additional injection of analgesia was given. Animals were allowed to recover in heated recovery chamber before being singly housed for one week, and then housed in groups of 3-4 animals per cage. Animals were monitored and weighed weekly for any sign of weight loss or distress. Progression of heart failure was assessed by echocardiography examination. At the designated end point, hemodynamic measurements were made.

2.1.2. Right Ventricular failure model

Monocrotaline (MCT) is a plant based pyrrolizidine alkaloid which, when activated by the liver (Kasahara et al., 1997), forms dehydro-MCT in a P450 dependent reaction. Dehydro-MCT is unstable in aqueous medium and a lysine modification occurs to the dehydro-MCT modified protein (Li et al., 2016), which is suggested to be the hepato and pulmonary toxic component. Exposure of activated MCT leads to vascular injury, via endothelial hyperplasia, thickening of the atrial medial leading to pulmonary artery hypertension (Huxtable, 1990). Male Wistar rats target weight 200 ± 20 g bred at the University of Leeds received an intra-peritoneal injection of 60 mL/kg MCT. Fresh MCT solution was prepared on the day of injection by dissolving 68 mg of MCT (Sigma, UK) in 0.5mL of 1M HCl before adding 140 mM NaCl and adjusting the pH to 7.4 to give a final concentration of 20 mg/mL MCT. Control (CON) rats were injected with an equivalent volume of saline solution (140 mM NaCl). Animals were housed 2-3 per cage. Rats were weighed weekly until day 21 post-injection, then daily until rapid weight loss was observed (10 g loss in a single day or a total loss of 20 g)(designated end point).

2.2. Metoprolol dosing

Chronic dosing with metoprolol has previously been shown to improve survival of MCT injected animals (Fowler and 2016). Animals were trained to receive a hand fed oral daily dose of Ribena® solution. From 15 days post MCT/saline injection animals were divided into three groups, a subset of MCT animals plus all of the CON animals received a daily dose (8 mL/kg) of placebo solution (0.3 M Sucrose, 20% Ribena® and water). The remaining MCT animals (MCT+BB) received a daily dose (8 mL/kg) of β-blocker solution (metoprolol 4.68 mM in placebo solution). Dosing was given 2 h before the commencement of the dark cycle. CON and MCT+BB animals were taken ± 3 days around the median day that the MCT animals went into failure (day 23 post MCT injection for the Leeds cohort of animals).

Short axis

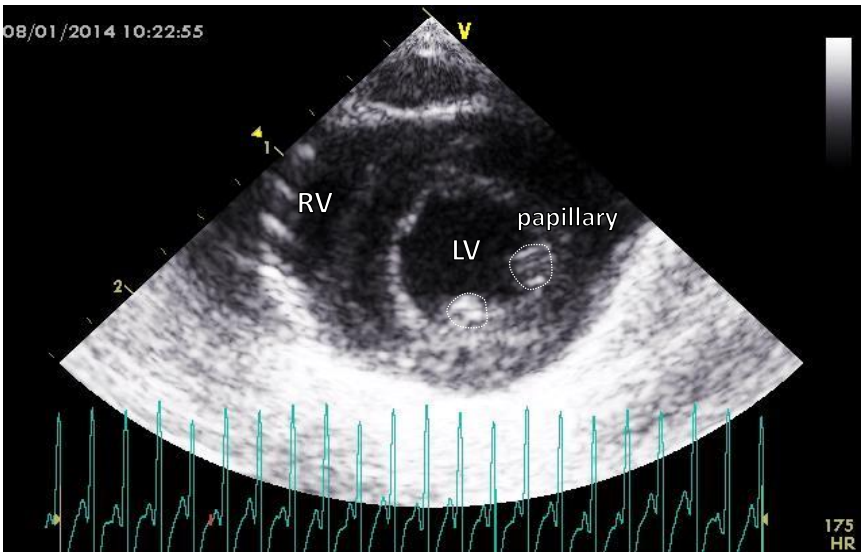

Long axis

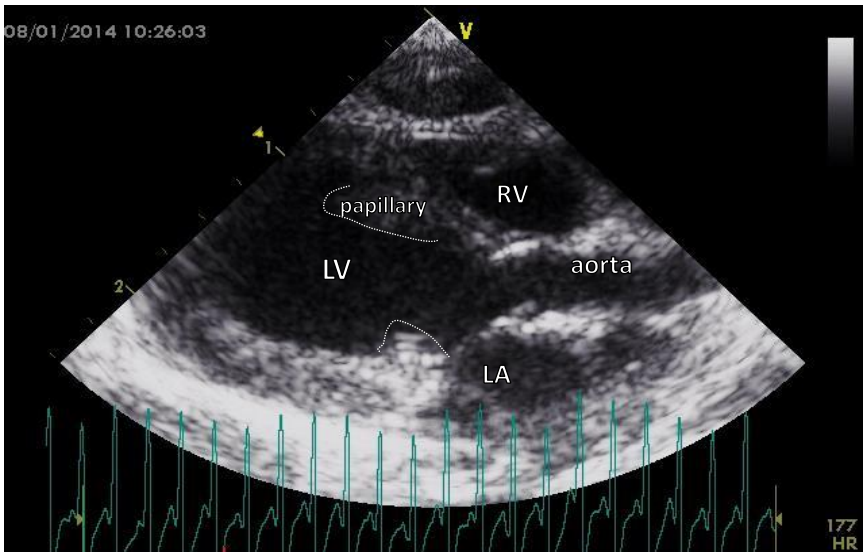

Figure 2-1 Short axis and long axis echocardiography image in AB animal

Short axis echocardiography images from AB animal (Surgery date – 29/08/13) taken 19 weeks post-surgery. In the short axis right (RV) and left ventricular (LV) chambers are highlighted as well as the papillary muscles. In the long axis the apex of the heart is off the left hand side of the display. The aorta and left atria (LA) can also be captured within this view. ECG recording is displayed at the bottom of the image as well as heart rate (HR) in the bottom right hand corner. Time and date of echocardiographic examination is displayed in the top left hand corner. Index down the left had side of the view screen is depth of echocardiography examination in cm.

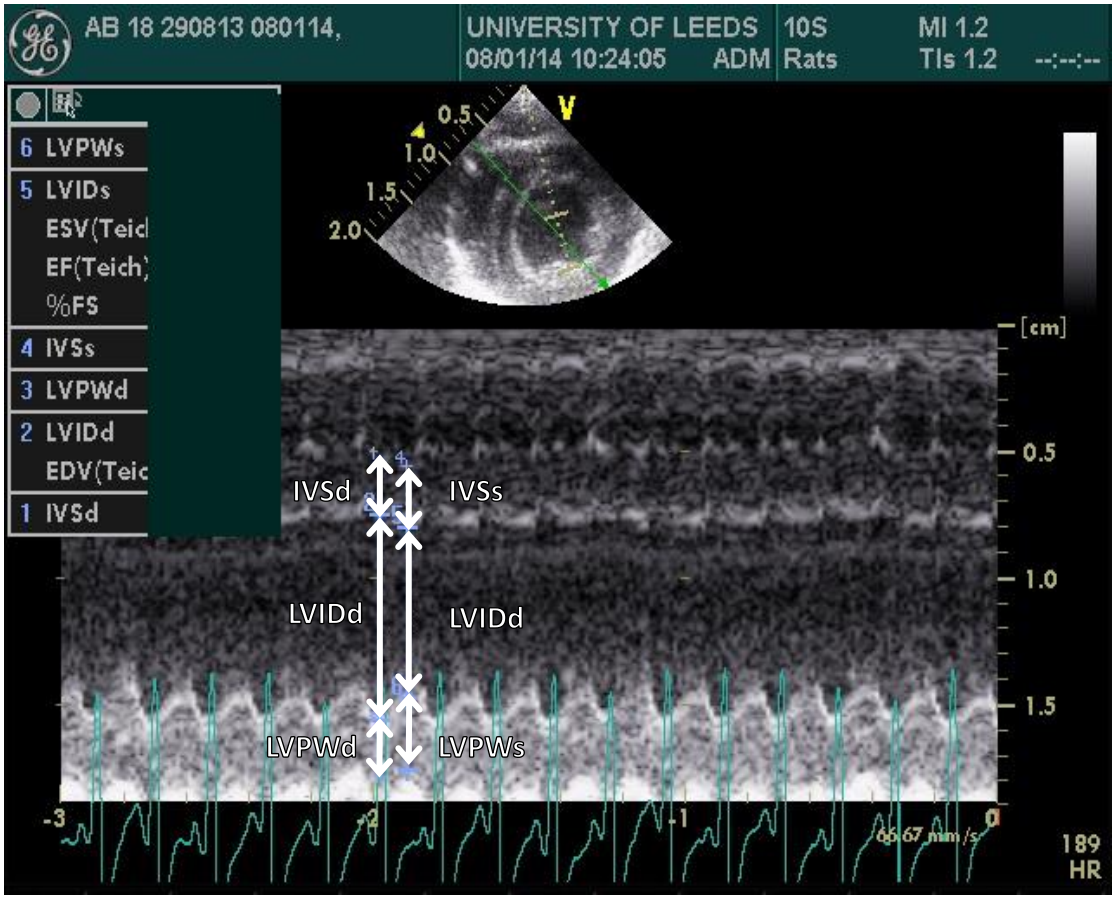

Figure 2-2 M-mode images of echocardiography examination of AB and sham banded animals

M-mode imaged in the parasternal short axis view from AB animal (Surgery date – 08/11/13) taken 19 weeks post-surgery. M-mode is taken running between the two papillary muscles and the interventricular septum (IVS). Left ventricle internal diameter (LVIS), left ventricle posterior wall (LVPW) measurements are also measured in systole and diastole (s/d). ECG recording is displayed at the bottom of the image and heart rate (HR) is in the bottom right hand corner. Time and date of echocardiography examination is displayed in the top left hand corner. Index down the right hand side of M-mode view screen is depth of echocardiography examination in cm. AB animals show reduced contractility.

2.3. In-vivo functional measurements

2.3.1. Echocardiography

A proportion of aortic banded (AB) and sham operated (Sham) animals underwent non-invasive echocardiography examinations to monitor heart function. A GE Vivid7 ultrasound machine with a 10S probe was used to perform the examinations. Rats were anesthetised and maintained under light anaesthesia (1.5-2% isoflurane), placed in a supine position on top of a heated mat with chest hair removed. A small amount of ultrasound gel (Cardiacare, Essex, UK) was applied to the chest wall to aid imaging. ECG recordings were taken simultaneously while echocardiography images were acquired at 11Hz in the parasternal short-axis of the heart at the level of the papillary muscles as well as long-axis video clips, representative images (Figure 2-1). For AB animals, ejection fraction (EF) was calculated using the inbuilt Vivid 7 computer's software (to determine if the ejection fraction had fallen below the 45% threshold set). Animals were taken immediately for hemodynamic measurements if ejection fraction was below the threshold. Images were analyzed offline for measurement of LV internal diameter in systole and diastole to calculate fractional area changed. In M-mode (motion mode) images inter-ventricular septum (IVS), LV posterior wall (LVPW) and LV internal diameter (LVID) were all measured in systole and diastole, a representative image is shown in Figure 2-2. From these measurements, EF and fractional shortening ([LVIDd - LVIDs/LVISd]*100 where LVID is measured as the left ventricular internal dimensions at the end of diastole and systole respectively) were calculated. Ejection fraction is calculated using the Teichholz calculation (Teichholz et al., 1976) (volume = [7.0/2.4 + internal dimension(D)] (D^3), and a squared calculation (((LVIDd^2 - LVIDs^2)/LVID^2)*100). Both these calculation have limitations due to assumptions of the left ventricle geometry and volume and heterogeneity of ventricular contractions (Wandt et al., 1999). MCT and saline animals have already been well characterized by echocardiography examination (Benoist et al., 2012), and more recently, MCT animals treated with β-blockers have been similarly characterised (Fowler and 2016). (Fowler et al., 2016 [in submission])

2.3.2. Hemodynamic measurements

Most AB and Sham animals underwent in vivo hemodynamic measurements at the designated end stage. After echocardiography examinations, animals were transferred to a heated surgical table where rats were mechanically ventilated and maintained under anaesthesia at 1.5% isoflurane mixed with medical O_2. Surgery was performed by Dr Mark Drinkhill. The chest wall was opened and a Millar conductance catheter (SPR-869, Millar

Instruments, TX) passed through the left ventricular free wall around the apex of the heart. Volume and pressure measurements of the left ventricle were recorded simultaneously. Volume was calculated using intravenous injections of a known volume of saline and corrected to the blood volume conductance measured in a cuvette (P/N 910-1048, Millar Instruments, TX) which was taken at the end of the experiment (Pacher et al., 2008). Once readings had settled to a steady state, pressure-volume (PV) loop relationships were recorded. End-diastolic pressure-volume relationships (ESPV) were measured by transient occlusions of the inferior vena cava in the abdominal region.

2.4. Cell Isolation

At the designated end point the right ventricular failure animals were killed by cranial stunning and cervical dislocation and hearts quickly extracted and mounted on a Langendorff apparatus (Figure 2-3). The aorta was cannulated and the coronary circulation was cleared through retrograde perfusion with isolation solution (I.S.) ((mM) 130 NaCl, 5.4 KCl, 1.4, $MgCl_2 \cdot 6H_20$, 0.4 NaH_2PO_4, 5 HEPES, 10 creatine, 20 taurine, 10 glucose pH 7.4) with calcium added (750 μM $CaCl_2$) at a constant flow rate of 7 mL/min. The heart was sequentially perfused with I.S. containing 0.1 mM EGTA for 4 min then a collagenase solution (3.2 mg protease (type XIV, Sigma, UK) and 40 mg collagenase type 2 (Worthington Biochemical, USA) in 40 mL I.S) for 7-8 min. The RV and LV were then dissected from the hearts and weighed before shaking in protease solution in conical flasks by a rotary shaker held in a 37 ^oC water bath. All solutions were continually oxygenated and heated to 37 ^oC. Cells were collected by straining tissue in collagenase solution through a gauze (200 μm^2 nylon mesh); myocytes collected from this centrifuged (50 x g for 40 s) supernatant removed and re-suspended in I.S. Isolated cells were kept in I.S. with 750 μM Ca^{2+} at room temperature until needed for experiments.

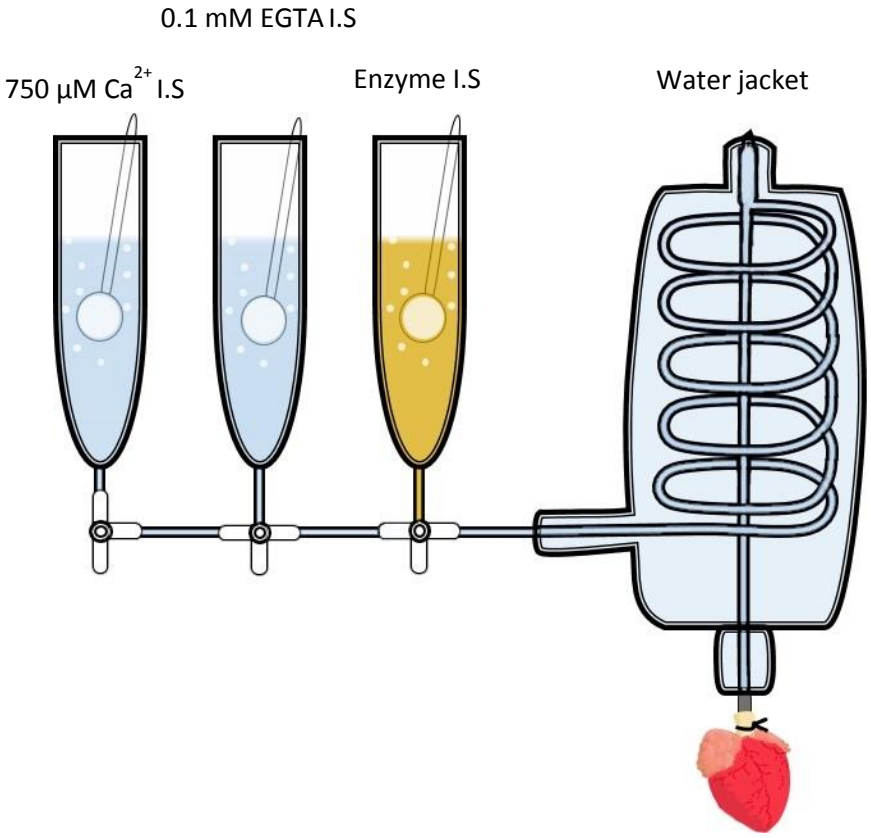

Figure 2-3 Langendorff system used for cardiac myocyte isolation

The aorta was cannulated and a silk suture tied around to secure it to the metal cannula. Hearts were retrogradely perfused with 750 µM Ca^{2+} isolation solution (I.S) (flow rate 7 mL/min) and the coronary circulation cleared before switching to 0.1 mM EGTA I.S for 4 min. The heart was then perfused with enzyme I.S which was recirculated for 7-8 min. All solutions were bubbled with 100% O_2 and heated in a water jacket to 37 ^{o}C

2.5. Trabeculae Dissection

Animals were decapitated following anaesthesia by isoflurane (5% medical O_2), hearts were quickly removed, weighed and placed into chilled Muscle Tyrode solution ((mM) 141.8 NaCl, 74.56 KCl, 1.2 $MgSO_4.H_2O$, 1.2 Na_2HPO_4, 10 HEPES pH 7.4) before transfer to the dissection chamber. The aorta was then cannulated while perfusing with Muscle Tyrode with (mM): 20 butanedione monoxime (BDM), 10 glucose and 0.25 Ca^{2+} bubbled with O_2. Free running trabeculae were dissected and mounted in a chamber connected to a force transducer as previously described (Kaur et al., 2016). In brief, trabeculae were transferred to a Perspex bath mounted on the stage of an inverted microscope (Nikon Diaphot 300, Japan) and perfused with Muscle Tyrode solution containing 10 mM glucose and 0.5 mM Ca^{2+} bubbled with O_2. One end of the trabeculae was cradled in a wire hook of the force transducer while the other end was held in a nylon snare extending from the end of a stainless steel tube attached to a micromanipulator. Trabeculae were field stimulated at 0.2 Hz at room temperature until stable contractions were observed, upon which the [Ca^{2+}] of the Tyrode's solution was increased to 1 mM before loading with Fura-2/AM (10 μmol/L; Teflabs, TX, USA) in 10 mL Tyrode at room temperature as previously described (Ward et al., 2003) for 2 h.

2.6. Selective β-adrenergic receptor stimulation

2.6.1. Pharmacological agents used

Selective β_1AR stimulation was achieved with the β_1AR agonist isoproterenol bitratrate (ISO) (Sigma I2760) in combination with ICI 118,551 (Sigma I127), a selective β_2AR antagonist. Various concentrations of ISO with ICI 118,551 (ICI) were made in Cell Tyrode solution ((mM) 136.9 NaCl, 5.4 KCl, 0.33 $NaH_2PO_4{\cdot}H_2O$, 0.5 $MgCl_2{\cdot}H_2O$, 5 HEPES, 5.6 Glucose, 1 $CaCl_2$, pH7.4). Selective β_2AR stimulation was achieved with the β_2AR agonist zinterol (Tocris 1051) in combination with CGP-20712A (Sigma C321), a selective β_1AR antagonist. Zinterol K_i for β_2AR (460 nM) (Bylund and Snyder, 1976). Concentrations of antagonists were chosen on the basis of previous use in the literature and the rat K_i values for β_1AR and β_2AR in the presence of the selective antagonist; ICI 118,551 K_i for β_2AR (1.78 nM) and K_i for β_1AR (194.98 nM) (Tsuchihashi et al., 1990), CGP 20712A K_i for β_1AR (1.3 nM) and K_i for β_2AR (600 nM) (Cerbai et al., 1995). Antagonist concentrations used: CGP-20712A (300 nM), ICI 118,551 (100 nM)

2.6.2. Contraction and Ca^{2+} recordings in isolated myocytes

Cell shortening and $[Ca^{2+}]_i$ transients were recorded simultaneously using digital edge-detection software (IonOptix, MA, USA) and an OptoScan monochromator [illuminating cells with 10 ms pulses of 340 and 380 nm light (Cairn Research, UK)]. Isolated cardiac myocytes from the right ventricle were field stimulated at 1 Hz after loading with the fluorescent Ca^{2+} indicator Fure-2 AM (F1221, Invitrogen, USA). Fura-2 has been a popular dye since it was first utilized (Grynkiewicz et al., 1985; Tsien et al., 1985) to study calcium content within cells including cardiomyocytes (Xu et al., 1997; Wier et al., 1987). The Fura acetoxymethyl (AM) attachment allows the dye to cross the cell membrane and once in the cells cytosolic esterases cleave the ester group forming an impermeable dye within the cell. Isolated cardiac myocytes (1-2 mL) were incubated with 1 μM FURA-2AM/ mL Cell Tyrode for 10 min before centrifugation (40 s, 500 rpm), removal of supernatant and re-suspension and incubation in fresh Cell Tyrode for 30 min to allow de-esterification. Cells were individually perfused using a solution switcher (MPRE8, CellMicro Controls, USA) containing different concentrations of ISO (Figure 2-4). All baseline recordings were made with selective antagonist (in the absence of antagonist) in Cell Tyrode. Bath solution was continually perfused with selective antagonist in Cell Tyrode. Both bath (by a HPRE2 Cell MicroControls, USA) and switcher solutions (inbuilt) were heated to 37 ^{o}C. Flow rate and rapid solution switching within the solution switcher were controlled by a channel flow controller (cFlow, Cell MicroControls, USA)

2.6.3. Force and Ca^{2+} recordings in trabeculae

Trabeculae force and $[Ca^{2+}]_i$ transients within a restricted window of approximately 300 μm^2 were recorded simultaneously using a spectrophotometry system (Cairn Research, UK) and a micro force sensor (AE801, Sensor One, USA). Base line recordings were taken when trabeculae were stretched to L.max (the length of the muscle at which developed tension was maximum) and field stimulated at 1 Hz (model D100; Digitimer, UK). Solutions were heated to 37 ^{o}C and recirculated.

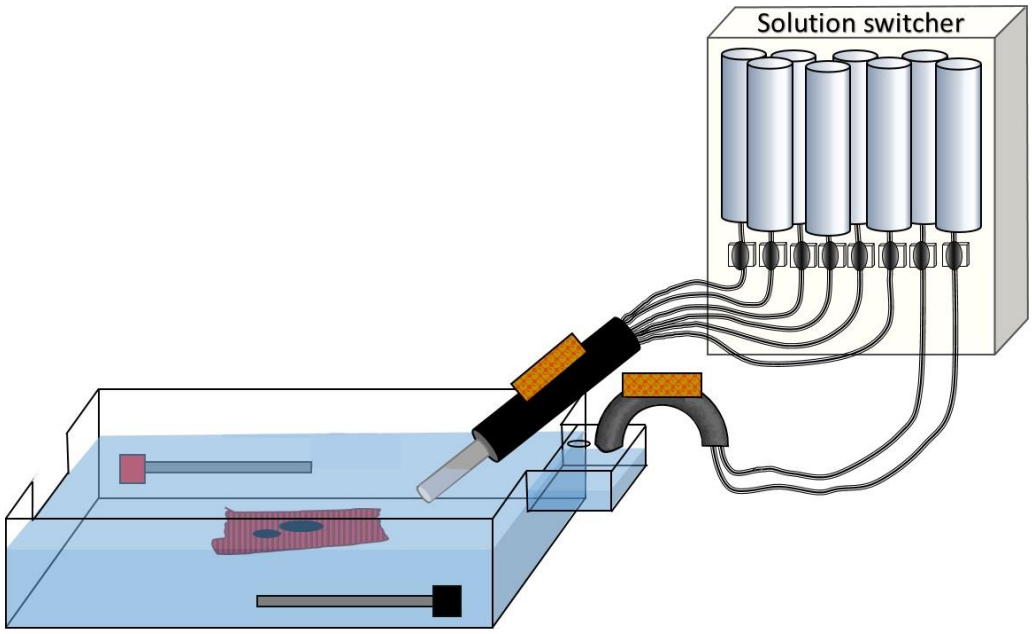

Figure 2-4 Solution switcher

Isolated cardiac myocytes were placed in the bath and allowed to settle on the glass cover slip before perfusion of the bath and field stimulation (at 1 Hz) was commenced. The rapid solution switcher mounted on a micromanipulator was then placed up-stream from the chosen cardiac myocyte and then the solution switcher turned on. This enabled rapid solution changing for individual cells. Cell shortening and $[Ca^{2+}]_i$ were simultaneously recorded. Both bath and solution switcher solutions were heated to 37^{o}C

2.7. Histology

2.7.1. Wax embedding sections

Tissue was wax-embedded to allow for sectioning and histological staining. Before wax embedding tissue samples were assigned a random 3 digit code generated on Excel, which was used to blind the samples. Un-blinding was not performed until the end of the image analysis. Longitudinal sections of ventricular tissue, approximately 100 mg in weight, were taken and placed in 4% PFA (PBS) solution overnight. Tissue was then dehydrated in an alcohol series of 25%, 50%, 70% ethanol (EthOH) in ultrapure water (MilliQ), 30 min in each, and stored in 70% EthOH at 4 ^{o}C until all the tissue was collected. The Thermo Citadel 2000 automatic processor was operated by Tim Lee to embed the tissue in paraffin wax. Wax embedded tissue was sectioned on a microtone at 10 μm thickness (American optical Spencer 820 microtome), floated on a heated water bath and then mounted on a coated glass cover slide (VWR polysine coated slices 48382-117).

2.7.2. Picro-sirius Red staining

Collagen content of the heart was indexed by picro-sirius red staining which is used to identify fibrosis within the heart (Michel et al., 1986; Tanaka et al., 1986). Sirius red stains all types of collagen and picric acid dye stains the myocytes yellow causing a colour contrast and allowing image thresholding and quantification by a light microscope. Sections were immersed in Histoclear 2 x 5 min (National Diagnostics, Atlanta, GA) to deparaffinise the sections and rehydrated in a 100%, 90%, 70% and 50% EtOH series, 2 min in each. Slides were then stained in 0.1% picrosirius solution (Direct Red 80, Sigma-Aldrich, Pool, UK, in saturated picric acid pH 2.15) for 90 min. Excess stain was then removed by washing with a 0.01M HCl solution and dehydrated in the same EtOH series. To clear the sections, slides were placed into Histoclear for 10 min before a drop of DPX (distyrene plasticiser (butyl, pfthalate, styrene), xylene; Sigma UK) mounting media was placed onto each section and a glass cover slip placed on top. Slides were left to dry and fix at room temperature overnight.

Images were taken using an upright Nikon Eclipse E600 light microscope at 20x magnification. Multiple images were taken from multiple sections for each animal. Only cross-sectional images of cardiac myocytes were used in the analysis; images with large capillaries within the frame were excluded. ImageJ (National Institute of Health, Bethesda, MA) was used for quantification by creating a Lab stack (Luminance (L) and two colour-opponent dimensions (a, b)) and then manually setting a threshold for red (collagen) and

blue (total cell and collagen staining minus background). Thresholds varied slightly from image to image depending on background staining.

2.8. Sample preparation

2.8.1. Homogenised tissue for protein analysis

For measurement of protein expression in myocardial homogenates, ventricular muscle was homogenised (Ultra-Turrax T8; Ika) 6 x 20 s each at full power (30000 rps) in Laemmli Sample buffer (63.5 mM Tris [pH 6.8], 10% glycerol, 2%SDS, 1x protease (Roche Applied Science) and phosphatase (Thermo Scientific Pierce) inhibitor cocktails. For measurement of protein distribution in different membrane fractions ventricular muscle was homogenised 6 x 20 s in detergent free buffer (500mM Na_2CO_3 (pH 11), 1x protease (Roche Applied Science) and phosphatase (Thermo Scientific Pierce) inhibitor cocktails. Both samples were stored at -20 ^{o}C until required.

2.8.2. Sucrose density gradient fractionation

Samples in detergent free buffer were thawed to 4 ^{o}C then sonicated (Vibra Cell; Sonics) 6 times each for 10 s at full power, kept on ice at all times. Samples were then centrifuged for 30 min at 5000 g, 4 ^{o}C, and 2 mL of supernatant mixed with 2 mL of 90% sucrose in MES-buffered saline (25 mM MES, 150 mM NaCl, 2mM EDTA, pH 6.5) to form a 45% sucrose solution. To create a discontinuous sucrose gradient 4 mL of 35% and ~4 mL 5% sucrose solution (MES-buffer saline with 250 mM Na_2CO_3) was layered on top. Sucrose gradients were centrifuged at 39000 rpm (Beckman SW40Ti rotor) at 4 ^{o}C for 17 h. After centrifugation 12 fractions were collected starting from the top using a Gilson pipette (p1000) (1 mL each), then frozen at -20 ^{o}C until required (Calaghan et al., 2008). Fractions 9-12 contain non lipid rich membrane fractions and cytosolic proteins are designated the heavy fractions. These fractions are considered to be fairly homogenous, so equal portions were loaded in a mixed sample for analysis with SDS-PAGE and Western blotting.

2.9. Cholesterol and Protein analysis

2.9.1. Amplex® red assay

Cholesterol content was measured by the Amplex® Red Cholesterol Assay Kit (Invitrogen, A12216). Fractionated samples from the sucrose gradient fractionation were diluted in 1 x reaction buffer (5 x reaction buffer (20 mL of 0.5 M potassium phosphate pH 7.4, 0.25 M NaCl, 25 mM cholic acid, 0.5% Triton X-100) diluted in MilliQ water) before loading duplicates of 50 µL into a 96 well plate. Reference standard (2 mg/mL cholesterol reference standard) was diluted in 1 X reaction buffer to give a range of 2-20 µL/mL cholesterol. Working solution was prepared and 50 µL added to each well (1.5% Amplex Red (dissolved in DMSO to make 20 mM stock), 1% horseradish peroxidase (HRP) (200 U/mL dissolved in 1 X reaction buffer), 1% cholesterol oxidase (200 U/mL cholesterol oxidase, from Streptomyces dissolved in 1 X reaction buffer), 0.1% cholesterol esterase (200 U/mL cholesterol esterase, from Pseudomonas dissolved in 1 X reaction buffer) and 96.4% 1 X reaction buffer. The plate was then protected from light and transferred to an incubator heated to 37 ^{o}C for 30 min. Fluorescence excitation was at 590 nm and emission measured at 545 nm with 12 nm bandwidth.

2.9.2. De-glycosylation by PNG-ase F

N-linked glycosylation is an asparagine-linked carbohydrate post-translational modification of a protein which aids in protein migration to lipid rich membranes. Peptide-*N*-Glycosidase F (PNG-ase F) can be used to test for N-linked glycosylation as this enzyme cleaves between the innermost GlcNAc and asparagine residue of the oligosaccharides from N-linked glycoproteins (Maley et al., 1989). This reduces the molecular weight of the protein, the reduction in molecular weight can then be detected by SDS-PAGE. PNGase-F was supplied by New England Biolabs (P0704S) and the denaturing protocol used. Sample containing glycoprotein (5-9 µL) was mixed with 1 µL Glycoprotein Denaturing Buffer (10X)(5% SDS, 0.4 M DTT) and H_2O when necessary to make up a reaction volume of 10 µL. Samples were then denatured by heating to 95^{o}C for 10 min before chilling samples on ice and centrifuging. The final reaction volume was then made up to 20 µl with 2 µL GlycoBuffer 2 (x 10) (0.5 M Na_2PO_4 pH 7.5), 2 µL 10% NP-40 and 6 µL milQ. H_20. 1 µL PNG-ase F (PNG-ase F purified from *Flavobacterium meningoseticum*, stored in 50 mM NaCl, 20 mL Tris-HCL pH 7.5, 5 mM Na_2EDTA and 50% glycerol) was then gently mixed into the sample and placed in an incubator held at 37 ^{o}C for 1 h. The enzyme reaction was terminated by addition of 5

x Laemmli sample buffer or heating sample to 75 °C for 5 min. Samples were analysed by SDS-PAGE.

2.9.3. Western blotting

2.9.3.1. Bicinchonincic acid (BCA) assay

A bicinchonincis (BCA) assay was used to determine total protein concentration. The BCA protein assay has the advantage over other protein assays as it can detect a wide range of protein concentrations and sample solution can contain up to 5% detergent. The BCA assay relies on a two reaction process, first the biuret reaction in which peptides containing three or more amino acid residues reduce the copper ion from cupric to cuprous form, then a chelation reaction of two BCA molecules with one cuprous ion to form the purple colour. 2-3 dilutions of each sample were made before loading duplicates of 10 µL into a 96 well plate along with 10 µL of bovine serum albumin (BSA) standards (2-10 µg/µL) used to construct a standard curve. 80 µL of a solution containing BCA (Sigma-Aldrich BCA1-1KT) and Cu_2SO_3 in a 50:1 ratio was then added to every well before placing the plate at 37 °C to incubate for 30 min. Absorbance at 570 nm was measured on a Varisoskan plate reader (Thermo Scientific) and this was used to calculate average protein concentrations by reference to the BSA standard curve. This allowed equal total protein loading of samples in Western blotting.

2.9.3.2. SDS-PAGE

Laemmli Sample buffer (62.5 mM Tris [pH 6.8], 10% glycerol, 2% SDS, 5% β-mercaptoethanol) was added to ventricular homogenates collected from the sucrose gradient fractionation, and 5% β-mercaptoethanol was added to myocardial samples homogenised in sampler buffer, before heating to 95 °C for 5 min. Proteins were separated by electrophoresis in SDS-PAGE gels (6-12% acrylamide) in SDS-PAGE running buffer (0.01% SDS in 25 mM TRIS, 192 mM glycine) and transferred to a polyvinylidene difluoride (PVDF) membrane by semi-dry blotting for 85 min at 60 mA per membrane (target protein below 100 kDa: 20% methanol, 0.0375% SDS in 48 mM TRIS, 39 mM glycine) (target protein above 100 kDa: 0.0375% SDS in 48 mM TRIS, 39 mM glycine). Methanol has been shown to impede the transfer of large molecular weight proteins (Beisiegel, 1986). Non-specific binding sites were then blocked in milk-TRIS buffer (5% no-fat dried milk powder, 0.1% Tween-20 in 50 mM TRIS/Hl, 150 mM NaCl) before staining with specific antibodies. Antibodies used listed in Table 2-1. Chemiluminescence (Amersham ECL Prime Western Blotting Detection Reagent, GE Healthcare, UK was used for low abundance proteins and

Thermo Scientific™ SuperSignal™ West Pico Chemiluminescent Substrate used for high abundance proteins) was used to detect secondary antibodies before either exposing and developing signals onto Fluorotrans 0.2 µm film (Pall international) or imaging signal intensity (Syngene G:BOX Chemi XT4). Band intensities were then quantified (Aida Image Analyzer). GAPDH was used as a normaliser, no difference in signal expression was observed between samples.

2.9.3.1. Phos-tag gel

Phos-tag™ Acrylamide reagent developed by the Department of Functional Molecular Science at Hiroshima University is used to study the phosphorylation of proteins for which phospho-specific antibodies are not available. Phosphorylation is a crucial post-translational modification which regulates protein function, localisation and targeting. Phos-tag™ Acrylamide provides a phosphate affinity which slows the migration of phosphorylated proteins during electrophoresis, which can be detected with Western blotting. Phos-tag™ reagent is added to SDS-PAGE gels to create a final concentration between 30-90 µM Phos-tag, in addition to equal concentrations of $MnCl_2$. The concentrations of all other components in the SDS-PAGE gel and running buffer remain the same. Gels were run slowly on ice before SDS-PAGE gel were washed 2x 10 min in transfer buffer (as stated above) with the addition of 2 mM EDTA and subsequently washed 2 x 10 min in transfer buffer without EDTA. The rest of the Western blot protocol continues as stated above with the transfer time being run twice as long as the usual gels.

2.10. Statistical analysis

Statistical analysis was performed on Prism 6/7 (Graphpad, La Jolla, CA). All data are expressed as mean ± S.E.M or of *n* = determinations (number of animal or number of cells). Normality was tested using Prism 6/7 normality tests (D'Agostino-Pearson omnibus or Shapiro-Wilk).

Significant differences between two independent groups were assessed by unpaired Student's t-test if data were normally distributed. Where data were non-normal Mann-Whitney U tests were used. If three or more independent groups were being tested for statistical differences a one-way ANOVA with Tukey's multiple comparison tests was used assuming that the data was normal. When data was non-normal a Kruskal-Wallis test was

used to compare more than two independent groups. Where multiple measurements were made and compared between different groups, a two-way repeated measure ANOVA was used.

To measure if there was a correlation between two variables the correlation coefficient with confidence intervals were calculated. A Pearson's test was used if the data were normal and a Spearman's rank test was used if data were non-normal.

To test for significant effects in binomial data a Chi-squared test was used to calculate expected values and determine if a significant difference was observed between the expected and observed values between one or more groups. For individual variations between expected and observed adjusted residual values were calculated with Bonferroni adjustment to test for individual statistical variation.

Where multiple measurements were taken over time, linear regression was calculated and line equation tested for significant deviation from a zero gradient.

Statistical significance is considered at $P<0.05$.

Antibody	Company, Cat #	Dilution	Species	MW (kDa)
AC	Santa Cruz 590	1:500	Rabbit	132
β_1AR	Santa Cruz 567	1:500	Rabbit	67
β_2AR	Alomone AAR-016	1:1000	Rabbit	55
BIN1	Santa Crus 30099	1:500	Rabbit	100, 75
Caspase 3	Cell signalling 9665	1:1000	Rabbit	17, 19, 35
Cav 1	BD Bioscience 610406	1:1000	Mouse	21-24
Cav 3	BD Bioscience 610421	1:5000	Mouse	18
Cavin 1	Proteintech 18892-1	1:4000	Rabbit	60
Cavin 4	Sigma HPA 021 021	1:2000	Rabbit	55
eNOS	BD Bioscience 610297	1:1000	Mouse	140
$G\alpha_i2$	Santa Cruz 13534	1:500	Mouse	41
$G\alpha_i3$	Santa Cruz 262	1:500	Rabbit	45
GAPDH	Sigma-Aldrich G9545	1:100000	Rabbit	37
GRK2	Santa Cruz 8329	1:500	Rabbit	75
JP 2	Santa Cruz 5131	1:500	Goat	90

Table 2-1 Table of antibodies used in Western blotting

The supplier, catalogue number, dilution used and predicted molecular weight (MW) band is given.

Chapter 3. Characterisation of aortic banding model leading to left ventricular failure

3.1. Introduction

According to the NICE guidelines around 0.9 million people are living with heart failure in the UK today (NICE, 2010). In the US, ~6 million are people living with heart failure and 1 in 5 adults over the age of 40 is likely to develop heart failure in their lifetime (NICE, 2010; Mozaffarian et al., 2016) . Failure of the left ventricle (LV) is most common with either systolic or diastolic dysfunction of the LV resulting in a reduced cardiac output to the body. In response to an initial insult on the heart, such as hypertension, the compensatory mechanism of the body is to increase sympathetic drive to the heart. Chronic sympathetic stimulation results in the desensitisation of the β-adrenergic receptors (β-AR) and further cardiac dysfunction (Steinfath et al., 1992). To study the β-AR and caveolar protein changes in LV heart failure a model with clinical relevance must first be established.

A rat model of aortic banding was chosen to determine these molecular changes in end stage heart failure. Aortic banding in rat is a slow progressive model of heart failure, which is a closer representation of clinical heart failure in humans compared to other faster onset models (Patten and Hall-Porter, 2009). A rat model is advantageous over a mouse model because of the larger mass of tissue, allowing for multiple different aspects to be studied (protein expression and membrane distribution, fibrosis etc.), but it is still inexpensive compared to larger animal models. This aortic banding (AB) model of heart failure was new to the University of Leeds so characterisation of the model was needed. It was imperative to be sure that end stage heart failure was reached before further studying the tissue at the molecular level. Previous studies have been criticised for not properly characterising heart failure within the model and only relying on single measurements to assume clinical heart failure (Houser et al., 2012; Patten and Hall-Porter, 2009).

Banding of the transverse limb of the arc of the aorta is used frequently to study multiple and varied aspects of heart failure (Miyamoto et al., 2000; Feldman et al., 1993; Litwin et al., 1995). Previous models of aortic banding have used echocardiography-Doppler measurements to assess LV function and progression of heart failure (Litwin et al., 1995; Miyamoto et al., 2000). In our model, echocardiography was used periodically to measure

the progression of heart failure, along with weekly body weight measurements to monitor any sudden changes in weight. In-vivo heamodynamic pressure volume loop measurements were taken at the end point to further analyses change in LV function. Dissected organ weights as well as fibrosis measurements were used to further characterise this heart failure model and give clinical relevance. Fibrosis is often present in human heart failure patients causing stiffness of the cardiac muscles (Tanaka et al., 1986), and is another clinical trait which can be measured in small animal models. By measuring a wide array of different parameters we hope to characterise this model of heart failure at Leeds, enabling the model to have clinical relevance.

3.2. Methods

Partial thoracotomy (2-3 ribs) was performed on male Wistar rats 80±20 g (target range) under anaesthesia (3-5% isoflurane) and a constriction (suture/clip) placed around the aorta (detailed in Methods section 2.2.2). Sham animals underwent the same surgery minus the constriction. Rats were then monitored and weights recorded weekly.

Progression of heart failure was monitored by echocardiography examination. ECG recordings were taken simultaneously while echocardiography images were acquired at the parasternal long and short-axis of the heart. Images were then analyzed offline to calculate fractional shortening and ejection fraction (Methods 2.3.1). Ejection fraction below 45% was used to define heart failure. Normal ejection fraction is considered to be > 50% (McMurray et al., 2012).

A proportion of AB animals with an ejection fraction below 45% were taken for hemodynamic measurements and pressure volume loop analysis (Methods 2.3.2). A proportion of Sham animals time matched to the AB also underwent the same procedure. Lung, liver, heart and dissected heart were all weighed post end point, and normalised to total body weight and tibia length. Longitudinal sections of the LV were taken and placed in 4% paraformaldehyde (PFA) in phosphate-buffered saline (PBS) overnight before dehydrating in an alcohol series and being wax-embedded and sectioned (as detailed in Methods section 2.7.2). Picro-sirius red staining was then used to identify collagen. Images were taken on an upright light microscope at 20x magnification. ImageJ was used to quantify images and calculate the percentage collagen staining per image (Methods section 2.7.2).

3.3. Results

3.3.1. Animal grouping

This was a new animal model to the University of Leeds and it became apparent when monitoring the animals with echocardiography that not all of the banded animals would reach the reduced ejection fraction used to define heart failure. The silk suture could have been absorbed within the aorta during growth or the metal clip may have slipped. Not all sutures/clips were found at the end point around the aorta of the banded animals. Feldman et al. 1993 observed, in a model of aortic banding, that 20-weeks post-surgery not all of the banded animals exhibited clinical signs of heart failure, but did present with moderate signs of hypertrophy (Feldman et al., 1993). In the present study, the size of the constriction placed on the aorta varied between animals and appeared to play a role in the severity and progression of heart failure. A few of the clips were kept and using imageJ the internal area (constriction) of the clip was calculated and plotted against weeks post-surgery/heart weight to body weight ratio (Figure 3-1). There was a significant correlation between the constriction placed on the aorta and the relationship between time taken to reach a heart failure phenotype and increased heart weight (R^2=0.9462, P<0.01). In vivo hemodynamic measurements and echocardiography revealed that not all the banded animals reached the cut off threshold of ejection fraction<45%. However in these animals there was an increase in posterior LV wall thickness and heart weight suggesting some degree of remodelling had occurred. Using the heart weight to body weight ratio and ejection fraction data, banded animals were split into two groups: banding with hypertrophy (AB(H)) which had a HW:BW ratio of greater than two standard deviations above the Sham mean and greater than 45% ejection fraction, and banding with end stage heart failure (AB (Fail)) with an ejection fraction below 45%. Out of the 28 animals that underwent aortic banding 9 animals reached an ejection fractions below 45% and 7 animals with ejection fraction above this had a HW:BW ratio which reached the AB(H) group definition. There were also three unexpected deaths which occurred within the first 6 weeks of surgery.

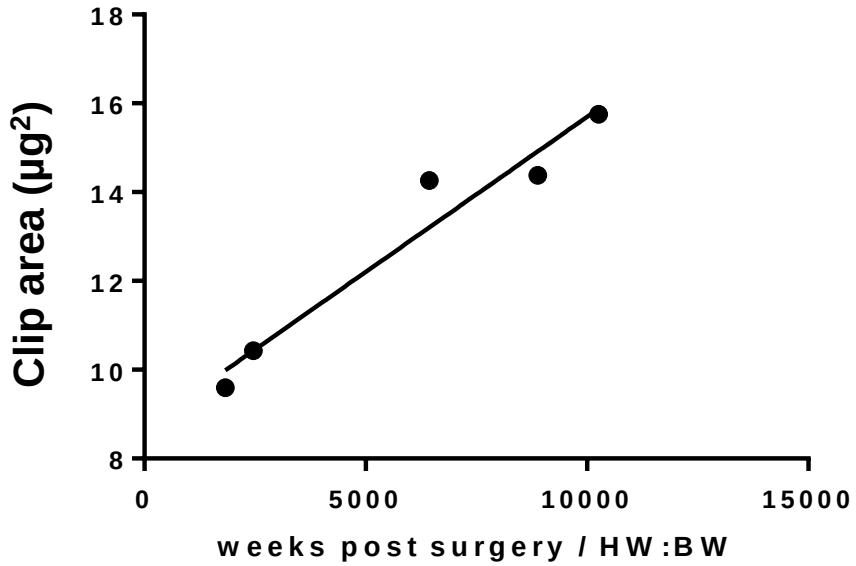

Figure 3-1 Correlation between aortic constriction and weeks post-surgery standardised by heart weight to body weight ratio

Internal area of titanium clip or silk suture was calculated on ImageJ and calibrated by a graticule placed in the same scanned image, which was then plotted against number of weeks post-surgery standardised to heart weight to body weight (HW:BW) . R_2=0.9462

3.3.2. Growth curves

Growth was measured by recording body weight weekly, monitoring for any sudden changes in weight. When animals were split into their retrospective groups based on surgery, ejection fraction and heart weight to body weight ratio, there was no significant difference in weight gain between groups over a 30 week period (Figure 3-2). One group of animals whose surgery was performed on the same day, two AB(Fail) and two Sham, did show a marked difference in growth, with a stunting in growth in the two AB(Fail) animals by over 10% from week 10 post surgery onwards(Figure 3-2) (Sham n=2). However this was a single example and other date- and surgery-matched AB(Fail) and Sham animals showed no difference in weight gain. Fluid on the lungs was often found in the AB(Fail) animals at end point, which could indicate oedema and fluid retention. This may mask any weight loss occurring in these animals.

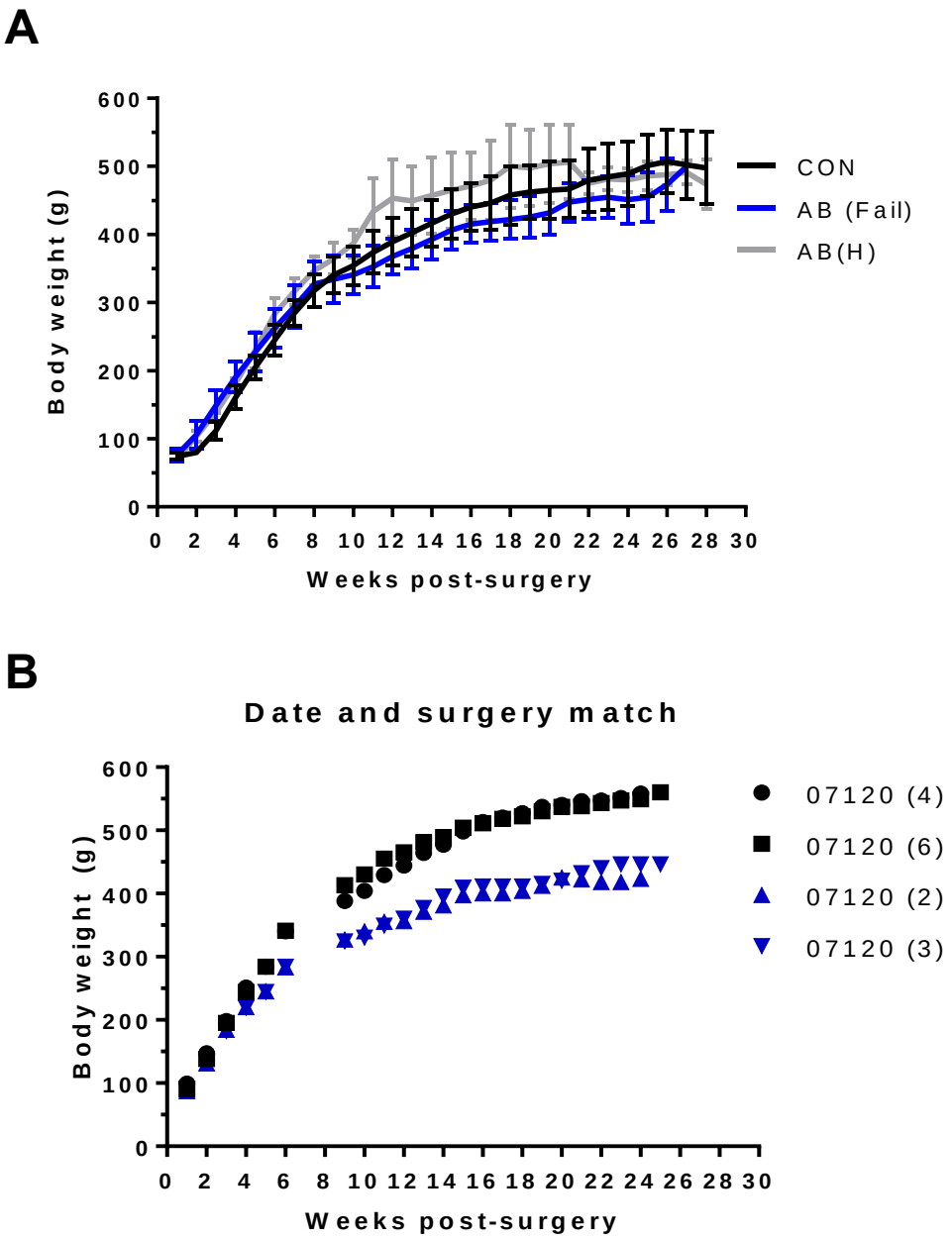

Figure 3-2 Growth Curve

Weight measurements were taken weekly to monitor for any sudden changes in weight from day of surgery. **A.** Grouped growth curve of all animals weights, mean ± SEM (Sham n=20, AB(H) n=7, AB(Fail) n=6) **B.** Individual growth curve of animals with same date of surgery (aortic banding 07120 (2+3) animal ID, sham operated 07120(4+6) animal ID)

3.3.3. Echocardiography and haemodynamic measurements

Echocardiography was performed to monitor changes in heart structure and function, and to identify the end-point within banded animals. A proportion of the sham animals also underwent the same monitoring. When ejection fraction was measured to be below 45% by echocardiography measurements, pressure volume loop analysis was performed. Further offline analysis was performed on multiple cineloop recordings and the average of 3-4 cineloops was taken to give the final measurements. Echocardiography measurements taken at the end point were then used to analyse LV geometry and wall thickness (Figure 3-3). There was no significant difference in interventricular septum (IVS) thickness between Sham, AB(H) and AB(Fail) animals in diastole or systole (Figure 3-4). Left ventricular posterior wall (LVPW) thickness in both AB(H) and AB(Fail) was significantly increased ($P<0.01$, $P<0.05$) during diastole with over a 50% increase in thickness from Sham, indicating left ventricular hypertrophy. AB (H) animals showed a reduced left ventricular internal diameter (LVID) in diastole and systole of up to a third compared with both Sham and AB(Fail)($P<0.05$, $P<0.01$)(Figure 3-4). By contrast AB(Fail) animals had a significantly larger internal diameter in systole than both Sham and AB(H)($P<0.001$), which would indicate systolic dysfunction and result in a reduced ejection fraction. This could suggest concentric hypertrophy in the AB (H) group which progressed to dilation in the AB (Fail).

Figure 3-3 M-mode images of echocardiography examination of AB and sham banded animals

A. M-mode imaged in the parasternal short axis view from AB animal (Surgery date – 08/11/13) taken 26 weeks post-surgery. **B.** Short axis image in M-mode from Sham animal (Surgery date – 12/03/13) taken 25 weeks post-surgery. **C.** Short axis image in M-mode from AB animal (Surgery date – 22/03/13). Short M-mode is taken running between the two papillary muscles and the interventricular septum (IVS). Left ventricle internal diameter (LVIS) and left ventricle posterior wall (LVPW) measurements are also made in systole and diastole (s/d). ECG recording is displayed at the bottom of the image as well as heart rate (HR) in the bottom right hand corner. Time and date of echocardiography examination is displayed in the top left hand corner. Index down the right had side of M-mode view screen is depth of echocardiography examination in cm.

A

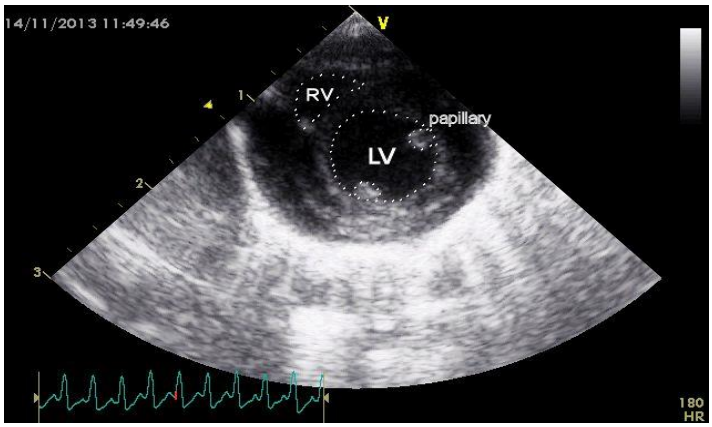
14/11/2013 11:49:46
RV
papillary
LV
180
HR

B

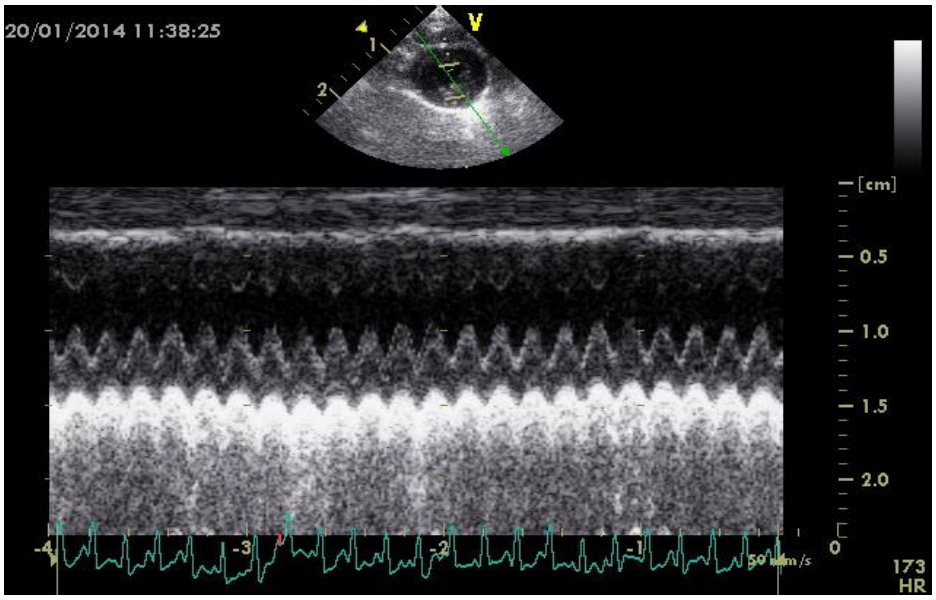
20/01/2014 11:38:25
[cm]
0.5
1.0
1.5
2.0
173
HR

C

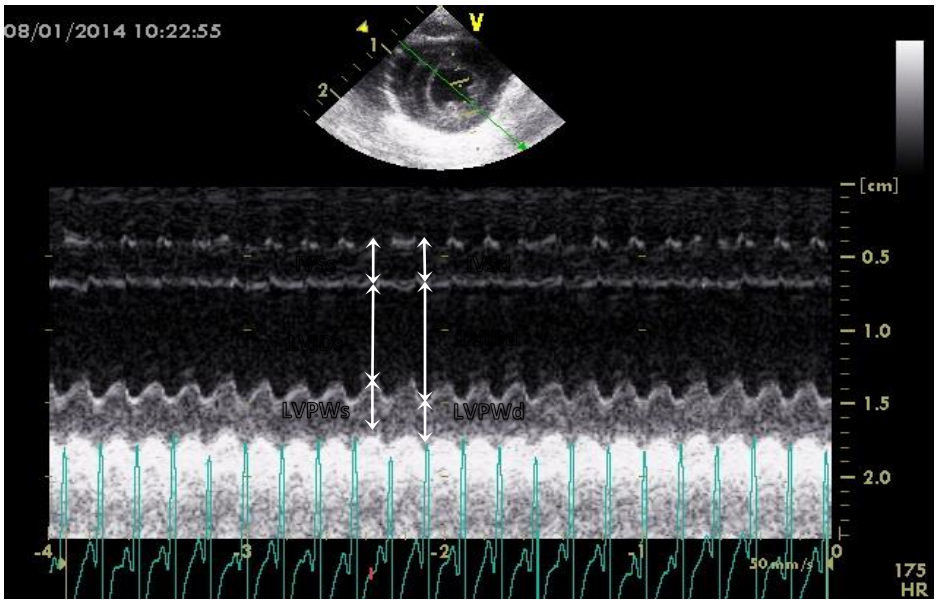
08/01/2014 10:22:55
[cm]
0.5
1.0
1.5
2.0
LVPWs
LVPWd
175
HR

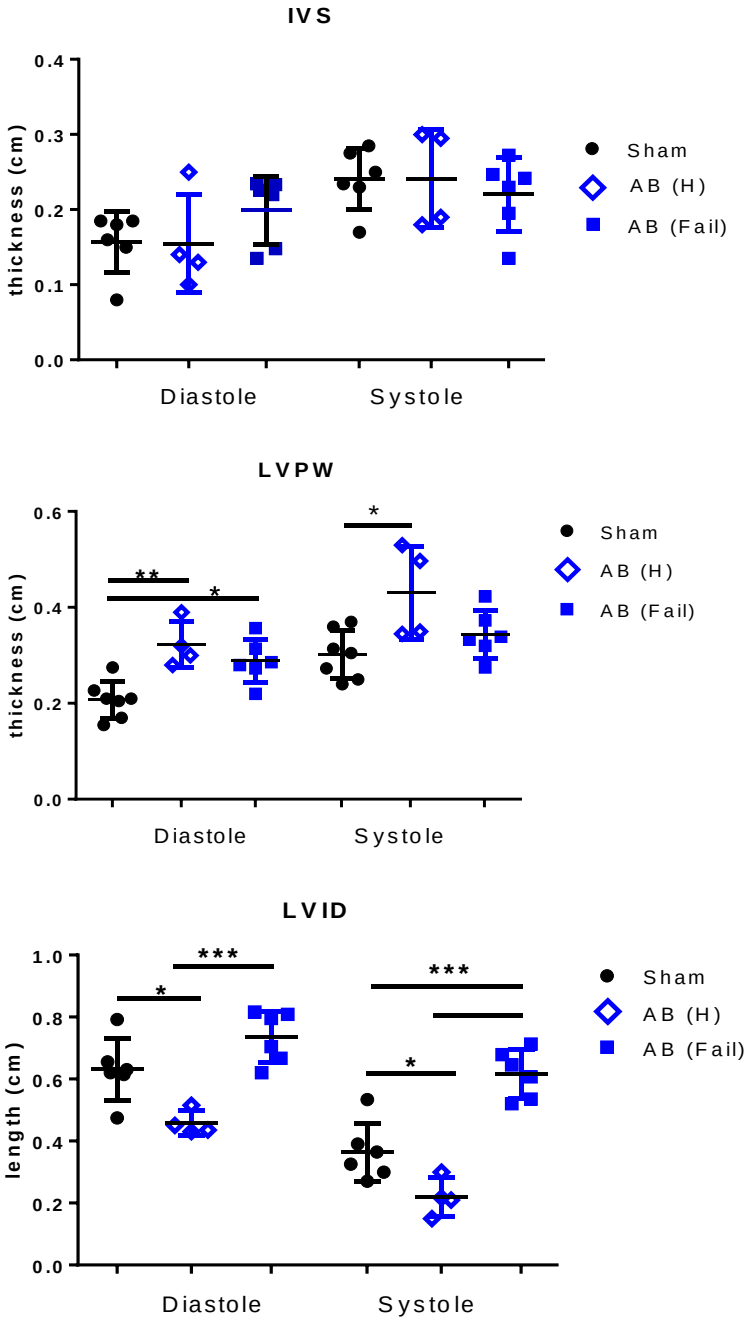

Figure 3-4 Echocardiography measurements taken at end point

Interventricular septum (IVS) and left ventricular posterior wall (LVPW) thickness as well as left ventricular internal diameter (LVID) were all measured at the end of diastole and systole in the short-axis parasternal M-mode. Data presented as dot plots ± SD (Sham n=6, AB(H) n=4, AB(Fail) n=7. One-way ANOVA comparison *P<0.05, **P<0.01, ***P<0.001.

Haemodynamic measurements were taken under anaesthesia with a pressure catheter (Figure 3-5) to measure LV pressure and volume during the cardiac cycle. Representative trace for AB(H) unfortunately do not fit completely with mean data in table. There was a large amount of variation within the end-diastolic volume measurement recorded and representative trace differs from the mean value. Haemodynamic measurements from AB(H) animals were the same as those of the Sham group apart from end-systolic pressure which was significantly increased ($P<0.05$). An increased end systolic pressure suggests increased afterload, indicative of some form of constriction placed on the aorta. End systolic pressure was also increased in the AB(Fail) ($P<0.01$) compared to Sham. End systolic volume was increased in the AB(Fail) animals compared to Sham and AB(H) ($P<0.01$) which fits with the increased LV internal diameter and reduced ejection fraction indicating LV systolic failure. Ejection fraction was significantly reduced in AB(Fail) compared with both AB(H) and Sham ($P<0.001$). There is a trend for a decrease in stroke volume in AB(Fail) compared with Sham animals which then results in a significant reduction in cardiac output as there is no significant change in heart rate. Arterial elastance, which is the calculated measurement of arterial load, is also increase in AB(Fail) compared with Sham. Many of these volume and pressure measurements are significantly different in AB(Fail) compared to Sham, however there is no significant difference between AB(Fail) and AB(H) in most of the measurements. This would indicate that the AB(H) animals are in an intermediate functional state. The AB(H) animals could be in a compensatory state, moving towards the failing state but without a dilated LV and with a preserved ejection fraction.

Figure 3-5 Haemodynamic measurements taken at end point

Pressure volume loops taken from Sham (black), AB(H) (green) and AB(Fail) (red) animals shown in top diagram. End systolic pressure volume loop relationship **(**ESPVLR). E_a = ESP(end systolic pressure)/SV(stroke volume). Data presented as mean ± SEM (Sham n=10, AB(H) n=4, AB(Fail) n=8. One-way ANOVA comparison *P<0.05, **P<0.01, ***P<0.001 AB(Fail) vs CON, †††P<0.001 AB(Fail) vs AB(H), #P<0.05 AB(H) vs CON.

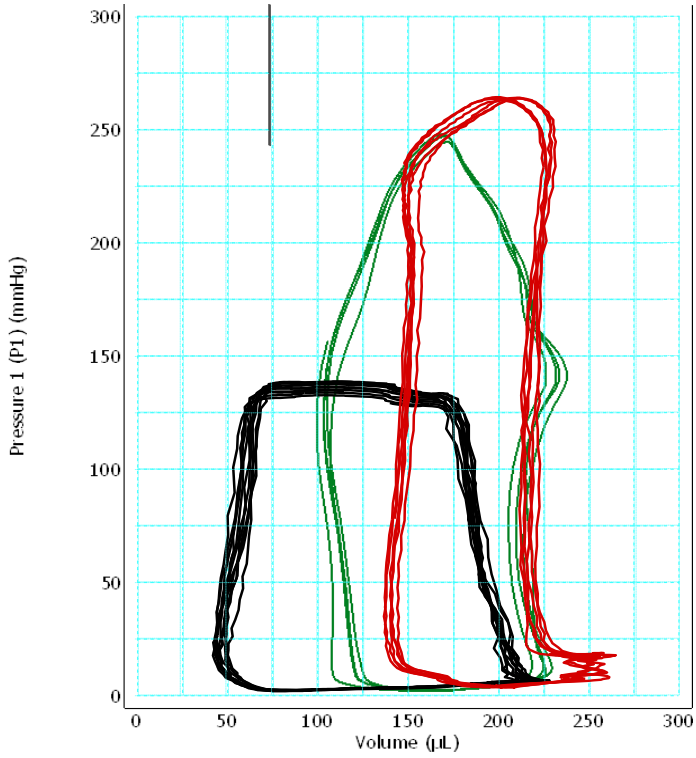

	Sham	AB (H)	AB (Fail)
Heart rate (bpm)	339 ± 8.72	351.5 ± 22.55	309 ± 13.33
End-systolic Volume (µL)	46.29 ± 7.38	73.43 ± 15.02	178.2 ±15.02 *** †††
End-diastolic Volume (µL)	165.6 ± 17.70	162.8 ± 24.60	217.3 ± 14.22
End-systolic Pressure (mmHg)	130.9 ± 9.41	199.8 ± 15.24 #	200.7 ± 11.59 ***
End-diastolic Pressure (mmHg)	8.335 ± 1.06	8.45 ± 1.85	14.23 ± 1.61 *
Ejection Fraction (%)	76.90 ± 2.60	68.59 ± 3.41	33.87 ± 3.57 *** †††
Stroke volume (µL)	132.3 ± 14.26	118 ±19.01	85.62 ± 12.06 (P=0.071)
Cardiac Output (µL/min)	45046 ± 4990	41793 ± 7867	26842 ± 4342 *
Cardiac Output/ Body weight ((µL/min)/g)	94.38 ± 11.69	84.64 ± 12.32	60.08 ± 8.59 (P=0.075)
Arterial Elastance (Ea) (mmHg/µL)	1.16 ± 0.21	1.88 ± 0.35	2.84 ± 0.52 **
ESPVR (linear)	0.059 ± 0.019	0.083 ± 0.043	0.211 ± 0.043 **

3.3.4. Organ weight ratios

Body weight, plus whole and dissected organ weights, were recorded at the end point, after hemodynamic measurements where these were made. The left tibia was dissected and measured with a pair of callipers. As mentioned previously, heart weight to body weight (HW:BW) ratio was used to allocate the banded animals to a AB(H) group which showed signs of hypertrophy. This was used as not all the banded animals showed signs of hypertrophy or other clinical symptoms and some appeared to have no apparent constriction placed on the aorta. In both AB(H) (n=7) and AB(Fail) (n=8) HW:BW ratio was significantly increased compared to control (n=13) ($P<0.01$, $P<0.001$ respectively),with the AB(Fail) HW:BW ratio over double of that of Sham (Figure 3-6). Heart weight normalised to tibia length (HW:Tibia) was also significantly increased in AB(H) and AB(Fail) compared to Sham($P<0.001$) (Figure 3-6). Body weight measurements showed a significant correlation with tibia length (Pearson correlation coefficient $P<0.05$) with no difference between the Sham and AB groups. To be consistent across the heart failure models body weight was used to normalise further measurements. For a small number of animals from the hypertrophy group, a method devised by MacDougall and Calaghan was employed to isolate single cells from the base, and prepare whole muscle samples from the apex, of the same heart (MacDougall and Calaghan, 2013). This meant that whole right ventricle (RV) and LV weight could not be obtained from these animals. There was a significant increase in the right ventricle to body weight (RV:BW) and left ventricle and septum to body weight (LV+S:BW) in the AB (Fail) group compared to Sham ($P<0.001$) (Figure 3-7). The AB(H) group showed no significant difference to the Sham or the AB (Fail) animals, indicating an in-between state between sham and failure. There was no difference in the LV to RV ratio for AB(H) or AB(Fail) compared with Sham suggesting a total heart hypertrophy instead of ventricle-specific hypertrophy. Lung weight in the AB(Fail) group was significantly increased compared with both Sham and AB(H) indicated by a significant increase in lung weight to BW (Figure 3-7). Fluid around the lungs of the AB(Fail) animals was often observed resulting from high pressure within the pulmonary vasculature, suggesting pulmonary oedema was present. Liver weight to body weight ratio was significantly increased in AB (Fail) compared to Sham, which may be a result of fluid retention.

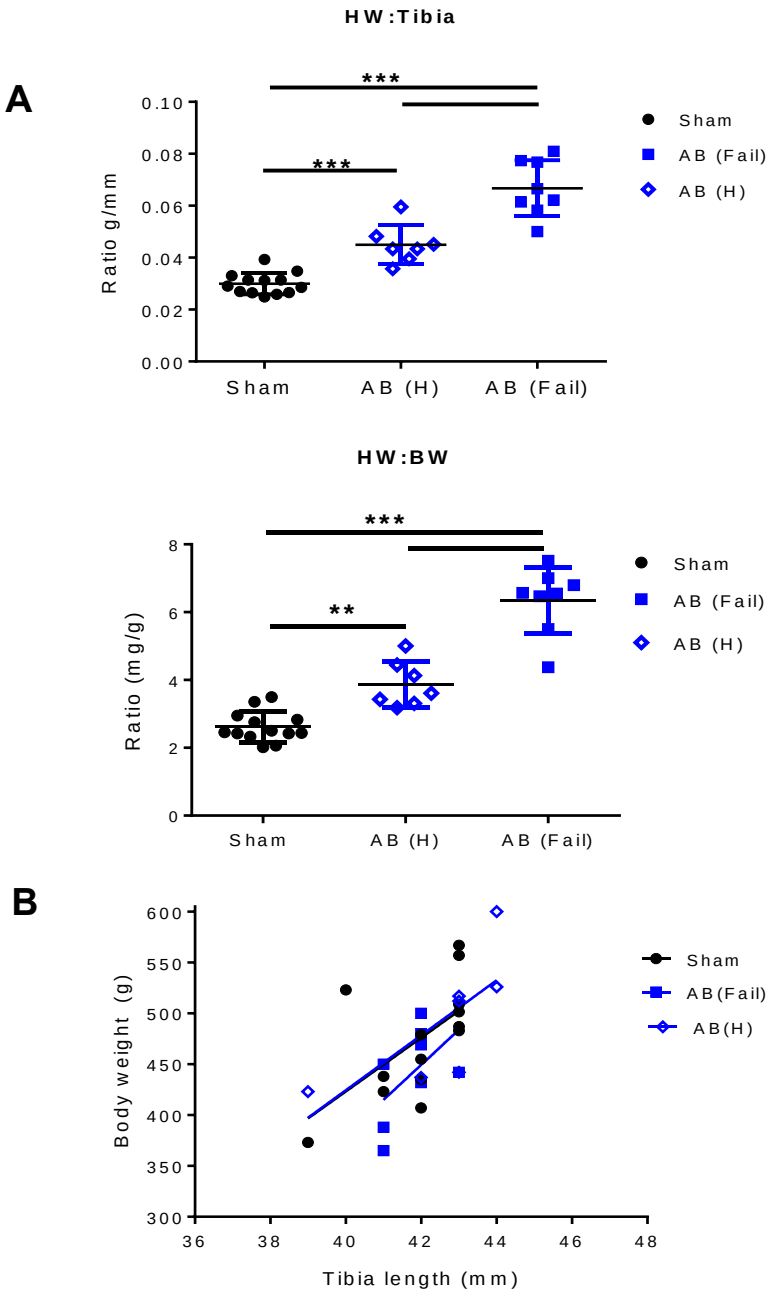

Figure 3-6 Post-mortem organ and body weight ratios

A. Body weight (BW) and whole heart weight (HW) were recorded at the end point of each animal. Left tibia was dissected and measured using callipers. Data presented as dot plots ± SD (Sham n=10, AB(H) n=4, AB(Fail) n=8). One-way ANOVA comparison *P<0.05, **P<0.01, ***P<0.001. **B.** Relationship between tibia length and body weight used to normalise organ weight (Sham n=14 R^2=0.359, AB (H) n=7 R^2=0.536, AB(Fail) n=8 R^2= 0.286)

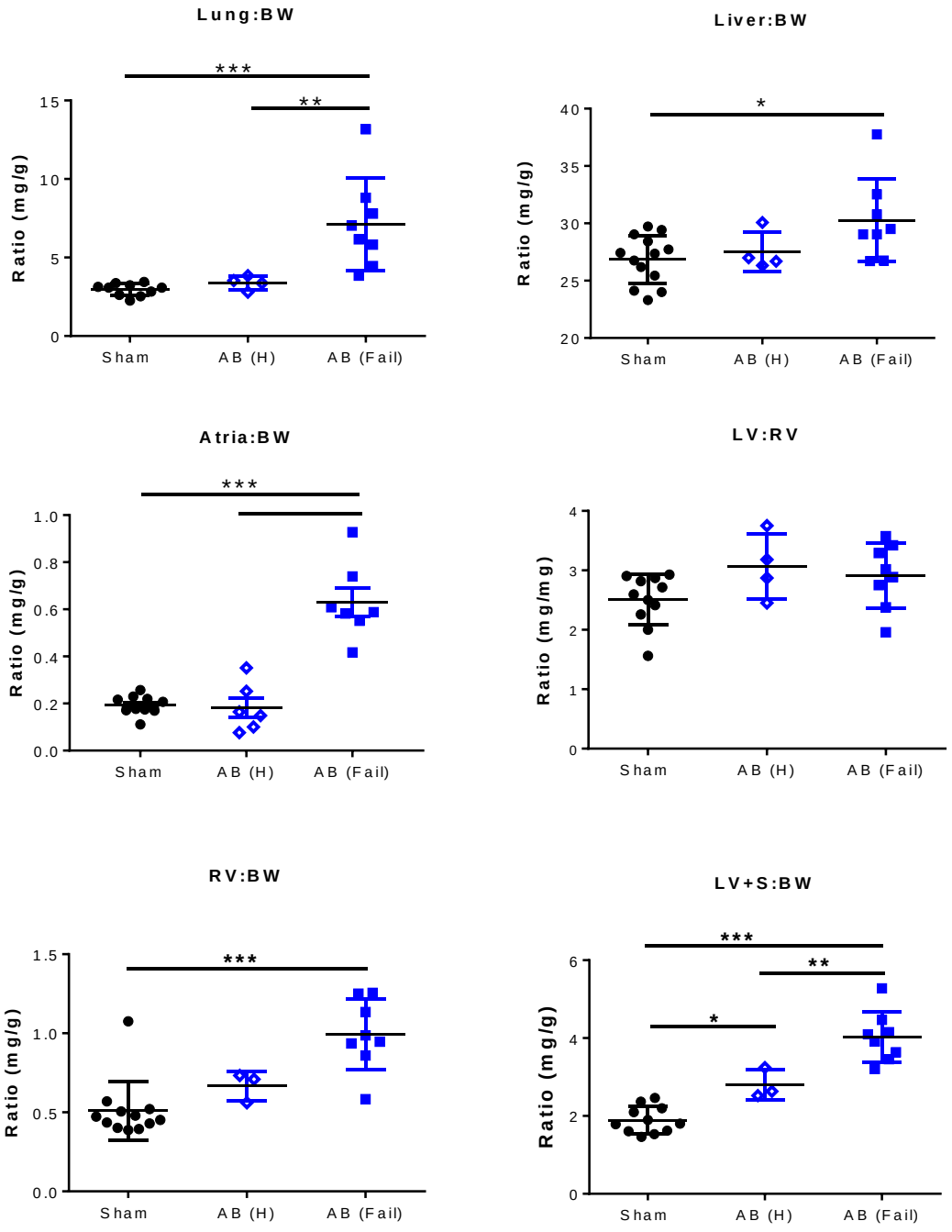

Figure 3-7 Post-mortem organ and body weight ratios

Body weight (BW) and dissected organ weight was recorded at the end point for each animal. Whole heart weight (HW) was recorded before dissecting into atria, right ventricle (RV) and left ventricle and septum (LV+S) which was then further dissected into left ventricle (LV) and septum. Data presented as dot plots ± SD (Sham n=10, AB(H) n=4, AB(Fail) n=8). One-way ANOVA comparison *P<0.05, **P<0.01, ***P<0.001.

3.3.5. Fibrosis staining

Longitudinal sections of the left ventricle were taken for picro-sirius red staining to assess fibrosis. Images were acquired using an upright light microscope, which did not differentiate between collagen type I and III, so these were measured together. When acquiring the images it was noted that there was an increased amount of fibrosis around the blood vessels in some of the samples which, when the samples were un-blinded, was revealed to be exclusively within the AB(Fail) samples (Figure 3-8). When analysing sections of tissue, images with blood vessels within the frame were excluded from analysis as equivalent size blood vessels were not found across all animals; if included this could create bias between animals. When fibrosis was quantified as a percentage per image there was a significant increase in percentage of fibrosis in the AB(Fail) group compared with both Sham and AB(H). AB(Fail) mean percentage fibrosis was increased two fold compared with the Sham group. AB(H) also showed a significant increase in fibrosis compared with the Sham group (Figure 3-8). Between 16 and 30 weeks post-surgery, time does not appear to have any effect on the percentage fibrosis in the Sham or AB(Fail) animals. However, within the same time period, there is a significant effect of time post-surgery on fibrosis in the AB(H) group. The linear relationship between mean fibrosis and weeks post-surgery significantly deviated from zero using a linear progression test within the AB(H) animals (Figure 3-9). This is unlikely to be due to age as the rats around 6 months are still classed as young in aging studies (Pacher et al., 2004), so is more likely to be the longer period of time with increased afterload on the heart or a delayed development of fibrosis due to a lesser constriction.

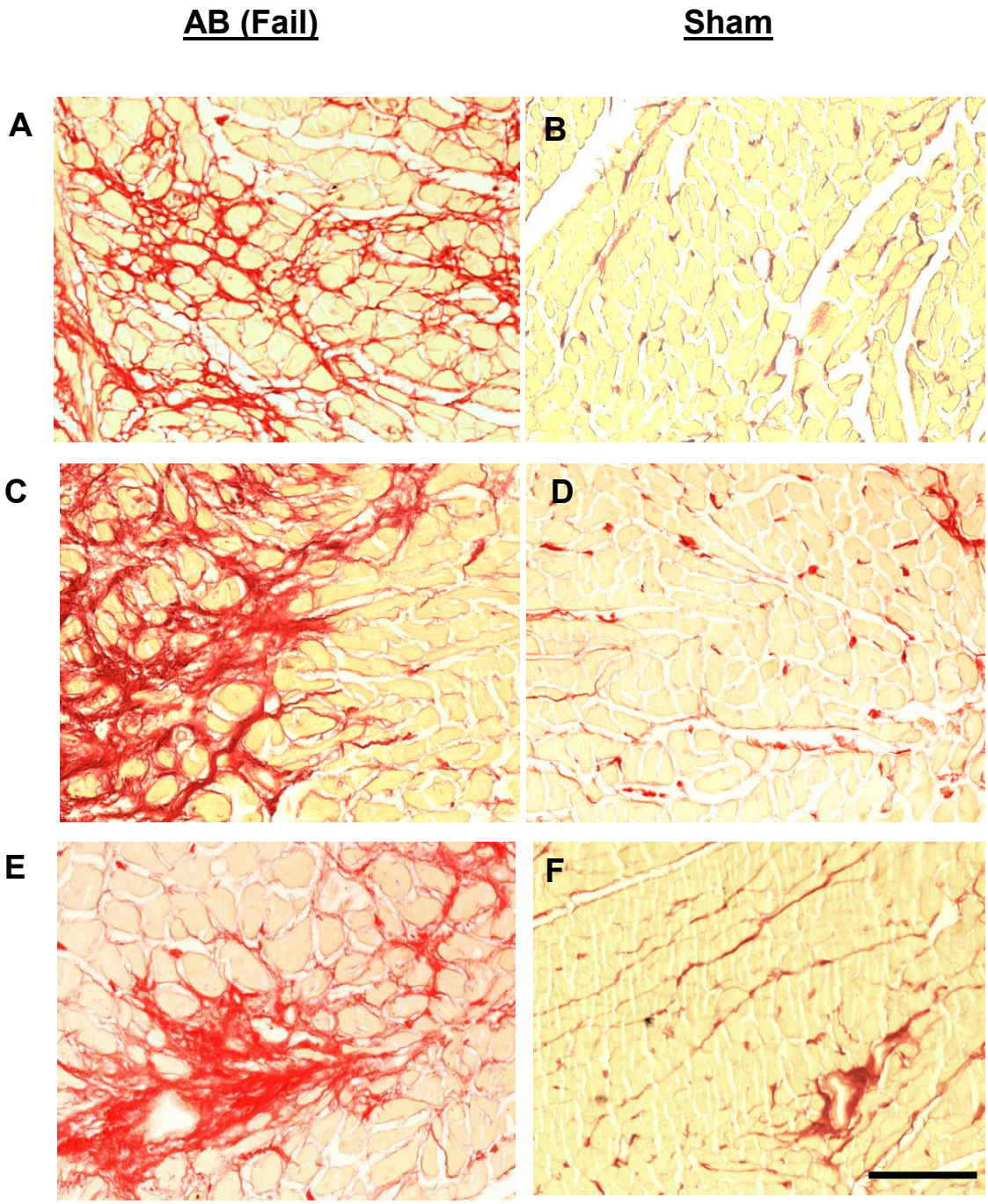

Figure 3-8 Representative images staining for fibrosis

Longitudinal sections of the left ventricle were fixed in PFA before dehydrating and wax embedding. Sections 10 µm thick were then stained with picro-sirius red, top four images are representative sections from AB(Fail) (A,C) and Sham tissue (B,D). **E.F** representative images of the perivascular fibrosis. Scale bar 100 µM

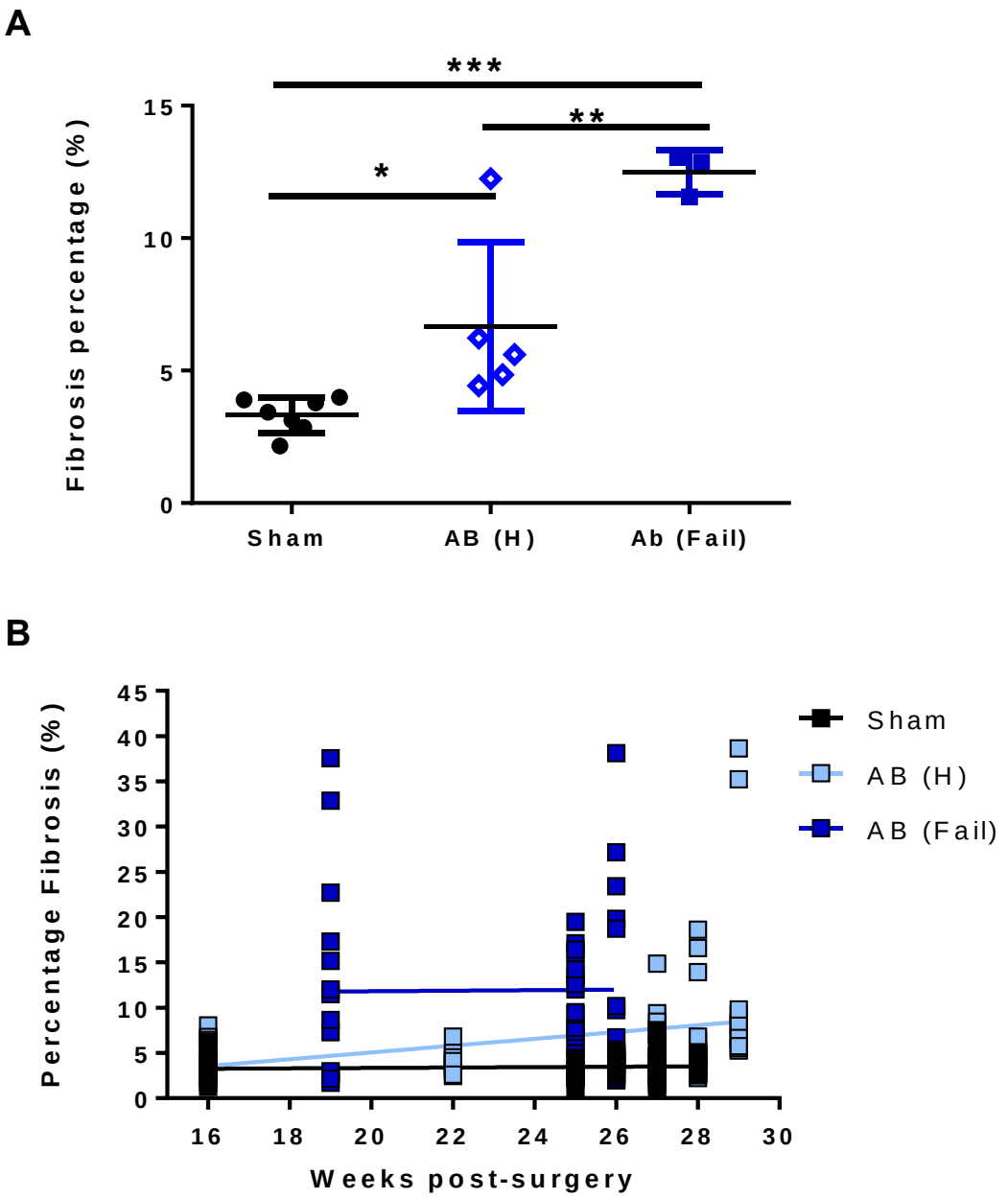

Figure 3-9 Picro-sirius red collagen staining

Sections of tissue were stained with Pico-sirius red to determine collagen content. At least 10 images from each animal were used to produce an index of fibrosis. **A.** Averaged fibrosis percentage. Data presented at mean ± SD (Sham n=8, AB(H) n=5, AB(Fail) n=3). One-way ANOVA comparison *P<0.05, **P<0.01, ***P<0.001. **B,** Individual image analysis for each animal plotted against time post-surgery, with linear regression calculated for each group (Sham n=8, AB(H) n=5, AB(Fail) n=3)

3.4. Discussion

These results collectively support the classification of animals in the AB(Fail) group being in end stage heart failure, showing many of the clinical signs of cardiac dysfunction seen in human patients. As mentioned previously not all of the animals reached this stage of heart failure. Some animals showed no signs of aortic constriction, probably as a result of absorbed sutures (Lygate, 2006) or slipping of the metal clip around the aorta. These were excluded from any analysis. Suture absorption has previously been reported in mice (Lygate, 2006) which result in the desired constriction not being applied. Those animals which did show an increase in heart weight to body weight ratio but still had an ejection fraction over 45% showed an intermediate stage of heart failure. Many of the functional pressure and volume measurements in the AB(H) group showed no significant difference to Sham or AB(Fail). This would suggest these animals are in a compensatory phase with increased left ventricular wall thickness and increased left ventricular end systolic pressure but with a preserved ejection fraction and cardiac output. Although the tissue from these animals cannot be grouped together with the failing tissue it may be interesting to analyse the differences within this transition phase. The end point of our study varied between 12 weeks to 36 weeks post-surgery, which could be ascribed to the degree of clip constriction placed on the aorta and is an important factor to consider when looking at molecular aspects of the model. The model of aortic banding progressing from concentric to dilated heart failure has previously been studied using echocardiography (Litwin et al., 1995). In this study six weeks after aortic banding concentric left ventricular hypertrophy was reported using echocardiography to have an increase in LV mass. Litwin et al.'s model progresses to a dilated diastolic and systolic dimension by 18 weeks after banding. The aortic constriction in our model is similar to that in the Litwin et al. model, which placed a tantalum clip of 0.58 mm (internal diameter) around the aorta of 60 to70 g Wistar rats. This produced comparable measurements for the left ventricular internal dimensions which reports both systolic and diastolic dysfunction.

3.4.1. Clinical translation

The typical clinical presentations of heart failure in human patients such as fatigue and exercise intolerance, which is used in part to define the stage of heart failure by the New York Heart Association guidelines (Association, 1964), are not easily tested in animals. Other clinical presentations such as fluid on the lungs and ejection fraction instead must be used to relate the clinical presentations of small animal heart failure to humans. The aim of

developing this model was to examine molecular changes within the myocardium at the end stage of heart failure. Although the nature of the initial insult to the heart may vary, the end result of the heart being unable to pump a sufficient output to the body to meet its metabolic needs is the same. The importance of being able to relate small animal models of heart failure to human patients is sometimes overlooked. Houser et.al have produced a statement from the American Heart Association with guidelines for what should be observed in animals models of heart failure, including their uses and limitation (Houser et al., 2012). This is a useful reference point to check with human clinical studies as well as other animal models. With each different type of initial insult to the heart, such as dilated cardiomyopathy, there are recommendations of clinical observations that are critical to replicate in the model in animals (in this case, relative wall thinning and eccentric hypertrophy). It also highlights the complexities within the disease and lists possible comorbidities often seen in these patients, such as diabetes and metabolic syndrome. The statement also references detailed methods papers, such as using pressure-volume conductance catheter techniques in mice and rats, to help standardize the calibrations made and basic parameters measured (Pacher et al., 2008). It is hoped that if more of these checkpoints were met that there would be a higher likelihood of clinical translation of the findings.

The concept of pressure overload or hypertension transitioning from compensatory heart hypertrophy to heart failure is well documented in both animal models and human cases (Frohlich et al., 1992; Dadson et al., 2016). The progression to heart failure normally begins with a preserved ejection fraction with increased ventricular pressure and wall thickness which then progresses towards dilation of the ventricle with increase end-diastolic and end-systolic left ventricular blood volumes, like that seen in the AB(Fail) group. Houser et al. list changes which should be seen in hypertensive heart disease leading to failure including: increased LV mass, changes in LV geometry, myocardial fibrosis which eventually leads to systolic/diastolic dysfunction. Pressure overload is also a listed method used to replicate the dilated cardiomyopathy phenotype, but with more focus on change in ventricular geometry with reduced output and elevated filling pressures (Houser et al., 2012). Progression of the AB(Fail) group was monitored by echocardiography but there were not enough time points recorded to be able to say whether the animals in this group went through a concentric hypertrophic phase before entering a dilatory failure phase. Image quality and reproducibility across groups was also not sufficient to look at long axis measurements of the left ventricular chamber (Teichholz et al., 1976; Bellenger et al., 2000). When analysing the heart in the short axis M-mode, several assumptions are made about

the geometry of the heart which may not always be valid in the AB(Fail) group if there has been dilation and structural remodelling, which is often seen in heart failure. From echocardiography measurements, animals in the AB(H) group have decreased left interventricular diameter in both diastole and systole and increased left ventricular posterior wall thickness. The AB(Fail) group only have an increased internal diameter in systole. This suggests that there may be concentric hypertrophy in the AB(H) group and systolic dysfunction and dilation in the AB(Fail) group

Increased fibrosis is a characteristic of the remodelling heart in response to an increased pressure; this is initially a compensatory mechanism in an attempt to normalise wall stress, which progressively leads to ventricular stiffness and becomes de-compensatory. There are two main types of fibrosis: reactive fibrosis, which follows the vasculature and is initially perivascular and then extends into the interstitial space; or replacement fibrosis which occurs after myocyte necrosis (Segura et al., 2014). The extracellular matrix plays an important structural and connective role within the heart and one of the main components within this is fibrillar collagen, which makes up around 2-4% of the myocardium in a healthy human heart (Knoebel and Weber, 1989). The collagen network consists of mainly type I collagen which provides tensile strength and determines myocardial stiffness, and a smaller proportion of type III which contributes to elasticity. Changes in the extracellular matrix and increased collagen and fibrosis have previously been linked with increased left ventricular end-diastolic pressure and reduced ejection fraction (Villarreal et al., 1993). Increased collagen and fibrosis has been repeatedly reported in hypertensive heart disease patients both by post-mortem analysis and in vivo measurements (Tanaka et al., 1986; Dadson et al., 2016). Without access to a polarised microscope, it is impossible to assess the different percentage of collagen I and III, however the total percentage of collagen has increased in the AB(fail) animals, with an apparent increase in perivascular fibrosis noted. A number of different factors play a role in the relationship between collagen synthesis and degradation; upregulation of cytokines, for example can tip the balance towards increased synthesis (Díez, 2007).

3.4.2. Study limitations

The data collection across all the parameters used to characterise heart failure is not complete for all animals. Not all the animals have full weekly growth data, echocardiography measurements and/or in vivo haemodynamic measurements. A summary is given in table (Table 3-1 and Table 3-2). While the echo and in vivo measurements hold the most value

for classifying heart failure, organ weight and fibrosis measurement are also needed to support its clinical relevance.

3.4.3. Final animal grouping

The aortic banding of this group of animals has produced a wide range of time and progression to heart failure, which in some part may be due to slight variations in surgery. This adds a large amount of variability to the study with an increasing number of different factors which would then need to be considered, reducing the power of any findings which may occur. For this reason it was decided to select a smaller range of animals to further study the molecular aspects of heart failure. Six AB(Fail) animals from 19-26 weeks post banding with time matched Sham animals were chosen, highlighted in blue in Table 3-1 and Table 3-2

3.5. Conclusion

This model of transverse aortic banding has produced a group of animals with heart failure which has been characterised with a number of clinically relevant parameters. Ensuring that the model has clinical translation is important for interpretation of what is seen at the molecular level and its relevance to human patients. Having multiple measurements indicating that heart failure is present within each individual animal aids further molecular analysis. Heart failure is not a simple definition of heart dysfunction measured by one parameter but more a graded progression of dysfunction in multiple aspects of the myocardium and vasculature. Having the individual function/structural measurements can facilitate correlations with molecular findings. Six AB(Fail) animals were selected with six time matched Sham animals with equivalent functional measurements to study changes in protein expression.

Animal ID	Surgery date	End date	Weeks post- surgery	ECHO	PV	Fibrosis	Organ W	Weight G
AB (3)	20/08/2013	14/11/2013	12		✓		✓	✓
AB (4)	01/08/2012	21/11/2012	16		✓	✓	✓	
AB (6)	30/08/2012	18/12/2012	16	✓	✓		✓	
AB (18)	29/08/2013	08/01/2014	19	✓	✓	✓	✓	✓
AB (13)	29/08/2013	14/01/2014	20	✓	✓		✓	✓
AB (3)	12/07/2012	14/12/2012	22			✓		
AB (2)	12/07/2012	17/12/2012	22			✓		
AB (8)	22/08/2013	28/01/2014	23	✓	✓		✓	✓
AB (2)	08/11/2012	02/05/2013	25		✓	✓	✓	✓
AB (3)	08/11/2012	07/05/2013	26	✓	✓	✓	✓	✓
AB (10)	14/11/2013	17/05/2013	26	✓			✓	✓
AB (2)	23/05/2012	26/11/2012	27	✓		✓	✓	
AB (1)	23/05/2012	26/11/2012	27	✓				
AB (2)	30/04/2013	17/10/2013	28	✓		✓		✓
AB (1)	17/10/2012	09/05/2013	29			✓		✓
AB (2)	08/01/2013	15/07/2013	29	✓	✓		✓	✓
AB (7)	22/08/2013	01/04/2014	32		✓		✓	✓

Table 3-1 Summary data of AB animal analysis

Animal ID	Surgery date	End date	Weeks post-surgery	ECHO	PV	Fibrosis	Organ W	Weight G
Sham(23)	20/08/2013	22/11/2013	13		✓		✓	✓
Sham(3)	01/08/2012	21/11/2012	16		✓		✓	
Sham(9)	30/08/2012	18/12/2012	16		✓	✓	✓	
Sham(7)	30/08/2012	18/12/2012	16			✓	✓	
Sham(20)	30/08/2013	14/01/2014	20	✓	✓		✓	✓
Sham(19)	30/08/2013	15/01/2014	20	✓	✓		✓	✓
Sham(1)	20/08/2013	28/01/2014	23		✓		✓	✓
Sham(4)	08/11/2012	02/05/2013	25		✓	✓	✓	✓
Sham(6)	08/11/2012	07/05/2013	26	✓	✓	✓	✓	✓
Sham(8)	14/11/2012	17/05/2013	26	✓	✓		✓	✓
Sham(12)	14/11/2012	17/05/2013	26				✓	✓
Sham(3)	23/05/2012	26/11/2012	27			✓	✓	
Sham(3)	17/10/2012	01/05/2013	28	✓		✓		✓
Sham(6)	22/08/2013	17/03/2014	30		✓		✓	✓
Sham(4)	12/03/2013	01/11/2013	32		✓		✓	✓

Table 3-2 Summary data of Sham animial analysis

Chapter 4. Changes in membrane protein expression and distribution in left ventricular heart failure

4.1. Introduction:

In heart failure, the initial insult to the heart can affect how the myocardium will respond and remodel; there may be different adaptive responses to different insults (Houser et al., 2012). The model of heart failure used in this study has been characterised by in vivo function (echocardiography and pressure volume loops) and post-mortem (fibrosis staining and organ to body weight ratios) measurements (Chapter 3). This gives the opportunity to link possible protein expression changes within the myocardium to specific functional measurements made. The rat aortic banding model has previously been used to study changes in Ca^{2+} current, ion channel and SERCA expression as well as being used for therapeutic interventions (Feldman et al., 1993; Miyamoto et al., 2000), but to date there has been no investigation of changes to caveolar proteins in detail including possible changes in membrane location.

Caveolin 3 (Cav 3) is considered to be the most highly expressed of the caveolar proteins in cardiac myocytes, and although prominently located within caveolae, is also found in non-caveolar sarcolemma membrane (Calaghan and White, 2006; Calaghan et al., 2008). Using sucrose gradient fractionation the majority of Cav 3 expression is found within the buoyant fraction, with a smaller proportion found within the heavy fractions which contain non-raft membranes. Along with cavin 1, Cav 3 is a major component involved in the formation of caveolae within the cardiac myocyte. The cavin proteins cavin 1 and cavin 4 (the latter being muscle specific), are highly expressed within myocardium (Bastiani et al., 2009; Briand et al., 2011). Caveolin proteins have been linked to changes in cardiac function numerous times (Taniguchi et al., 2016; Ogata et al., 2014; Wright et al., 2014), but many aspects of the remodelling of caveolae and cavin proteins in heart failure remain unexplored.

The response of the ventricular myocyte to sympathetic stimulation - positive inotropy and lusitropy - relies on effective signalling of the β-adrenergic receptors (β-AR) (Richardson et al., 1967; Reddy, 1976). The two main subtypes β_1AR and β_2AR are both located within the caveolar domain. However, evidence from several groups suggest that only a small proportion of β_1AR is located within the caveolae, while β_2AR populations are mainly localised within caveolae This difference in sarcolemmal distribution is suggested to play a

significant role in controlling downstream signalling (Head et al., 2005; MacDougall et al., 2012).

The response of the heart to an increased afterload, such as aortic banding, is to increase sympathetic stimulation to the heart to maintain cardiac output. When sympathetic stimulation becomes chronic the heart goes through a remodelling phase, which is initially compensatory but eventually becomes de-compensatory (Triposkiadis et al., 2009). Hearts from the failing aortic banded (AB (Fail)) animals have a significantly reduced ejection fraction and cardiac output. This suggests that these hearts have entered a de-compensatory phase causing disruption to the protein composition and expression at the membrane. It is predicted that there will be changes in protein expression and membrane organisation in a number of caveolar and β-AR signalling proteins in this model of heart failure. To test this hypothesis we measured caveolar and β-AR signalling protein expression, as well as changes in these proteins location within the membrane with a view to linking these to the functional changes observed.

4.2. Methods:

At the designated end point AB and Sham animals were humanely culled using an appropriate listed Schedule 1 technique. The coronary circulation was then cleared using a cannula attached to a 1 mL syringe to perfuse the heart through the aorta with Tyrode solution prepared fresh on the day. Hearts were then weighed and right and left ventricles dissected and weighed. A 100 mg longitudinal strip of LV free wall was cut and placed in a labeled Eppendorf and snap-frozen in liquid nitrogen to be homogenised in Laemmlli sample buffer for the study of protein expression (as stated in Methods 2.8.1). For analysis of protein distribution in different membrane fractions, approximately 350 mg LV free wall was homogenised 6 x 20 s in detergent free buffer (500 mM Na_2CO_3 (pH 11), 1x protease (Roche Applied Science) and phosphatase (Thermo Scientific Pierce) inhibitor cocktails). Samples were then stored at -20 ^{o}C till samples were ready to be run on a discontinuous sucrose gradient.

Sucrose gradient fractionation was performed as stated in Methods (Section 2.8.2). In brief, samples were sonicated and then centrifuged before layering on to a discontinuous sucrose gradient. Gradients were centrifuged overnight at 4 ^{o}C and fractions were then collected and frozen at -20 ^{o}C until required.

The protein concentration of fractioned samples and LV muscle homogenate was measured using a bicinchonincic acid (BCA) assay as stated in Methods 2.8.5.1. This enabled equal protein loading for protein analysis by SDS-page and Western blot (Section 2.8.5.2.)

De-glycosylation experiments were performed on both muscle homogenates and fractionated samples as described in Methods section 2.8.4. PNG-ase F had not previously been used within the research group so a number of optimisation steps were also performed. To determine which conditions should be used to de-glycosylate the β_2AR a non-denaturing protocol was also tested which omitted the denaturing step and incubated sample and PNG-ase F for 20 h. For denaturing conditions, samples (5-9 µL) were mixed with 1 µL denaturing buffer and denatured at 95 ^{o}C for 10 min. The volume of 10% NP-40 was adjusted for each reaction to ensure the final concentration was equal to that of the SDS in solution. As initial experiments could not replicate the shift in molecular weight bands seen in previous studies of the cardiac β_2AR by Rybin et.al., an experiment was designed to replicate the conditions stated in (Rybin et al., 2003; Rybin et al., 2000). Freshly isolated ventricular cardiac myocytes were homogenised in cell buffer ((mM) 15 Tris-HCl (pH 7.5), 60 NaCl, 1.25 EDTA and 1% SDS) as used in Rybin et al. The resulting homogenate was centrifuged at 16000g at 5 ^{o}C and supernatant removed (Rybin et al., 2000). AB and Sham samples homogenised in Laemlli sample buffer were also analysed in this test run, with 8 µL of input sample being subjected to the PNG-ase F protocol (Section 2.8.4). Enzyme incubation time was extended to 2 h at 37 ^{o}C with the reaction being terminated by the addition of 5 x Laemlli sample including bromephenol blue and β- mercaptoethanol to replicate conditions outlined.

Phosphorylation of proteins was studied by the use of phos-tag gels as described in Methods (Section 2.8.5.3). Briefly, Phos-tag™ was added to the SDS-PAGE gel which slows the migration of phosphorylated proteins compared to non-phosphorylated proteins through the gel. This can be detected in Western blotting as additional bands when compared to normal gels.

4.3. Results

4.3.1. Altered protein expression in left ventricular myocardium following aortic banding

4.3.1.1. Caveolar proteins

Western blotting of left ventricle myocardial homogenate from AB animals showed a significant reduction in Cav 1 expression compared to Sham animals ($P<0.01$). AB Cav 1 protein expression was around 50% of that seen in the Sham animals. Cavin 1 protein expression was also significantly reduced in AB animals when compared with Sham ($P<0.05$) (Figure 4-1). There was no change in Cav 3 expression between the two groups. Cavin 4 expression on the other hand was significantly increased by almost 50% in the AB animals compared to Sham ($P<0.05$) (Figure 4-1). A strong positive correlation ($R^2=0.684$) was observed between Cav 1 protein expression and ejection fraction, (the latter being one of the key measurements used to define cardiac function)(Figure 4-1). Protein expression of the other caveolar proteins were examined for links with functional measurements such as ejection fraction, heart weight (HW) to body weight (BW) and left ventricular (LV) weight to BW ratios but no significant correlations were revealed (Figure 4-2).

4.3.1.2. β-adrenergic signalling proteins

Cardiac β_1AR expression in the AB animals was significantly reduced to and around half that measured in the Sham animals ($P<0.05$) (Figure 4-3). The β_2AR expression showed no significant difference between groups, although there was a wide range in expression levels among banded animals. This was, in part, due to a slightly higher molecular weight band (Figure 4-3); the reason for this higher molecular weight band is addressed later in the chapter. There was a ~50% reduction in AC 5/6 expression in the AB left ventricle as compared with Sham ($P<0.05$). G-protein receptor kinase 2 (GRK2) expression in the left ventricle of the AB animals was significantly increased compared with the sham animals ($P<0.05$) (Figure 4-3). There was no difference in the expression levels of eNOS or $G\alpha_i3$ between the AB and Sham animals (Figure 4-3). Two AB animals showed higher expression levels of $G\alpha_i3$ although there appeared to be no obvious link to supressed cardiac function, as measured by ejection fraction, or correlation with β_2AR expression.

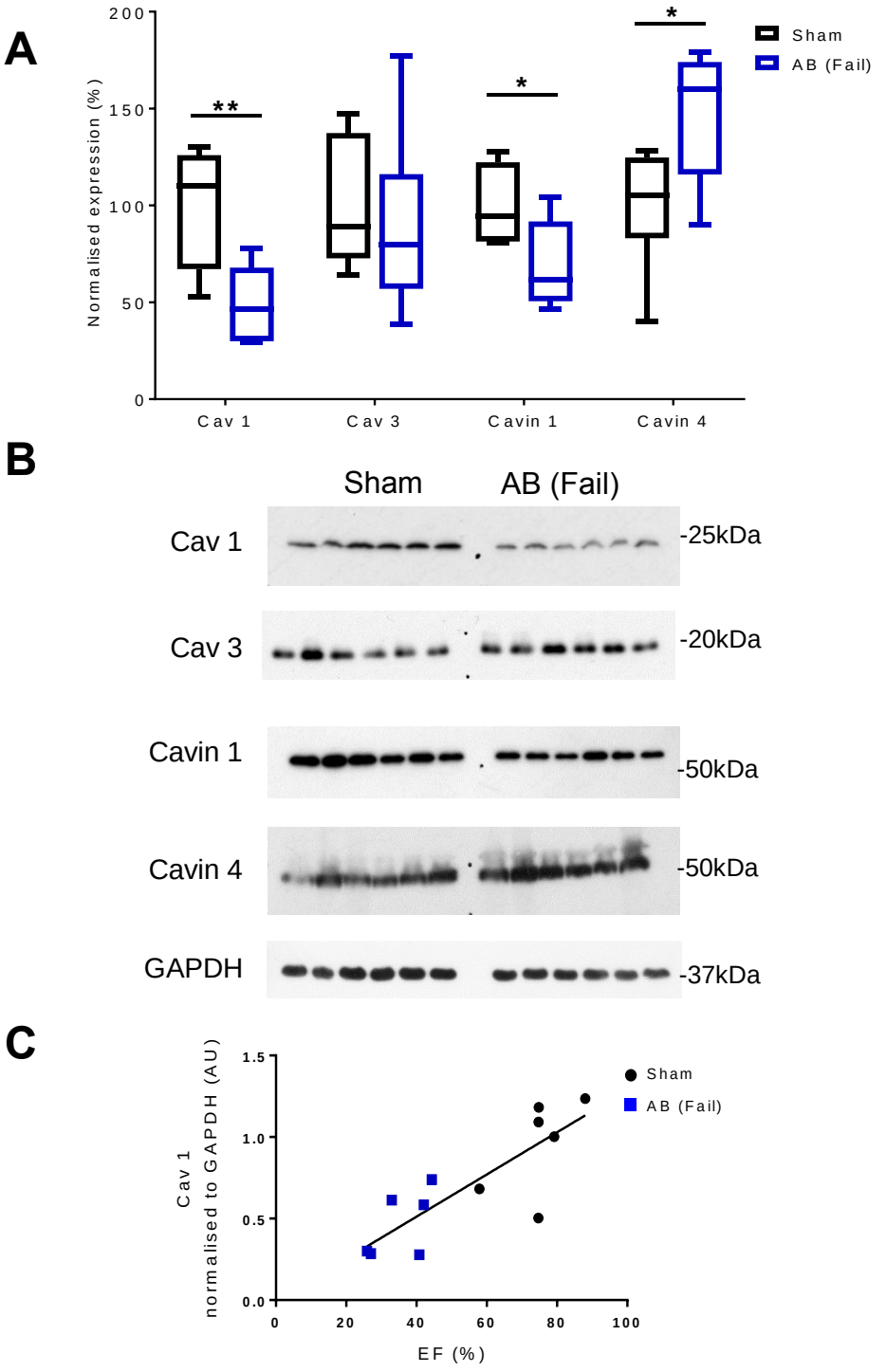

Figure 4-1 Caveolar protein changes in left ventricular heart failure.

A. Western blot of left ventricular muscle homogenised in Laemmli sample buffer, signal normalised to GAPDH and expressed as a percentage of mean Sham value, box and whisker graph. Sham n=6, AB n-6, Student t-test, *P<0.05, **P<0.01. **B.** Representative Western blot. **C.** Cav 1 protein expression plotted against ejection fraction (EF) recorded from haemodynamic measurements.

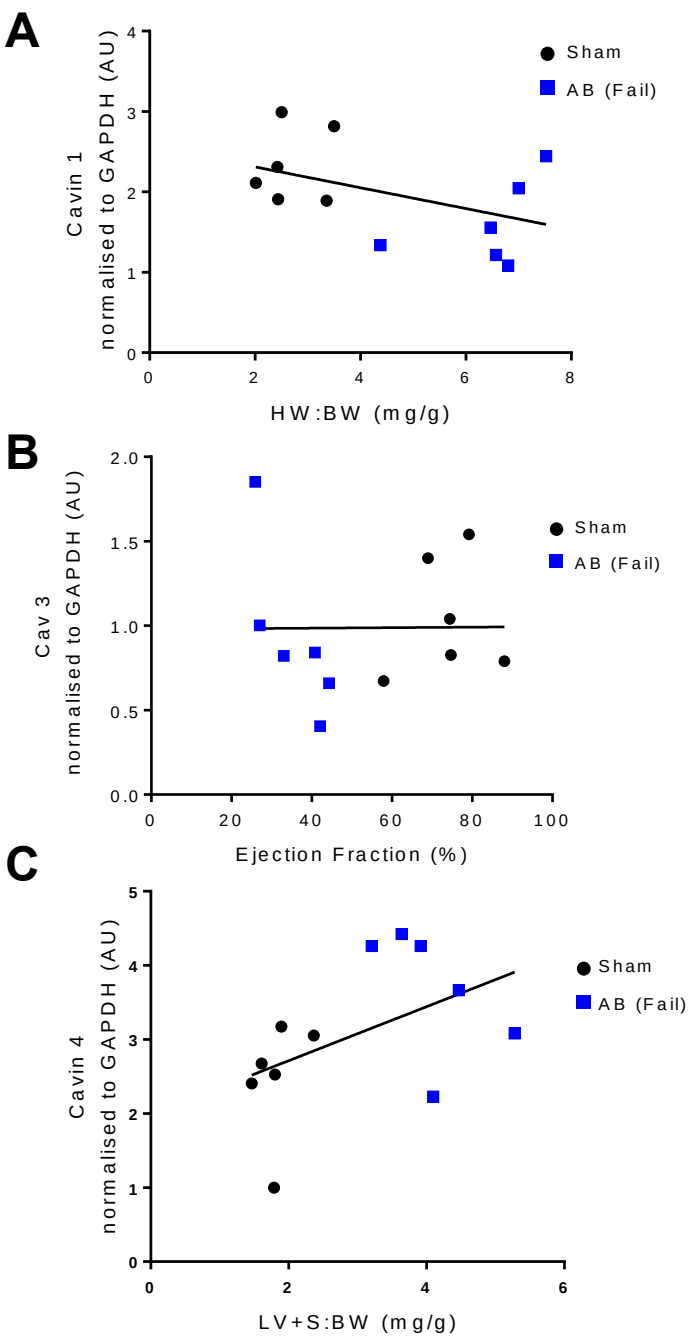

Figure 4-2 Caveolar protein correlated with heart measurements

A Cavin 1 protein expression plotted heart weight to body weight (HW:BW) ratios. **B.** Cav 3 protein expression plotted against ejection fraction (EF) recorded from haemodynamic measurements **C.** Cavin 4 protein expression plotted against left ventricular and septum (LV+S) weight normalised to body weight (BW).

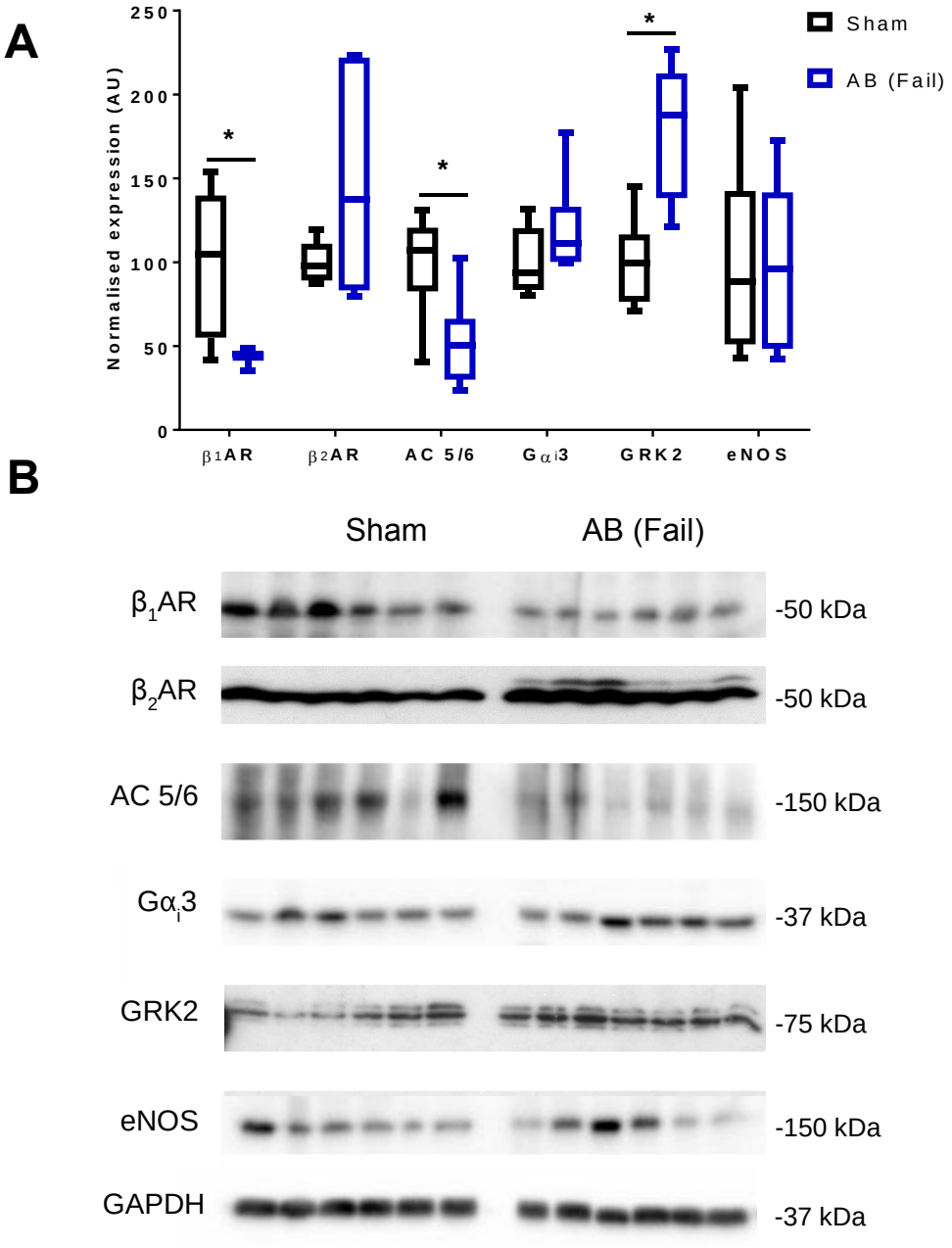

Figure 4-3 β-adrenergic (β-AR) signalling protein changes in left ventricular heart failure

A. Western blot of left ventricular muscle homogenised in Laemmli sample buffer, signal normalised to GAPDH and expressed as a percentage of mean Sham value, box and whisker graph. Sham n=6, AB n-6, Student t-test, *P<0.05, **P<0.01. **B.** Representative Western blot.

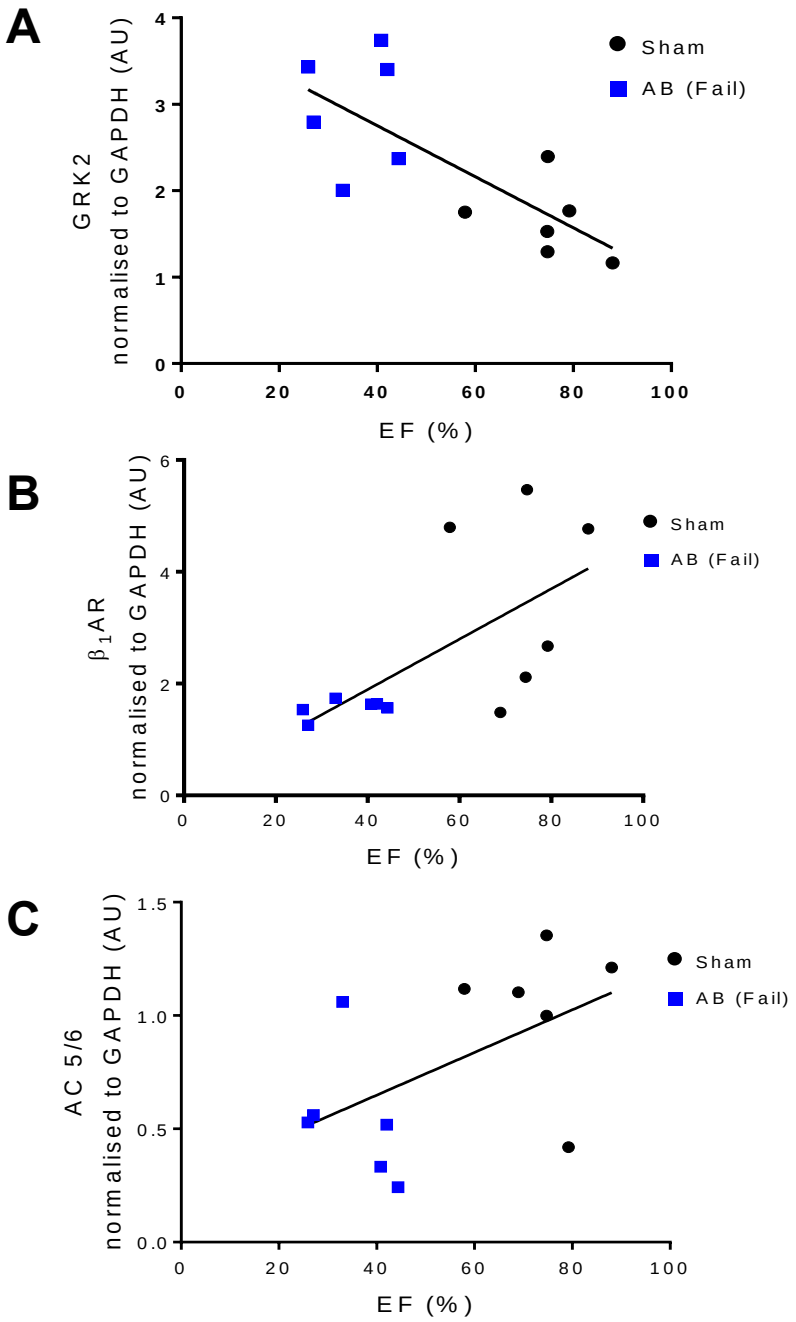

Figure 4-4 Correlation of βAR signalling proteins and ejection fraction

A. G-protein receptor kinase (GRK2) protein expression normalised to GAPDH plotted against ejection fraction (EF), R^2=0.566, (Persons correlation P<0.01). **B.** β_1AR protein expression normalised to GAPDH plotted against EF, R^2=0.412 **C.** Adenylyl cyclase (AC 5/6) protein expression normalised to GAPDH plotted against EF, R^2=0.281

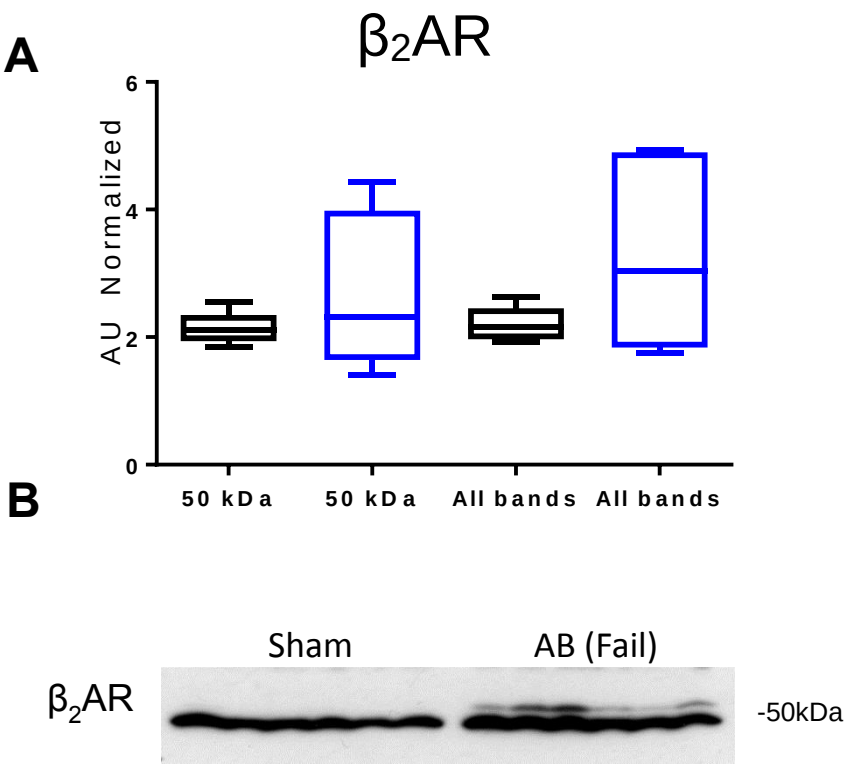

Figure 4-5 β_2-adrenergic (β_2AR) double band analysis

A. Western blot of left ventricular muscle homogenised in Laemmli sample buffer, signal normalised to GAPDH, box and whisker graph of band at 50 kDa only, and with the addition of the upper band. Sham n=6, AB n-6, Student t-test, *P<0.05, **P<0.01. **B.** Representative Western blot.

Protein expression of other βAR signalling proteins were also examined for links with functional measurements such as ejection fraction, heart weight (HW) to body weight (BW) and left ventricular (LV) weight to BW ratios with most showing no clear correlation (Figure 4-4). GRK2 expression did appear to be negatively correlated with function, as measured by ejection fraction (R^2=0.566) (Figure 4-4). Changes in protein expression from myocardial homogenate suggest altered remodelling of the caveolae and β-AR signalling complexes; the membrane distribution of these proteins also plays an important role in caveolae and β-AR function.

4.3.2. Altered protein membrane distribution following aortic banding

4.3.2.1. Caveolar proteins

Fractions are collected starting at the top of the sucrose gradient (5% sucrose) with fraction 1. Fraction 4 and 5, which sit at the boundary of the 5% and 35% sucrose, are the buoyant/caveolar containing fractions and fractions 9-12 are the heavy fractions which represent non-raft sarcolemma and cytosolic proteins (Wypijewski et al., 2015). Around 50-60% of total Cav 3 expression was located within the caveolar fractions, with a smaller percentage (20-30%) found within the heavy fraction (Figure 4-6), which is similar to previous results (Calaghan et al., 2008). There was no difference between the Sham and AB animals in Cav 3 distribution and no correlation between Cav 3 distributions and function, as measured by ejection fraction or time post-surgery (Figure 4-6). Cav 1 was found solely within the caveolar fractions for both AB and Sham animals (Figure 4-6). It was noted that the banding pattern for cavin 1 and cavin 4 was altered in fractionated samples compared with muscle homogenate samples. In myocardial homogenate a clear band was seen just above 50 kDa, whereas in the fractionated samples bands around 37 kDa and below were present (Figure 4-7). The predicted molecular weight for cavin 1 is 43 kDa, but it routinely runs at a higher molecular weight due to multiple post-translational modifications including phosphorylation and ubiquitination (Liu and Pilch, 2016). These lower bands could be the de-ubiquitinated form of the protein. Further experiments using a control peptide identical to the original immunizing peptide would determine whether the observed bands were truly cavin 1 or the result of non-specific antibody binding to a different protein. Given that such a peptide was not available at the time, the identity of the bands could not be confirmed. Cavin 4 has previously been shown to run at 43 kDa (Bastiani et al., 2009) which is lower than what is seen in the whole LV muscle homogenate (Figure 4-1). Due to uncertainty of banding pattern seen results were not analysed. Phos-tag gels were used to look at the phosphorylation state of cavin 1 in Sham and AB LV muscle homogenate. This revealed multiple bands (Figure 4-7). There was no difference between the AB and Sham groups in these phosphorylated bands, although analysis was slightly impaired by the intensity of the 50 kDa band.

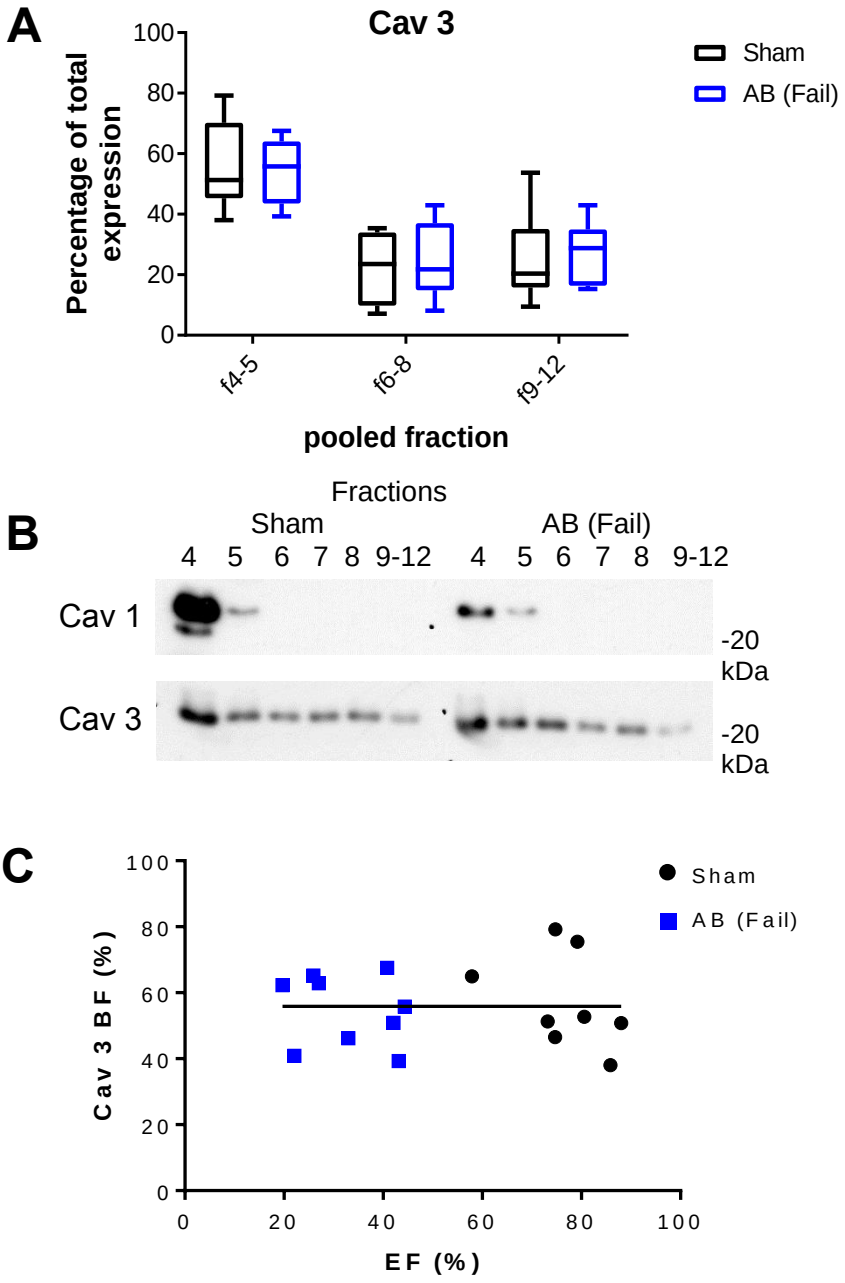

Figure 4-6 Caveolar protein membrane distribution changes in left ventricular heart failure

A. Western blot of left ventricular muscle homogenised in Na_2CO_3 buffer run on a sucrose gradient. Equal volumes of each fraction 4-8,(9-12) were loaded with equal total protein loading between AB and aged matched Sham. Protein expression in fractions expressed as a percentage of total expression from all fractions (4-12) box and whisker graph. Sham n=9, AB n-9, **B.** Representative Western blot. **C.** Percentage of Cav 3 expression located within the buoyant fractions plotted against ejection fraction (EF)

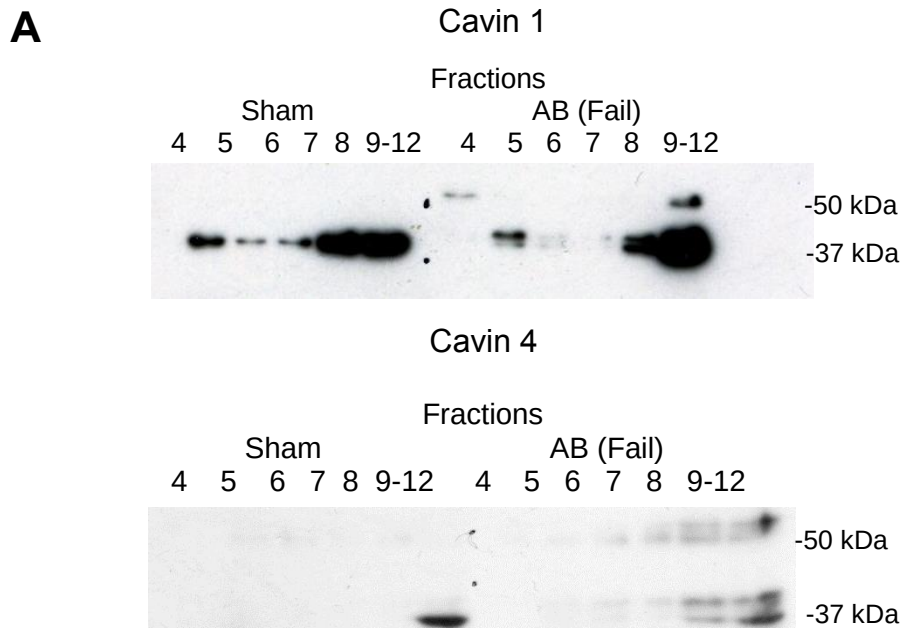

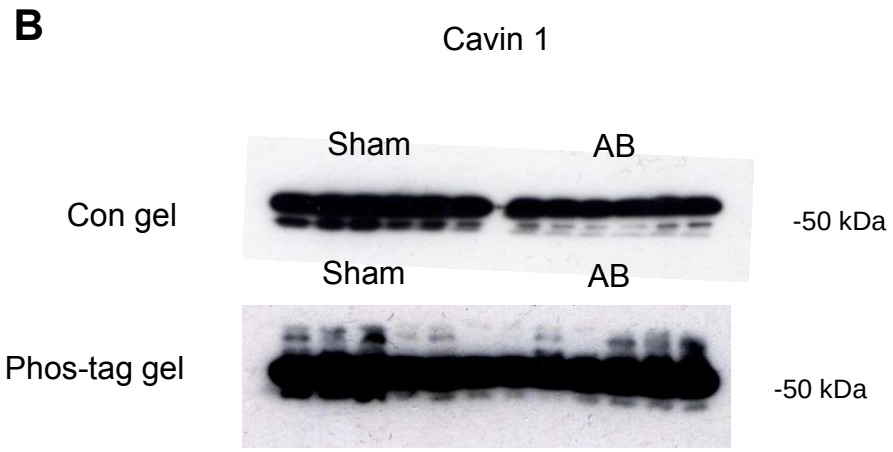

Figure 4-7 Caveolar protein membrane distribution and phosphorolation

A. Western blot of left ventricular muscle homogenised in Na_2CO_3 buffer run on a sucrose gradient. Equal volume of each fraction 4-8 +(9-12) were loaded with equal total protein loading between AB and aged matched Sham. Sham n=9, AB n-9, **B.** Representative Western blot of left ventricular muscle homogenate in Laemmli sample buffer with control and phos-tag gel.

4.3.2.2. β-adrenergic signalling proteins

Previous studies have observed that β_1AR can localise within the caveolar membrane or on the non-caveolar sarcolemma (Rybin et al., 2000). The predicted molecular weight of β_1AR is 51 kDa however when blotting for β_1AR there was often only a very faint band (or no band) around 50 kDa which made analysis of β_1AR distribution too variable to give meaningful results. The predicted molecular weight for the β_2AR is 46 kDa and β_2AR membrane distribution showed a clear band at 50 kDa in the caveolar fractions and in the heavy fractions. There was also a higher molecular weight band, which was apparent at high exposures in the LV homogenate sample, which only appeared in the caveolar fractions (Figure 4-8). This caused a significant increase in buoyant fraction to heavy fraction ratio in the AB animals compared to the Sham ($P<0.05$) (Figure 4-8). This higher molecular weight band was calculated to be around 63 kDa with the lower molecular weight band calculated at 55 kD, making an 8 kDa shift between the bands (Figure 4-9). This higher band was confirmed as β_2AR receptor with the use of a specific blocking peptide (Figure 4-9).

4.3.2.3. Additional β_2AR band

The molecular weight shift in the β_2AR in the buoyant fractions was thought to be too large to be caused by a phosphorylation. The β_2AR has previously been shown to have N-linked glycosylation which promote targeting to the caveolae and affect the receptor's binding to $G\alpha_i3$ (Rybin et al., 2003). The additional sugar moiety from glycosylation could explain this size shift. To test to see if the band at 63 kDa could be a glycosylated version of β_2AR, PNG-ase F was used on samples from fraction 4 and 5 to cleave the N-linked glycosylation. This should result in a single band analysed with Western blotting. After a number of attempts using the PNG-ase F on the fractionated samples, with no change seen in the molecular weight of the bands (Figure 4-9), and consulting the product manufacturers about the salt and sucrose concentrations which may affect the reactivity of the PNG-ase F enzyme, it was decided to run an experiment and replicate the conditions from the original paper which reported glycosylation of the cardiac β_2AR (Rybin et al., 2003).

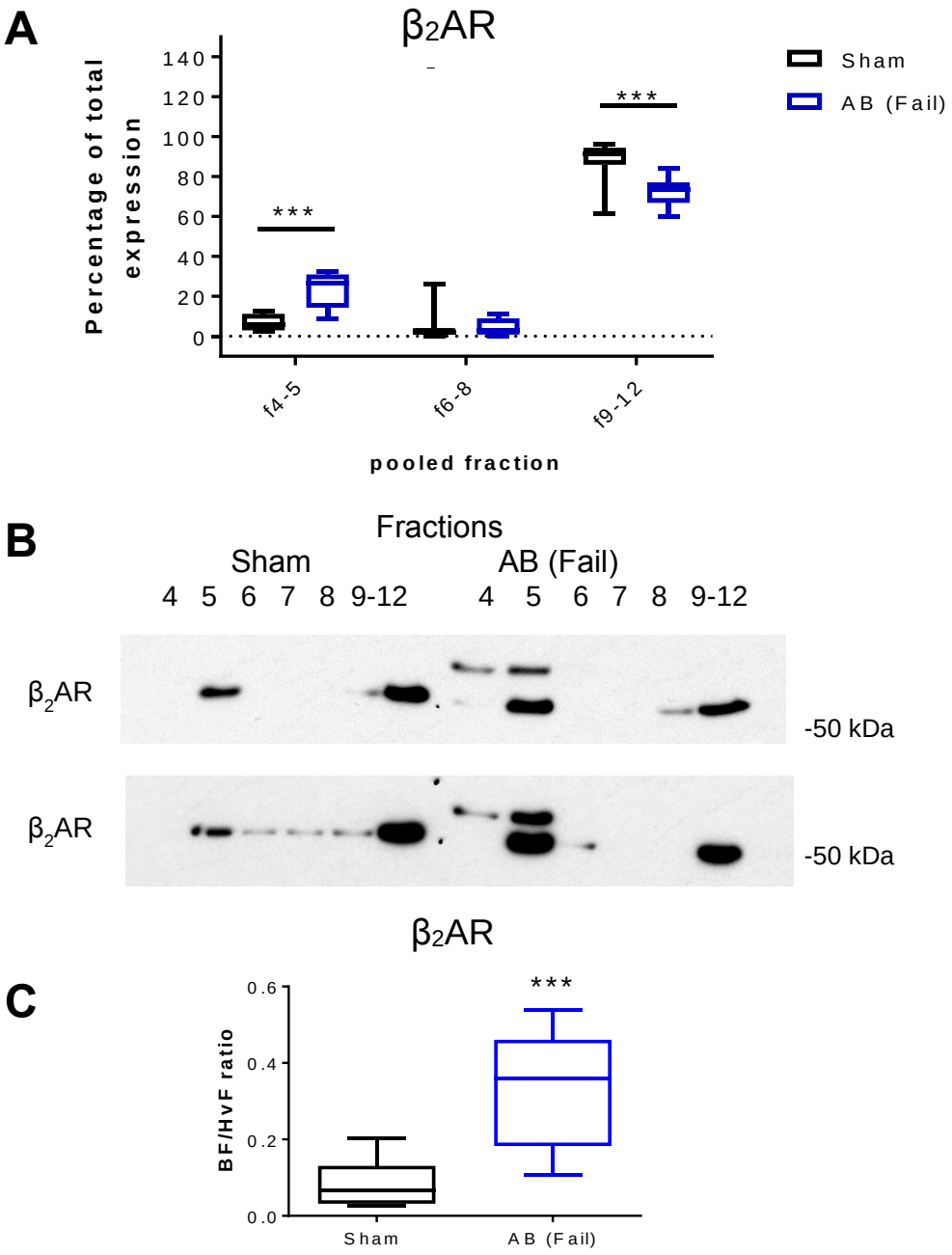

Figure 4-8 β_2AR protein membrane distribution changes in left ventricular heart failure

A. Western blot of left ventricular muscle homogenised in Na_2CO_3 buffer run on a sucrose gradient. Equal volume of each fraction 4-8 + (9-12) were loaded with equal total protein loading between AB and aged matched Sham. Protein expression in fractions expressed as a percentage of total expression from all fractions (4-12) box and whisker graph. Sham n=9, AB n-9, **B.** Representative Western blot. **C.** Buoyant fraction (fraction 4+5) (BF) to heavy fraction (fractions 9-12) (HvF) ratio, percentage of totally expression in sample, Sham n=9, AB n=9, student t-test ***P<0.01.

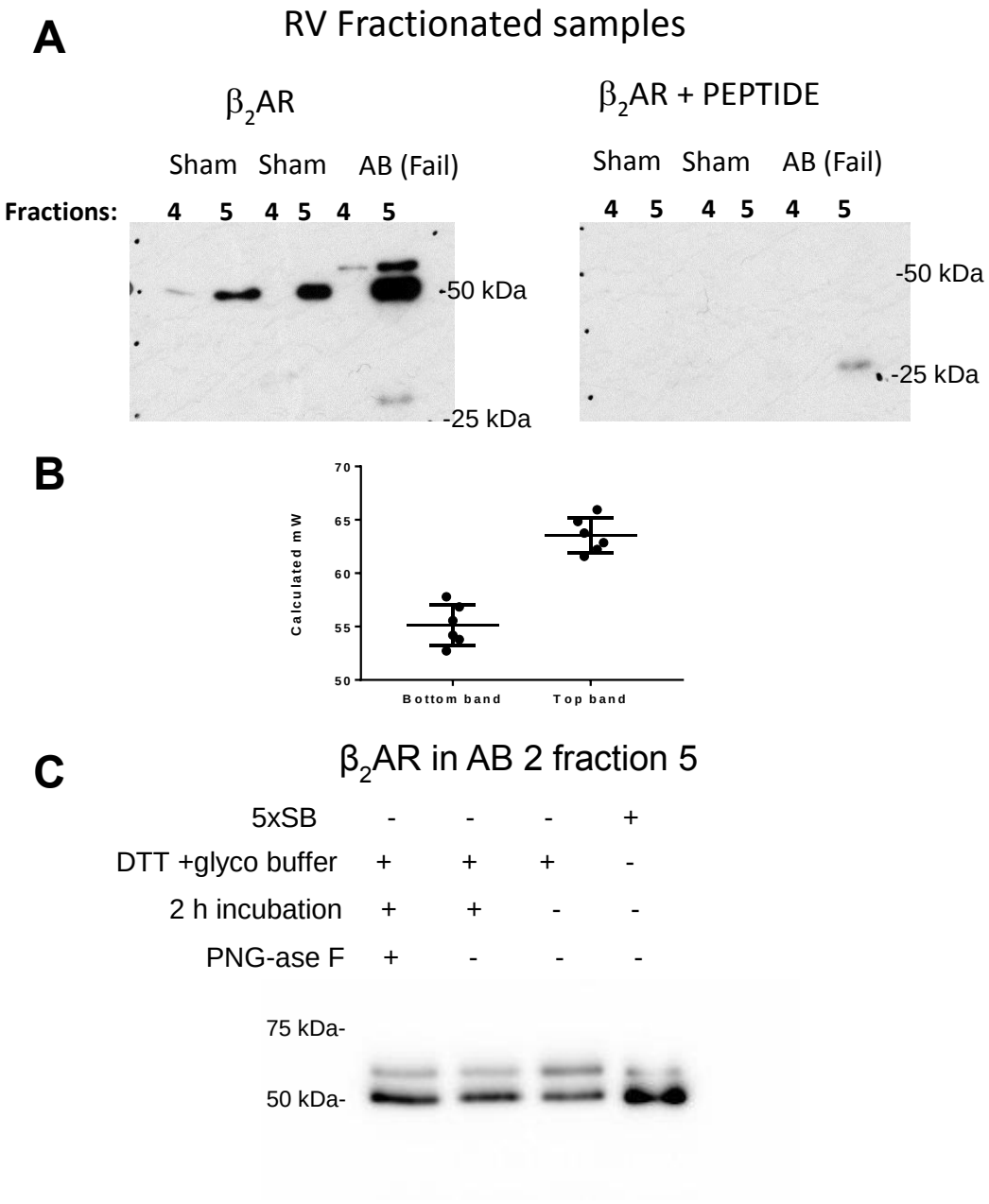

Figure 4-9 β_2AR higher molecular weight band calculations

A. Western blot of left ventricular muscle homogenised in Na_2CO_3 buffer run on a sucrose gradient with and without the pre-incubation of primary antibody with antibody peptide to test for specific banding, **B.** Molecular weight of higher band was calculated by plotting the molecular weight marker and calculating the exponential line, this was then used to calculate the predicted weight from the migration distance of the lower and higher bands. **C.** Example of PNG-ase F experiment testing different conditions and controls on sample from fraction 5 in Na_2CO_3 AB (Fail) animals. Sample buffer (SB), glycosylation buffer (glycol buffer)

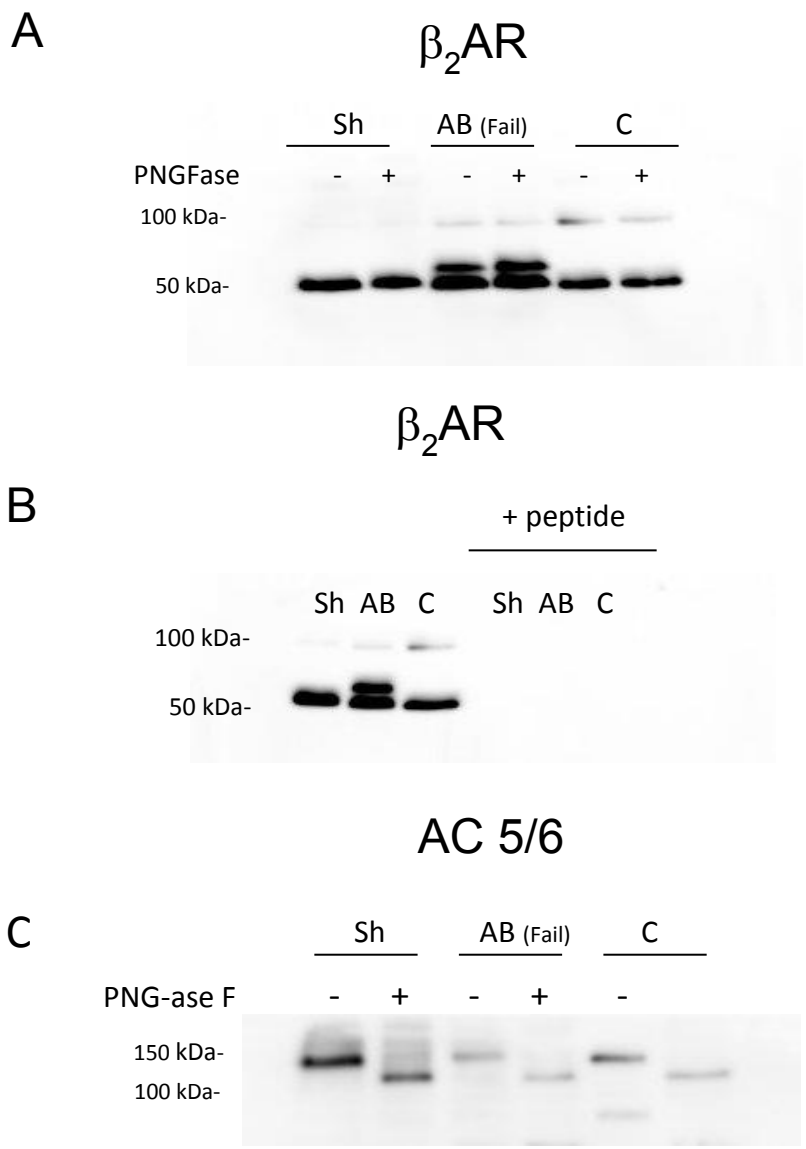

Figure 4-10 De-glycosylation by PNG-ase F.

A ~20 µg samples of Sham (Sh), aortic banded (AB (Fail)) homogenised left ventricle and homogenised cells (C) were incubated for 2 h with PNG-ase-F or equivalent volume of 50% glycerol in dH_2O before Western blot for β_2AR. **B.** Identical samples run on a separate Western blot with and without pre-incubation of β_2AR primary antibody with peptide. **C.** Membrane A was stripped and re-probed for AC to ensure enzyme was active.

LV muscle which had been homogenised in Laemmli sample buffer was used in the test run as this contained a lower salt and sucrose content, and had previously been seen to contain the 63 kDa band. Of note, Rybin et al. 2003 also characterised the difference between isolated adult cardiac myocyte samples and whole ventricular homogenate in rat. The experimental run to replicate Rybin et al. 2003 included freshly isolated cardiac myocytes which were homogenized in cell buffer, on the day of the experiment (Figure 4-10). To ensure that all of the bands were correctly identified as β_2AR, samples were tested with the epitope blocking peptide provided with the antibody (Figure 4-10). The addition of PNG-ase F caused no change in the molecular weight in any of the bands. The molecular weight of the band seen in the isolated cardiac myocytes sample was identical to that in the LV homogenate; this differs from what was previously seen in isolated adult cardiac myocytes, which ran at a lower molecular weight. Rybin et al. had previously looked at the glycosylation of other proteins within cardiac myocytes using PNG-ase F (Rybin et al., 2000). In this earlier paper, AC 5/6 was shown to migrate at a higher than predicted molecular weight due to N-linked glycosylation which, after PNG-ase F treatment, shifts to a molecular weight around 120 kDa. The PVDF membrane in Figure 4-10.A. was washed in Western blotting stripping buffer, to remove primary and secondary antibodies, and re-probed with a AC 5/6 antibody to test if the enzyme was working in the set conditions used to produce a similar result to the Rybin et.al (2000). With the addition of PNG-ase F there was a shift in molecular weight of the band for Sham and AB LV homogenate samples, as well as the isolated cardiac myocytes sample, suggesting that the enzyme was working in the conditions used. From this it was concluded that the 63 kDa band observed was not caused by an N-linked glycosylation of β_2AR.

4.3.3. Correlations in protein expression

A correlation between Cav 1 protein expression and function was noted earlier in the chapter (Figure 4-1.). Cav 1 was seen to be solely located within the caveolar fractions; this is where the increase in β_2AR expression was seen. When comparing myocardial Cav 1 expression with β_2AR expression in the buoyant fractions there was a significant negative correlation (R^2=0.682)(Pearson's $P<0.05$) (Figure 4-11). When comparing the percentage of β_2AR expression within the buoyant fraction with function (ejection fraction) there is a slight negative correlation (R^2=0.595)(Pearson's $P<0.05$) (Figure 4-11).

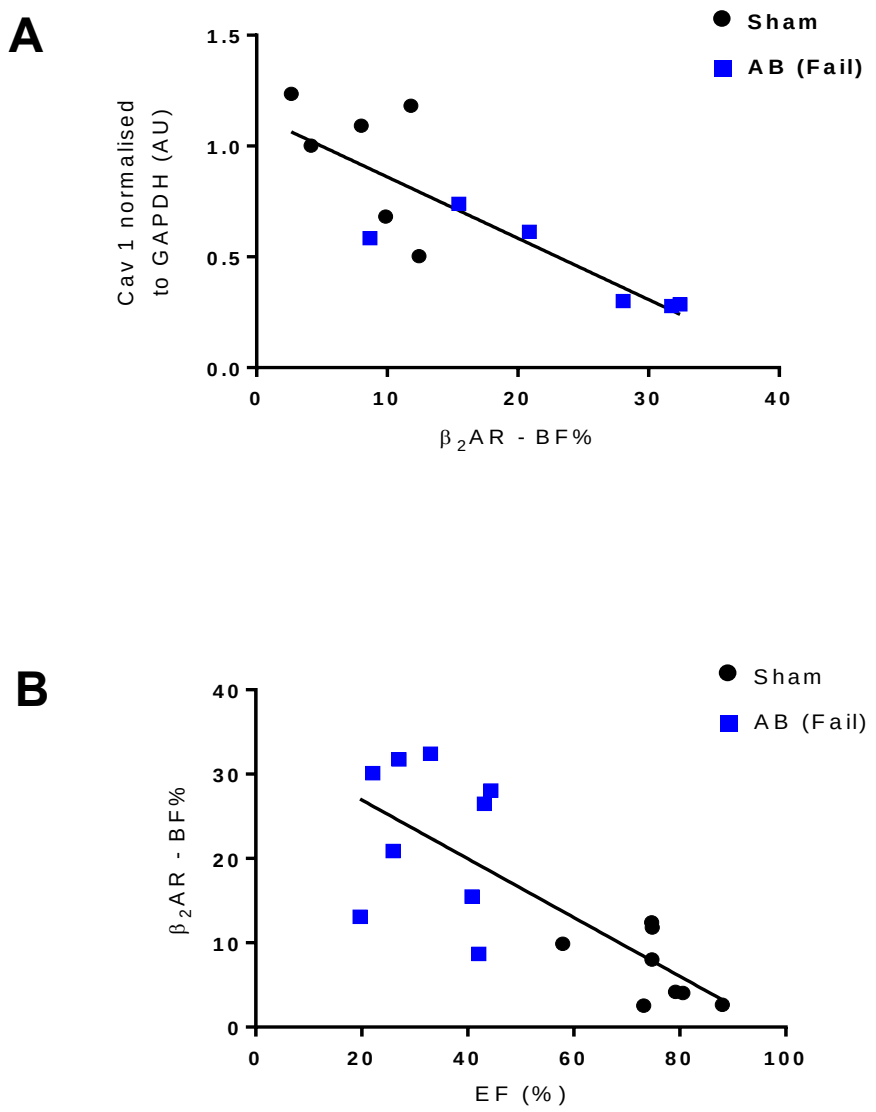

Figure 4-11 Correlation data.

A. Cav 1 protein expression normalised to GAPDH plotted against percentage of β_2AR total expression located in the buoyant fraction, R^2=0.682, P<0.05 **B.** Percentage of β_2AR total expression located in the buoyant fraction against ejection fraction (EF) as recorded from haemodynamic experiments R^2=0.588, P<0.05

4.4. Discussion:

One of the advantages of the aortic banding model is the detailed collection of functional data which can be linked with protein expression in LV homogenate as well as distribution of membrane proteins. Ventricular remodelling should also be consistent throughout the ventricle due to the effect of pressure overload on the whole chamber, unlike the more regional variations in remodelling seen with myocardial infarction models. Aortic banding in rat is an established model of heart failure and has been successfully employed numerous times to examine a multitude of cardiac parameter, from global function to protein and mRNA expression (Pacher et al., 2004; Feldman et al., 1993; Tsutsui et al., 1993).

A handful of studies to date have examined the impact of pressure-overload on the β-AR and other components of caveolae. Kikuchi et al. measured an increase in Cav 3 protein expression in a model of pressure overload in rat (Kikuchi et al., 2005). In this paper animals were banded for 28 days before blood pressure measurements were taken from the right carotid artery. The carotid artery hemodynamic measurements along with the LV to body weight ratios in Kikuchi et al. are more comparable to the AB (H) within this study than the AB(Fail) group. In the present study, LV to bodyweight ratio in the AB(Fail) group is double that of Sham, compared to the 27% increase reported by Kikuchi et al. In some initial Western blots performed on a small group of Sham and AB without reduced EF, animals Cav 3 protein expression in myocardium was increased (data not shown): this may be an initial compensatory mechanism in response to elevated afterload on the heart. A canine pressure overload model produced a reduction in β-AR receptor number as well as reduced responsiveness to stimulation (Vatner et al., 1984). Isolated cardiac myocytes from hypertrophied hearts induced by aortic banding in rat show a reduced sarcoplasmic reticulum Ca^{2+} ATPase (SERCA2a) activity as well as an impaired response to stimulation by isoprenaline (Miyamoto et al., 2000). Some of the remodelling responses of the heart to pressure overload have been shown to be reversible with SERCA therapy and unloading of the heart in animal models (Dadson et al., 2016; Miyamoto et al., 2000). Although these treatments were applied after a relatively short period of time it does show that the myocardium may hold some reverse re-remodelling potential. Reverse re-modelling of protein and gene expression has been reported in heart failure patients fitted with left ventricular assisted devices (LVAD) which helps to unload the heart in a bridge to transplantation (Uray et al., 2003; Heerdt et al., 2000; Uray et al., 2002).

4.4.1. Caveolin 3

One of the surprising findings from experiments using this model of heart failure was the lack of effect on Cav 3, protein expression (left ventricular muscle homogenates) and distribution across the membrane (from sucrose gradient fractionation). Cav 3 has been the focus of many studies linking change in Cav3/caveolae with cardiac function (Wright et al., 2014; Woodman et al., 2002; Feiner et al., 2011). In mice cardiac specific Cav-3 over expression is cardio protective and attenuates cardiac hypertrophy (Horikawa et al., 2011; Markandeya et al., 2015) as well as mimicking ischemic preconditioning (Tsutsumi et al., 2008). On the other hand, deletion of the Cav 3 gene in the heart results in loss of cardiac caveolae, hypertrophic dilation and reduced fractional shortening (Woodman et al., 2002). Wright et al. have used adenoviral transfection with a mutant Cav 3, which lacks three nucleotides within the caveolin scaffolding domain (CSD) and acts in a dominant negative fashion (preventing effective binding to CSD), to disrupt the regulatory control of Cav 3 on β_2AR signaling. This has a similar impact to that observed in the myocardial infarction model of heart failure. This phenotype in heart failure was rescued when Cav 3 was over expressed (Wright et al., 2014). The conclusion that this is only due to Cav 3 however is based on; the assumptions that there are no caveolae within the t-tubules; that Cav 3 has a direct regulatory action on β_2AR; and that functional changes are not achieved through other proteins within the micro domain the caveolae creates. The Cav dominant negative used in this study resulted in a significant decrease in caveolae as seen by electron microscopy (Wright et al., 2014).

There are many key contractile proteins which are found to co-localise with Cav 3 in caveolae including a sub-population of L-type Ca^{2+} channels. L-type Ca^{2+} channels (LTCC) are responsible for triggering Ca^{2+} induced Ca^{2+} release and the majority are involved in EC coupling (Bers, 2002). Cav 3 plays a crucial role in regulating the phosphorylation of L-type Ca^{2+} channel within the t-tubules (Bryant et al., 2014). This was determined by disrupting the Cav 3 scaffolding domain with a trans-activating transcriptional activator sequence (TAT)-tagged peptide (C3SD) (MacDougall et al., 2012), which resulted in a decrease in staining intensity of a phospho-specific LTCC antibody within the transverse striations (Bryant et al., 2014). The A-kinase anchoring protein 5 (AKAP5) aid in targeting AC, PKA and a sub-population of LTCC to Cav 3 complexes in the membrane (Hall et al., 2007). In a AKAP5 KO mouse model, only the subpopulation of LTCC bound with Cav 3 is found to be phosphorylated by PKA via sympathetic stimulation (Nichols et al., 2010). The presence of Cav 3 within the dyad however is contested when imaging cardiac myocytes using super

resolution microscopy. Although the presence of Cav 3 staining in immunocytochemistry of cardiac myocytes within the t-tubules and co-localised with the RYR2 is high, Cav 3 is thought to be excluded from the majority of RYR2 junctions, suggesting exclusion from the dyad (Jayasinghe et al., 2009; Wong et al., 2013). This sub-population of LTCC which is presents in the Cav 3 complexes has shown not to be involved in EC coupling in feline cardiac myocytes (Makarewich et al., 2012). Instead this sub-population is suggested to modulate the size of the cardiac myocyte (Makarewich et al., 2012).

4.4.2. Caveolin 1

Published studies often conclude that Cav 3 is the only important caveolar protein in cardiac myocytes and that Cav 1 does not exist in these cells (Taniguchi et al., 2016; Wunderlich et al., 2006). Many studies of KO Cav 1 mouse models which see cardiac re-modelling and reduced cardiac function completely rule out any possible change to the cardiac myocytes and explain the cardiac remodelling entirely through other cells located within the heart (Zhao et al., 2002; Murata et al., 2007). The presence of Cav 1 in cardiac myocytes is discussed in a Chapter 7.

Caveolin 1 has been demonstrated to be expressed in cardiac myocytes from different species including humans (Hagiwara et al., 2002; Yang et al., 2010; Robenek et al., 2008; Wunderlich et al., 2008; Kozera et al., 2009), although its presence in the cardiac cell is not universally accepted (Chapter 7). Despite knock-out (KO) of Cav 1 not affecting the formation of caveolae in the cardiac myocytes this does not rule out any other functional roles it may have within the cell. Uray et al. found a significant increase in both protein and mRNA levels of Cav 1 in human ventricular tissue after LVAD insertion with no change in Cav 3 protein levels (but an increase in mRNA), when compared to tissue samples from before fitting of the device (Uray et al., 2003). The role of Cav 1 within the cardiac myocyte has been somewhat overlooked so far. In the model of heart failure used in the current study there was a correlation between Cav 1 protein expression and cardiac function as measured by ejection fraction. More recently, there has been some interest in Cav 1's functional role within the cell (Bai et al., 2016) – see Chapter 7.

4.4.3. Cavins

In the last 5 years, the cavin proteins have been discovered to play an important role in caveolae formation and function within the cardiac myocyte (Briand et al., 2011). KO of cavin 1 reduced the number of caveolae in cardiac myocytes (Liu and Pilch, 2008). Increased

cavin 4 expression in the heart has been linked with increased hypertrophy (Ogata et al., 2014). Overexpression of the coiled-coil domain in cavin 4, by plasmid transfection, in the heart also increased interstitial fibrosis (Naito et al., 2015). Cavin 4 protein expression in this model of heart failure is significantly increased compared to Sham animals in association with a significant increase in LV+S:BW ratio and fibrosis within the myocardium. Unfortunately there were not enough measurements of fibrosis to match these directly with cavin 4 expression in individual animals to see if there is link between the two. No correlation was seen between cavin 4 expression and LV:BW or HW:BW. Dissected organ ratios cannot be directly used as an indication of fibrosis, as there also appeared to be an increase in cell size, most likely from cellular hypertrophy (Korecky and Rakusan, 1978). A more recent study has linked a KO of the cavin 1 gene with an increase in fibrosis in cardiac tissue (Taniguchi et al., 2016). However, in the present study there was no obvious correlation between cavin 1 protein expression and fibrosis measurements collected. It was not possible to measure the distribution of the cavin proteins within the membrane due to multiple banding patterns which may be explained by cavin protein degradation within the samples. These samples were collected over a period of over a year, and stored in Na_2CO_3 at -20 ^{o}C during this time. Even with protease and phosphatase inhibitors this may not prevent de-ubiquitination of proteins. The storage solution was detergent free, due to the nature of the sucrose gradient fractionation experiment, meaning that break down of tissue is reliant upon the homogenisation which may not effectively expose all the cellular content to protease and phosphatase inhibitors.

4.4.4. β-AR changes in heart failure

Hearts from the aortic banded animals in this study, in general, showed a decrease in protein expression of β-AR signalling components promoting cAMP signalling and an increase in the inhibitory components. Although β_2AR protein expression in LV myocardium did not change, the β_2AR membrane distribution changed, with an increase in expression in buoyant fractions due to the presence a higher molecular weight band. In heart failure, reduction in β_1AR protein expression as well as mRNA expression is routinely observed which is linked to a decrease in β-AR responsiveness (Hata et al., 2004; Engelhardt et al., 1996). The reduction in β_1AR is routinely seen in rat models of heart failure and is linked with a blunted response to β-AR stimulation (Gorelik et al., 2013; Zhu et al., 2003; Houser et al., 2012). GRK2 is activated by β-AR signalling and phosphorylates the activated β-AR targeting the receptor for internalisation. An increase in GRK2 protein and mRNA has been linked with a reduced β_1AR expression and reduced cardiac function in human heart failure

(Freedman et al., 1995; Ungerer et al., 1993b). In the present study there is a significant increase in GRK2 protein expression in AB animals which is correlated with a reduction in function. This would promote binding of β-arrestin and uncoupling of the β-AR from cognate G-protein subunits. AC 5/6, are key signalling proteins in the β-AR signalling pathway which are often reported to be down regulated and uncoupled from the β-AR in heart failure (Marzo et al., 1991; Bristow et al., 1989). In the present model of heart failure there is a decrease in protein expression of AC, again this would be expected to contribute to reduced β-AR intracellular signalling.

While β_1AR is commonly seen to be reduced in the failing heart, there is often no change in protein expression of the β_2AR subtype which causes a shift in the β_1AR:β_2AR ratio (Steinfath et al., 1992). A reduction in total cardiac β_1AR protein expression is recorded in the banded animals in this study, with no change in β_2AR expression. This decreases the β1AR:β2AR. β_2AR differs to β_1AR in its ability to couple both Gαs or Gαi enabling stimulation or inhibition of AC production of cAMP (Xiao, 2001). The downstream cAMP production of β_2AR differs from that of the β_1AR which produces a more global response, due to several mechanisms including Gαi coupling, and regulation through phosphodiesterases (PDEs) (Isidori et al., 2015). This in part has been shown to be caused by regulation through caveolae (MacDougall et al., 2012). When cholesterol was depleted by methyl-β-cyclodextrin (MBCD) in isolated cardiac myocytes, which disrupts caveolae, there was an increase in fractional shortening and Ca^{2+} transient amplitude in response to β_2AR stimulation (Haque et al., 2016; MacDougall et al., 2012).

Studies aimed at clarifying the effects of induced heart failure on cardiac β AR signalling tend to agree on findings relating to β_1AR but disagree in relation to β_2AR (Zhu et al., 2012; Nikolaev et al., 2010). Experiments in failing rat cardiac myocytes which used FRET-based biosensors to image cAMP signalling demonstrate a reduction to selective β_1AR signalling while β_2AR signalling increased (Nikolaev et al., 2010; Gorelik et al., 2013). By contrast in failing mouse cardiac myocytes, the contractile response to β_2AR stimulation was reduced, which was in part due to a $G\alpha_s$ to $G\alpha_i$ switch mediated by GRK2 (Zhu et al., 2012). The location of the β_2AR is also contested; at a membrane level, some results from sucrose gradient fractionations show the β_2AR solely within the caveolae containing fractions (Rybin et al., 2000; Xiang et al., 2002) while others show it distributed throughout the membrane (MacDougall et al., 2012; Head et al., 2006). At a cellular level there are also conflicting results as to whether the β_2AR is located and active only within the t-tubule

membranes (Nikolaev et al., 2010) or whether there is a cell surface component too (Wright et al., 2014). The disparity in results may, however, highlight the dynamic and complex signalling of the β_2AR. Different approaches to studying function divergent methods of preparing cardiac myocytes may also contribute.

4.4.4.1. Higher molecular weight band β_2AR

In Western blotting of myocardial homogenates and fractionated samples an additional higher molecular weight band for β_2AR was observed. This higher molecular weight band appeared at around 63 kDa, was found only within the caveolar fractions and is most likely to be a post translational modification. This was not an N-link glycosylation, as it is not sensitive to PNG-ase F. This result contradicts what has previously been reported of the β_2AR in adult ventricular myocardium (Rybin et al., 2003). Rybin et al. proposed that all β_2ARs are glycosylated in the ventricles which aids in migration of the receptor to the caveolar membrane. PNGase-F was used to test for N-linked glycosylations in both these experiments, with the main difference between these two experiments being the β_2AR antibody used. Rybin et al. use a commercially available antibody sourced from Santa Cruz which targets a 20-30 amino acid region close to the C terminus. The antibody used in the present study was from Alomone and targets N-terminal amino acids 14-30 (Figure 4-12). There are two N-linked glycosylation sites in the β_2AR, N^6 and N^{15}, with a third glycosylation site in humans 187^{EL2} (Selvam et al., 2012). The second amino acid recognition site of the Alomone antibody cross over the N^{15} site; this should not have an effect on protein recognition as the proteins are de-natured and tertiary structures removed before addition of PNG-ase F, but it may cause recognition issues. Another point of interest is the difference between the molecular weight of the band in isolated cardiac myocytes and homogenised ventricular myocardium. In this study there is no difference in molecular weight, compared to the Rybin et al. study where the molecular weight of β_2AR in isolated cardiac myocytes is lower, which is reasoned to be due to the cleavage of the N-linked glycosylation site (Rybin et al., 2003). One explanation could be that the Alomone antibody does not recognise the glycosylated form of β_2AR, although this would then suggest a large amount of β_2AR is un-glycosylated within the membrane. This however does highlight the issues with studying these complex and dynamic GPCR within the heart. If antibodies supplied do not recognise the correct protein, or all possible version of the protein then a false positive result could be obtained.

A

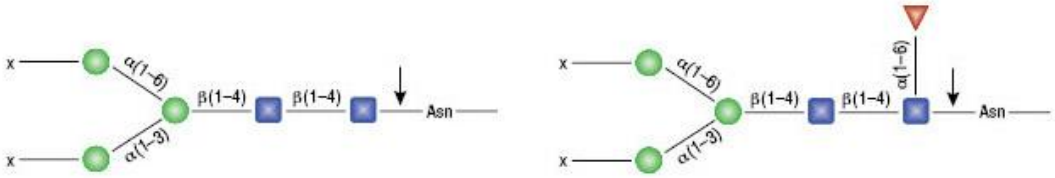

A. PNGase F can cleave when an a1–6 Fucose is on the core GlcNAc

B

RAT – β_2AR – protein FASTA

MEPHG **N** D SDFLLAP **N** G SRAPGHDITQERDEAWVVGMAILMSVIVLAIVFGNVLVITA
IAKFERLQTVTNYFITSLACADLVMGLAVVPFGASHILMKMWNFGNFWCEFWTSIDVLCVTA
SIETLCVIAVDRYVAITSPFKYQSLLTKNKARVVILMVWIVSGLTSFLPIQMHWYRATHKQAIDC
YAKETCCDFFTNQAYAIASSIVSFYVPLVVMVFVYSRVFQVAKRQLQKIDKSEGRFHAQNLSQ
VEQDGRSGHGLRRSSKFCLKEHKALKTLGIIMGTFTLCWLPFFIVNIVHVIRANLIPKEVYILLNW
LGYVNSAFNPLIYCRSPDFRIAFQELLCLRRSSSKTYGNGYSSNSNGRTDYTGEQSAYQLGQEK
ENELLCEEAPGMEGFVNCQGTVPSLSIDSQGRNCNTNDSPL

Figure 4-12 PNG-ase F action and β_2AR amino acid protein sequence

A. Figure modified from BioLabs® PNGase F description, arrow demonstrates where the sugar molecule is cleaved from its N-link to the target protein **B** FASTA protein sequence taken from PUBMed of *Rattacus* β_2-ardernergic receptor (β_2AR). The two "N" underlined are the residues where N-linked glycosylation occurs, highlighted in blue is the target epitope sequence for the Alomone antibody, highlighted in orange is the range of amino acids in which a 20-30 epitope is targeted (SantaCruz does not give specific target sequences)

The higher molecular weight band in this study was only seen in the buoyant fractions, so is only found within caveolae (or other lipid rafts). This band was also predominantly within the banded animals, which may suggest a switch in function. The percentage of total β_2AR expression located in the caveolar fractions, when plotted against the Cav 1, shows a negative correlation; this might suggest a regulatory control of Cav 1 with recruitment of β_2AR to the caveolae. There was also a slight negative correlation of the percentage of β_2AR total expression located within the caveolae fractions and function, as measured by ejection fraction.

4.5. Limitations

There are many different approaches to studying molecular changes in cardiac myocytes, with each possessing advantages and disadvantages. Studying changes in protein expression and distribution offers a snap-shot of the molecular mechanisms and can suggest links to changes that may be occurring, even if myocyte contraction and $[Ca^{2+}]_i$ cannot be studied. High resolution imaging gives an idea of 3-D structure and architecture of fixed cells and enables visualisation of possible intersections. Using live intact cells to test function through techniques such as patch clamping can give a detailed knowledge of the cells' functional capacity. One of the difficulties in studying the caveolae and β-ARs is the dynamic nature of these proteins which can show rapid change in sarcolemmal location in response to a stimulus (Wypijewski et al., 2015). Differences may arise in cellular and tissue processing due to stress on animals/tissue or mechanical handling.

4.6. Conclusion

The results from this animal model provide an insight into possible links between heart failure and caveolar protein localisation and function, adding to the growing wealth of information in this area of research. Reduction in Cav 1 and cavin 1 protein expression suggest possible disruption to caveolar organisation within the heart, which coupled with the Cav 1 correlation with function may induce negative functional effects on the heart. The changes in β_2AR membrane location and the addition of a post-translational modification may indicate a change in signalling of the β_2AR which is again seen to be linked with a deterioration in cardiac function.

Chapter 5. β-adrenergic responses in right ventricular heart failure

5.1. Introduction:

Right ventricular (RV) heart failure is the leading cause of death in patients with pulmonary artery hypertension (PAH). PAH causes an increased afterload on the RV resulting in hypertrophy of the ventricle, which eventually develops into RV failure. The prognosis for PAH patients is poor, with one third of patients dying within the first three years of diagnosis (Humbert et al., 2010). Current treatment strategies for PAH target the remodelling in the pulmonary vasculature and the increased pressure in the pulmonary arteries. No treatments are directly targeted at improving the failing RV (Gurtu and Michelakis, 2015).

β-adrenergic desensitisation is common in both RV (Bristow et al., 1992) and LV (Ungerer et al., 1993b) heart failure, secondary to an increase in sympathetic drive, and is characterised by decreased β_1AR expression and receptor uncoupling (Bristow et al., 1982). Increased sympathetic drive is a compensatory response to increase cardiac output and is essential in periods of increased metabolic demand. However chronic sympathetic stimulation leads to maladaptive changes in the myocardium. β-blockers are routinely prescribed to treat LV failure and have been shown to improve the β-AR functional response and receptor coupling, however the use of β-blockers in PAH leading to RV failure is controversial. When faced with increased afterload, the RV does not have the same ability to increase force as the LV (MacNee, 1994). Heart rate is suggested to play a vital role in maintaining sufficient RV cardiac output, so the possible negative chronotropic actions of β-blockers may not to be well tolerated. Contrary to this, there are emerging studies (de Man et al., 2012; Bogaard et al., 2010) which support the benefits of treating animal models of PAH with β-blockers, but none have yet looked at the direct effect on the β-ARs.

Monocrotaline (MCT) induced PAH and RV failure is a well-established model within the research group (Stones et al., 2013; Benoist et al., 2011; Benoist et al., 2012; Fowler et al., 2015). Treatment with the selective β_1AR antagonist metoprolol has previously been shown to significantly improve the median survival of MCT animals from day 23 (post MCT injection) to day 31 ($P<0.05$) (Fowler and 2016). MCT induced PAH closely mimics the cardiovascular remodelling observed in PAH human patients, making it an appropriate

model for studying metoprolol treatment and the effect on βAR receptors and signalling. Metoprolol treatment does not prevent heart failure in this animal model, but enables the heart to maintain function for longer under increased pulmonary pressure (Fowler and 2016).

The aim of this chapter was to investigate the effects of β-blockers on the RV in the MCT model, focusing on β-AR function. All functional experiments were performed around the median day that the MCT group went into failure. Two different heart preparations were used to look at βAR function in these animals, isolated cardiac myocytes and sections of free running heart muscle from the ventricular wall (trabeculae carneae). The trabeculae carneae are composed of linearly arranged myocytes and are commonly used to study myocardial force production (Hunter et al., 1998; Goo et al., 2009).

5.2. Methods:

For isolated cardiac myocyte experiments male Wistar rats (target weight 200 ± 20 g) received an intra-peritoneal injection of saline (CON) or 60 mg/kg of monocrotaline (MCT) as described in Methods (Section 2.1.2). MCT induces PAH and RV hypertrophy which progresses to RV heart failure, when clinical signs of heart failure are apparent (e.g. weight loss, lethargy) (Benoist et al., 2012). From 15 days post MCT injection a voluntary oral dose of placebo solution (Sucrose 0.3 M in Ribena® and water) was given to the MCT and CON group, and a β-blocker solution (metoprolol 4.68 mM in placebo solution) was given to the MCT+BB group, at 8 mL/kg body weight/daily.

At the designed end point, cardiac myocytes were isolated from the RV and LV as described in Methods (Section 2.4). Cell shortening and $[Ca^{2+}]_i$ transients were simultaneously recorded in RV myocytes field stimulated at 1Hz and loaded with the fluorescent Ca^{2+} indicator FURA-2 AM (1 μM). Cell shortening was expressed as a percentage of resting cell length. Selective β-AR stimulation was achieved with either the β_1AR agonist isoprenaline bitratrate (ISO) in combination with ICI 118,551 (100 nM), a selective β_2AR antagonist, or a selective β_2AR agonist zinterol in combination with CGP-20712A (300 nM), a selective β_1AR antagonist. Various concentrations of ISO/zinterol with ICI 118,551/CGP-20712A were made in Cell Tyrode solution ((mM): 136.9 NaCl, 5.4 KCl, 0.33 $NaH_2PO_4 \cdot H_2O$, 0.5 $MgCl_2 \cdot H_2O$, 5 HEPES, 5.6 glucose, 1 $CaCl_2$ pH7.4). Isolated cells were individually perfused with different concentration of agonist using a solution switcher (Section. 2.6.2) All myocytes were

continually perfused via bath solution with selective antagonists in Cell Tyrode. All base line recordings were made with selective antagonist, in the absence of angonist, in Cell Tyrode. Both bath and switcher solutions were heated to 37^{o}C. Statistical analysis was performed on cell recordings of factional shortening and Ca^{2+} transients that fell within two standard deviations of the mean of each concentrations within each group.

Experiments on trabeculae were performed at the University of Auckland, where the MCT model had recently been set up. Due to the nature of trabeculae dissection (which requires larger hearts), animals were injected at a heavier weight resulting in a longer time post injection before exhibiting clinical symptoms of failure. Male Wistar rats 325±25 g (target range) bred at the University of Auckland received an intra-peritoneal injection of saline or 60 mg/kg MCT solution (as described in Methods 2.1.2). Animal were housed 3-4 per cage. Animals were weighed twice weekly until day 20, then daily until overt weight loss (15 % body weight in one day or more than 20% total loss in body weight) or other symptoms of failure were observed (piloerection, dyspnea, lethargy, cold lower body).

Echocardiography measurements were not used to characterise when the β-blocker treatments should commence, in contrast with experimental procedures performed at the University of Leeds, due to time restraints. From studying weight records of animals at the University of Auckland, MCT animals on average begin to plateau in weight gain around day 20. Assuming that heart failure progressed in a linear manner dependent on the initial weight at which animals were injected, day 20 would be a similar proportion of time as day 15 (for University of Leeds animals) toward the median day of heart failure. For these reasons day 20 was chosen to start metoprolol treatment. Treatment regimens were identical to that at the University of Leeds, detailed in Methods 2.2.

At the designated end point animals were killed by a listed schedule 1 procedure and hearts quickly extracted and cannulated in a dissection chamber. Trabeculae were dissected from the RV as described in (Kaur et al., 2016) and transferred to the experimental rig, detailed in Methods 2.5. Trabeculae were continually superfused with solution. Baseline recordings were made in the presence of selective antagonist in Muscle Tyrode ((mM) 141.8 NaCl, 6 KCl, 1.2 $MgSO_4.H_2O$, 1.2 Na_2HPO_4, 10 HEPES, 10 glucose, 1 Ca^{2+}, pH 7.4) heated to 37 ^{o}C and bubbled with medical O_2. Muscles were stretched to L.max. Agonist and antagonist were the same as those used in isolated cell experiments. Details of protocol are given in (Figure 5-1).

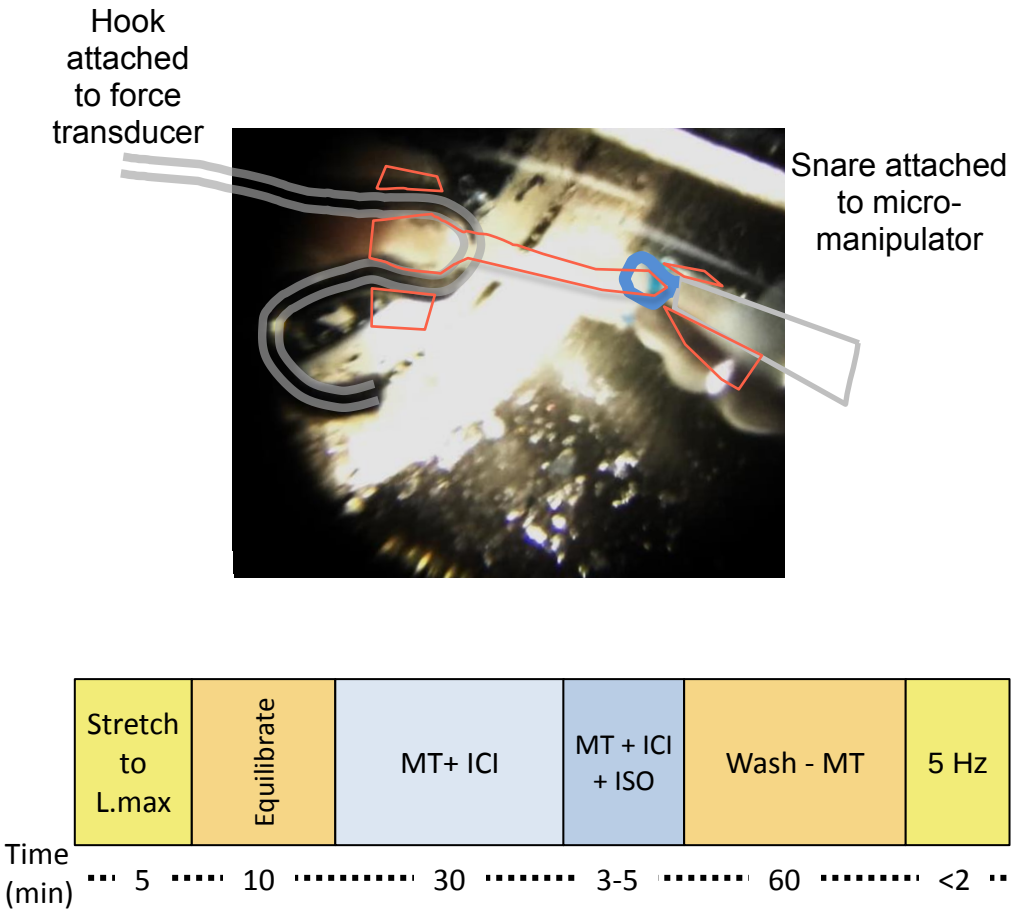

Figure 5-1 Trabecula carneae experimental protocol

Trabeculae were mounted on a stage and secured to a micromanipulator and a force transducer and continually superfused with Muscle Tyrode (MT) heated to 37 °C bubbled with O_2. After trabeculae had been loaded with Fura-2 field stimulation was increased to 1 Hz and muscles stretched to L.max (the length of the muscle at which developed tension was maximum). Trabeculae were then allowed to equilibrate before switching bath solution to MT containing ICI 118,551 (ICI). After 30 min superfusion with solution containing ICI, isoprenaline (ISO) was added to the solution to create a 1 µM ISO final concentration in ICI MT. ICI and ISO were then washed out by switching the bath solution back to MT before field stimulating at 5 Hz.

5.3. Results

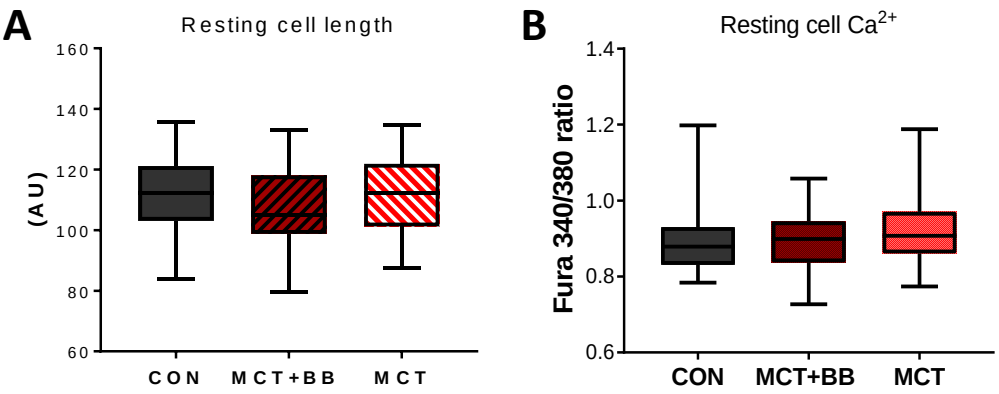

Figure 5-2 Resting cell length and $[Ca^{2+}]_i$

Data presented in box and whisker graph, mean, interquartile range and full data range shown. CON n=70, MCT+BB n=72, MCT n=68, one-Way ANOVA

5.3.1. Myocyte survival at 100 nM isoprenaline

Isolated cardiac myocytes were superfused with a range of ISO concentrations (1 nM – 100 nM). This range of ISO concentrations has previously been shown to produce a graded increase in contraction in rat cardiac myocytes, with 100 nM and above causing a plateau in response (Tamada et al., 1998; Collins and Rodrigo, 2010; McMartin and Summers, 1999). The initial concentration range included 200 nM ISO but it very quickly became obvious that none of the MCT cells would survive this concentration. When stimulating cells at 100 nM it was observed that some cells would spontaneously contract and then stop contacting or become hypercontracted. These cells did not recover when solution was switched back to ICI alone. Cells that stopped contracting or become hypercontracted when perfused with 100 nM ISO were defined as dead cells in this instance, recorded and compared across groups.

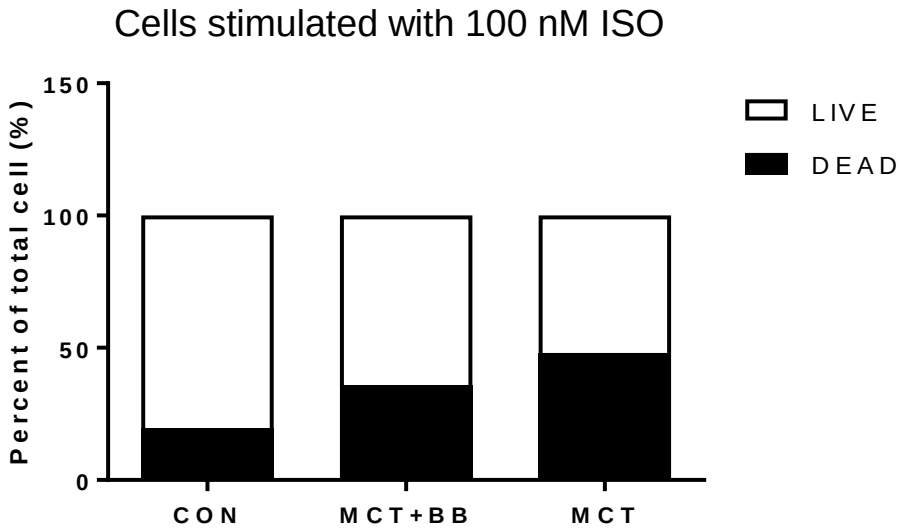

Figure 5-3 Cell survival when stimulated with 100 nM isoprenaline:
Some cardiac myocytes locally perfused with 100 nM isoprenaline (ISO) become spontaneously contractile, or hypercontracted or stopped contracting. Cell death was defines as irreversible cessation of contraction or hypercontraction. Percentage survival compared across the three groups, was significantly different (P=0.0183, X^2 test). MCT cells percentage survival was significantly lower than expected (Adjusted residual, ʐ<-1.6) Con n=41, MCT+BB n=70, MCT n=50

Cells which exhibited spontaneous contractions or waves but returned to normal contractions with each stimulation pulse when solution was returned to ICI alone were not counted within this group. The percentage of cell death was different across the groups (P=0.0183, X^2 test) with CON cells having the lowest percentage cell death (8/41). MCT cells were found to have a significantly higher percentage cell death (24/50) than expected value (X^2 with adjusted residual, ʐ<-1.6). For MCT+BB cells, the percentage of cell death (25/70) was no different than expected (Figure 5-3)

5.3.2. Changes in myocyte fractional shortening in response to β_1AR stimulation

Representative contraction and $[Ca^{2+}]_i$ transients are shown at baseline and following stimulation with 100 nM ISO in CON, MCT+BB and MCT RV myocytes (Figure 5-4). Baseline contraction recordings were made in the presence of a selective β_2AR antagonist (ICI

118,551). At baseline, there was no significant difference between CON, MCT+BB and MCT in fractional shortening or time to 50% relaxation. Upon locally superfusion with ISO to selectively stimulate the β_1AR, cells produced a positive inotropic and lusitropic response. Mean concentration data are shown in Figure 5-5 to 5-8.

At 1 nM ISO, RV myocytes exhibited a small increase in fractional shortening, although this was not significantly different from baseline recordings. MCT cells showed a larger percentage shortening compared to MCT+BB at 1 nM ISO ($P<0.05$), but this was not significantly different to CON (Figure 5-5). There was no difference in time to 50% relaxation at this concentration between groups (Figure 5-6).

At 30 nM ISO, which was above the EC_{50} of the concentration response curve of all the groups, fractional shortening had increased more than two-fold compared to baseline recordings. There was no difference between the groups in cell fractional shortening at this concentration and no difference in EC_{50} between groups. Time to 50% relaxation was significantly slower in MCT compared to both CON and MCT+BB at 30 nM ISO ($P<0.05$). CON time to 50% relaxation was significantly faster than baseline recordings, while there was no significant decrease in time to 50% relaxation from the MCT group compared with baseline recordings. In cells from the MCT+BB group time to 50% relaxation was also significantly faster at 30 nM compared to baseline recordings ($P<0.05$) (Figure 5-6).

Fractional shortening was significantly blunted in the MCT cells in response to the highest concentration (100 nM) of ISO compared with both CON and MCT+BB groups ($P<0.001$, $P<0.01$) (Figure 5-5). From 30 nM to 100 nM ISO stimulation, the mean percentage shortening increased by around 3% in both CON and MCT+BB whereas MCT cells showed no further increase in percentage shortening (Figure 5-5 A). At 100 nM ISO time to 50% of relaxation was significantly blunted in the MCT group compared with CON ($P<0.01$). There was no significant difference in time to 50% relaxation between MCT+BB and CON or MCT at the highest ISO concentration, showing an intermediate state. MCT blunts the increase in fractional shortening and reduced time to 50% relaxation at high concentrations of ISO stimulation compared to CON; this is partially recovered with metoprolol treatment.

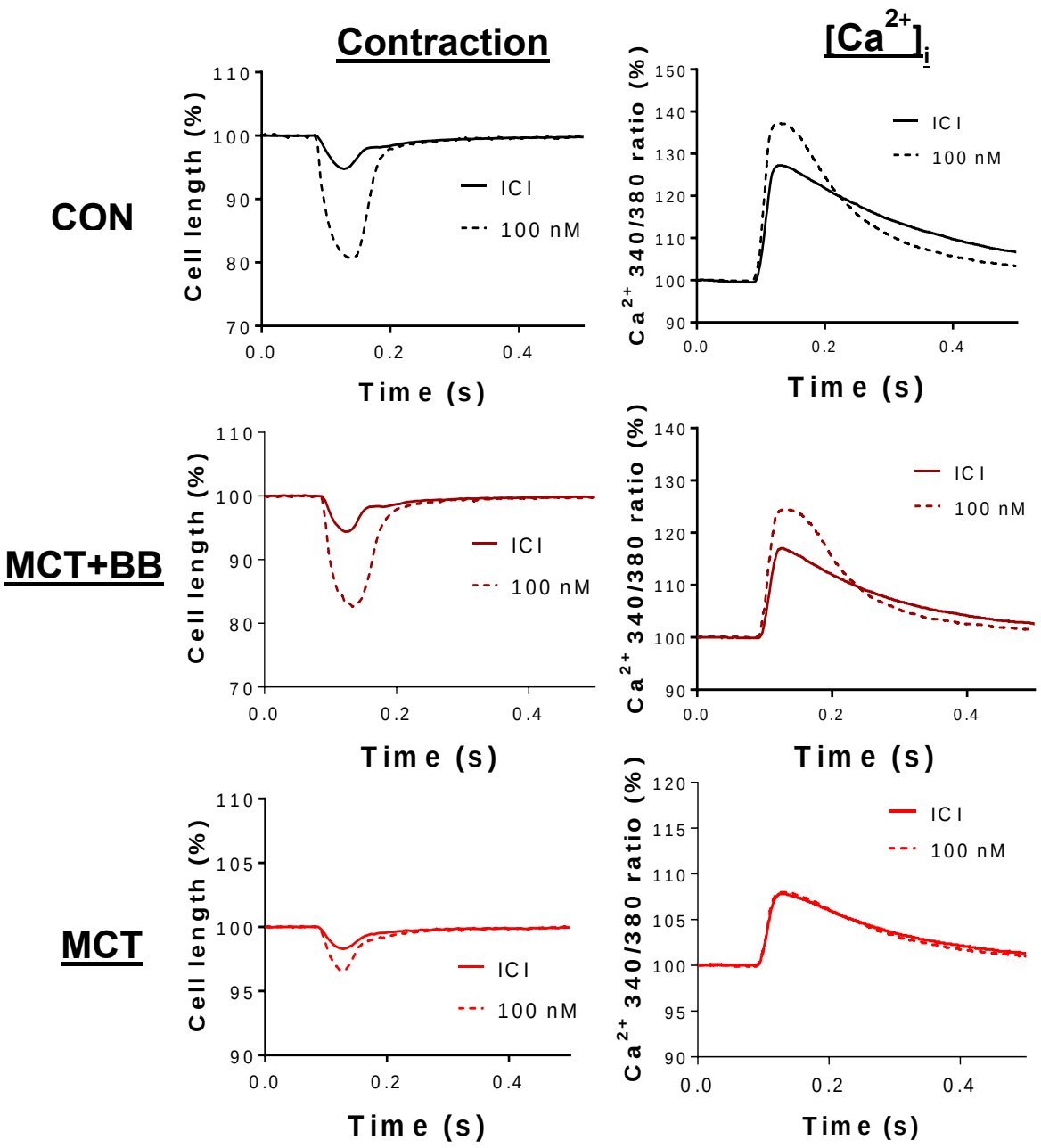

Figure 5-4 Representative cell length and $[Ca^{2+}]_i$ transient traces at baseline and 100nM isoprenaline stimulation

Contraction is plotted as a percentage of resting cell length. Baseline recordings in the presence of of ICI 118,551 (ICI) are shown as a solid line. Local perfusion of the cell was then switched to 100 nM isoprenaline (ISO) shown as a dotted line. 10-20 contractions/$[Ca^{2+}]_i$ transients were used to create each average trace.

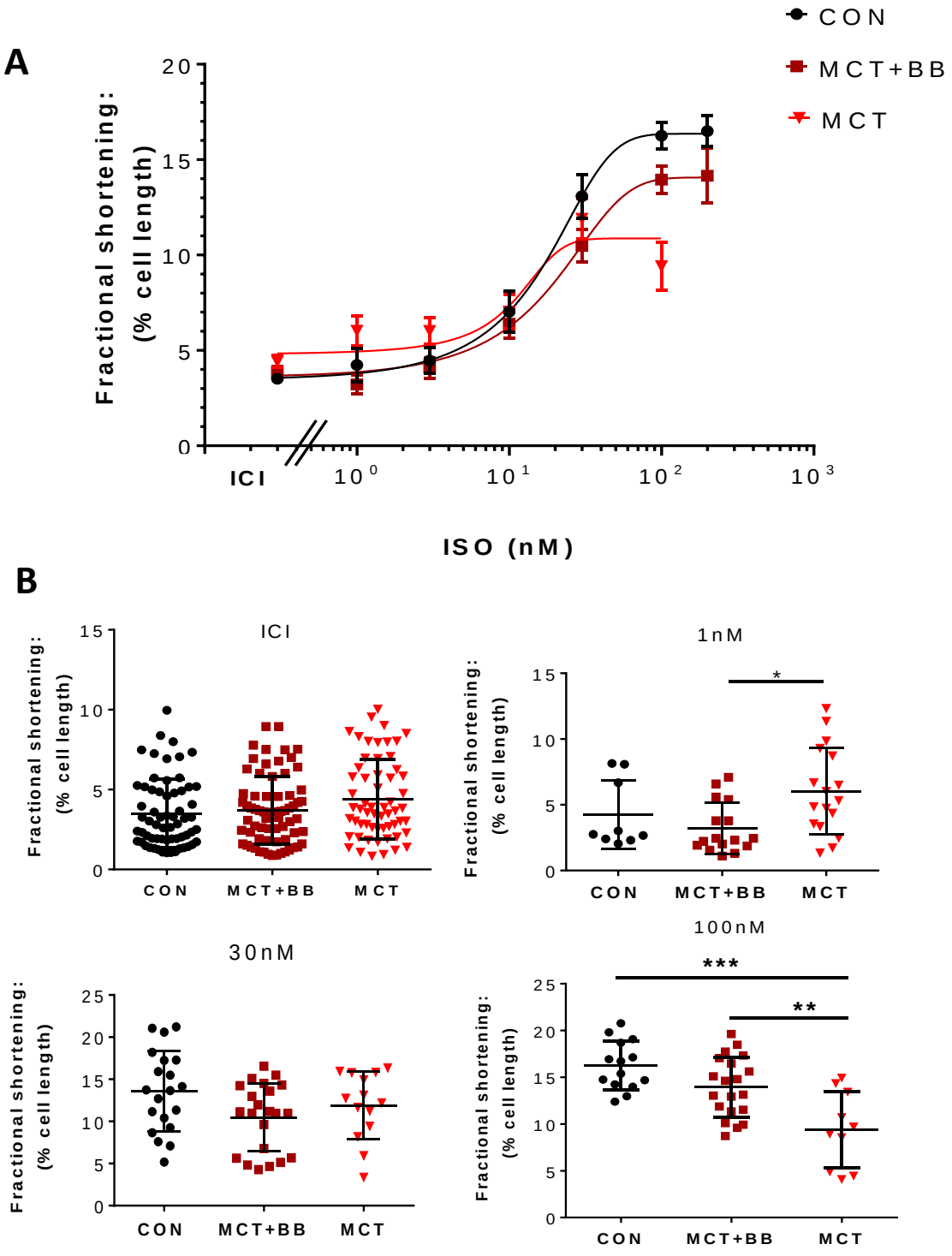

Figure 5-5 Change in fractional shortening in response to β_1AR stimulation

Cell shortening is expressed as a percentage of cell length. All recordings were made in the presence of the β_2AR antagonist ICI 118,551 (ICI). **A.** Concentration-response curve to isoprenaline (ISO), mean ± SEM. **B.** Dot plots of individual cell shortening with ICI alone and 1, 30 and 100 nM ISO, mean ± SD. *P<0.05, **P<0.01, ***P<0.001 (One-way ANOVA), (Krus Willis).

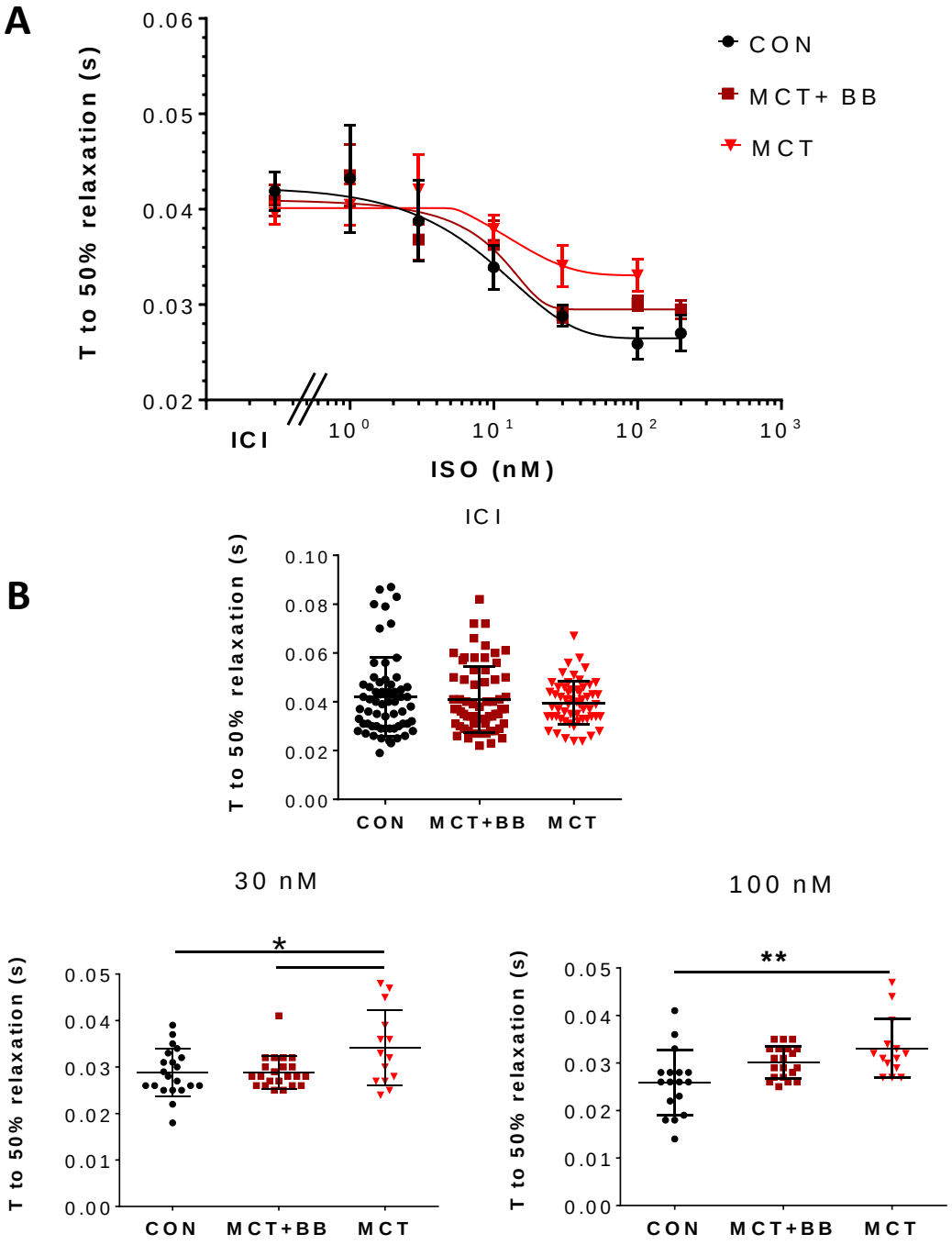

Figure 5-6 Change in time to 50% relaxation in response to β_1AR stimulation

Cell relaxation is expressed as time to 50% total cell length, mean ± SEM. All recordings were made in the presence of the β_2AR antagonist ICI 118,551 (ICI). **A.** Concentration-response curve to isoprenaline (ISO), mean ± SEM. **B.** Dot plots of individual cell data with ICI alone and 30 and 100 nM ISO, mean ± SD. *P<0.05, **P<0.01, ***P<0.001 (One-way ANOVA).

5.3.3. Changes in myocyte Ca^{2+} handing in response to β_1AR stimulation

Similar trends were observed when measuring myocyte $[Ca^{2+}]_i$ handling, as seen in the representative traces (Figure 5-4). Data are expressed as change from baseline recordings due to gradual decay in signal over time, which was observed in all cells. This signal decay resulted in the recordings at low concentrations of ISO (1 nM and 3 nM) being below 100% of that recorded at baseline. Selective β_1AR stimulation increased the $[Ca^{2+}]_i$ transient amplitude in CON cells, which was significantly blunted in MCT cells at the highest concentration of ISO ($P<0.05$)(Figure 5-7). There was no difference in the MCT+BB cell $[Ca^{2+}]_i$ transient amplitude compared with either CON or MCT at the highest ISO concentration. MCT cells also showed a significantly prolonged time to 50% Ca^{2+} decay compared with CON cells at 100 nM ISO ($P<0.001$). In MCT+BB time to 50% Ca^{2+} was significantly reduced from MCT cells ($P<0.05$), with no difference compared to CON. MCT blunts the increase in $[Ca^{2+}]_i$ transient amplitude and time to 50% Ca^{2+} decay at high concentrations of ISO stimulation compared to CON; this again is partial recovered with metoprolol treatment.

5.3.4. Effects of FURA-2 AM in cells

It was noted while measuring cell fractional shortening in the presence of ICI that there was a trend for a greater percentage shortening in the MCT cells compared with CON (Figure 5-5). MCT fractional shortening at 1 Hz has previously been shown to be significantly greater than that of CON, which is suggested to be a result of the higher $[Ca^{2+}]_i$ content in MCT cells (Benoist et al., 2012). To examine whether the effect of FURA-2 AM buffering the $[Ca^{2+}]_i$ has a greater effect in cells with a lower resting $[Ca^{2+}]_i$ content, fractional shortening was measured in ICI alone and then with the addition of 30 nM or 100 nM ISO in cells which had not been loaded with FURA-2 AM (Figure 5-9). At baseline there was a significant increase in fractional shortening in unloaded cells, compared to the FURA loaded cells, in both the CON and MCT+BB group ($P<0.05$, $P<0.001$), with a trend to increase in the MCT cells. This difference was abolished at 100 nM ISO. The MCT response to selective β_1-AR stimulation was still significantly blunted compared to both CON and MCT+BB in the unloaded FURA cells ($P<0.01$). Buffering of $[Ca^{2+}]_i$ by FURA only appears to have an effect on shortening at lower levels of Ca^{2+} with a greater effect in CON and MCT+BB cells.

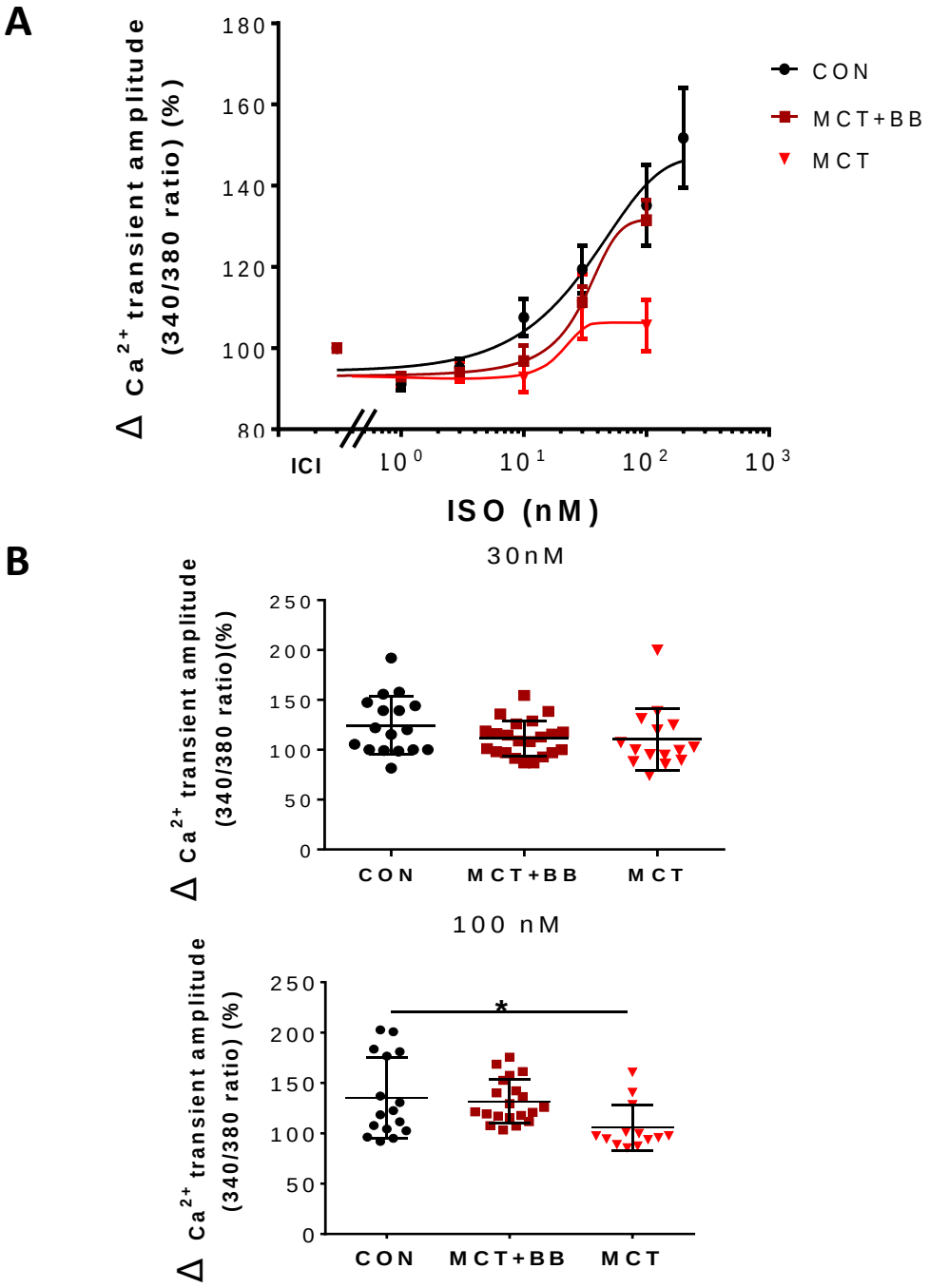

Figure 5-7 Change in $[Ca^{2+}]_i$ cell transient amplitude in response to β_1AR stimulation

$[Ca^{2+}]_i$ transient amplitude is expressed as a percentage change from baseline [amplitude (340/380 ratio). All recordings were made in the presence of the β_2AR antagonist ICI 118,551. **A.** Concentration-response curve to isoprenaline (ISO), mean ± SEM. **B.** Dot plots of individual cell data at 30 and 100 nM ISO, mean ± SD. *P<0.05 (One-way ANOVA).

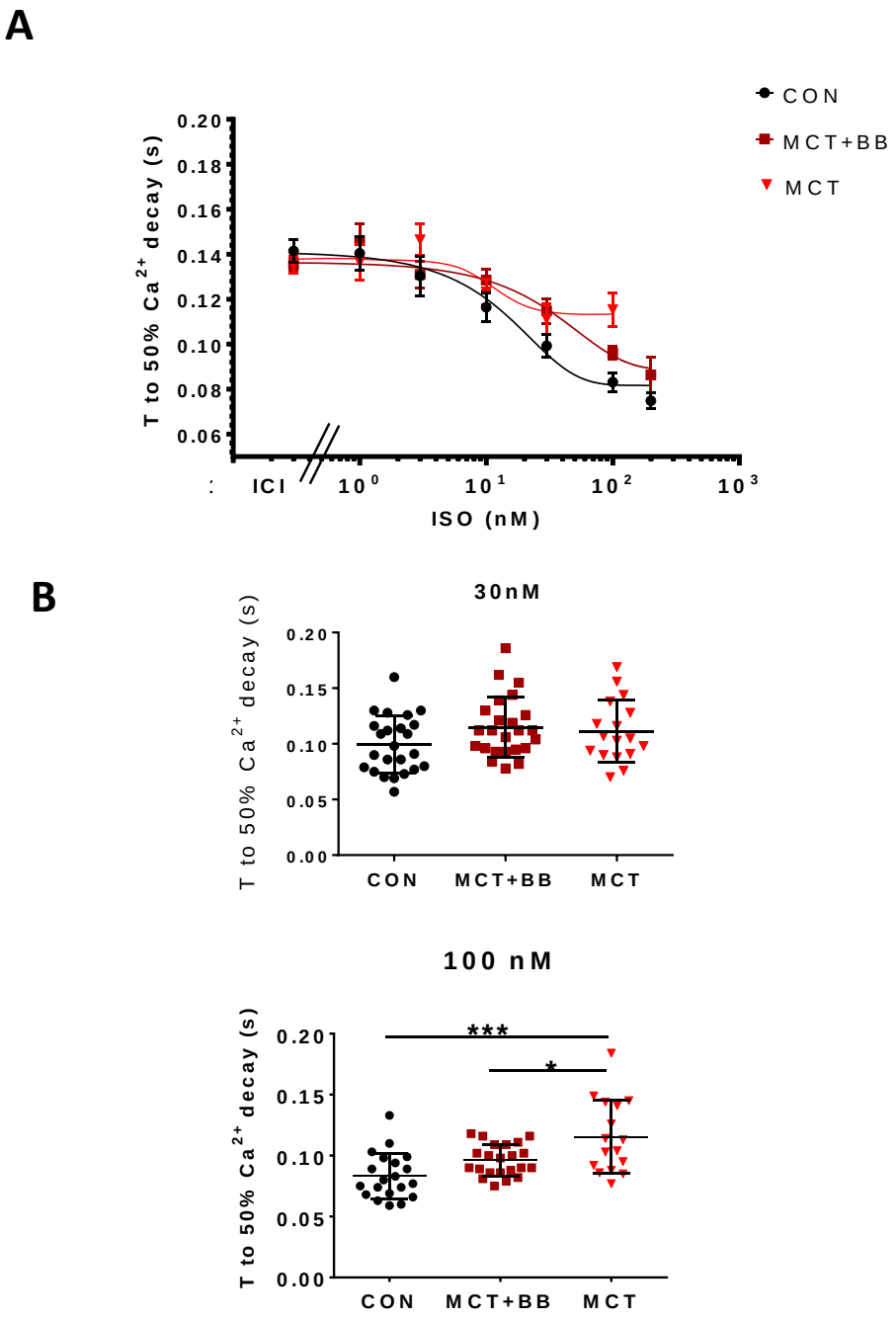

Figure 5-8 Change in time to 50% $[Ca^{2+}]_i$ decay in response to β_1AR stimulation

Time to 50% $[Ca^{2+}]_i$ decay is measured as the time taken to return 50% towards $[Ca^{2+}]_i$ levels recorded at baseline. All recordings were made in the presence of the β_2AR antagonist ICI 118,551 (ICI). **A.** Concentration-response curve to isoprenaline (ISO), mean ± SEM. **B.** Dot plots of individual cell data at 30 and 100 nM ISO, mean ± SD. *P<0.05, **P<0.01, ***P<0.001 (One-way ANOVA)

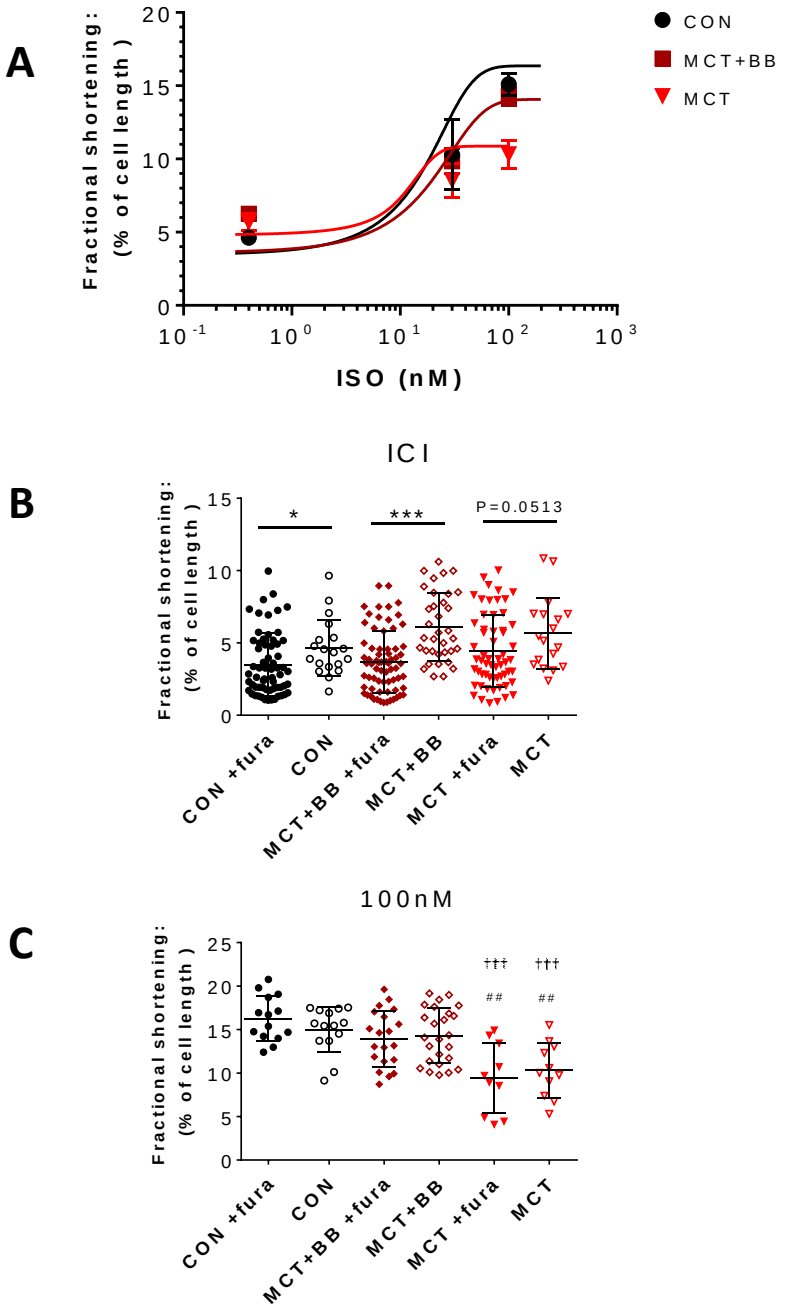

Figure 5-9 Change in fractional shortening in response to β_1AR stimulation: effect of Fura loading

A. Cell shortening is expressed as a percentage of resting cell length. Concentration response curve shows mean fractional shortening ± SEM, fitted with the curve from the previous graph (Fig 5-5A) with Fura loaded cells. **B.C.** Dot plots of cell shortening with ICI 118,551 (ICI) only and 100 nM isoprenaline (ISO) showing which cells were loaded with Fura-2 AM. Student t-test (*P<0.05, ***P<0.001, ***P<0.001). One-way ANOVA (##P<0.01 MCT+BB vs. MCT, †††P<0.001 CON vs. MCT)

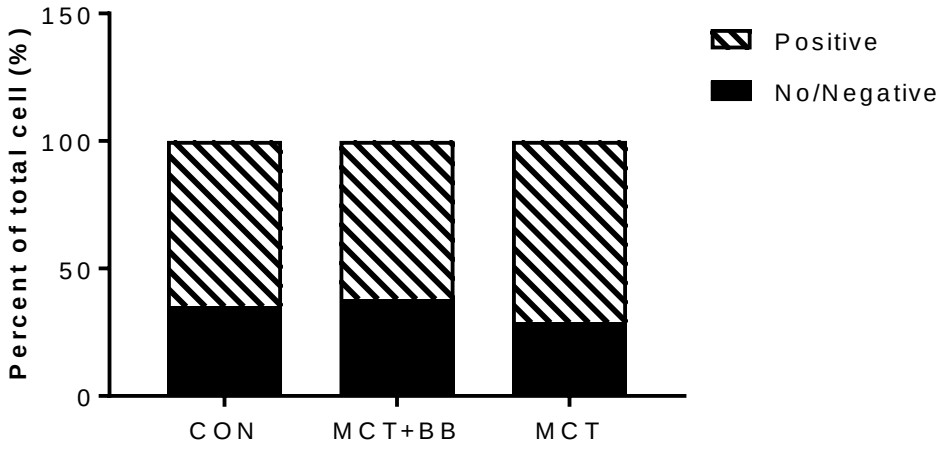

Figure 5-10 Cell response to β_2AR stimulation

Cardiac myocytes were locally superfused with a range of zinterol concentrations in the presence of the selective β_1AR antagonist CGP 20712A. Not all cells showed a positive inotropic response. The number of cells which showed no response or a negative inotropic response to zinterol were counted and compared across groups. There was no difference in the proportion of cells shortening no response or a negative response. (X^2) CON n= 91, MCT+BB n= 63, MCT n= 52

5.3.5. Response to selective β_2AR stimulation in cardiac myocyte

When stimulating with the selective β_2AR agonist zinterol, in the presence of the β_1AR antagonist CGP-20712A, not all cells exhibited a positive inotropic response (Xiao et al., 1999a). The number of cells which did not show a positive inotropic response was recorded and compared across the groups. The total proportion of positive to non/negative responders did not change between the three groups (X^2 P>0.05)(Figure 5-10). All further analysis on selective β_2AR stimulation is only performed on cells which showed a positive inotropic response.

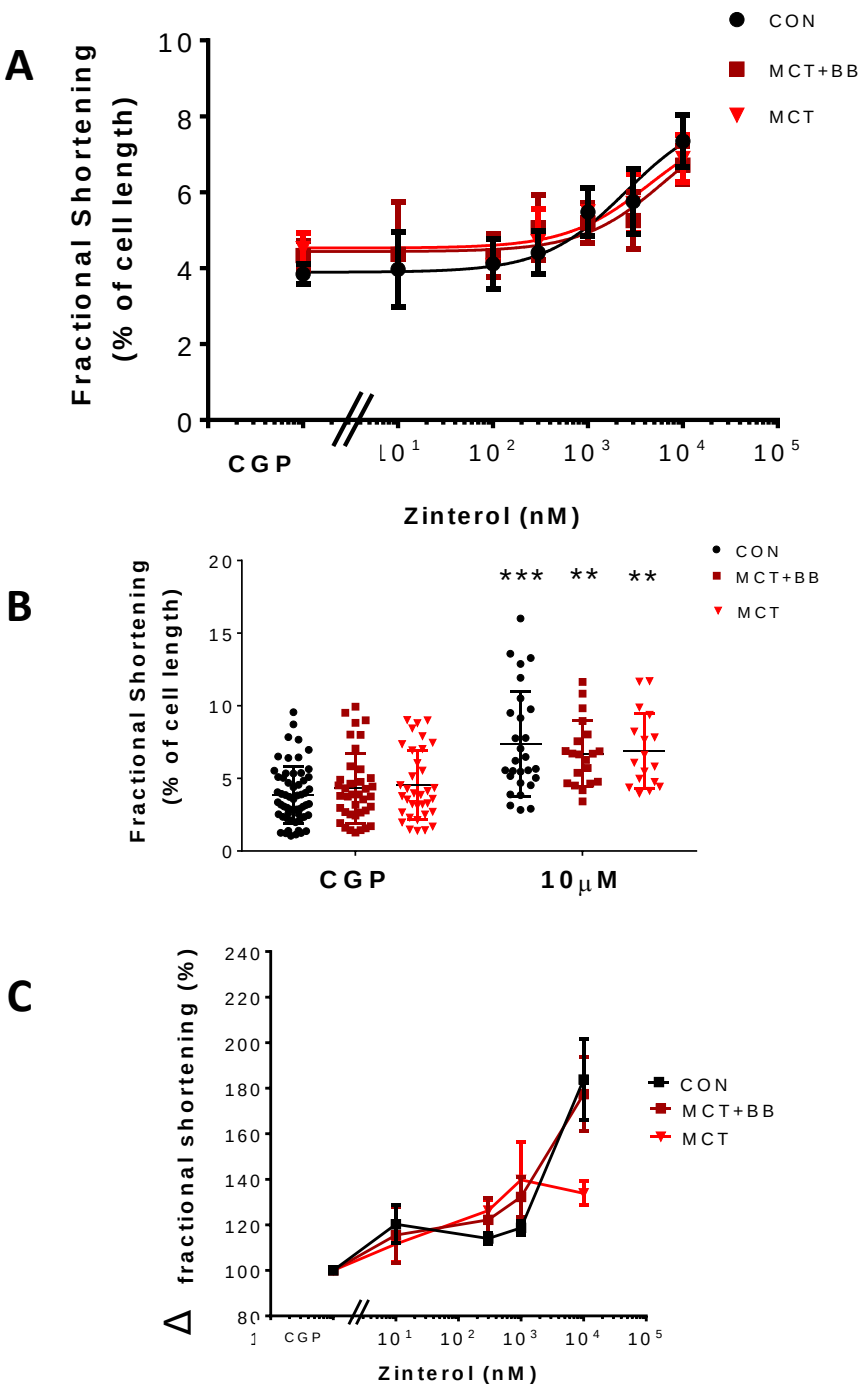

Figure 5-11 Change in fractional shortening in response to β_2AR stimulation

Cell shortening is expressed as a percentage of resting cell length. All recordings were made in the presence of the β_1AR antagonist CGP-20712A (CGP). **A.** Concentration-response curve to zinterol, mean ± SEM. **B.** Dot plots of individual cell data with GCP alone and 10 μM zinterol, mean ± SD. **C.** Cell shortening is expressed as a percentage increase from baseline. **P<0.01, ***P<0.001 vs. baseline (CGP) (Two-way ANOVA).

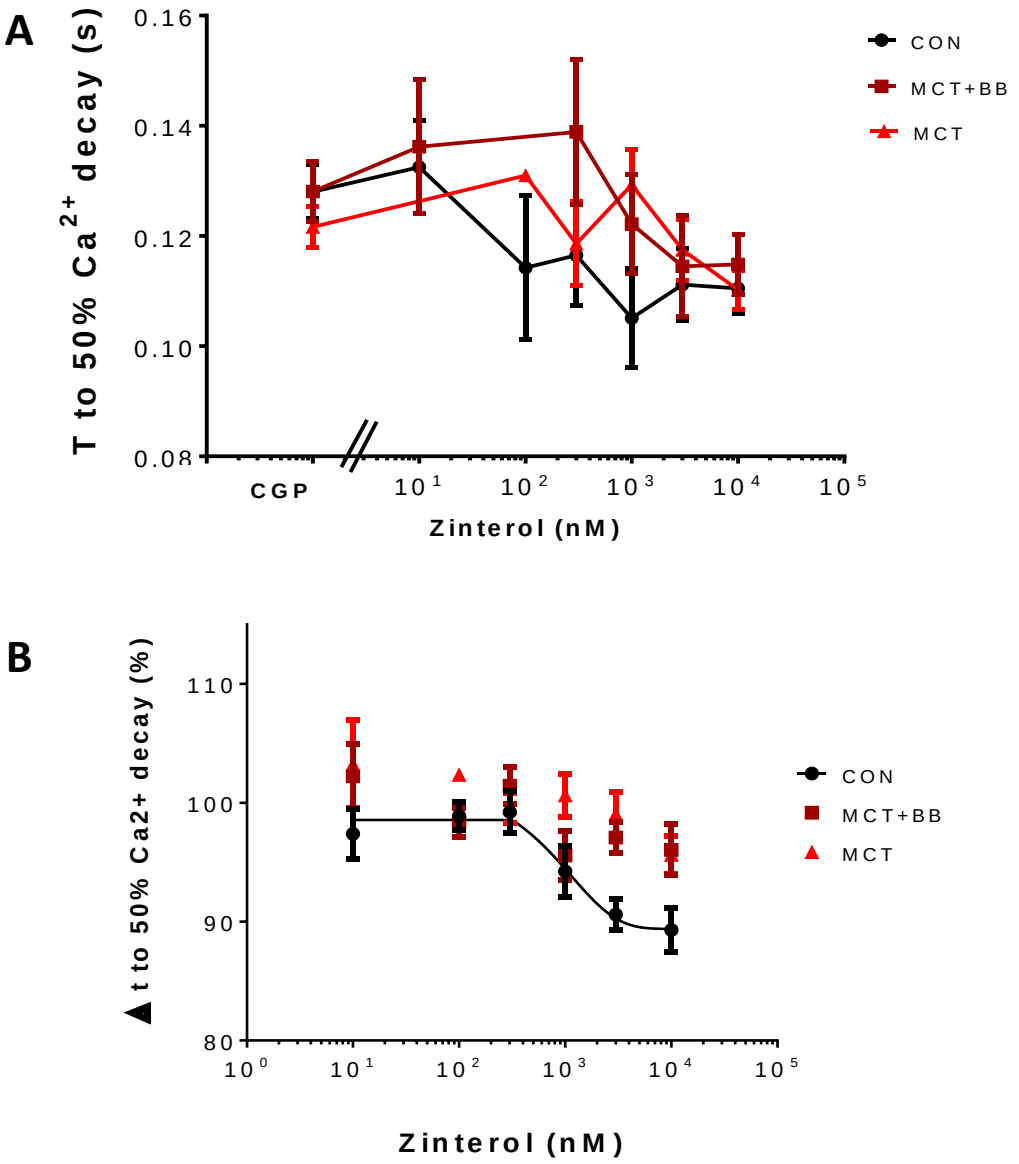

Figure 5-12 Change in time to 50% $[Ca^{2+}]_i$ decay in response to β_2AR stimulation

Time to 50% $[Ca^{2+}]_i$ decay is measured as time taken to return 50% towards $[Ca^{2+}]_i$ levels recorded at baseline. All recordings were made in the presence of CGP -20712A (CGP). **A.** Concentration-response curve to zinterol, mean ± SEM. **B**. Concentration-response curve to zinterol, measured as a percentage change from baseline recordings, mean ± SEM.

Selective β_2AR stimulation increased the contraction of cells, as measured by fractional shortening, in all three groups. This increase became significant at 10 μM zinterol ($P<0.01$) (Figure 5-11 B). There was no difference in fractional shortening at baseline or with 10 μM zinterol between the three groups, although there was a trend for a larger increase in shortening in response to 10 μM zinterol in CON compared with MCT cells ($P=0.14$). Time to 50% relaxation was significantly decreased from baseline in CON cells with the addition of 10 μM zinterol ($P<0.01$). However this decrease was not significantly different between groups and there was no significant difference in relaxation times at baseline or 10 μM zinterol (Figure 5-12). There was no change in $[Ca^{2+}]_i$ transient amplitude or time to 50% $[Ca^{2+}]_i$ decay in any of the groups (Figure 5-12). At high levels of zinterol stimulation CON, MCT+BB and MCT all show an increase in fractional shortening, which is not different between the groups although only CON cell show a reduction in time to 50% relaxation.

5.3.6. Growth and organ weight ratios in Auckland animals

Animals at the University of Auckland were injected with MCT at a larger weight due to the nature of the trabeculae dissection; this resulted in a longer period of time post injection before animals exhibited signs of heart failure. Animals were weighed regularly up until day 20, when daily weights were recorded. Mean group weight data were plotted and show CON continuous weight gain over time, while MCT+BB and MCT animals initially gained weight but this slowed over time (Figure 5-13). Individual daily weight changes were plotted to closely examine trends in weight variation: CON mean weight variation showed animals continued to gain weight in a fairly consistent manner from injection to the designated end point (illustrated by the line of best fit), while MCT plateau and the mean change in weight becomes negative around day 24 (straight line intersecting the x-axis)(Figure 5-14). In the MCT+BB group, the mean change in daily weight starts to plateau and approach zero towards day 24-30 post injection (Figure 5-14). The fall in weight seen in the mean data plotted in Figure 5-14 is due to a single animal losing weight at that time point. Both MCT+BB and MCT daily weight change significantly deviate from zero (linear regression, $P<0.05$).

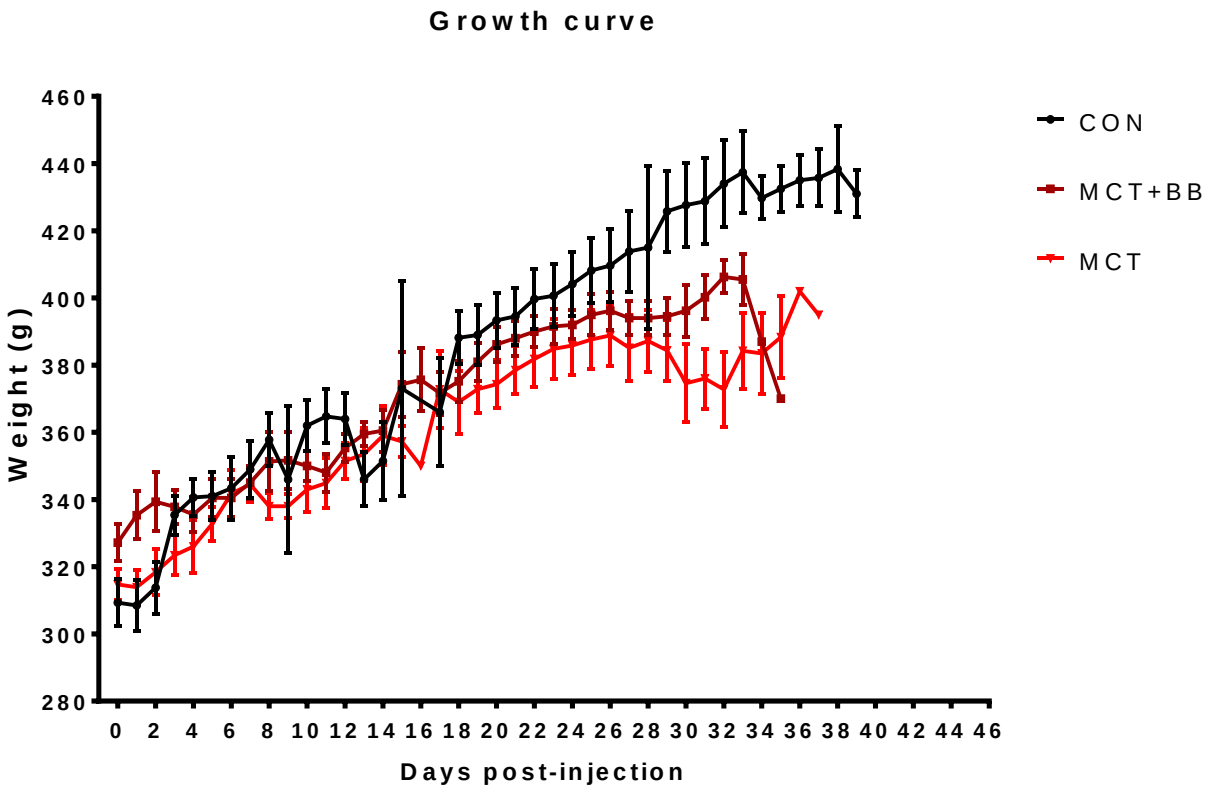

Figure 5-13 Growth curve of CON, MCT+BB and MCT animals (Auckland)

Animals were weighed regularly from day of injection to day 20, then daily until designated end point. Mean animal weight from each group is plotted ± SEM. MCT+BB and MCT weight begins to plateau around day 20-24 while CON continue to gain weight. CON n=6, MCT+BB n=6, MCT n=5

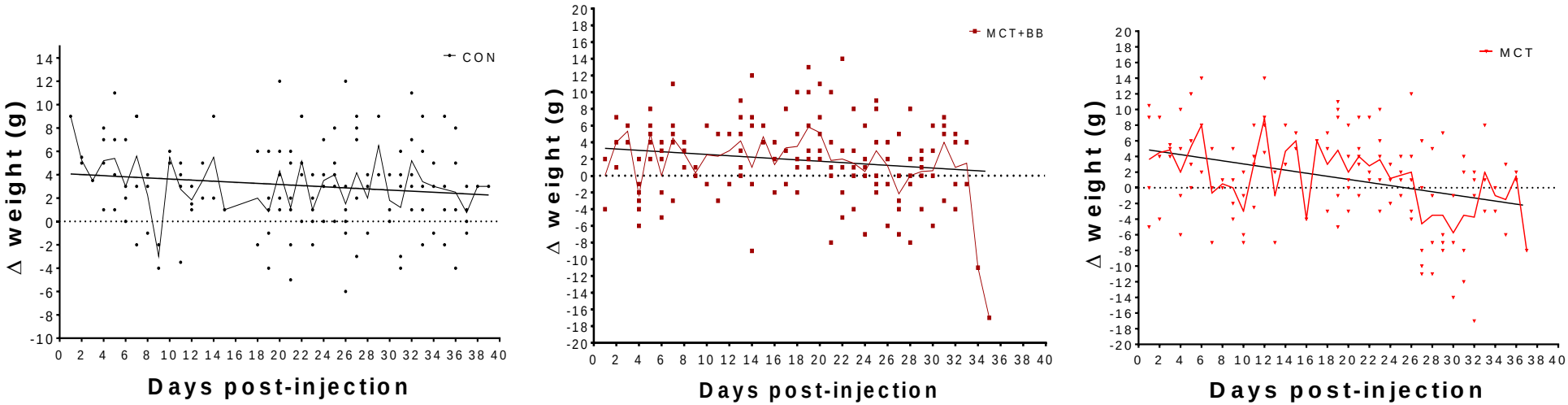

Figure 5-14 Daily change in weight post MCT/Saline injection

Weight change from the previous day was calculated and individual weight change plotted for each group. Line of best fit for the data is plotted in black and linear regression calculated. MCT+BB and MCT slop of the line is significantly deviated from zero ($P<0.05$). CON animals show a continual average gain in weight over time, while MCT+BB begins to plateau in weight gain towards the end and MCT plateaus and becomes negative from day 25. CON n=6, MCT+BB n=6, MCT n=5

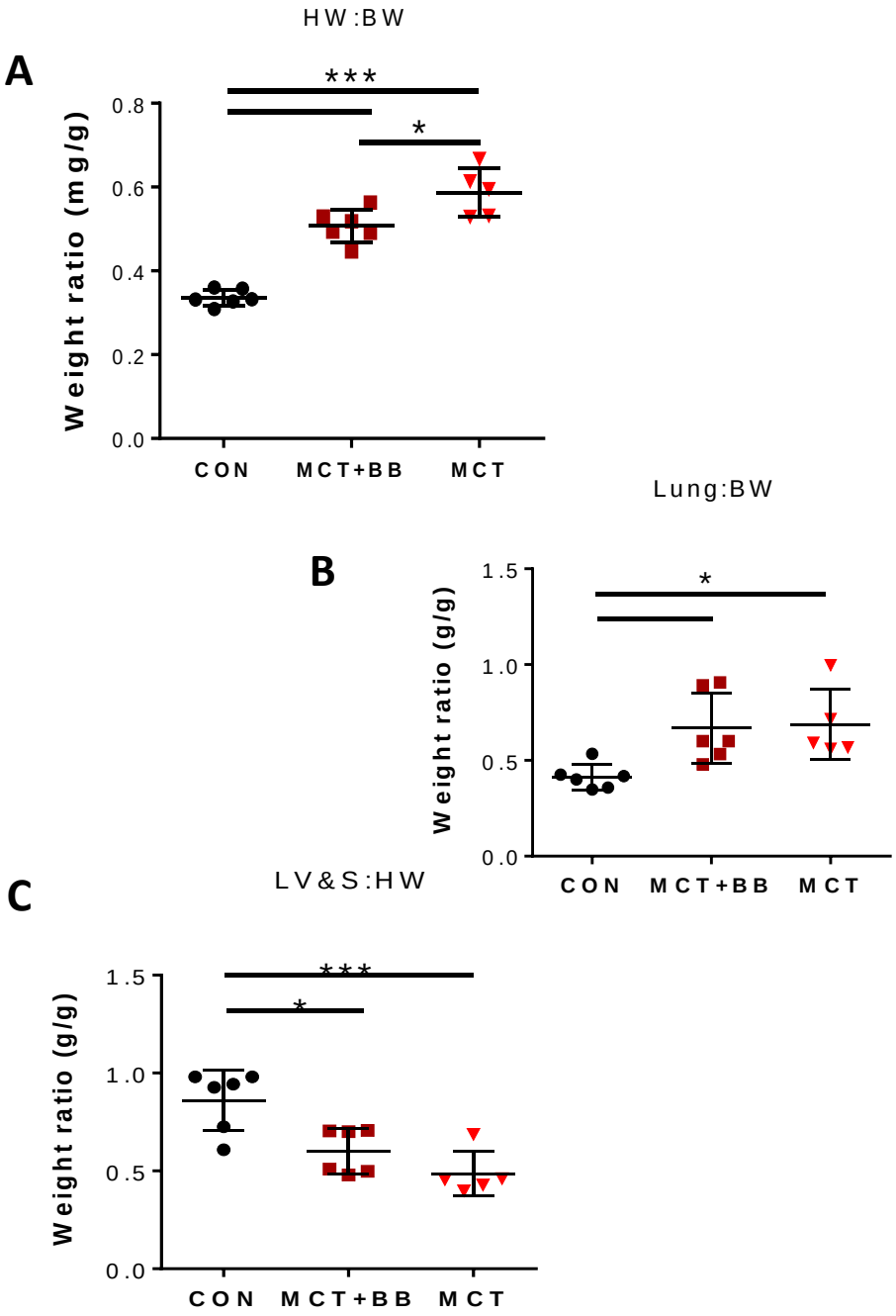

Figure 5-15 Changes in organ weight ratios

At the designated end point hearts were quickly dissected out and whole heart weight recorded (HW). Lung weight was also recorded. Dissected organ weights were normalised to body weight (BW). After trabeculae dissection the left ventricle and septum (LV&S) were weighed. CON n=6, MCT+BB n=6, MCT n=5, One-way ANOVA (*P<0.05, **P<0.01, ***P<0.001).

Heart weight to body weight (HW:BW) ratios were significantly increased in both MCT+BB and MCT animals compared to CON indicating hypertrophy of the heart ($P<0.001$)(Figure 5-15). The HW:BW ratio was significantly greater in the MCT animals compared to the MCT+BB animals ($P<0.01$). The trabeculae carneae are sensitive to stretch and other mechanical stress so needed to be dissected out first, meaning right ventricle free wall weight recordings were not possible. Instead, LV and septum to heart weight (LV+S:HW) ratios were used as a reverse index for the RV to the heart weight ratio. The LV+S:HW ratio was significantly reduced in MCT and MCT+BB compared to CON ($P<0.05$, $P<0.001$). Lung weight to body weight ratio was also significantly increased in both MCT+BB and MCT compared to CON animals ($P<0.05$). Pulmonary edema was noted in a few of the MCT+BB and MCT animals.

5.3.7. Change in trabeculae stress in response to β_1AR stimulation

Isometric force was measured in mN and normalised to trabeculae cross-sectional area to index muscle stress (force production per unit area). Baseline recordings were measured at L.max in the presence of ICI. At baseline MCT+BB trabeculae produced significantly more stress than CON trabeculae. There was no difference between CON and MCT or MCT and MCT+BB. When CON trabeculae were superfused with 1 μM ISO, stress production was significantly increased ($P<0.05$)(Figure 5-16). No significant change in stress production was observed in either MCT+BB or MCT trabeculae. However, the CON increase in stress production was not significantly different to the change in stress of MCT or MCT+BB trabeculae (Interaction $P>0.05$, Paired Two-way ANOVA). There was no difference in the stress measurements during ISO superfusion between the three groups. Time to 50% relaxation did not differ between the three groups at baseline and there was no change with β_1-AR stimulation.

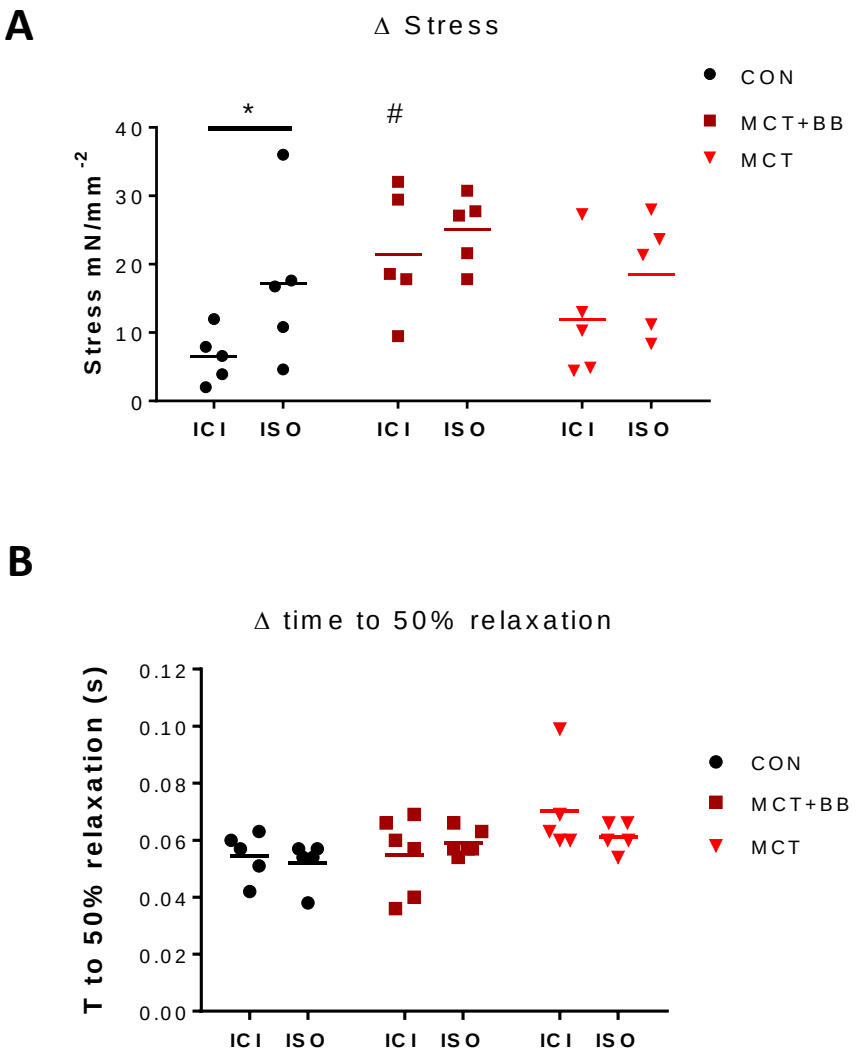

Figure 5-16 Change in stress production and relaxation in response to β_1AR stimulation in trabeculae carneae

All recordings were made in the presence of the β_2AR antagonist ICI 118,551 (ICI). Individual recordings are plotted in ICI alone and then with the addition of isoprenaline (ISO). **A.** Stress (force per unit area) production is measured as peak force (in mN) divided by the cross-sectional area of the trabeculae (mm^2). **B.** Time to relaxation is measured as expressed as time to 50% resting force. CON n=5, MCT+BB n=6, MCT n=5, Two-way ANOVA (*P<0.05, CON ICI vs CON ISO, #P<0.05, CON ICI vs MCT+BB ICI).

5.3.8. Change in trabeculae Ca^{2+} handling in response to β_1AR stimulation

$[Ca^{2+}]_i$ was simultaneously measured with stress. There was no difference in $[Ca^{2+}]_i$ transient amplitude between the three groups at baseline (Figure 5-17). The $[Ca^{2+}]_i$ transient amplitude was significantly increased in CON trabeculae when selective β_1AR stimulation was applied ($P<0.05$). There was no significant increase in $[Ca^{2+}]_i$ transient amplitude with addition of ISO in the MCT or MCT+BB groups. However there was no difference in $[Ca^{2+}]_i$ transient amplitude between the three groups when ISO was applied. There was no difference in time to 50% Ca^{2+} decay between the three groups at baseline and there was no change with selective β_1AR stimulation (Figure 5-17). CON trabeculae were the only group to show a significant increase in both stress and $[Ca^{2+}]_i$ transient amplitude.

5.3.9. Trabeculae stimulated at 5 Hz

After superfusion with ISO, bath solution was changed back to Muscle Tyrode for 60 min to allow for the washout of ISO/ICI. Stress production before ISO stimulation and after washout was not significantly different in any of the groups. Trabeculae stimulation frequency was then increased to 5 Hz for less than 2 min. When pacing was increased to 5 Hz, MCT and MCT+BB trabeculae showed a negative stress frequency relationship ($P<0.05$). There was no significant difference in stress production of CON trabeculae when pacing at 5 Hz compared with 1 Hz (Figure 5-18). The $[Ca^{2+}]_i$ transient amplitude after washout was not significantly different from recording before ISO stimulation in any of the groups. When pacing was increased to 5 Hz there was a significant reduction in $[Ca^{2+}]_i$ transient amplitude in the CON and MCT+BB group ($P<0.05$) with a trend for a reduction in the MCT group ($P=0.06$). At 5 Hz stimulation there was no difference in stress of contraction or $[Ca^{2+}]_i$ transient amplitude between the three groups.

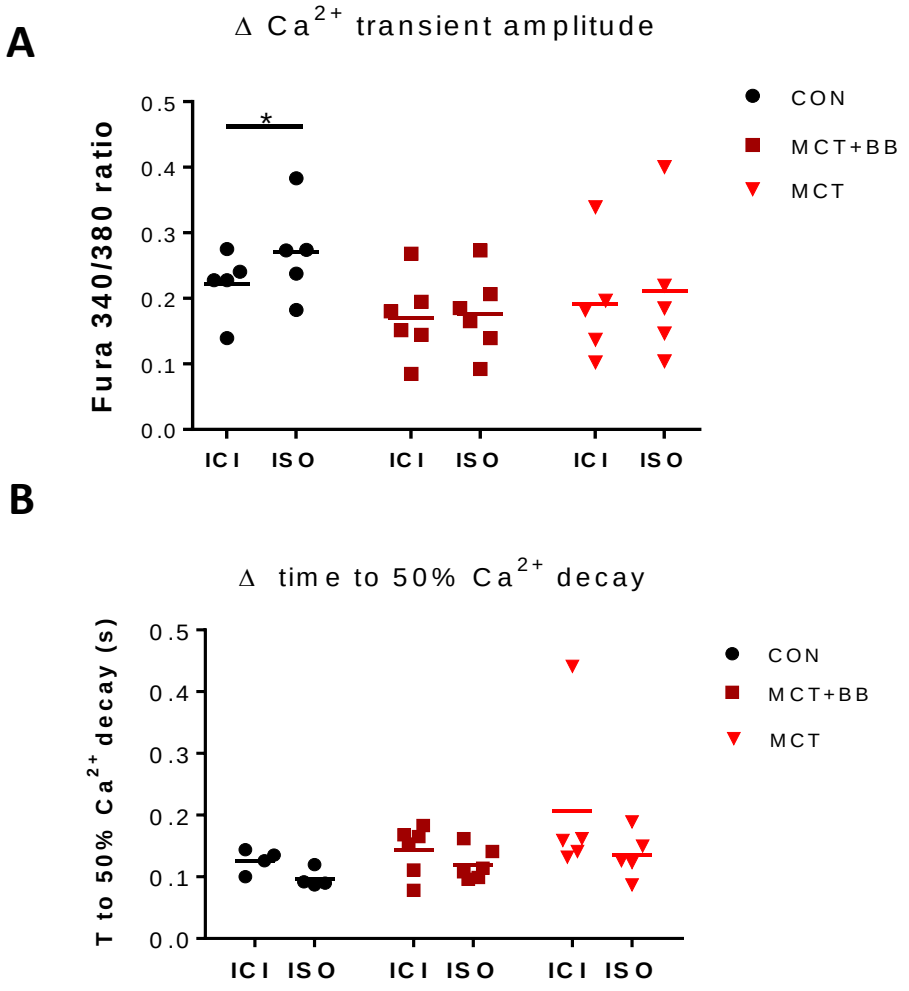

Figure 5-17 Change in $[Ca^{2+}]_i$ trabeculae amplitude and decay in response to β_1AR stimulation

All recordings were made in the presence of the β_2AR antagonist ICI 118,551 (ICI). Individual recordings are plotted in ICI alone and then with the addition of isoprenaline (ISO) **A.** Trabeculae $[Ca^{2+}]_i$ transient amplitudes is expressed as peak 340/380 ratio from baseline recordings . **B.** Trabeculae time to 50% $[Ca^{2+}]_i$ decay was measured as the time taken to reach 50% of the $[Ca^{2+}]_i$ levels recorded at baseline . CON n=5, MCT+BB n=6, MCT n=5 .Two-way ANOVA (*P<0.05, CON ICI vs CON ISO)

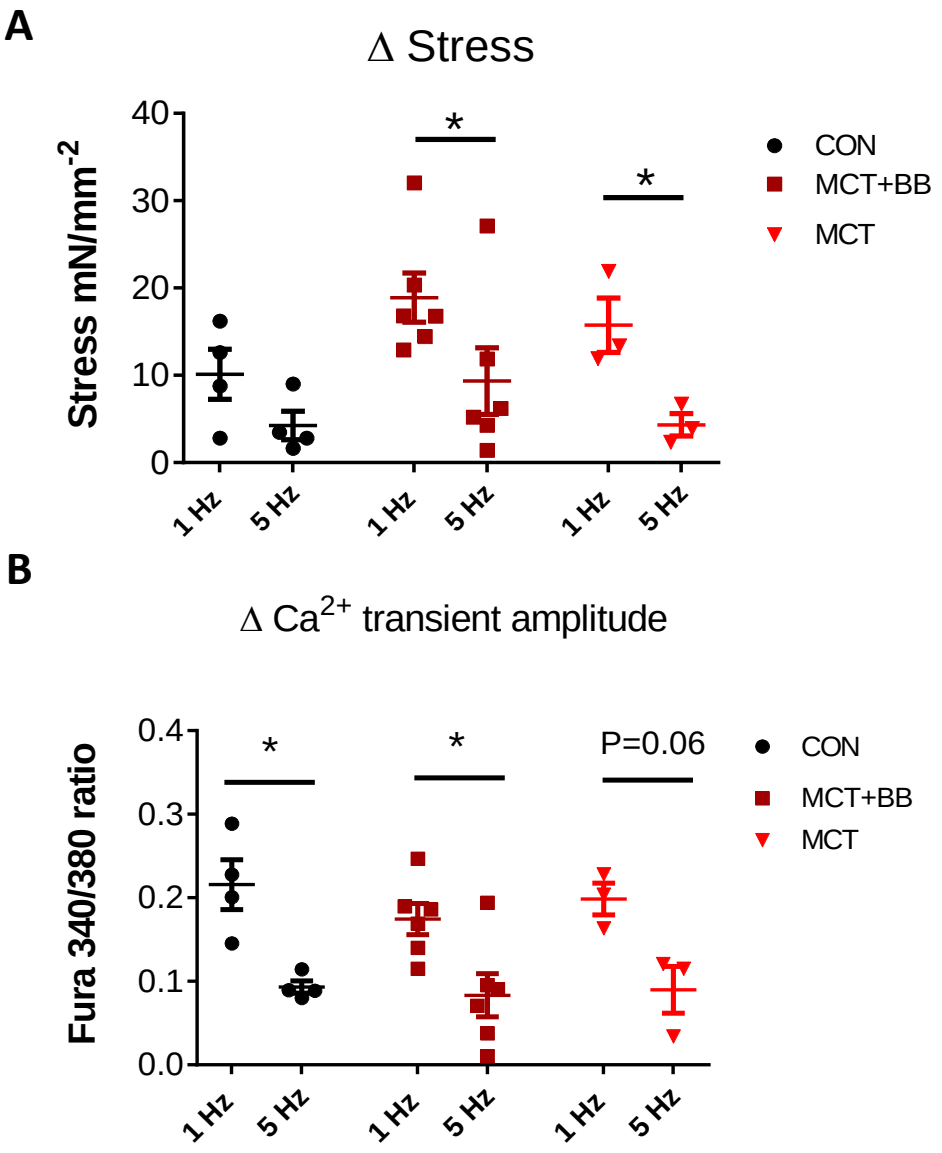

Figure 5-18 Change in stress production and $[Ca^{2+}]_i$ transient amplitude in response to pacing at 5 Hz

Individual recordings are plotted with field stimulation at 1Hz at the end of the washout period and then at 5 Hz **A.** Force production (mN) was normalised to the cross sectional area of the trabeculae (mm^2). CON n=4, MCT+BB n=5, MCT n=3, Two-way ANOVA (*P<0.05, 1Hz vs. 5Hz).

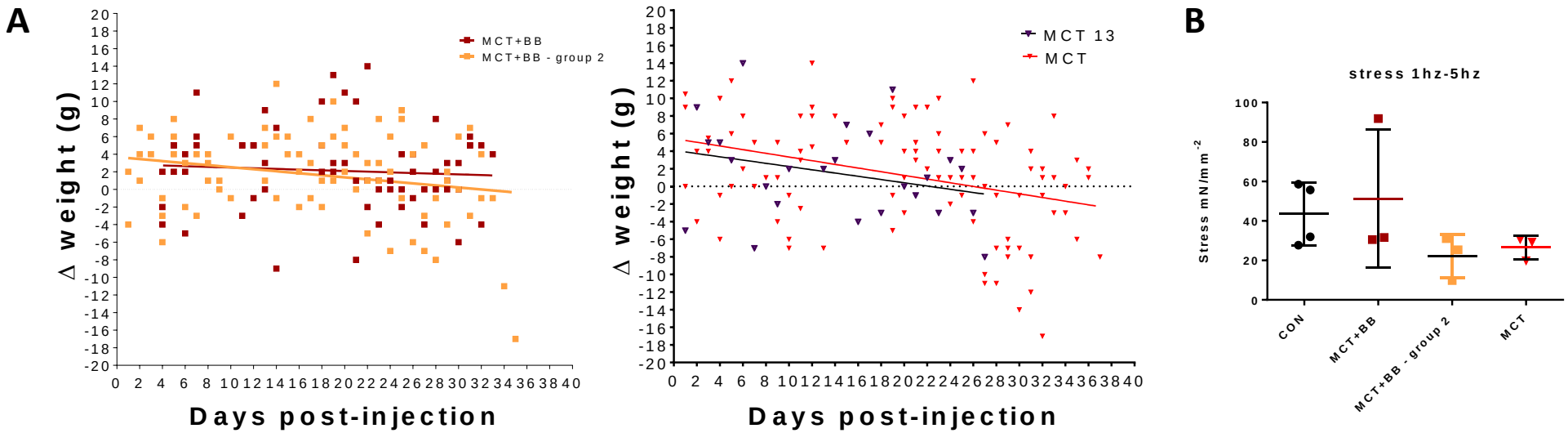

Figure 5-19 Comparison of daily weight variation and response to 5 Hz stimulation between different vials of MCT injected

A.Weight change from the previous day was calculated and individual weight change plotted for each group. Line of best fit for the data is plotted for each group and linear regression calculated. For MCT+BB (group 2) and MCT the slope of the line is significantly deviated from zero ($P<0.05$). MCT+BB n=3, MCT+BB- group 2 n=3, MCT n=4, MCT 13 n=1. **B.** Individual recordings are plotted of percentage change in stress produced when field stimulation was increased to 5 Hz. Force production (mN) was normalised to the cross sectional area of the trabeculae (mm^2). CON n=4, MCT+BB n=3, MCT+BB – group 2 n=3, MCT n=3, Two-way ANOVA

5.4. Discussion:

Selective stimulation of the β_1ARs in CON myocytes caused increased fractional cell shortening and $[Ca^{2+}]_i$ transient amplitude, and decreased the time to 50% relaxation and 50% $[Ca^{2+}]_i$ transient decay. This response was significantly blunted in failing myocytes from MCT animals compared to CON. MCT+BB myocytes showed a partial recovery from the MCT blunted phenotype, with no significant difference between CON in these parameters. In vivo heart function of MCT animals treated with metoprolol has previously been characterised within the group, through haemodynamic and echocardiography measurements (Fowler and 2016). MCT+BB animals had a significantly improved survival compared to the MCT animals ($P<0.05$), increasing the median survival day to 31 from 23. RV end diastolic pressure recordings in MCT and MCT+BB were almost double that of CON animals, with vascular resistance was also showing a significant increase in both MCT and MCT+BB compared with CON. Metoprolol was not expected to affect the pulmonary vasculature, in which β_2AR are present, due to the selectivity of metoprolol for the β_1AR. Improved RV function is therefore assumed to be the cause of increased median survival day in MCT+BB animal. Treatment with metoprolol started 15 days post injection of MCT; an increase in pulmonary artery pressure as well as an increased HW to BW ratio and RV to LV+S ratio has been reported at this time point, indicating RV hypertrophy (Lee et al., 1997). It is important that treatment is started after signs of hypertrophy have already begun to develop for clinical relevance; PAH is normally only diagnosed in later stages of the disease when RV hypertrophy is already present. Other studies using the MCT model treated with β-blockers have also observed an increase in survival (de Man et al., 2012) (Bogaard et al., 2010). These studies have used bisoprolol and carvedilol respectively; however neither has investigated effects on βAR activity. The present study is the first to examine selective β_1AR and β_2AR responsiveness in MCT animals treated with β-blockers.

5.4.1. β_1-adrenergic changes in PAH

Typically in LV heart failure, after an initial insult, there is an increase in sympathetic drive which leads to a reduction in β_1ARs and desensitisation of the β-AR response. The extent to which sympathetic nerve activity is increased in PAH induced heart failure is not as clear. A number of studies have indicated that sympathetic activity is increased in PAH patients: Nagaya et al. observed increased plasma noradrenaline levels in end-stage heart failure PAH patients compared to patients with minimally impaired heart function (Nagaya et al., 2000); Velez-Roa et al. observed significantly higher sympathetic nerve activity within skeletal

muscles of PAH patients compared to control patients, which indicated an increased neuronal sympathetic drive (Velez-Roa et al., 2004). However Velez-Roa et al. and other studies have questioned whether the observed increase in sympathetic activations reaches pathophysiological relevance (Nootens et al., 1995; Velez-Roa et al., 2004; Lowes et al., 1997), although correlations between increased sympathetic nerved activity and clinical deterioration of patients have been observed (Ciarka et al., 2010).

Despite the increase in sympathetic drive not always being apparent, a reduction and desensitisation of the cardiac β-AR receptors is more routinely seen in PAH patients with RV heart failure (Bristow et al., 1992; Lowes et al., 1997). In the MCT model, reduced β_1AR protein expression and mRNA levels have been shown as well as evidence for receptor desensitisation (Piao et al., 2012). Ishikawa et al. have reported an increase in plasma noradrenaline (as well as Kögler et al.) and tissue adrenaline and noradrenaline within the RV of MCT animals compared to CON, suggesting an increased sympathetic drive in the MCT (Ishikawa et al., 1991; Kögler et al., 2003). Leineweber et al. and others have used a (−)-[^{125}I]-iodocyanopindolol (ICYP) radioligand binding assay (Brodde et al., 1981) to measure β_1AR membrane density within the heart. Using this method on isolated myocytes showed that the β_1AR subtype made up 75% of the total β-AR population in CON. The β_1AR membrane density was significantly decreased in MCT animals compared to CON (Leineweber et al., 2003), this reduction was only seen in the RV. Using different concentrations of ISO in a competitive binding assay, Leinewber also demonstrated a reduction in ISO binding in MCT. Ishikawa et al. also used the ICYP radioligand binding assay in the MCT model to measure β-AR membrane density in myocardium (Ishikawa et al., 1991). Unlike Leinebeter et al, this group showed a reduction in β_1AR density in both the RV and LV. The reduction of β_1AR density in LV myocardium was suggested to come from changes to non-myocyte cells in the sample. Levels of cAMP were also measured in Leineweber et al. via a radioimmunoassay after cardiac myocytes were incubated with ISO. The amount of cAMP produced in MCT myocytes after ISO stimulation was significantly reduced, by about 68%, compared to CON. In the present study mean fractional shortening was reduced by 57% in MCT myocytes compared to CON at 100 nM ISO. Although measuring total cAMP activity to ISO stimulation is a useful functional assessment, it fails to elucidate possible variation within the different cAMP compartments, which is seen to change in heart failure (Gorelik et al., 2013). Assessing individual cardiac myocyte function, by measuring cell shortening and $[Ca^{2+}]_i$ transient amplitude, prevents measurements of non-myocyte being included and gives a better idea of individual cell responses to β-AR stimulation. The present study shows a desensitisation of the response to selective β_1AR stimulation in

cardiac cells from the MCT animals at high concentrations of ISO. This fits with previous work that reports decreased cAMP activity and increased GRK2 activity in MCT myocytes (Piao et al., 2012).

When β_1ARs were stimulated in isolated RV cardiac myocytes a blunted response in both contraction amplitude and rate of relaxation was observed in the MCT group compared with CON (representative traces Figure 5-2). This is comparable to the decreased βAR response seen in human LV HF patients (Bristow et al., 1982), which results in a reduced exercise tolerance in patients and inability to increase cardiac output in response to demand. The reduced response in shortening appears to be linked with the $[Ca^{2+}]_i$ handling in these cells, as $[Ca^{2+}]_i$ transient amplitude and time to 50% $[Ca^{2+}]_i$ decay were also blunted in the MCT group compared with CON. Prolonged decay of the $[Ca^{2+}]_i$ transient is linked with reduced reuptake of Ca^{2+} into the sarcoplasmic reticulum (SR) and cardiac alternans (Díaz et al., 2004), which can lead to potential fatal arrhythmias and sudden cardiac death. In MCT rats a reduction in SERCA protein expression has previously been recorded (Xie et al., 2012), as well as reduced mRNA and SERCA activity (Benoist et al., 2014). When locally perfusing isolated cardiac myocytes with 100 nM ISO, a higher percentage of cells from the MCT animals became spontaneously contractile, then stopped contracting compared with the CON and MCT+BB groups. This may be due to early after depolarisation (EADs) or delayed after depolarisation (DADs). Increased SR Ca^{2+} content of the MCT cells with reduced mRNA expression phospholamban (PLN) has been reported within the research group (Fowler et al. in submission) could cause cellular Ca^{2+} overload when stimulating at higher ISO concentrations and result in DAD explaining the increased number of cells developing alternans in the MCT group.

5.4.2. β_2-adrenergic changes in PAH

Within the literature, studies of patients and animal models of PAH which examine possible β-AR changes in the heart tend to focus mainly on the β_1AR components. This may be because in normal physiology β_2AR makes up only a small proportion of the total βAR pool within the heart and produces a smaller inotropic response to stimulation. In PAH patients the density of the β_2AR has not been seen to change within the RV (Bristow et al., 1992). In LV heart failure models the total β_2AR density in myocytes is similarly unaltered, although the membrane location of the receptor is suggested to be relocated, which alters downstream signalling (Wright et al., 2014; Nikolaev et al., 2010). In the present study, when the cardiac β_2AR were selectively stimulated not all cells showed a positive inotropic

response. Varying results have been reported in the literature with some studies not seeing an increase in percentage shortening with selective β_2AR stimulation (MacDougall et al., 2012), while others see a robust increase in contraction (Xiao et al., 1999a). This, in part, may be due to to species, disease and/or agonist used (Xiao et al., 1999b; Staus et al., 2016). The functional response to selective β_2AR stimulation varies within different mammals from no contractile response being seen in mouse, to a moderate response in canines and a robust inotropic and lusitropic response in the failing human heart (Kaumann et al., 1999). In the present study, of those cells that did show a positive response there was a significant increase in fractional shortening, which was observed in all three groups (CON, MCT+BB and MCT) at 10 μM zinterol in the presence of a selective β_1AR antagonist. Time to 50% relaxation was also reduced in CON cells with 10 μM zinterol. Although the functional response to selective β_2AR stimulation did not vary between the groups, this does not rule out possible changes to the β_2AR coupling and membrane location. The ability of β_2AR to couple to either $G\alpha_s$ or $G\alpha_i$ further complicates the issue. Redistribution of the β_2AR and changes to the cAMP signaling have been reported in animal models of LV HF (Wright et al., 2014; Nikolaev et al., 2010) but functional changes in myocyte β_2AR responsiveness were not measured. Changes in protein levels and membrane location of the β_2AR proteins will play an important role in this study to determine any possible changes occurring within the cells which are undetectable by the functional measurements made in this study (Chapter 6).

5.4.3. The use of β-blockers in PAH

Under current treatment guidelines for PAH there are no specific targets for the failing RV and β-blockers are not recommended. The RV is structurally and functionally different from the LV and has a limited ability to increase stroke volume; therefore β-blockers are not thought to be well tolerated, due to possible negative chronotropic effects. Recent studies have started to question if β-blockers could be used to improve RV function in PAH patient; animal models of PAH have tolerated the treatment well (Bogaard et al., 2010; de Man et al., 2012; Pankey et al., 2016). The importance of which β-blocker (1st, 2nd or 3rd generation) is used has recently been highlighted in response to an observational study looking at survival and the used of β-blockers (Malenfant and Perros, 2016; Bandyopadhyay et al., 2015). The initial study showed no change in long term survival of those PAH patients who were prescribed β-blockers for co-morbidities compared with those not taking them. The letter to the editor highlights that the conclusions from the article may be more positive than described in the initial paper, showing that there were was no detrimental effects on

survival when taking these drugs (Malenfant and Perros, 2016). The generation or specificity of β-blockers plays an important role, as many first generation drugs target both the β_1AR and β_2AR receptors which could lead to smooth muscle contraction and vasoconstriction within the pulmonary vasculature provoking further pulmonary hypoxia and increasing afterload on the RV (Leblais et al., 2008). Metoprolol is a second generation β-blocker which is a complete inverse agonist specifically of the β_1AR and has been shown to bind to agonist sites and hold the receptor in a constitutively inactive state (R), which prevents phosphorylation of the receptor (Maack et al., 2000). This would prevent internalisation of the receptor through the β-arrestin pathway. Bucindolol and carvedilol, 2nd and 3rd generation β-blockers respectively, which have been used in the MCT model have a lower inverse agonist activity and under some conditions show partial agonist signalling through the receptor (Lattion et al., 1999).

One of the advantages of metoprolol is that it is already a licenced drug which is prescribed to patients with LV heart failure and has been shown to improve patient survival and decrease New York Heart Association (NYHA) functional class (Hjalmarson et al., 2000). Chronic metoprolol treatment in human patients with LV heart failure increases the β_1AR and density re-sensitises the LV (Gilbert et al., 1996), and reduces the instances of sudden cardiac death (Group, 1999).

In this model of MCT, chronic β-blocker treatment with metoprolol appears to aid in the re-sensitization of the β_1AR and improve the β-response in isolated cardiac myocytes. Fractional shortening was significantly improved compared with the MCT group at the highest concentration of ISO and time to 50% relaxation was also improved. The $[Ca^{2+}]_i$ measurements mirror improvements seen in contraction. Metoprolol's action through partially blocking over stimulation of the β_1AR could prevent the receptor internalisation and degradation. There was no difference in the functional response to selective β_2AR, which is perhaps not surprising as metoprolol is a selective β_1AR blocker and there is lack of β_1AR-β_2AR crosstalk. The precise mechanism by which the β-blockers are acting to make these functional improvements has not been definitively proven and there may yet be other effects of metoprolol on signalling downstream from the receptor. The potential mechanisms by which β-blocker improve heart function have yet to be examined in depth in the RV. Despite the anatomical differences between the RV and LV, the selective β-blocker metoprolol appears to have similar functional benefits.

5.4.4. Trabeculae carneae

Experiments using trabeculae were carried out on a visit to the University of Auckland where there is established expertise in measuring force and $[Ca^{2+}]_i$ simultaneously in this preparation (Kaur et al., 2016; Shen et al., 2016). In Auckalnd, animals took longer to the develop signs of heart failure following injection of MCT, even though the animals were given the same dose of MCT per kg of body weight (compared with studies conducted in Leeds). There appears to be a correlation with injection weight and time taken to exhibit signs of heart failure. The reason behind this is not known. In the literature, injection weight and average days post injection to reach failure are not routinely stated.

Previous studies of trabeculae stress/force production in the MCT model reflect what has been shown in the present work measuring isolated cardiac myocytes fractional shortening and $[Ca^{2+}]_i$ measurements. Trabeculae from MCT animals show a reduction in force production and $[Ca^{2+}]_i$ handling compared to CON (Versluis et al., 2004; Miura et al., 2011; Kögler et al., 2003). $[Ca^{2+}]_i$ wave prolongation was observed, as well as an increase in diastolic $[Ca^{2+}]_i$ within trabeculae from MCT animals stimulated at 2 Hz (Miura et al., 2011). In the present study there were no differences baseline stress or $[Ca^{2+}]_i$ transient amplitude between CON and MCT, although this may be due to poor controls. Extracting the trabeculae from the heart is done by fine dissection being careful not to mechanically damage or stretch the trabeculae, which is technically demanding. Stress production at the length-tension maximum (L.max) in CON animals was almost half of what has previously been reported in the literature (Miura et al., 2011; Raman et al., 2006). This would suggest that some of the CON trabeculae may have been damaged in the dissection procedure. Despite this low baseline force production the trabeculae experiments still show similar tends to those see in the isolated cells. CON trabeculae showed a significant increase in force and $[Ca^{2+}]$ transient amplitude when perfused with ISO, while the MCT trabeculae did not. There was also a trend for a faster time to 50% relaxation in the CON animals compared to the MCT, suggesting more efficient SR Ca^{2+} uptake.

Unfortunately the metoprolol treatment did not appear to have been as beneficial in the Auckland animals as in the Leeds animals, which may be due to using a new (more potent) vial of MCT in the last cage of animals. This cage contained one placebo treated and three metoprolol treated animals. When comparing these animals to the rest of their cohort, the MCT animal showed clinical signs of failure 6 days earlier than the median day of the other MCT animals (Figure 5-19.). The MCT+BB animals from the first batch, when plotting

change in weight over time maintained a steady positive change in weight (as seen by the line of best fit Figure 5-19), whereas MCT+BB from the second batch have a negative change in weight gain over time which deviated significantly from zero (linear regression ($P<0.05$) Figure 5-19). The timing of dosing is crucial due to the fast progression of HF in this model; ensuring that dosing is early enough to have time to affect the heart, whilst waiting until changes in RV dynamics (wall thickness/pressure) appear. Further force experiments would require the proper characterisation of MCT animals' progression to failure at the heavier weight (with echocardiography measurements), to enable the correct assignment of a day for dosing to begin.

5.5. Conclusion

We have shown for the first time that metoprolol treatment of PAH induced RV failure improved the β_1-AR response in isolated rat cardiac myocytes. These data along with other supporting evidence (de Man et al., 2012; Fowler and 2016) show the functional benefits that could be achieved with β-blocker treatment in PAH patients. The improved β-AR function of the heart and potential block of detrimental remodelling signals could help, delay if not prevent, the onset of RV HF from RV hypertrophy. The molecular mechanisms of β-blockers are still not fully understood; even though they have been shown to functionally improve the heart and increase β-AR protein and mRNA expression, there may be other pathways contributing to this bar the simple blocking of overstimulation of the β_1AR. Measuring changes at the molecular level of the β-AR signaling cascade in heart failure and remodeling within β-blocker treatment may begin to reveal how these functional improvements are being achieved. Regulatory proteins of the β-AR signalling pathway such as the caveolar proteins, have previously been seen to be reduced in human patients and animal models of LV heart failure (Feiner et al., 2011; Woodman et al., 2002), but have not been studied in RV heart failure. Cav-1 peptide administration has previously been shown to prevent HF in the rat MCT model (Jasmin et al., 2006). Although this was mainly ascribed to primary effects within the pulmonary vasculature, concurrent actions on the ventricle were not ruled out. Caveolae have previously been shown to play a key role in regulating downstream processes of the β-AR signalling across different agonist concentrations (MacDougall et al., 2012; Agarwal et al., 2011). How these proteins change and where they are located in the membrane may help explain some of the functional observation seen with β-blocker treatment.

Chapter 6. Protein changes in right ventricular failure

6.1. Introduction

The functional response to selective β_1AR stimulation in isolated cardiac myocytes from MCT animals was blunted compared to that of CON animals. Treatment with the selective β_1AR blocker metoprolol improved the MCT phenotype towards the response seen in CON cells (Chapter 5). Previous examination of this model within the research group revealed a reduced t-tubular network and transverse-orientation, as well as reduced Ca^{2+} handling ability in the MCT myocardium (Fowler et al., 2015; Stones et al., 2013). This was partially restored with β-blocker treatment. The right ventricle (RV) of MCT animals showed a blunted β-AR response and a reduction in β-AR binding with ICYP radioligand binding assay (Leineweber et al., 2003). The impact of β-blocker treatment of MCT animals on proteins of the β-AR cascade or related signalling proteins has not previously been examined. This was the focus of the present study.

Caveolae are crucial for compartmentalisation of β_2AR signalling (Rybin et al., 2000; MacDougall et al., 2012), with many of the crucial β-AR signalling proteins located within buoyant caveolar fractions following sucrose gradient fractionation, or co-immunoprecipitating with caveolar proteins (Agarwal et al., 2011; Insel et al., 2005). Disruption to caveolae and the caveolin proteins is linked with disorganised cAMP signaling from the β_2AR in left ventricular (LV) heart failure (Wright et al., 2014; Feiner et al., 2011). Indeed much of what is known about changes to caveolae in heart failure has been studied in models of LV heart failure. Although there are similarities between ventricles, there are also significant differences (e.g embryological origin, pressure development), and assumptions must not be made that both ventricles act identically to stress, as this is not always the case. In heart failure induced by pulmonary artery hypertension (PAH), β-AR abnormalities are mainly isolated to the RV (Seyfarth et al., 2000). When comparing increased overload of the RV and LV across multiple studies, structural remodelling of the ventricles appears to share some common features (Bristow and Quaife, 2015), with a similar degree of down regulation of the β-AR being reported (Mak et al., 2012; Bristow and Quaife, 2015). This might predict that similar changes would be seen to the β-AR signalling and caveolar proteins in RV as in the LV heart failure model. This premise has also been used to argue the use of β-blocker in PAH patients. Changes to caveolae and caveolar proteins have not previously been studied in the heart of MCT animals.

Here we look at the remodelling of caveolar and β-AR signalling proteins in the MCT animals as well as the impact of β-blocker treatment on these changes. At the heart and cellular level of MCT animals, treatment with β-blockers improves function. To study if this improvement in function is due to restoration of the β-AR signalling signaling proteins and/or changes in their regulation by caveolae both protein expression and protein distribution across the membrane was studied.

6.2. Methods

At the designated end-point animals were humanly culled using a listed schedule one technique. For whole RV homogenate, hearts were quickly removed and dissected. The RV free wall was removed and 100-200 mg of tissue was snap-frozen in liquid nitrogen ready for processing at a later date. Frozen sections of RV were homogenised in homogenisation buffer 100 mg/mL ((mM) 5 HEPES, 1 EDTA, 5 $MgCl_2$, 0.1% Triton-X100) 5 x 20 s on ice. Samples were then centrifuged at 16000 g at 6 ^{o}C and supernatant aspirated. Before SDS-PAGE and Western blot an aliquot of 5 x Laemmli sample buffer was added to samples to create a 1x final concentration.

For sucrose gradient fractionation, hearts were quickly removed and the coronary circulation cleared of blood on a Langendorff apparatus through retrograde perfusion with Cell Tyrode solution. Hearts were then weighed and RV free wall dissected and ~250 mg homogenised in detergent free buffer (500 mM Na_2CO_3 (pH 11), 1 x protease (Roche Applied Science) and phosphatase (Thermo Scientific Pierce) inhibitor cocktails). Samples were then sonicated, centrifuged and layered onto a discontinuous sucrose gradient and spun overnight (As detailed in Methods 2.8.2). Fractions were then collected (1 mL each) and stored at -20 ^{o}C until used for Western blotting.

Total protein concentration was measured in samples using a bicinchoninic acid (BCA) assay (as detailed in Methods 2.8.5.1). RV homogenate samples were run on Precast Midi Protein Gels (567-1035, 567-1045, 567-1085, BIO-RAD, UK) before transferring to a PVDF membrane described in (Methods 2.8.5.2). Samples from sucrose gradients were run on and mini gels (Methods 2.8.5.2). Western blotting performed as described in (Methods 2.8.5.2).

6.3. Results

6.3.1. Altered protein expression in right ventricular muscle homogenate

6.3.1.1. Caveolar proteins

In RV muscle homogenate from MCT animals there was a significant reduction (~50%) in caveolin 1 (Cav 1) protein expression compared with saline animals (CON) ($P<0.001$) (Figure 6-1). Cav 1 protein expression was also significantly reduced in MCT+BB animal compared to CON ($P<0.01$). Similar effects were seen for Caveolin 3 (Cav 3); protein expression was significantly reduced in MCT animals compared to CON ($P<0.01$). MCT Cav 3 protein expression was also significantly reduced compared with MCT+BB ($P<0.05$), however by comparison with data for Cav 1, there was no difference between MCT+BB and CON, suggesting that β-blocker treatment attenuates effects of MCT on Cav 3. Cavin 1 RV protein expression was significantly decreased by around 20% in MCT animal compared to CON ($P<0.05$). There was no difference between MCT+BB cavin 1 expression and CON or MCT, again suggesting that β-blocker treatment attenuates effects of MCT on cavin 1 expression. Cavin 4 protein expression was similar in all three groups.

6.3.1.2. β-adrenergic signalling proteins

Figure 6-2 summarises changes in expression of the β-AR cascade proteins. β_1AR protein expression in MCT RV homogenate was significantly reduced by around 30% compared with CON ($P<0.01$). There was no difference in β_1AR protein expression between MCT+BB and either CON or MCT. In this heart failure model a single band at around 50 kDa was observed for the β_2AR in Western blot. This contrasts with the double bands seen in the AB model (discussed in Chapter 4). The β_2AR protein expression levels did not significantly differ between the CON and MCT animals. In MCT+BB, β_2AR expression was significantly reduced compared to CON ($P<0.05$), with no difference between MCT+BB and MCT. Adenylyl cyclase (AC) 5/6 protein expression was significantly reduced by over 50% in MCT animals compared to CON ($P<0.001$). AC 5/6 expression in the MCT group was also significantly reduced compared to MCT+BB animals ($P<0.01$). Expression of the inhibitory $G\alpha_i$ 3 subunit was significantly increased in MCT by >100% compared with CON ($P<0.001$) and the $G\alpha_i$ 3 expression was also significantly higher in MCT compared to MCT+BB ($P<0.001$). Compared to CON, MCT RV G -protein receptor kinase 2 (GRK2) protein expression was doubled ($P<0.001$). GRK2 expression in MCT was also significantly increased compared to that of MCT+BB animals ($P<0.001$).

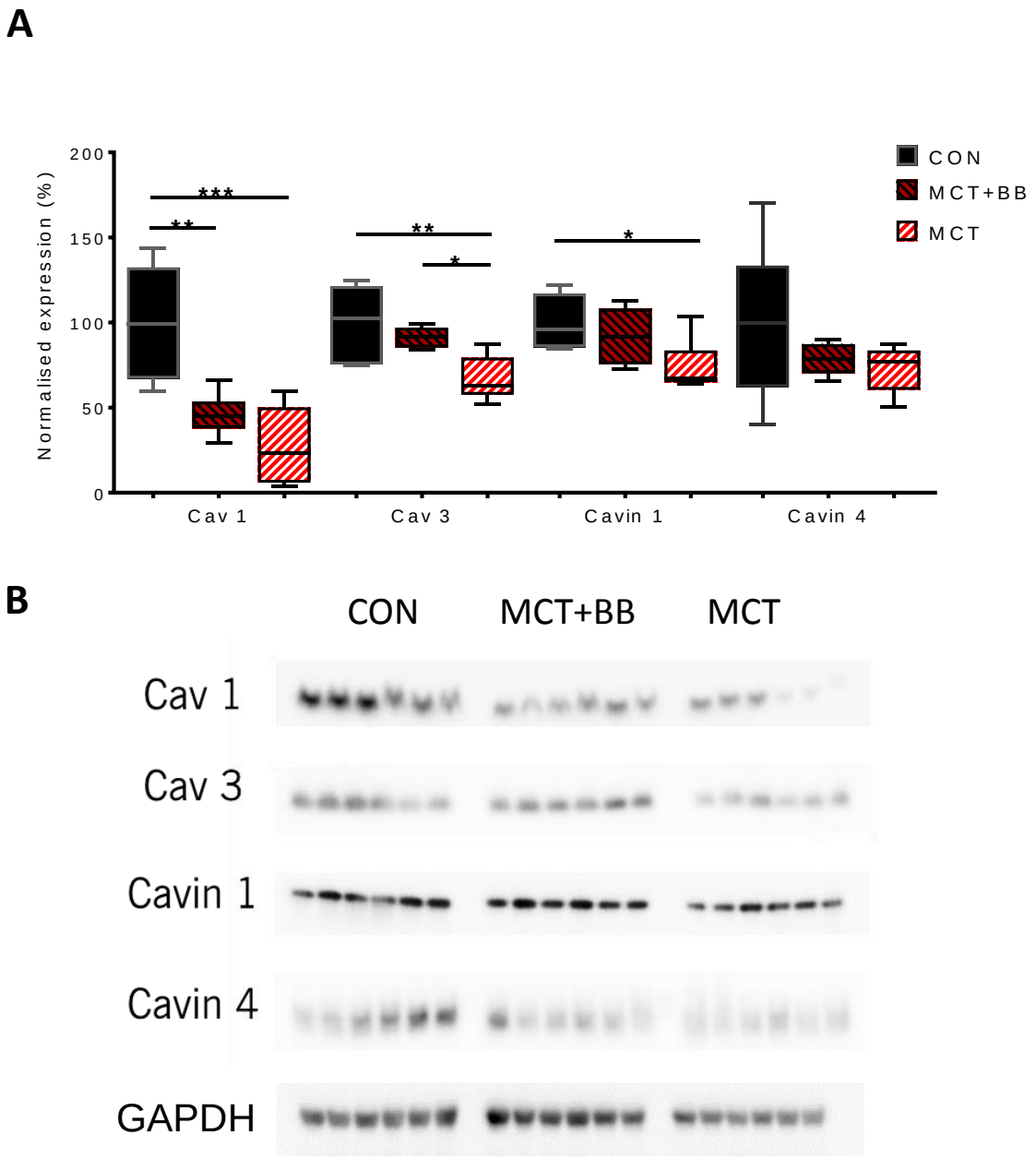

Figure 6-1 Caveolar protein expression in right ventricular heart failure

A. Western blot of right ventricular muscle homogenised in Laemmli sample buffer. Expression is normalised to GAPDH and expressed as a percentage of mean CON value, box and whisker graph. CON n=6, MCT+BB n=6, MCT n=6 One-way ANOVA, *P<0.05, **P<0.01, ***P<0.001. **B.** Representative Western blot.

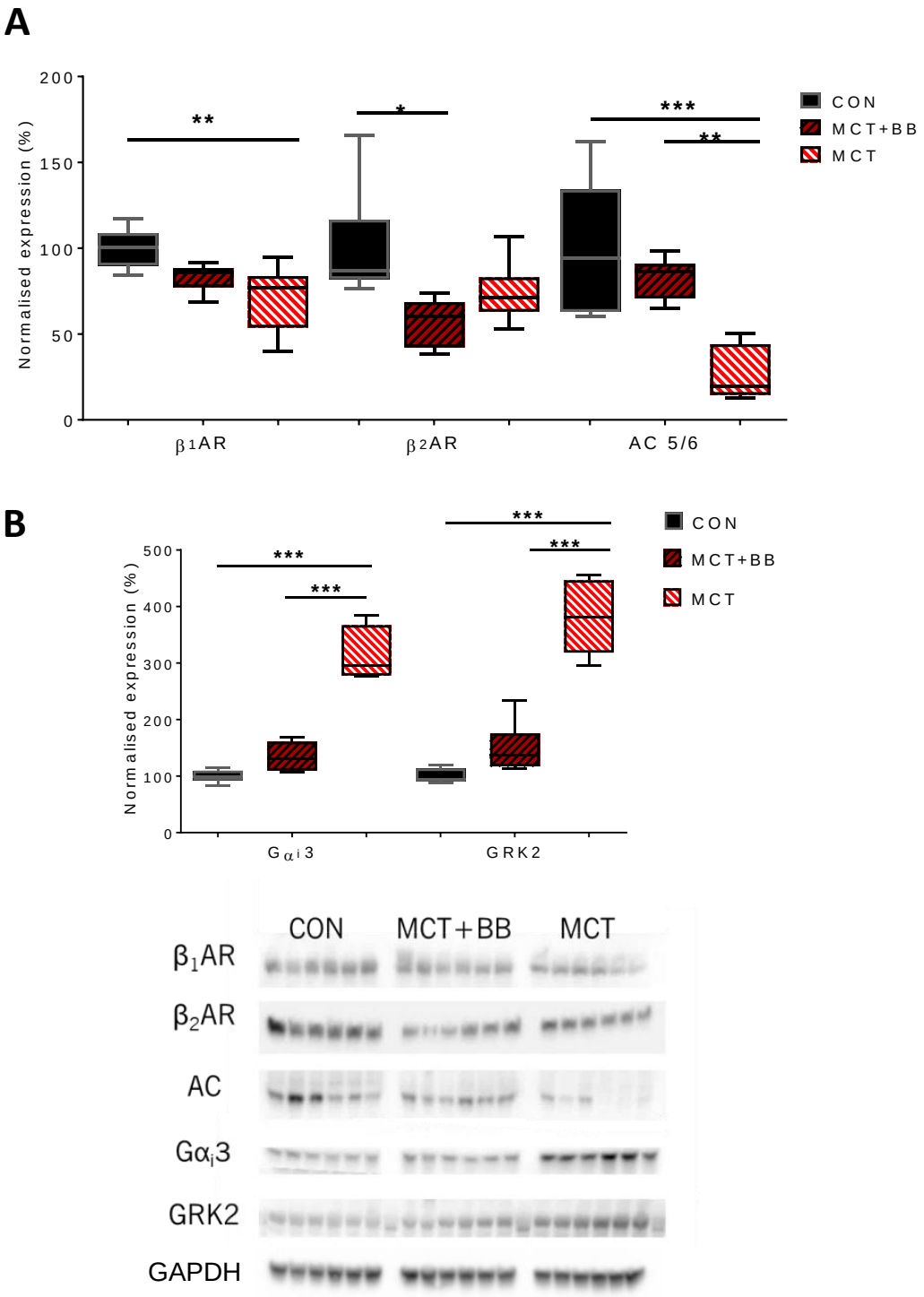

Figure 6-2 β-adrenergic signalling protein in right ventricular heart failure

A. Western blot of right ventricular muscle homogenised in Laemmli sample buffer. Expression is normalised to GAPDH and expressed as a percentage of mean CON value, box and whisker graph. CON n=6, MCT+BB n=6, MCT n=6 One-way ANOVA, *P<0.05, **P<0.01, ***P<0.001. **B.** Representative Western blot.

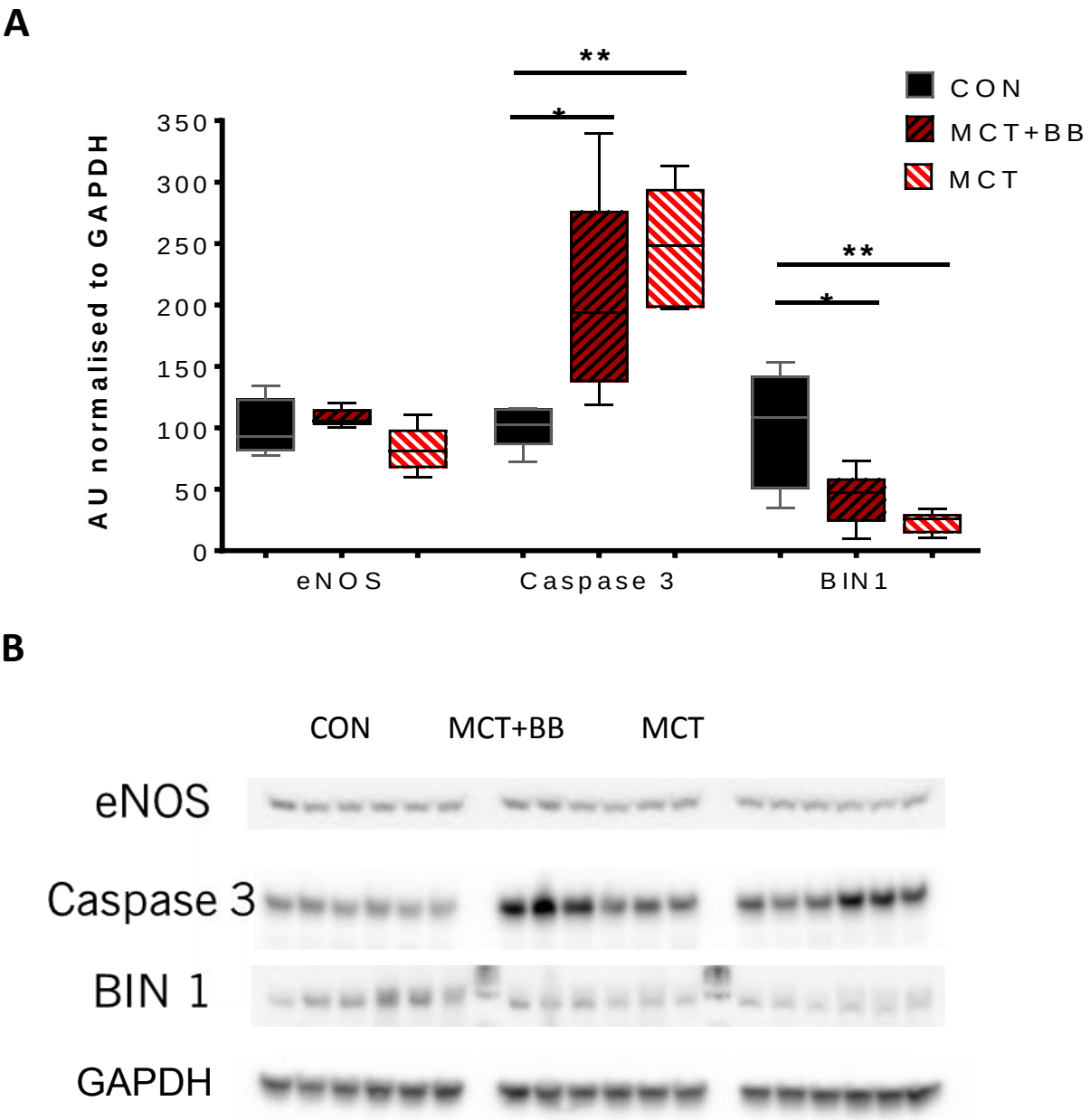

Figure 6-3 Cellular remodelling protein changes in right ventricular heart failure

A. Western blot of right ventricular muscle homogenised in Laemmli sample buffer. Expression is normalised to GAPDH and expressed as a percentage of mean CON value, box and whisker graph. CON n=6, MCT+BB n=6, MCT n=6 One-way ANOVA, *P<0.05, **P<0.01, ***P<0.001. **B.** Representative Western blot.

To summarise, MCT resulted in a reduction in expression of β_1AR and AC and an increase in expression of $G\alpha_i$ 3 and GRK2 proteins, all these changes were normalised to some extend by β-blocker treatment.

6.3.1.3. Cellular remodelling proteins

Figure 6-3 shows that expression of endothelial nitric oxide synthase (eNOS) protein in the RV was similar in all three groups ($P>0.05$). The expression of caspase-3 was significantly increased in the MCT compared to CON ($P<0.01$). Caspase-3 expression was also significantly increased in MCT+BB compared to CON ($P<0.05$). We could not detect fragments of cleaved (activated) caspase-3 in any group. Bridging integrator 1 (BIN 1) protein expression within the RV homogenate was significantly reduced in the MCT group compared to CON ($P<0.01$). BIN 1 expression was also significantly decreased in MCT+BB compared to CON ($P<0.05$). To summarise, expression of proteins linked with remodelling of the heart during failure progression were reduced in the MCT group compared with CON, but treatment with metoprolol had no significant effect on this.

6.3.2. Membrane protein distribution changes in right heart failure

Using data from fractionated samples, the distribution of membrane proteins has been analysed in two ways which give different results and have different meanings (See Figures 6-4). The first **(A)** is by normalising each individual blot by signal intensity; on a single blot the total amount of protein across the fractions 4-12 is equally loaded in CON, MCT+BB and MCT, as calculated by BCA assay. Comparisons were made across animals which were time-matched to days post injection. Values are given as absolute expression percentage normalised to the highest intensity band on the individual blots; this enabled comparison across multiple blots and allowed analysis of changes in expression within specific fractions. The second way **(B)** is to normalise to distribution across the membrane in individual animal hearts; by calculating the total signal expression per heart and calculating expression in different fractions as a percentage of this. Values are given as expression in each fraction as a percentage of the sum of expression across all fractions; this enabled the analysis of membrane distribution to be studied.

6.3.2.1. Caveolae proteins

In CON the majority of the Cav 3 expression is located within the buoyant fractions (fraction 4+5). The expression of Cav 3 in the caveolar containing fractions was significantly decreased in MCT animals compared to CON (Figure 6-4. A) ($P<0.01$). There was no difference in expression in the other fractions. Membrane distribution of Cav 3 changed in the MCT animals, with a significant reduction in the proportion present in the buoyant fraction ($P<0.01$) and a significant increase in the heavy fractions ($P<0.05$) compared to CON RV (Figure 6-4. B). There was no difference in Cav 3 distribution in the buoyant or heavy fractions in MCT+BB compared with CON. To summarise there was a reduction in Cav 3 expression within the buoyant fraction and a change in membrane distribution in MCT animals which is partially restored with β-blocker treatment.

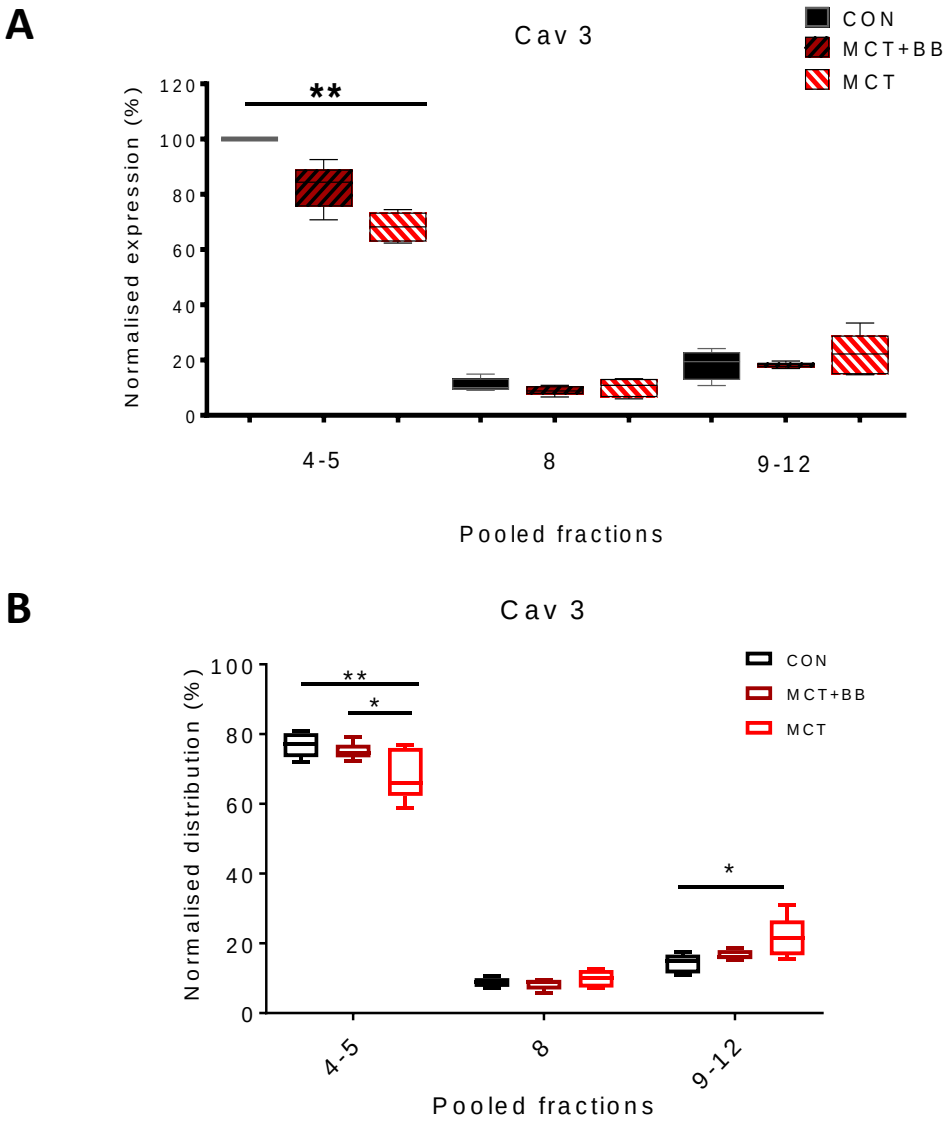

Figure 6-4 Caveolin 3 (Cav 3) protein membrane distribution in right ventricular heart failure

Western blot of right ventricular muscle homogenised in Na_2CO_3 buffer and fractionated on a sucrose gradient. Equal volumes of each fraction (4, 5, 8 and 9-12) were loaded with equal total protein loading between MCT and aged matched CON and MCT+BB. **A.** Individual Western blot comparing age-matched CON, MCT+BB and MCT were normalised to protein expression intensity on each membrane, box and whisker graph **B.** Protein expression in fractions was expressed as a percentage of total expression from all fractions (4-12) box and whisker graph. CON n=6, MCT+BB n=6, MCT n=6 **C.** Representative Western blot.

6.3.2.2. β-adrenergic signalling proteins

With the β_1AR distribution, similar problems occurred with the fractioned samples as previously experienced in the AB animals. After several attempts only three blots could be used for analysis. These gave varying results when analysing signal intensity within individual blots. There was no significant difference between the groups when data were presented as normalised expression (Figure 6-5. A). However, when data were presented as normalised distribution a different pattern emerged (Figure 6-5. B). There was a significant shift in the distribution of β_1AR across the different fractions, from the buoyant fraction to the heavy fraction in MCT ($P<0.01$). This shift was also significant in the MCT group compared to MCT+BB ($P<0.001$). This would suggest a redistribution of β_1AR from the caveolar membranes to the non-caveolar membranes in MCT. For the β_2AR there was no significant change in expression levels within the different fractions and no significant change in distribution between the different fractions between groups (Figure 6-6).

There was a significant decrease in adenylyl cyclase (AC) 5/6 expression within the caveolar fraction in MCT animals compared to CON ($P<0.05$) with no difference in heavy fraction expression (Figure 6-7. A). There was also a significant decrease in the expression of AC within the buoyant fractions in the MCT+BB animals compared to CON. For the $G\alpha_i$ 3 expression there was a trend for an increase in the MCT buoyant caveolar fractions compared to CON ($P=0.19$) (Figure 6-8. A). A significant increase in the expression of $G\alpha_i$ 3 in the caveolar fractions in MCT+BB compared to CON was shown ($P<0.05$). In the heavy fractions there was a significant increase in expression in the MCT animals compared to CON ($P<0.01$). There was a trend for an increase in the G-protein receptor kinase (GRK) 2 expression levels in the heavy fraction in MCT compared to CON ($P=0.064$)(Figure 6-9. A). MCT+BB show a significant increase in GRK2 expression in the heavy fraction compared to CON ($P<0.01$). For the AC 5/6, $G\alpha_i$ 3 and GRK2 the proportion of protein found in different membrane fractions significantly differ between the three groups. This highlights the advantages of studying distribution using both methods. Although there may be a reduction of expression observed within the caveolae/buoyant fractions (as seen in AC 5/6), as the majority of the protein expression is located here, changes in distribution may be too small to cause significant differences.

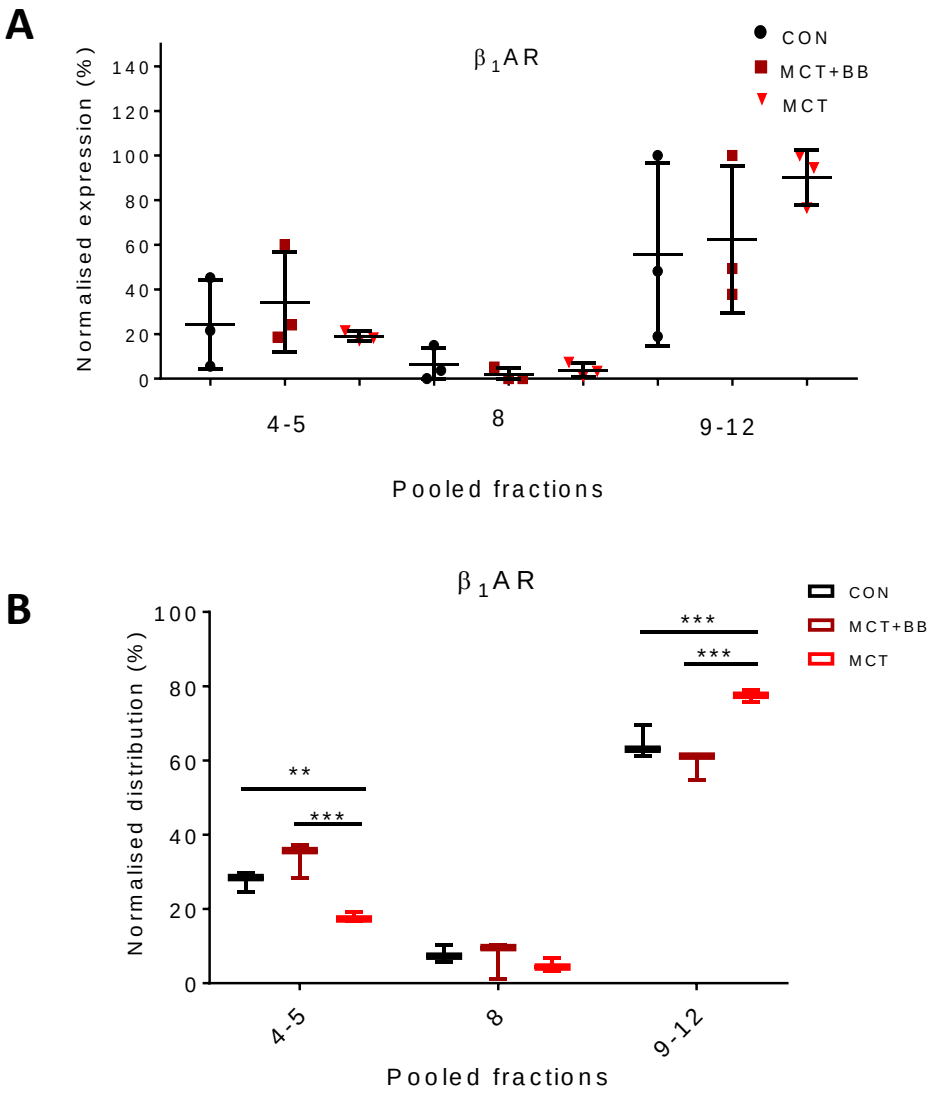

Figure 6-5 β_1 adrenergic receptor (β_1AR) protein membrane distribution in right ventricular heart failure

Western blot of right ventricular muscle homogenised in Na_2CO_3 buffer and fractionated on a sucrose gradient. Equal volumes of each fraction (4, 5, 8 and 9-12) were loaded with equal total protein loading between MCT and aged-matched CON and MCT+BB. **A.** Individual Western blot comparing age matched CON, MCT+BB and MCT were normalised to protein expression intensity on each membrane, box and whisker graph **B.** Protein expression in fractions was expressed as a percentage of total expression from all fractions (4-12) box and whisker graph. CON n=3, MCT+BB n=3, MCT n=3

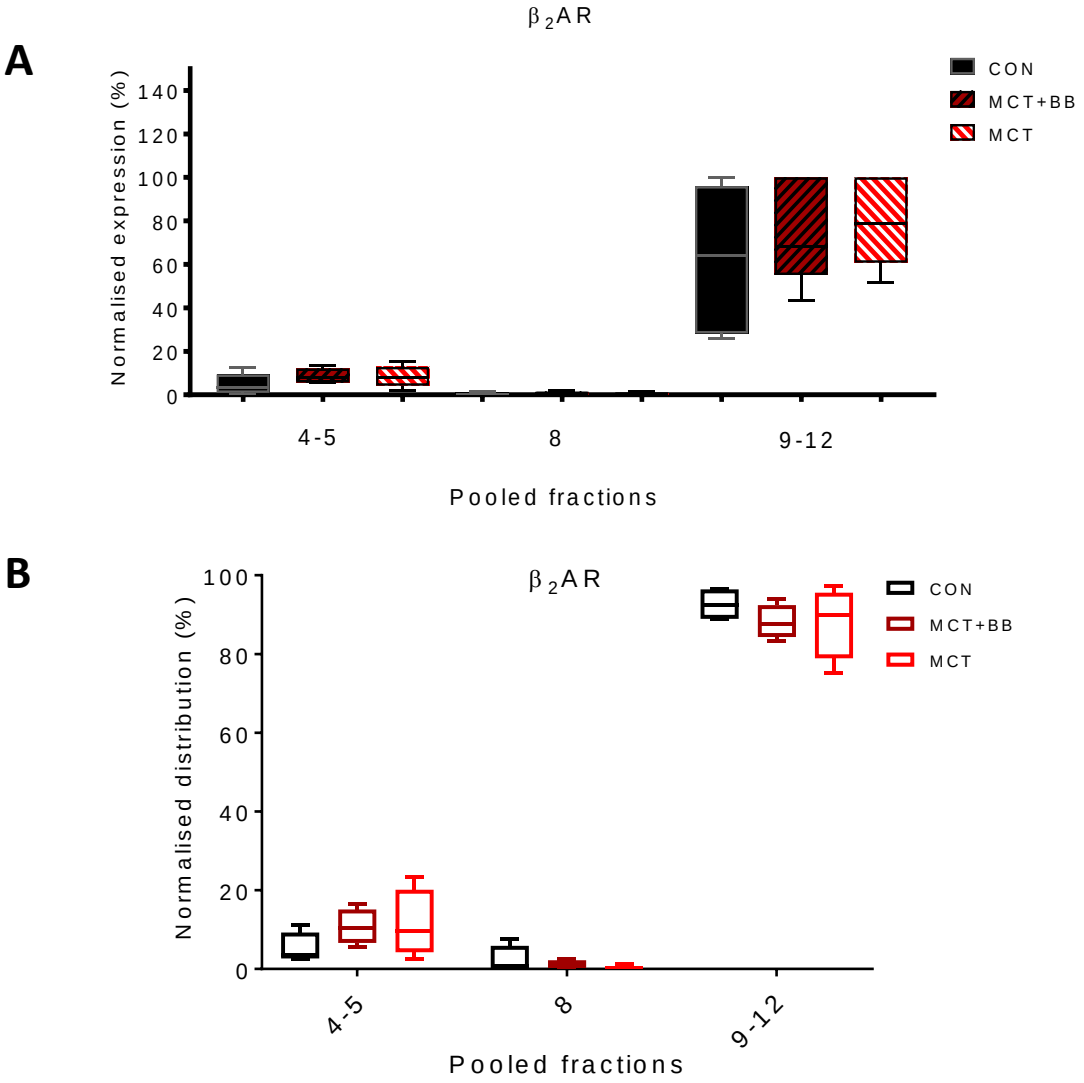

Figure 6-6 β_2 adrenergic receptor (β_2AR) protein membrane distribution in right ventricular heart failure

Western blot of right ventricular muscle homogenised in Na_2CO_3 buffer and fractionated on a sucrose gradient. Equal volume of each fraction (4, 5, 8 and 9-12) were loaded with equal total protein loading between MCT and aged-matched CON and MCT+BB. **A.** Individual Western blot comparing age matched CON, MCT+BB and MCT were normalised to protein expression intensity on each membrane, box and whisker graph **B.** Protein expression in fractions was expressed as a percentage of total expression from all fractions (4-12) box and whisker graph. CON n=6, MCT+BB n=6, MCT n=6

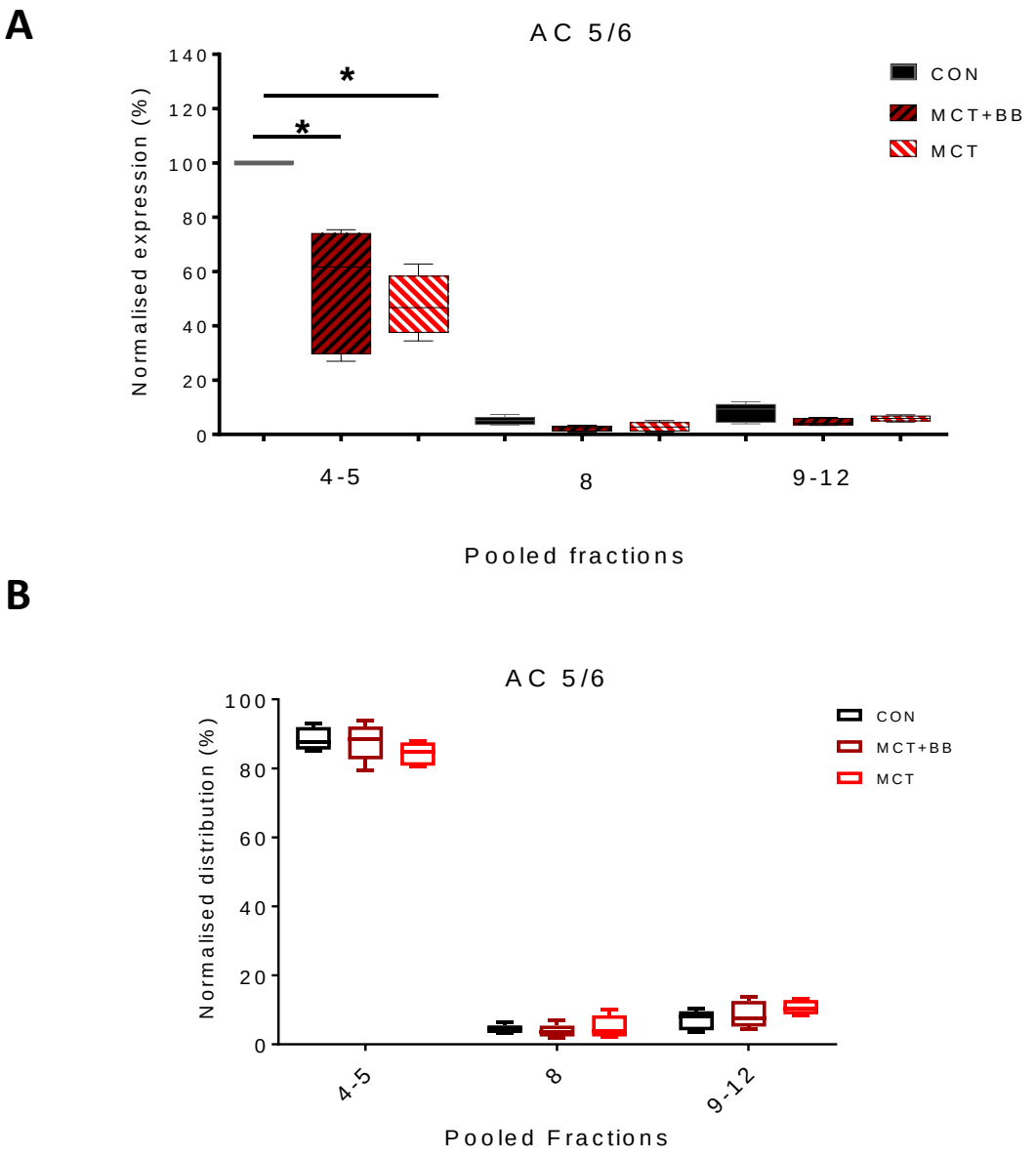

Figure 6-7 Adenylyl cyclase (AC) 5/6 protein membrane distribution in right ventricular heart failure

Western blot of right ventricular muscle homogenised in Na_2CO_3 buffer and fractionated on a sucrose gradient. Equal volumes of each fraction (4, 5, 8 and 9-12) were loaded with equal total protein loading between MCT and aged-matched CON and MCT+BB. **A.** Individual Western blot comparing age matched CON, MCT+BB and MCT were normalised to protein expression intensity on each membrane, box and whisker graph **B.** Protein expression in fractions was expressed as a percentage of total expression from all fractions (4-12) box and whisker graph. CON n=6, MCT+BB n=6, MCT n=6

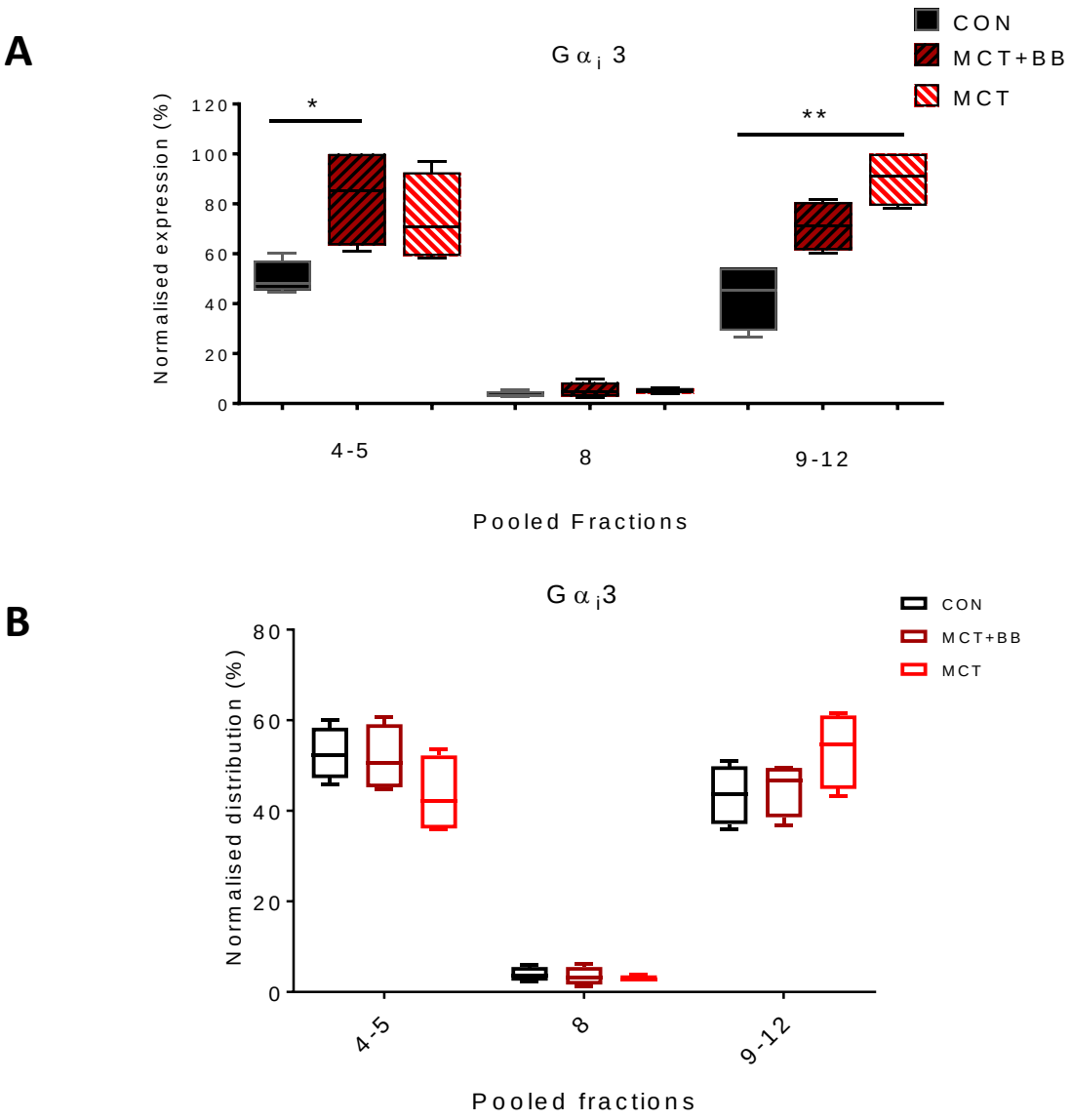

Figure 6-8 Gαi3 protein membrane distribution in right ventricular heart failure

Western blot of right ventricular muscle homogenised in Na_2CO_3 buffer and fractionated on a sucrose gradient. Equal volume of each fraction (4, 5, 8 and 9-12) were loaded with equal total protein loading between MCT and aged-matched CON and MCT+BB. **A.** Individual Western blot comparing age matched CON, MCT+BB and MCT were normalised to protein expression intensity on each membrane, box and whisker graph **B.** Protein expression in fractions was expressed as a percentage of total expression from all fractions (4-12) box and whisker graph. CON n=6, MCT+BB n=6, MCT n=6

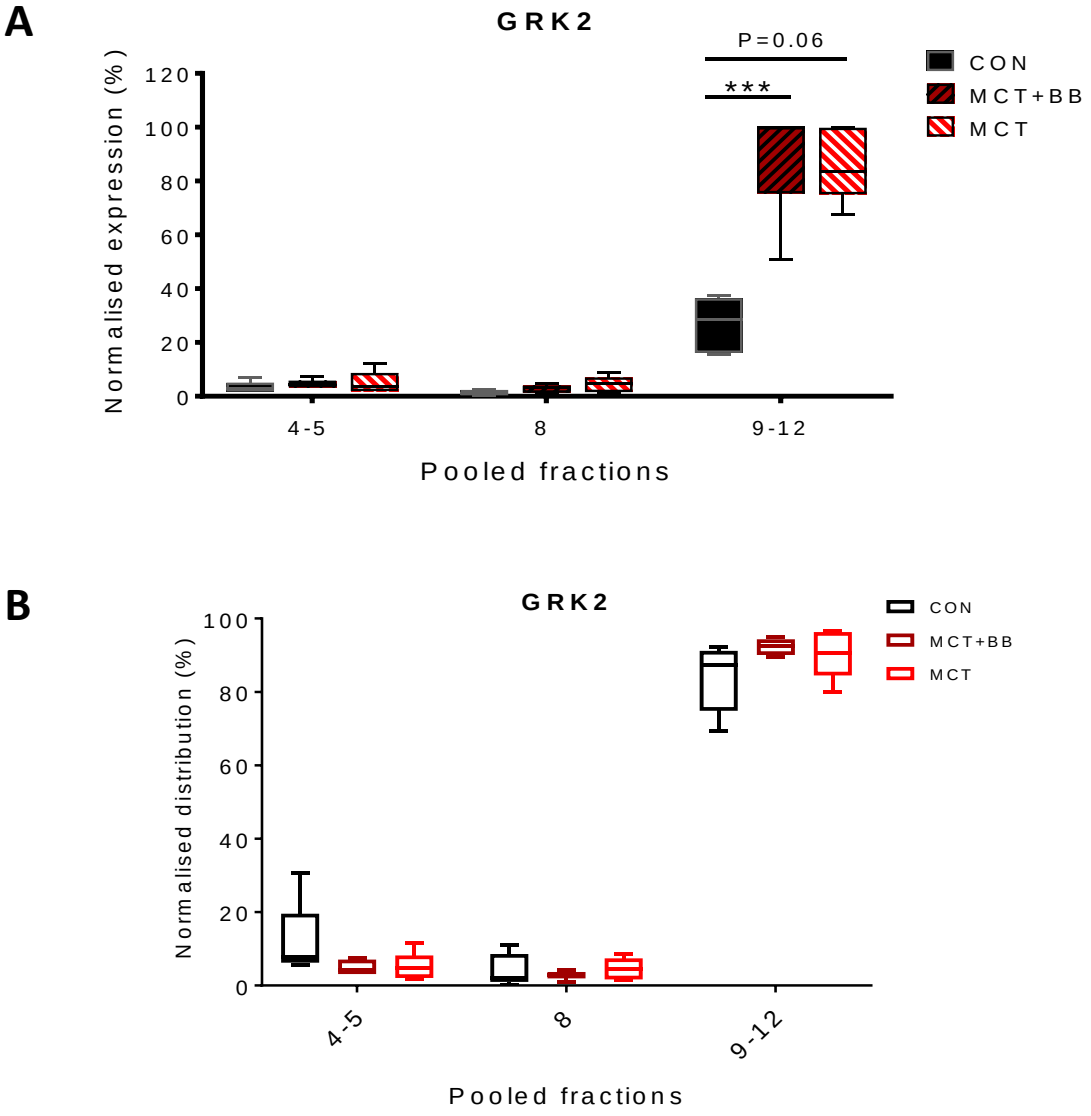

Figure 6-9 G-protein receptor kinase 2 (GRK2) protein membrane distribution in right ventricular heart failure

Western blot of right ventricular muscle homogenised in Na_2CO_3 and fractionated run on a sucrose gradient. Equal volumes of each fraction (4, 5, 8 and 9-12) were loaded with equal total protein loading between MCT and aged matched CON and MCT+BB. **A.** Individual Western blot comparing age-matched CON, MCT+BB and MCT were normalised to protein expression intensity on each membrane, box and whisker graph **B.** Protein expression in fractions was expressed as a percentage of total expression from all fractions (4-12) box and whisker graph. CON n=6, MCT+BB n=6, MCT n=6

6.4. Discussion

As with the functional measurements of β-AR responsiveness made in isolated myocytes, protein expression of some caveolar and β-AR signalling proteins in the MCT animals treated with β-blocker is improved towards expression levels seen in CON animals. The MCT RV failure model has previously been extensively characterised within the research group (Benoist et al., 2011; Benoist et al., 2012; Benoist et al., 2014; Stones et al., 2013), although the caevolar and β-adrenergic signalling proteins have not been studied to date. Metoprolol treatment of these MCT animals has been reported to improve survival and Ca^{2+} handling dysfunction (Fowler et al. in submission).

Changes to the βAR and its signalling proteins in RV heart failure using the MCT model have been previously been reported. A significant reduction in the β-AR density has been observed in isolated right ventricular myocytes (Leineweber et al., 2003), seen specifically in the β_1AR population which significantly changes the β_1AR:β_2AR ratio within the RV myocytes. Downstream production of cAMP was measured in response to stimulation with isoprenaline, which was significantly reduced in MCT treated animals (Leineweber et al., 2003). Similar results have been observed in intact right ventricular muscle (Kasahara et al., 1997; Seyfarth et al., 2000). The 50% reduction in β-AR density as measured with (−)-[125I]-iodocyanopindolol (ICYP) is not dissimilar to the reduction in protein expression observed within the present study (although Western blotting is semi-quantitative). The β-blocker treated animals show a stepped improvement of β_1AR expression with no difference compared with either the CON or MCT group. There is a shift in distribution of the β_1AR across different membrane fractions in the MCT animals, which appears to be recovered back to CON distribution with β-blocker treatment. This would suggest that selective blocking of the β_1AR aids, in part, by restoring β_1AR expression and distribution within the membrane. Expression of AC 5/6 in the RV is reduced in the MCT animals, which is comparable with previous studies showing a reduction in cAMP production in MCT animals (Leineweber et al., 2003). Again, this change in expression in MCT is recovered with β-blocker treatment. Expression and membrane distribution of the β_2AR receptor does not change in the MCT animals compared to CON, similar to previous been reports (Seyfarth et al., 2000). This links with functional data showing no difference in fractional shortening in response to selective stimulation of the β_2AR in isolated cardiac myocytes from MCT compared to CON (Chapter 5). Most LV heart failure models similarly see no change in β_2AR expression, although some have reported a change in the β_2AR distribution moving from

caveolae to non-caveolar sarcolemmal membranes resulting in a change in β_2AR cAMP production (Wright et al., 2014).

Increased sympathetic drive and excessive stimulation of β-ARs as seen in both RV (Velez-Roa et al., 2004) and LV (Floras, 2009) heart failure patient studies in humans, leads to a decrease in both mRNA and protein expression of the β_1AR (Bristow et al., 1982) as well as G-protein receptor uncoupling (Ungerer et al., 1993b) in the myocardium. Desensitization of the β_1AR is caused by Gβγ activation of the GRK2 which phosphorylates the β_1AR causing it to be targeted by β-arrestin preventing further activation of the receptor and receptor internalization (Lohse et al., 1990); elevated levels of GRK2 have been reported in human HF patients (Ungerer et al., 1993b). In the present study there in an increase in GRK2 protein expression in the RV of the MCT animals; this was significantly reduced with metoprolol treatment. Seyfarth et al. have shown in the same model there is a reduction β_1AR and uncoupling from its functional G-protein subunit, as well as a reduction in the $G\alpha_s$ protein in the RV (Seyfarth et al., 2000). Protein expression of the $G\alpha_s$ was not measured in this study, although there was a significant increase in expression of the $G\alpha_i3$ in the MCT animals, which again was significantly reduced with metoprolol treatment.

6.4.1. Caveolar changes in right ventricular failure

The reduction in Cav 1, Cav 3 and Cavin 1 expression in RV homogenate of MCT animals would suggest a decrease in caveolae number within this chamber. However due to time constraints it was not possible to show this using electron microscopy. Cav 3 and cavin 1 protein expression levels are partially recovered with β-blocker treatment suggesting a partial restoration of the caveolar microdomain. In the double KO of Cav 1 and Cav 3, increased RV wall thickness has been reported (Park et al., 2002). LV wall thickness is also increased in double Cav1/3 KO animals; interestingly there was no significant increase in LV thickness in the singular Cav 1 null or Cav 3 null animals compared with wild type. This may suggest that both Cav 1 and Cav 3 are needed within normal myocardial function. However, it should be noted that in other studies of KO mice, Cav 1 or Cav 3 KO both showed an increase in RV wall thickness (De Souza et al., 2005).

The shift in the distribution of Cav 3 in the fractionated samples from the MCT animals, and the reduction of Cav 3 expression in the buoyant fraction would also suggest a reduction in caveolae. A significant reduction in the buoyant fraction and an increase in the heavy fraction of Cav 3 was reported in an model of myocardial ischemia and myocardial infarction (Ballard-Croft et al., 2006) (Ratajczak et al., 2003). This was also paired with a reduction of

cholesterol content in the buoyant fractions, as well as a reduction in Cav 1 expression suggesting a reduction in caveolae. Interestingly in both these models there was no difference in the total Cav 3 expression, unlike what was seen in this MCT model of heart failure. This could be due to the nature of the heart failure models use; myocardial ischemia and myocardial infarction cause regional variation within the ventricles resulting from an acute initial insult to the heart. The MCT model is a whole ventricle pressure overload which is expected to cause homogenous changes to the ventricle, so homogenous reduction in Cav 3. Changes to caveolae or caveolar proteins within the RV of PAH patients or animal models have not previously been studied. Our understanding of changes in caveolae in heart failure relies on what has been studied within the LV, which may not be applicable to the right ventricle.

There was no change in muscle specific cavin 4 expression in the MCT or MCT+BB animals. Increased cavin 4 expression has previously been linked with an increase in hypertrophy and fibrosis within the heart (Ogata et al., 2014). The MCT animal model is a fast onset model of heart failure and although there is an increase in RV and heart weight to body weight ratios and an increase in cellular hypertrophy there is no evidence of increased fibrosis (Fowler, 2016, in submission) (Fowler and 2016). The membrane distribution of the cavin proteins could not be studied in this model as described previously (Chapter 4) due to the presence of multiple bands instead of a single band at 50 kDa on Western blotting. Interestingly, it was noted is that degradation of the 50 kDa band was most prominent in the CON animals. The reason for degradation of the cavin proteins within the fractionated samples is currently unknown.

6.4.2. β-AR and the microenvironment

Scaffolding proteins are important for ensuring correct protein grouping at the sarcolemma to provide effective and accurate downstream β-AR signalling. Caveolin and A-Kinase Anchoring Proteins (AKAP) have both been shown to play important scaffolding roles in aiding regulation of the βAR response (Kritzer et al., 2012; Insel et al., 2005).

Caveolin isoforms all have a conserved region toward the N terminus, the caveolin scaffolding domain (CSD), which allows interaction with other proteins (Couet et al., 1997). The CSD can bind to the G-protein α subunit, GRK2 and protein kinase A (PKA). The Cav 3 CSD sequence binds both AC5 and phosphodiesterase (PDE) 4 which acts to restrict the cAMP being produced (Timofeyev et al., 2013). Through recruitment and binding of additional proteins, caveolins aid in controlling β-AR signalling (Rybin et al., 2003) and have

a direct role in the compartmentalization of β_2AR signal (MacDougall et al., 2012). Disruption of these scaffolding proteins (Cav 3 and AKAP) has been observed in human heart failure (Zakhary et al., 2000; Feiner et al., 2011) and linked with ventricular dysfunction. Within the MCT model we observe a change in distribution of the Cav 3 from the buoyant fraction to the heavy fraction. This may then in turn affect the distribution of other proteins within the buoyant fractions. The distribution of AC 5/6 does not change between the three groups, but there is a significant decrease in AC 5/6 expression within the buoyant fraction of the MCT and MCT+BB animals. This is due to the majority of the AC 5/6 expression locating within the buoyant fractions, which may result in any changes in membrane distribution being too small to reach significance in this sample size. Reduction in AC 5/6 within caveolae may have an impact on downstream cAMP production and suggest uncoupling/disruption of the β-AR signalling cascade.

The distribution of the β-AR and their signalling proteins from sucrose gradient fractionations is highly varied from study to study (Rybin et al., 2000; MacDougall et al., 2012; Balijepalli et al., 2006). Some report that the β_2AR is solely located within the buoyant fractions, while others report a more diffuse distribution. This could be, as mentioned previously (Chapter 4), due to the antibody recognition. Distribution of the β_2AR between the different fractions of the sucrose gradient was the same in both CON (MCT model) and Sham (AB model) animals. There are also mixed reports of the location of β_1AR within different fractions of sucrose gradients. Sucrose gradient fractionation shows a proportion of β_1AR located within the caveolar fractions in some studies (Balijepalli et al., 2006; Rybin et al., 2000; Ostrom et al., 2001), while others report that it is only found on non-caveolar sarcolemmal membranes (Nikolaev et al., 2010). In the present study the proportion of the β_1AR location in the buoyant fractions was slightly higher than the proportion of β_2AR in these fractions. Although there was no difference in expression levels of the β_1AR between fractions in any of the three groups, there was a shift in the distribution of β_1AR in the MCT animal compared to CON, which was restored metoprolol treatment. The difference in results was partly due to the variability within the β_1AR expression between different Western blots.

6.4.3. Remodelling in the RV

PKA signalling is not the only downstream pathway from the β_1AR, the β_1AR also activates the mitogen-activated protein kinase MAPK pathway (Bogoyevitch et al., 1996) which promotes extracellular signal-regulated kinase (ERK) and janus kinase 2 (JAK) signalling resulting in hypertrophy and remodelling of the myocardium. Elevated levels of ERK and

JAK have both been observed in a model of heart failure induced by chronic ISO treatment in the rat (Takemoto et al., 1999; Zhang et al., 2005). Myocyte hypertrophy is initially a compensatory mechanism to cope with the increased afterload placed on the heart, but increased inflammation (Rondelet et al., 2012) and fibrosis (Vonk-Noordegraaf et al., 2013) eventually leads to decompensation of the RV and RV failure. Prolonged β_1AR stimulation can also induce apoptotic signalling in a PKA independent manner through the Ca^{2+}/calmodulin pathway (Zhu et al., 2003). As mentioned previously there is no increase in fibrosis found within this model of MCT (Fowler and 2016), which may be due to the short onset of this model and limited time the failing heart is under stess.

Other G-protein coupled receptors which activate hypertrophic signalling include the α_1AR, which is also able to active ERK signalling (Ogata et al., 2014). When a selective β_1-blockers was used to treat a model of excess ISO stimulation, there was a significant reductions in fibrosis of the heart (Brouri et al., 2004). Metoprolol treatment may be, indirectly, having an effect on aspects of remodelling due to stimulation of other receptors and effect receptor cross-talk.

6.4.4. Molecular mechanisms of metoprolol

The use of β-blockers to successfully treat LV heart failure patients and pulmonary artery hypertensive animal models has been reported, each proposing mechanisms of how this may be achieved (Böhm et al., 1997; Bogaard et al., 2010; Group, 1999; Heilbrunn et al., 1989). However many aspects of the changes which occur with β-blocker treatment are not fully understood. Not only has metoprolol been reported to aid in increasing β-adrenergic density, it also helps to restore the cAMP response to stimulation through the PDE3 inhibitor milrinone (Böhm et al., 1997) via β-AR independent effects. This could be through the re-coupling of the β-AR to $G\alpha_s$ protein subunits and AC, as β-blocker treatment has also been shown to reduce GRK2 activity and expression (Iaccarino et al., 1998). These works demonstrated that long term activation of the β-AR leads to increased levels of GRK2 mRNA, protein and activity. In the present study, GRK2 protein expression is significantly increased in the MCT animals, and this effect is reverse towards CON levels with β-blocker treatment.

Metoprolol treatment of the MCT model within the group has previously been reported to improve Ca^{2+} handling by restoring SR content and reducing Ca^{2+} waves in isolated cardiac myocytes (Fowler and 2016). The Ca^{2+} wave synchronicity within the isolated cardiac myocytes was also disrupted in the MCT animals, which was restored with β-blocker treatment. This, in part, is suggested to be linked with the restoration of the t-tubular system

(Fowler and 2016). Similar restoration of wave propagation was seen in metoprolol treatment of a genetic mouse model of heart failure (sympathetic hyperactivity-induced heart failure)(Bartholomeu et al., 2008). PP1 expression was increased in this model of heart failure which was returned towards control levels with metoprolol treatment. A reduction in both CaMKII and troponin I phosphorylation were also observed. Within isolated cardiac myocytes metoprolol acts to prevent the reduction in β-AR membrane receptor density and preserve the response to isoprenaline stimulation after incubation with isoprenaline (Flesch et al., 2001). This would suggest that selective blocking of the β_1AR prevents against overstimulation and receptor down regulation.

In the setting of diabetes induced heart dysfunction and failure, metoprolol treatment has been shown to have reverse remodelling effects on the heart (Sharma et al., 2011). These works showed that metoprolol attenuated the reduction in myocardial Cav 3 expression and was linked with prevention of the excessive activation of caspase-3 which is suggested to be Cav 3 dependent. In diabetes, treatment with the β-blocker metoprolol is suggested to decrease the overstimulation of the cAMP/PKA signalling pathway (Sharma and McNeill, 2011). In the present study metoprolol treatment of MCT animals aids in restoration of the Cav 3 protein expression and membrane distribution towards CON levels. In Sharma et al. metoprolol treatment was suggested to work by Cav 3 preventing the caspase-3 from being activated by sequestering away from its targets (Sharma et al., 2011). There is an elevation in protein expression of caspase-3 in MCT and MCT+BB. Although there were still high levels of caspase-3 expression in MCT+BB, with the restoration of Cav 3, this may aid in preventing excess activation. Due to time restriction the distributions of caspase-3 was not studied. Furthermore, cleaved (activated) caspase-3 could not be detected in samples from any groups, meaning a more direct comparison with the effect of metoprolol treatment on diabetes cannot be made. Cav 3 expression has also been linked with preventing cell death within vascular smooth muscle cells exposed to oxidized low density lipoproteins (oxLDL), again linked with a reduction in cleaved caspase-3 (Gutierrez-Pajares et al., 2015). However, in this case, the suggested protective mechanism was by Cav 3 inhibition of Oxidized low-density lipoprotein receptor 1 (OLR1) activating down downstream signalling pathways to induce cell death (Gutierrez-Pajares et al., 2015).

Chapter 7. The role of Caveolin 1 in protein membrane distribution

7.1. Introduction

It is well known that caveolin 1 (Cav 1) is not required for the formation of caveolae within the cardiac myocyte, as Cav 1 knock-out (KO) animals still form caveolae (Park et al., 2002). This may be one reason why several groups have put forward the view that Cav 1 is not expressed within the cardiac myocyte (Taniguchi et al., 2016; Wunderlich et al., 2006). However, Cav 1 protein expression have been reported several times within cardiac myocytes of different species (Yang et al., 2010; Robenek et al., 2008; Kozera et al., 2009). Although Cav 1 does not regulate the formation of caveolae in cardiac myocytes, this does not rule out a possible functional role within the caveolae. To date there is only a small handful of studies which has investigated Cav 1 and the functional role it may play within the cardiac cell (Bai et al., 2016; Patel et al., 2007).

In both the left ventricular (LV), aortic banding, and right ventricular (RV), pulmonary artery hypertension, models of heart failure Cav 1 protein expression is reduced in myocardial homogenate samples compared to respective control animals (Chapter 4, Chapter 6). Within the LV model of heart failure a correlation was observed between reduced Cav 1 protein expression and a decrease in heart function, as measured by ejection fraction (Chapter 4). There was also a trend for a negative correlation between Cav 1 protein expression and an increase in β_2AR expression within the buoyant fractions (fractions 4-5). These data suggest that there may be a link between Cav 1 expression and the β-ARs in the heart. Within the present study, Cav 1 protein expression was solely found within the buoyant fractions run on a discontinuous sucrose gradient fractionation, suggesting the Cav 1 is only associated with caveolae. It should also be noted that other cell types within the heart (endothelial cells, fibroblasts, vascular smooth muscle cells) also express Cav 1.

A collaboration was established with a group in Manchester which provided the opportunity to study Cav 1 KO mouse hearts. Due to the nature of the tissue fixation (frozen tissue), functional studies of the heart could not be performed, however, assessment of protein expression and membrane distribution was possible. The location of β-AR signalling proteins within the membrane can play an important role in cardiac myocyte function (Wright et al., 2014; Rybin et al., 2000). Cav 3 has previously been shown to play a role in

compartmentalising a number of different proteins involved in β-AR signalling, although the same has not been done for Cav 1. To test the hypostasis that Cav 1 plays a role in orchestrating the location of the membrane location of the β-AR cascade proteins and caveolar proteins, membrane distribution was studied using a sucrose gradient fractionation.

7.2. Methods

Due to the smaller size of the mouse heart ~100 mg, in comparison to the rat heart 1-2 g, all of the ventricular tissue (right ventricle, septum and left ventricle) was used for the sucrose gradient fractionation.

7.2.1. Mouse heart sucrose gradient fractionation

The Cav 1 KO mouse hearts, along with littermate wild type hearts, were a kind gift from Dr Toryn Poolman at the University of Manchester. C57BL/6 mice, 8-10 weeks old, were killed via an overdose of pentobarbital. For the test sucrose gradient, spare cardiac tissue from 20 week old wild-type C57BL/6 mice (University of Leeds) was used.

The established sucrose gradient fractionation protocol (Methods section 2.8.2) needed to be tested for its suitability and adapted for use of murine tissue. After an initial run on mouse tissue it was predicted that over or under sonication were giving misleading results. Three different sonication protocols were then tested on spare mouse hearts to see the impact on protein distribution between fractions. Snap frozen hearts (~100 mg) were partially defrosted to be able to remove the atria and aorta before ventricular tissue was quickly cut into smaller pieces and homogenised in detergent-free Na_2CO_3 buffer (detailed in Methods 2.8.1) 6 x 20 s. Samples were then further sonicated 3, 6 or 9 x 10 s before being centrifuged at 5000 g for 30 min at 4^{o}C. The supernatant was layered onto a scaled-down discontinuous sucrose gradient (total volume reduced from 12 mL to 4.8 mL (0.8 mL 45% sucrose and sample, 1.6 mL 35% sucrose, 1.6 mL 5% sucrose)). A SW55Ti rotor, which works with 5 mL swing bucket tubes, was used instead of the SW40 which contained 12mL swing buckers tubes. Sucrose gradients were centrifuged at 45000 rpm for 15 h at 4 ^{o}C (SW55Ti rotor, Beckman UK); this subjects the sucrose gradient to the equivalent g force as produced in the larger rotor as calculated by Beckman G-force calculator. After centrifugation, 12 fractions were collected from the top using a Gilson pipette (p1000) (400 µL each), then frozen at -20 ^{o}C until required. A BCA assay was used to measure the protein

concentration and an Amplex Red® assay used to measure cholesterol content within each fraction (as detailed in Methods 2.9.3.1 and Methods 2.9.1 respectively). SDS-PAGE and Western blotting were performed on samples as detailed in Methods 2.9.3.2).

7.2.2. Limitations

Snap frozen hearts from the University of Manchester had varying amounts of blood within the heart. The atria and aorta were removed and most of the blood cleared before whole ventricular tissue (right ventricle, septum and left ventricle) was homogenised in detergent free buffer. The whole ventricular tissue was used due to the limit in tissue size (~100mg). KO of Cav 1 is known to cause cardiac hypertrophy, fibrosis and dysfunction (Murata et al., 2007; Zhao et al., 2002). This would cause an increase in extracellular matrix, and possibly an increase in other non-myocyte cells within the heart. For this reason, and because of the addition complication of unknown amounts of blood in the samples, total expression across the different fractions (see Chapter 6 for example) was not compared. Due to a limited sample number the same statistical analysis, comparison of target protein expression in different fractions by a two-way ANOVA (as performed in Chapter 6), was not possible on these samples. Therefore only the trend for differences between membrane distribution of proteins in WT and KO mouse heart can be reported, without statistical significance.

7.3. Results

7.3.1. Mouse heart sucrose gradient test run

Sucrose gradient fractionation of mouse tissue has not previously been performed within the research group. When a scaled down version of the rat protocol (described in Methods 2.8.2) was used for the mouse heart, the distribution of specific proteins in the gradient did not fit with the distribution previously seen. It was thought that due to a smaller volume of solution being used (because of the smaller size of the mouse heart compared to rat) the samples may have been over-sonicated. Sonication is an important step within the sucrose gradient fractionation protocol (Waugh et al., 2011; Smart et al., 1995); samples need to be sonicated enough to break up the membrane into fragments which are small enough to separate caveolar membrane from the rest of the sarcolemma, without completely fragmenting the membrane (Macdonald and Pike, 2005).

Three different sonication protocols were used (n=2 hearts) to test the impact on the distribution of different proteins across the membrane. Membrane protein and cholesterol content in the different fractions is depicted in Figure 7-1. Fractions 1 and 2 were not studied; no protein was detected in these fractions as lipid rich membrane fractions do not float to this level in detergent free fractionation (Smart et al., 1995; Song et al., 1996a). There was a reduction in protein concentration and cholesterol concentration in the buoyant fractions (fraction 4 and 5) from the 9 x 10 s protocol compared to the 3 x 10 s and 6 x 10 s protocols. This could suggest that 9 periods of 10 s sonication is over-sonicating the samples resulting in a redistribution of caveolar/membrane raft proteins and cholesterol to the heavy fractions.

Figure 7-2 shows the change in protein expression distribution of Cav 3, hydroxyacyl-CoA dehydrogenase/3-ketoacyl-CoA thiolase/enoyl-CoA hydratase (trifunctional protein), alpha subunit (HADHA) and clathrin heavy chain (clathrin HC) with the different sonication protocols. Protein distribution of HADHA (a marker for mitochondria), and clathrin HC (a marker for non-caveolar membrane) are similar across the different protocols and is comparable to what has previously been observed (Wypijewski et al., 2015). The largest difference between protocols was seen in the membrane distribution of Cav 3. In samples sonicated for 3 x 10 s there was an average of 40% of Cav 3 located within the buoyant fractions, while those sonicated for 6 x 10 s and 9 x 10 s had an average of 22% and 18% in the buoyant fractions respectively. The Cav 3 distribution following 3 x 10 s is most consistent with previous reports in the heart using a detergent-free sucrose gradient

fractionation in the rat (Wypijewski et al., 2015; Calaghan et al., 2008). For this reason the 3 x 10 s sonication protocol was implemented in all subsequent experiments with mouse tissue. Caveolin 1 KO hearts

The Cav 1 KO hearts came from global Cav 1 KO mice. Hearts from wild type (WT) littermate mice were used as a control. Cav 1 KO was confirmed from heart muscle homogenate samples not used in the sucrose gradient fractionation (Figure 7-3). In WT and KO hearts total protein distribution between fractions was almost identical, and there was no marked change in the distribution of the clathrin HC and HADHA proteins (Figure 7-4). Expression of the Clathrin HC and HADHA across the different fractions was also similar to that seen in the test run using the 3 x 10 s sonication protocol.

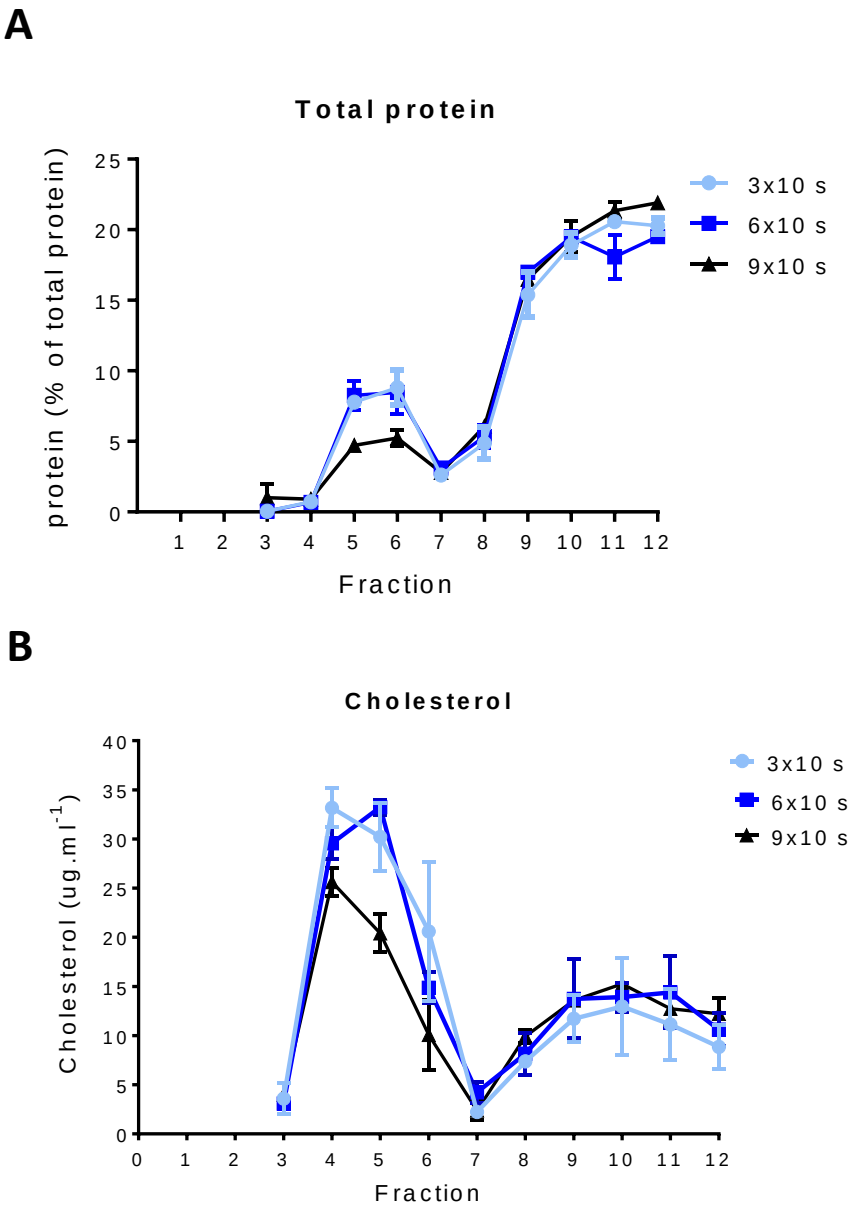

Figure 7-1 Protein and cholesterol distribution in fractions from different sonication protocols using mouse heart

Three different sonication protocols were used, 3 x 10 s, 6 x 10 s, and 9 x 10 s, (n=2), Data are expressed as mean ± SEM.

A. Protein concentrations in different fractions as measured by a BCA assay **B.** Cholesterol concentrations in different fractions as measured by an Amplex Red assay.

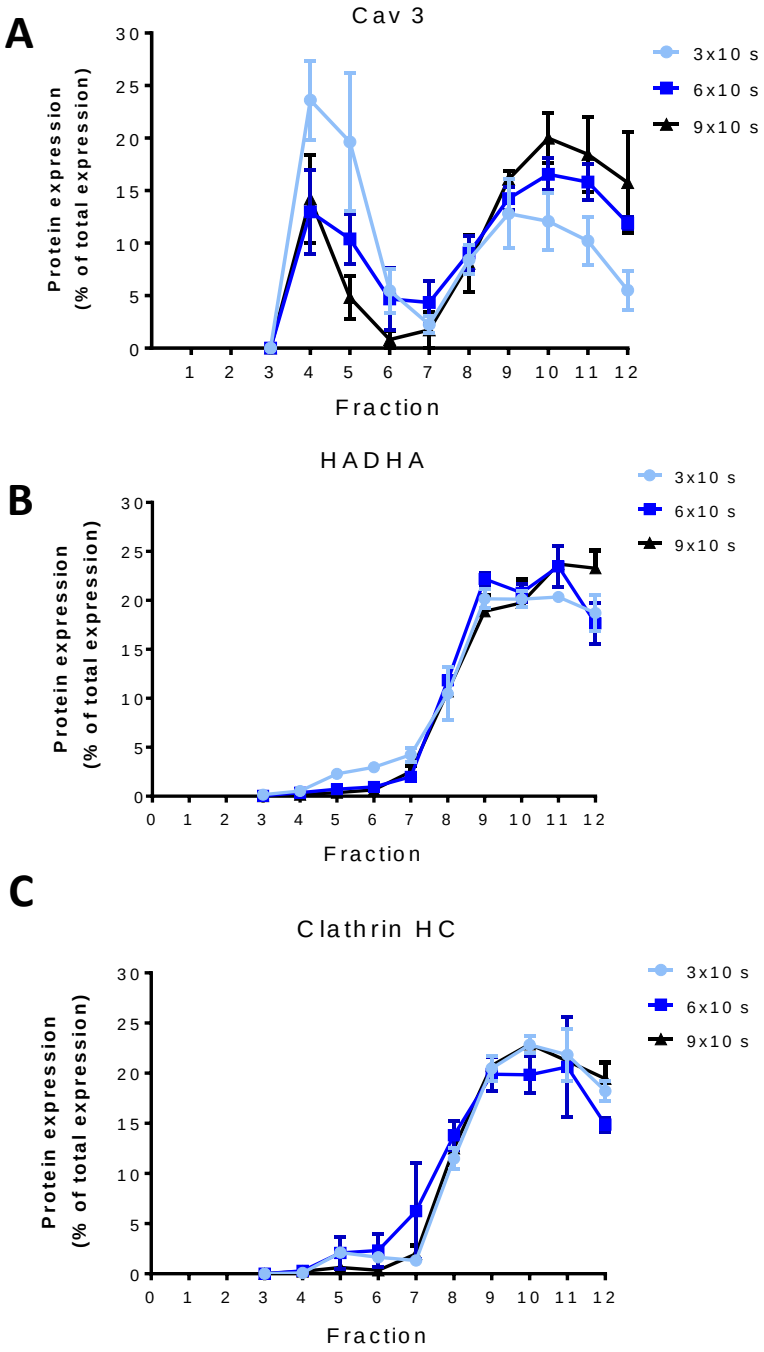

Figure 7-2 Protein distribution of membrane compartment markers following three different sonication protocols in house heart

Western blot of three different sonication protocols were used, 3 x 10 s, 6 x 10 s, and 9 x 10 s, (n=2), Data are expressed as mean ± SEM. **A.** Distribution of Caveolin 3 (Cav 3) protein expression **B.** Distribution of HADHA protein expression **C.** Distribution of clathrin heavy chain (clathrin HC) protein expression.

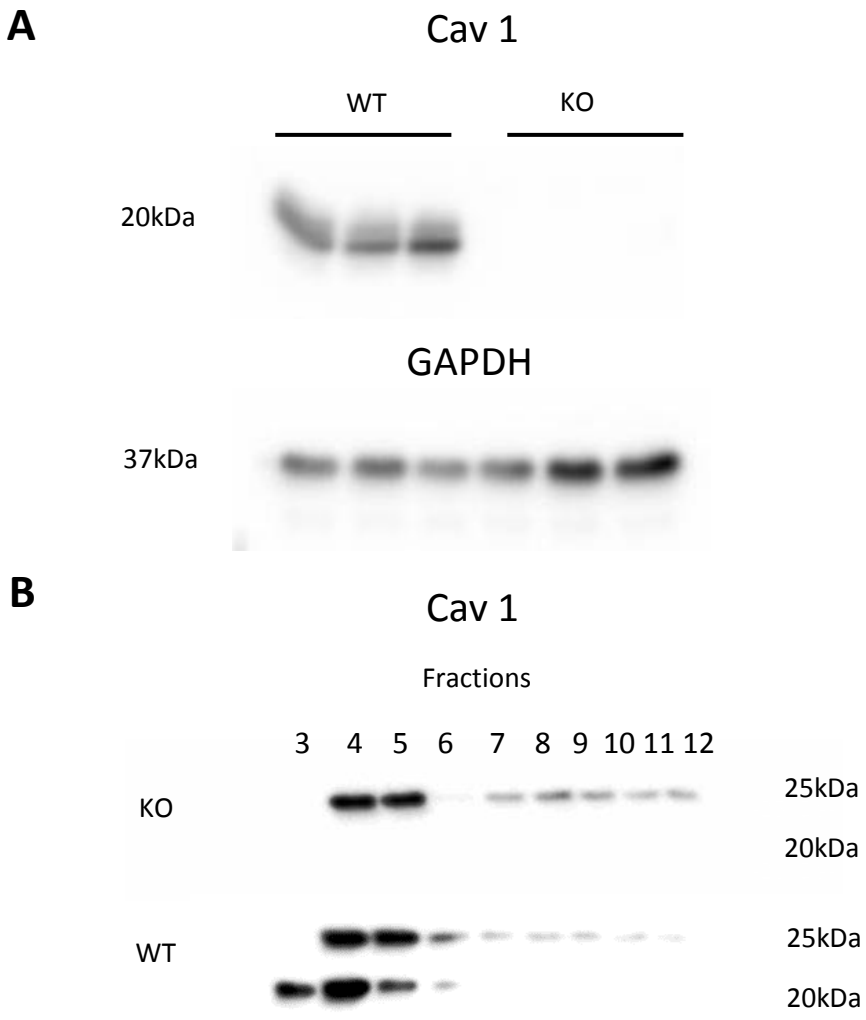

Figure 7-3 Western blot confirming Cav 1 KO

A. Ventricular muscle homogenate from wild type (WT) mice and caveolin 1 (Cav 1) knock-out (KO) mice, WT n=3, KO n=3. **B.** Ventricular muscle homogenate distribution from sucrose gradient fractionation. Non-specific band seen at 25 kDa.

7.3.1.1. Caveolar protein distribution

Figure 7-5 shows the membrane distribution of the caveolar proteins in WT and Cav 1 KO hearts. The majority of Cav 3 expression (30-50%) is located within the buoyant fractions (fractions 4-5) in both the WT and KO hearts. There was no significant difference in percentage expression of Cav 3 within each fraction between groups; however there was a greater variation in Cav 3 expression in buoyant fraction 4 of the KO hearts compared with WT. In the Western blot of the cavin 1 fractionated samples a single band at 50 kDa was observed. Cavin 1 expression is mainly located within the heavy fractions (fraction 9-12), with a smaller percentage located within the buoyant fractions (5-10% in WT and 3-9% in KO). The cavin 1 distribution across the fractions is similar between groups, apart from fraction 4 which has slightly less in the KO (mean 1.93% ± 0.705 SEM) compared to the WT (mean 3.74% ± 0.350 SEM), although this was not significantly different. Western blot of cavin 4 expression showed a doublet band at 50 kDa (close to the predicted molecular weight). The distribution of cavin 4 is unlike any of the other proteins studied before, with highest expression in fractions 5-7. Cavin 4 membrane distribution, as measured with a discontinuous sucrose gradient, has not been reported in the literature before. Around 60% of the cavin 4 expression is located within these fractions in both KO and WT. The distribution of cavin 4 in all fractions was similar in both groups. The Western blot of cavin 1 and cavin 4 showed bands which were different to what had previously been observed in fractionated samples of rat tissue (Chapter 4 and Chapter 6). Previous Western blots of fractionated samples, cavin 1 and cavin 4, showed multiple bands below 50 kD and often no band present at 50 kDa. The reason for a single band at 50 kDa in the murine samples was proposed to be the limited time tissue spent in storage. In the KO mouse experiments time from initial homogenisation in the detergent free buffer to sonication and running in a sucrose gradient was very short (one day), where previous samples were stored in the Na_2CO_3 buffer for longer periods of time (1 month – 2 years) before processing.

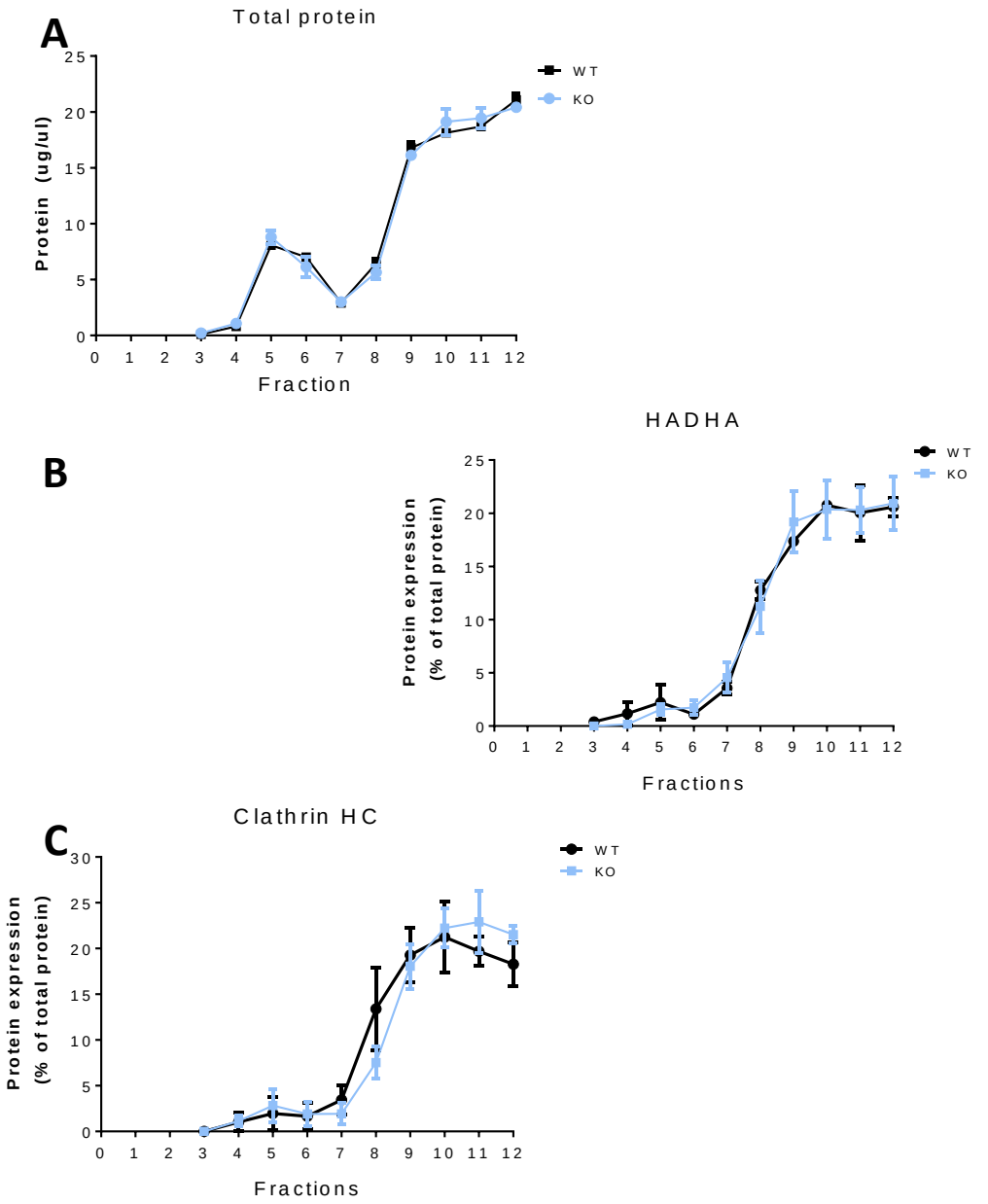

Figure 7-4 Distribution of total protein and membrane compartment markers in wild type (WT) and Cav 1 knockout (KO) mice

Western blot of ventricular muscle homogenate from WT mice and Cav 1 KO mice, (n=3), Data are presented as mean ± SEM. **A.** Protein concentrations in different fractions as measured by a BCA assay **B.** Distribution of HADHA protein expression **C.** Distribution of clathrin heavy chain (clathrin HC) protein expression

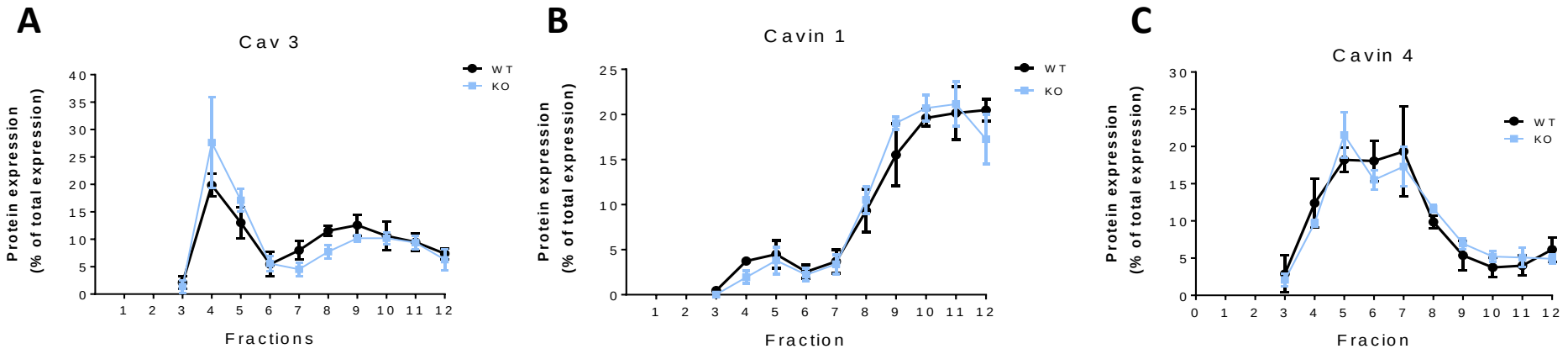

7-5 Caveolar protein membrane distribution markers in wild type (WT) and Cav 1 knockout (KO) mice

Western blot of ventricular muscle homogenates from WT mice and Cav 1 KO mice, (n=3), Data are presented as mean ± SEM **A.** Distribution of Caveolin 3 (Cav 3) protein expression **B.** Distribution of cavin 1 protein expression **C.** Distribution of cavin 4 protein expression.

7.3.1.2. β-adrenergic signaling protein distribution

Figure 7-6 shows a summary of the distribution of β-AR signalling proteins between fractions in WT and KO animals. The majority of adenylyl cyclase (AC) 5/6 expression is located in the buoyant fractions (~60%) in both the KO and WT mouse hearts. The distribution of AC 5/6 is very similar in WT and KO animals and comparable to what was observed in normal (CON) rats (Chapter 6). In WT mouse hearts only a small percentage of the β_2AR protein expression was found in the buoyant fractions with the majority of protein located within the heavy fractions, which replicates data in the rat (Chapter 6). Cav 1 KO had a marked impact on β_2AR distribution. In the KO animals, even at very high exposures (time developing Western blot), no β_2AR could be detected within the buoyant fractions. In the KO hearts β_2AR protein expression was solely located within the heavy fractions. In the WT hearts $G\alpha_i$ 3 protein expression was mainly located within the buoyant fractions (~50%); KO hearts had an almost identical membrane distribution of $G\alpha_i$ 3 to the WT heart. This also resembled the distribution of $G\alpha_i$ 3 found within the myocardium of normal (CON) rats (Chapter 6). As mentioned previously (Chapter 4 and Chapter 6), Western blotting of the β_1AR in fractionated samples had caused difficulty as a clear band at the predicted molecular weight (50 kDa) was not always evident. Two of three WT fractionations showed a band which would be analysed at 50 kDa but none of the KO animals produced a clear band suitable for analysis at 50 kDa. The β_1AR Western blot produces multiple non-specific bands, as seen with peptide blocking. Overall, KO of Cav 1 had no impact on the protein distribution of AC and $G\alpha_i$ 3 within the membrane, but it appeared to prevent the localisation of β_2AR within the buoyant/caveolae fractions.

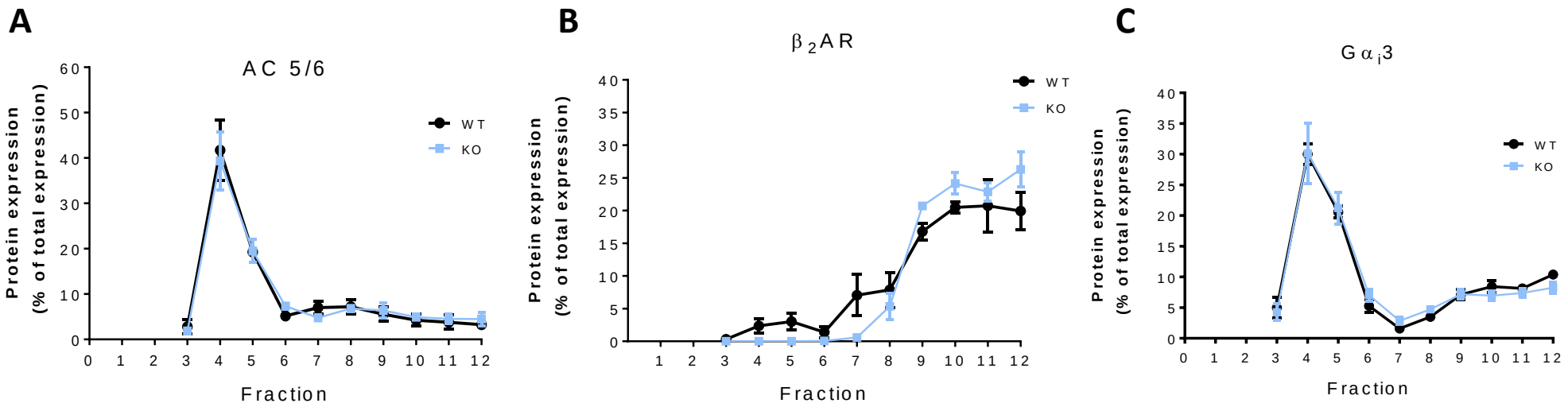

Figure 7-6 β-adrenergic signalling protein membrane distribution markers in wild type (WT) and Cav 1 knockout (KO) mice

Western blot of ventricular muscle homogenates from WT mice and Cav 1 KO mice, (n=3), Data are presented as mean ± SEM **A.** Distribution of adenylyl cyclase 5/6 (AC 5/6) protein expression **B.** Distribution of β_2AR protein expression **C.** Distribution $G\alpha_i$ 3 protein expression.

7.3.2. β-adrenergic protein expression in myocardium

Due to the differences observed in the distribution of β_2AR in the KO mice, whole protein expression was examined in small aliquots of myocardial homogenate which had not been layered onto the sucrose gradient. β_1AR was also examined due to the fact that none of the fractionated samples in the KO hearts showed a clear single band at 50 kDa. There was no significant difference in protein expression ($P>0.05$) of the β_1AR in the KO hearts compared to WT (Figure 7-7). There was also no difference ($P>0.05$) in β_2AR expression in KO compared to WT. There is a trend for a decrease in the β_2AR ($P=0.2$), but due to the limited sample size these comparisons are underpowered (alpha = 0.53).

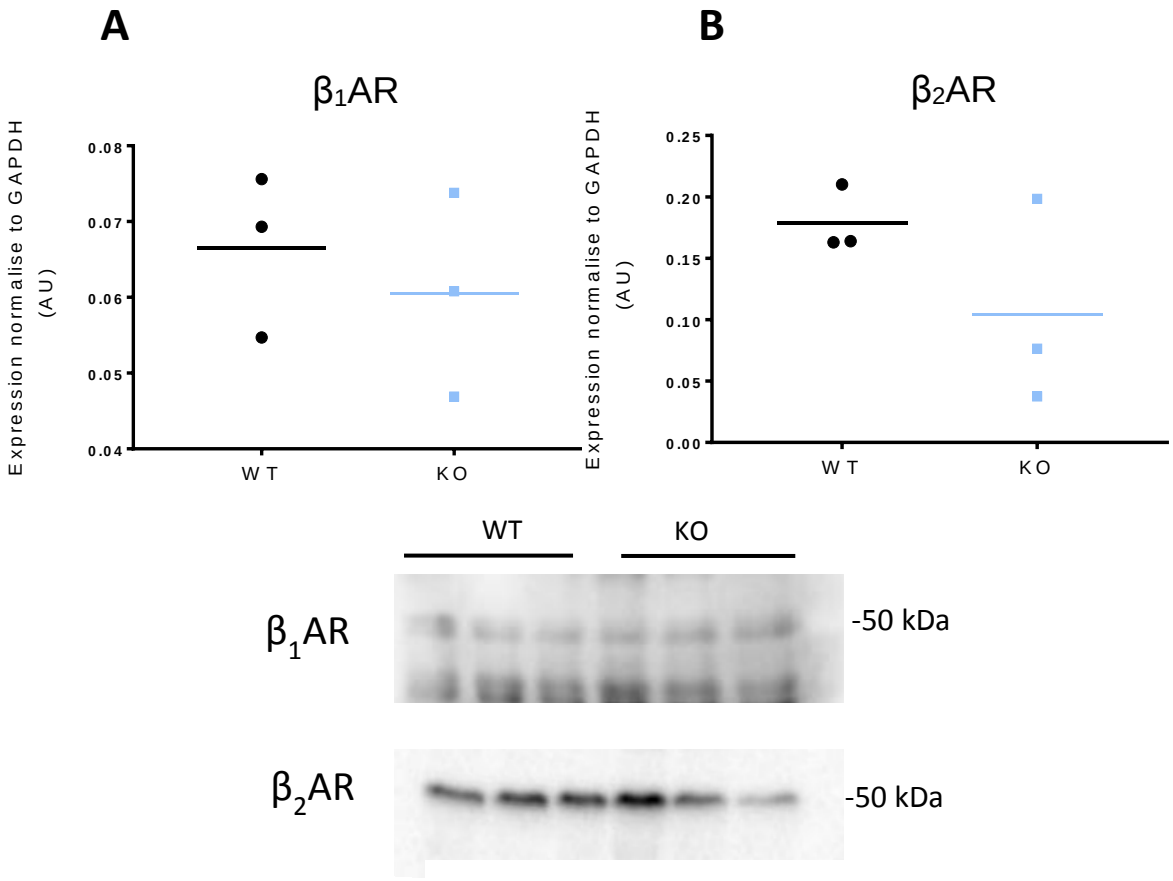

Figure 7-7 β-adrenergic protein expression in wild type (WT) and Cav 1 knockout (KO) mice

Western blot of ventricular muscle homogenate from WT mice and Cav 1

KO mice, **A.** β_1AR protein expression **B.** β_2AR protein expression. Signal normalised to GAPDH protein expression. WT n=3, KO n=3. Dot plot with mean

7.4. Discussion

The membrane distribution of the caveolar proteins and most components of the β-AR signalling cascade in the heart remain unchanged with knock-out of Cav 1. The notable exception to this is β_2AR, which is no longer located within the buoyant fractions in the absence of Cav 1 expression. This would go some way towards suggesting that, although Cav 1 does not determine membrane location of other caveolar proteins or the β-AR signalling proteins, it does have a role in the recruitment of the β_2AR to caveolae.

7.4.1. β_2-adrenergic receptor and caveolae

In the present study, the percentage of β_2AR expression within the buoyant fractions was lower than that reported previously (Rybin et al., 2000; MacDougall et al., 2012; Balijepalli et al., 2006), although these previous studies have not quantified percentage expression there are apparent bands in the buoyant fractions without overexposure of the heavy fractions. The variability in the membrane location of β_2AR may be due to variable antibody recognition of different β_2AR conformations, as mentioned previously (Chapter 4 section 4.1.2). There are a limited number of commercially available antibodies, and most Western blotting experiments use the antibody produced by Santa Cruz (Rybin et al., 2003; Rybin et al., 2000; Head et al., 2005; MacDougall et al., 2012), which in our hands produced variable results. The functional response to selective β_2AR stimulation also varied in cardiac myocytes from the same heart, as seen in the present study (Chapter 4) and between different studies with some seeing no increase in contraction and $[Ca^{2+}]_i$ while others see distinct cAMP signalling within the t-tubules and an increase in I_{Ca} (Wright et al., 2014; MacDougall et al., 2012; Barbagallo et al., 2016; Bryant et al., 2014). This highlights the variability seen within the study of β_2AR.

In two models of LV heart failure, the β_2AR shows a redistribution from its usual location within the caveolae to other non-caveolar sarcolemma membranes which increased the downstream cAMP response to stimulation, as examined with fluorescence resonance energy transfer (FRET) (Barbagallo et al., 2016; Wright et al., 2014). Within the present study, the LV heart failure model showed an increased in β_2AR protein expression within the buoyant fractions compared to sham animals (Chapter 4). These are two different approaches to examine the location of β_2AR, with different interpretations drawn from them. Neither directly proves that β_2AR moves in or out of caveolae, but instead suggests it as a reasonable conclusion of the data. The conclusions of Barbagallo et al. and Wright et al. that β_2AR is relocated from caveolae is based upon the assumption that β_2AR cAMP

production is solely regulated by Cav 3 in caveolae. In the models of heart failure used in these studies, decrease in Cav 3 was observed in association with an increase in β_2AR cAMP production, ascribed to β_2AR relocation from caveolae (Barbagallo et al., 2016; Wright et al., 2014). Similarly, in sucrose gradient fractionation, an increase in β_2AR protein expression within buoyant fractions does not directly translate to an increase in β_2AR within caveolae, as there are lipid rich non-caveolae membranes also located within buoyant fractions. Interestingly though the majority of AC 5/6, which is the primary target for $G\alpha_s$ to produce cAMP, is located within the buoyant fractions within this present study and in others (Rybin et al., 2000).

The data from Cav 1 KO mice in the present study suggest that in normal physiology of the heart, Cav 1 plays a role in the recruitment of β_2AR to the buoyant fractions/caveolae. When cholesterol is extracted from normal myocyte membranes with methyl β cyclodextrin, there is an increase in β_2AR cAMP signalling (MacDougall et al., 2012), suggesting that lipid rafts/caveolae exert compartmentalisation control of the β_2AR cAMP. As assessed by sucrose gradient fractionation, isoprenaline stimulation results in a re-location of β_2AR out of caveolae, as (Rybin et al., 2000), and selective β_2AR stimulation also results in recruitment of cavin 1 to caveolae (Wypijewski et al., 2015). The different studies of the β_2AR are difficult to fit into one coherent model of caveolar control. One issue which may have been slightly overlooked is the protein composition of caveolae in heart disease, and that in fact there may be different caveolae with different pools of proteins. The role of Cav 1 and the cavins has also not been considered in most studies to date. If there was a reduction in caveolae and also a change to the proteins located within the caveolae then simple KO of Cav 3 or disruption to the Cav 3 protein may not in fact correctly represent the disease phenotype, but may still produce similar responses to β-AR stimulation. This may overlook the complex structural makeup of caveolae and overlook potentially proteins which are functionally important.

7.4.2. Caveolar protein membrane distribution

Fraction 4 from the sucrose density gradient, which has previously been used to study proteins within caveolae (Wypijewski et al., 2015), shows the widest amount of variation in Cav 3. This could be a result of variation between fractionation, although this is unlikely as expression of total protein, and other proteins located within the buoyant fraction (AC 4/5 and $G\alpha_i$ 3) are not as varied. Instead this could reflect an increased variation of Cav 3 located in caveolae from Cav 1 null mice. Cavin 1 protein expression was mainly located within the heavy fractions, which concurs with similar patterns in cavin 1 membrane distributions

seen when studied by sucrose gradient fractionations (Wei et al., 2015). Within the buoyant fractions, the cavin 1 expression within fraction 4 and fraction 5 was fairly even. As mentioned above, cavin 1 membrane location has been shown to be highly dynamic following selective β-AR stimulation (Wypijewski et al., 2015). The pattern of Cavin 4 membrane distribution in the murine heart is dissimilar to all other proteins assessed within the present study. Most studies of caveolae by sucrose gradient fractionation only report data on buoyant fractions (fraction 4-5) and the heavy fractions (fractions 9-12), and fail to mention the fractions in between (Head et al., 2005; Smart et al., 1995; Rybin et al., 2000). Bastiani et al. show that cavin 4 co-localised with Cav 1 and is dependent on Cav 1 for its location on the plasma membrane in a BHK cell line (Bastiani et al., 2009). In addition, partial co-localisation of cavin 4 with Cav 3 in muscle cells as imaged by immunolabelling was reported by this group (Bastiani et al., 2009). The different caveolar proteins show different distributions across the membrane, and in particular different concentrations in fraction 4 and 5. This supports the idea that there may be different populations of caveolar composed of different caveolar proteins. There is still much which is unknown about cavin 4, but from the results of the Cav 1 KO hearts we can suggest that Cav 1 is not needed for the location of cavin 1 or 4 within the plasma membrane in the cardiac myocyte.

7.4.3. Difference in sucrose gradient fractionation

Measuring membrane protein distribution using sucrose gradient fractionation gives divergent results within the literature. Although the same basic protocol may be implemented there can still be user variability and small differences in the procedure which make a significant difference - as observed when first applying a scaled-down protocol from rat tissue to use in murine tissue. The reduced volume resulted in over sonication of the sample with implications for caveolar protein distribution. The degree of sonication applied to a sample is not routinely stated within the literature.

Many papers concur with the results shown in this study that Cav 1 is expression solely located within the buoyant fractions, as seen with homogenates from endothelia cells and cultured cell line (Wei et al., 2015; Lisanti et al., 1994; Yao et al., 2009). However, there are other reports in the literature of a more diffuse distribution of Cav 1 expression with the majority of Cav 1 expression within the buoyant fraction but also expression in the heavy fractions in mouse and rat (Bai et al., 2016; Kozera et al., 2009); these studies have looked specifically at distribution within cardiac myocyte preparations. Interestingly a previous study of mouse heart homogenate run on a discontinuous sucrose gradient found the majority of Cav 1 expression within the heavy fractions (Patel et al., 2007). It was noted

when performing Western blot on fractionated samples that a non-specific band appeared at 25 kDa with the Cav 1 antibody. Both Bai et al. and Kozera et al. use a Cav-1 antibody purchased from BD Transduction Laboratories (#610058 and #610406). Our antibody was from the same company (#610406) but the two antibodies differ in the epitope against which the antibody was raised. Another variation in protocol which may explain differences between studies relates to samples loading discrepancies for SDS PAGE. The approach in the present study is to load equal volumes of samples from each fraction. As demonstrated in Head et al., the alternative approach of loading an equal amount of protein gives a very different result when studying Cav 3 distribution, skewing the distribution towards the buoyant fractions (Head et al., 2005). Many studies do not explicitly state that equal volumes of samples in each fraction are loaded. The addition of the detergent Triton-X to the sucrose gradient has been shown to disrupt the distribution of Cav 1 in cultured 3T3-L1 cell line (Yao et al., 2009). Yao et al. also raise the point that, while the non-detergent Na_2CO_3 buffer-based fractionation is useful for isolating caveolar membrane fractions, these will also be contaminated with non-caveolar lipid rafts. They go on to detail a modified protocol which adds an addition layer to the conventional sucrose gradient (a 21% sucrose solution between the 35% and 5% solution). This extra layer of sucrose positioned where lipid rich fractions would normally be located, further separates the fractions so that light low-density insoluble membrane fractions were located towards the 21% and 35% gradient border. The Cav 1 rich micro-domains were located towards the 21% and 35% gradient border which contains morphologically identifiable caveolae when imaged with electron microscopy (Yao et al., 2009).

7.4.4. Caveolin 1 KO mouse models

In Bai et al. knock-out of Cav 1 caused a reduction of Cav 2 protein within cardiac myocytes, but no change in Cav 3 protein expression or Cav 3 membrane distribution as measured with a sucrose gradient fractionation (Bai et al., 2016). It was noted however that phosphoinositide-3 kinase (PI3K), protein kinase B (Akt) and β_1 subunit of Na^+/K^+-ATPase was slightly reduced in the caveolar fractions. In another Cav 1 KO mouse model isolated working hearts were examined in response to an increase in preload and isoprenaline stimulation (Chow et al., 2010). Surprisingly Cav 1 KO hearts showed an increase in cardiac output and cardiac work compared to control mice. In response to the highest levels of isoprenaline stimulation there was a significant increase in heart rate and rate pressure product (beats per min x mmHg) compared to control mice. It should be noted that these functional studies were performed on KO Cav 1 mice 6-8 weeks old, which is well before

cardiac hypertrophy and fibrosis develops (4-5 months) (Murata et al., 2007; Zhao et al., 2002). In the present study, there appears to be a redistribution of the β_2AR to the non-caveolar sarcolemma membranes in Cav 1 KO myocardium which could in turn enhance the inotropic response to β_2AR stimulation; as described for the effect of cholesterol depletion in cardiac myocytes which causes an increase in selection β_2AR stimulation (MacDougall et al., 2012).

Chapter 8. Quantitative Western blotting of myocardial and myocyte samples

Homogenised myocardium has been used throughout the present study to measure changes in protein expression and membrane distribution in disease models and transgenic animals. An alternative approach is to isolate cardiac myocytes and use myocyte homogenates for the same assessments. Each technique has its own advantages and disadvantages. In myocardial homogenates, cardiac myocytes are not the only cell within the sample and are suggested to make up ~30% of the cell count within the heart; other cells include fibroblasts and endothelial cells (Vliegen et al., 1991). However myocytes are the largest cell in the myocardium and are suggested to make up ~80% of the volume in myocardial samples (Vliegen et al., 1991). These estimates are for the normal healthy hearts; in heart disease there is typically an increase in extracellular matrix, which decreases the proportion of protein that myocytes contribute to a myocardial sample (Schwab et al., 2013; Vliegen et al., 1991). By contrast, myocyte homogenates only contain protein from myocytes, eliminates protein contamination of the sample from other cell types. The disadvantages to using myocyte preparations include the process by which cells are isolated which may place some stress (mechanical and chemical) on the cardiac myocytes. Even when maximising the cell viability of preparations, myocyte homogenates will still contain a proportion of dead cells, and this small/varying percentage of dead cells will have an impact on the protein content. Use of cell sorting to enrich myocyte suspensions in live cells is problematic as conventional cell sorting protocols are not generally appropriate for large rod shaped cardiac myocyte. Another consideration is the possible bias of cell selection, that by the process of isolating cardiac myocytes this may inevitably selective the healthier cells within the heart. This effect could be further compounded in disease models. As mentioned previously (Chapter 4, Chapter 6 and Chapter 7) caveolae and the β-AR are highly dynamic components within the myocyte which can change within minutes (Wypijewski et al., 2015; Rybin et al., 2000). The time to sample fixation is much longer for myocyte preparations than myocardial preparations and this may cause changes to the membrane location of proteins within this time.

Caveolin 3 (Cav 3) and cavin 4 are muscle specific caveolar proteins whereas caveolin 1 (Cav 1) and cavin 1 are ubiquitously expressed in all the cell types within the heart. In a myocardial sample it is not known how much of the ubiquitously expressed caveolar protein expression comes from cardiac myocytes and how much is from non-myocyte cells

in the heart. It is well known that in cardiac myocyte β_1AR has a higher expression than β_2AR, with β_1AR contributing to around 70% of the total βAR population. By comparing protein concentrations of β_1AR and β_2AR in myocytes could be used as a positive control.

Here we looked to assess the difference in relative expression of caveolar protein isoforms between myocyte and myocardial homogenate samples using new tools for protein quantification. A collaboration with Prof. John Colyer and the University of Liverpool was established which enabled the absolute quantification of protein expression within a sample in Western blotting. The CavCAT (caveolarCAT) standard tools used are based on Quantification concatamers (QconCAT) (Brownridge et al., 2012; Mackenzie et al., 2016; Brownridge et al., 2013), in which artificial proteins are created expressing the same amino acid recognition site (epitope) as the desired protein being quantified, these are then loaded into a Western blot at known expression levels to create a standard (calibration) curve, so that band density can then be extrapolated to absolute protein expression. A capillary based Western blotting system (Simple Western from ProteinSimple®) was used, which eliminates the transfer step of traditional SDS-PAGE and Western blotting, and has been proven to be a more quantitative approach to Western blotting that the traditional protocol (O'Neill et al., 2006; Chen et al., 2015; Chen et al., 2013).

8.1. Methods

Peptide design was performed at the University of Leeds; CavCAT protein sequence was designed in the University of Liverpool by Mr Richard Bennett and Prof Rob Beynon. Expression, purification, quantification and optimisation steps of the CavCAT peptide and final Western blots were performed by Mrs Victoria Harman. Final analysis and interpretation of results was done in the University of Leeds.

8.1.1. CavCAT synthesis

The first CavCAT design included the study of six proteins (Cav 1, Cav 3, cavin 1, cavin 4, β_1AR and β_2AR), details of the protein amino acid sequences and amino acid recognition sights are detailed in Figure 8-1. Some of the antibodies used in previous studies (e.g. Cav 1 and cavin 1) were not suitable for use in this work; a short epitope sequence (optimum 10-30 resides) was required for synthesis of the calibrating peptide. Initially all protein epitopes were included in one CavCAT peptide, however, this showed poor expression

levels when the sequence was transfected into E*scherichia coli.* and so was redesigned as two separate CavCAT peptides. In addition, not all antibodies used in traditional Western blotting are compatible with the Simple Western system, which is thought to be due to the immobilization step securing the protein to the capillary glass tube modifying antibody recognition. This was the case for the β-AR in our study. Due to unusual banding patterns in the β-AR Western blotting results and limitations on time, the study of the β-AR proteins was discontinued. CavCAT contain the epitope recognition site of the chosen antibodies, with additional amino acids either side (Figure 8-2). A hexa-His Tag (highlighted in green) at the C terminus was added to enable purification of the protein. At the N-terminus a glufibrinopeptide was added to allow for CavCAT standard quantification.

Detailed methods of CavCAT protein production and quantification can be found in Brownridge et al., which is the protocol employed here (Brownridge et al., 2012). In brief, CavCAT sequences were sent to Eurofins Genomics (Edersberg, Germany) for gene synthesis. The genes were then transfected into E*scherichia coli.* which were driven to express the CavCAT protein heterologously. For extraction, pellets of cell culture (50 mL) were sonicated in 25 mM ammonium bicarbonate buffer with protease inhibitor. Samples were centrifuged at 6000 g for 6 min and the soluble fraction removed. The remaining inclusion body pellets (which contained the CavCAT) were solubilised in purification Buffer A (mM: 20 sodium phosphate, 50 NaCl, 10 imidazole, 6 M guanidine HCl). Solubilised inclusion bodies were purified using a His-trap 1 mL column on the ÄKTA start system (GE healthcare, UK). Fractions were eluted using a 20 mL gradient elution from 0% to 100% (500 mM imidazole final). CavCAT optimisation was performed to calculate a detectable linear range for CavCAT loading the matching antibodies. As a set volume of sample was loaded per Western blot, a range of sample dilutions were trialed to ensure that the protein signal fell within the linear range of the CavCATs signal.

RAT – Caveolin 3

MMTEEHTDLEARIIKDIHCKEIDLVNRDPKNINEDIVKVDFEDVIAEPEGTYSFDGVWRVSYT
TFTVSKYWCYRLLSTLLGVPLALLWGFLFACISFCHIWAVVPCIKSYLIEIQCISHIYSLCIRTFCNPLF
AALGQVCSNIKVVLRREG

BD (610421) – Rat peptide (antibody raised in mouse)

TEEHTDLEARIIKDIHCKEIDL

RAT -Caveolin 1

MSGGKYVDSEGHLYTVPIREQGNIYKPNNKAMADEVNEKQVYDAHTKEIDLVNRDPKHLNDDVVK
IDFEDVIAEPEGTHSFDGIWKASFTTFTVTKYWFYRLLSTIFGIPMALIWGIYFAILSFLHIWAVVPCIK
SFLIEIQCISRVYSIYVHTFCDPLFEAIGKIFSNIRISTQKEI

Boster (PA1514)– Human peptide (antibody raised in rabbit)

GKIFSNVRINLQKEI

RAT – Cavin 1 (PTRF)

MEDVTLHIVERPYSGYPDASSEGPEPTPGEARATEEPSGTGSDELIKSDQVNGVLVLSLLDKIIGA
VDQIQLTQAQLEERQAEMEGAVQSIQGELSKLGKAHATTSNTVSKLLEKVRKVSVNVKTVRGSLE
RQAGQIKKLEVNEAELLRRRNFKVMIYQDEVKLPAKLSVSKSLKESEALPEKEGDELGEGERPEED
AAAIELSSDEAVEVEEVIEESRAERIKRSGLRRVDDFKKAFSKEKMEKTKVRTRENLEKTRLKTKEN
LEKTRHTLEKRMNKLGTRLVPVERREKLKTSRDKLRKSFTPDHVVYARSKTAVYKVPPFTFH
VKKIREGEVEVLKATEMVEVGPDDDEVGAERGEATDLLRGSSPDVHTLLEITEESDAVLVDKSDSD

Origen (NP_036364) – Human peptide (antibody raised in rabbit)

CLVPAERREKLKTSR

RAT Cavin 4 (MURC)

MEHNGSASNAGKIHQNRLSSVTEDEDQDAALTIVTVLDRVATVVDSVQASQKRIEERHREMGNAI
KSVQIDLLKLSQSHSNTGYVVNKLFEKTRKVSAHIKDVKARVEKQQVRVTKVETKQEEI
MKKNKFRVVIFQEDVPCPASLSVVKDRSLPENEEEAEEVFDPPIDLSSDEEYY
VEESRSARLRKSGKEHIDHIKKAFSKENMQKTRQNFDKKVSGIRTRIVTPERRERLRQSGERLRQ
SGERLRQSGERFKKSISNATPSKEAFKIRSLRKPKDPKAEGQEVDRGMGVDIISGSLALGPIHEFH
SDGFSETEKEVTKVGYIPQEGGDPPTPEPLKVTFKPQVRVEDDESLLLELKQSS

Sigma (HPA021021)– Human peptide (antibody raised in rabbit)

KVSAHIKDVKARVEKQQIHVKKVEVKQEEIMKKNKFRVVIFQEKFRCPTS
LSVVKDRNLTENQEEDDDDIFDPPVDLSSDEEYYVE

Figure 8-1 Design of CavCAT recognition sights.

For each target the FASTA protein sequence (acquired from PubMed protein library) from *Rattus norvegicus* is matched with the amino acid recognition site. Antibody amino acid recognition sequence highlighted in orange and used for CavCAT design. Any discrepancies in the antibody epitope from the FASTA sequence are highlighted in blue. Under each target are details of antibody: company, catalogue number, species from which peptide sequence was raised against and species peptide raised in.

CavCAT1_1
(Cav 1, Cavin 4, β_2AR)

MGTREGVNDNEEGFFSARAIGKIFSNIRISTQKEIREVT
KVGYIPQEGGDPPTPEPLKVTFKPQQIDLLKLSQSHSN
TGYVVNKLFEKTRFLLAPNGSRAPGHDITQERDEAWV
VRIQCISRVYSIYVHTFCDPLFEAIGKIFSNIRFDGIWKAS
FTTFTVTKYWFYRENLYFQGQDRKTRKVSAHIKDVKA
RVEKQQVRVTKVETKQEEIMKKNKFRVVIFQEDVPCP
ASLSVVKDRSLPENEEEAEEVFDPPIDLSSDEEYYVEE
SRSPDFRIAFQELLCLRRSSSKTVIAVDRYVAITSPFKY
QSLLTRAGAGAAGHHHHHH

CavCAT1_2
(Cav 3, Cavin 1, β_1AR)

MGTREGVNDNEEGFFSARGLRVIALDRYLAITLPFRYQ
SLLTCYNDPKCCDFVTNRAYAIARGTRLVPVERREKLK
TSRDKLYSLCIRTFCNPLFAALGQVCSNIKVVLRREVVP
CIKSYLIEIQCISHIYSLCIRTFCNPRENLYFQGQDRMMT
EEHTDLEARIIKDIHCKEIDLVNRDPKLSLLDKIIGAVDQI
QLTQAQLEERQAEMEGRDKLRKSFTPDHVVYARSKTA
VYEKSDDDDDDAGATPPARLLEPWAGCNGGTTTVDS
DSSLDEPGRQGFSSESKVGRAGAGAAGHHHHHH

Figure 8-2 CavCAT final gene sequence

Final gene sequence of CavCATs, each CavCAT is named with a list of protein targets underneath. Amino acid recognition sights highlighted in orange, with additional ammino acids either side underlined. Glufibrinopeptide (Glufib) sequence highlighted and underlined in green and hexa-His Tag at C terminus highlighted in green. The β-AR target sequences are highlighted in red. A tobacco etch virus protease cleavage site is in bold.

8.1.2. Sample preparation

Cardiac myocyte samples were prepared using freshly isolated cells (detailed in Methods 2.4) from the left ventricle of saline-injected animals (Methods 2.1.2). Cells were centrifuged, supernatant removed and then re-suspended in Laemelli Sample buffer before homogenising 4 x 20 s. Samples were then centrifuged for 10 min at 16000 g 6^{o}C, supernatant removed and stored at -20 ^{o}C. Myocardial samples were prepared from left ventricular free wall from saline-injected animals (Methods 2.1.2) snap-frozen in liquid N_2 and stored at -80 ^{o}C. Myocardium was quickly defrosted and processed as detailed in Methods (Section 2.8.1). Protein concentration was measured using a BCA assay as detailed in Methods (Section 2.9.3.1).

8.1.3. Simple Western, Western blotting

Protocol for Western blotting followed the manufacturer's guidelines (ProteinSimple, 2016). Samples were diluted to the desired concentration, calculated in the optimization steps, and mixed with the fluorescent master mix. Both biotinylated ladder and samplers were denatured by heating to 95^{o}C for 5 min. Five CavCAT standards, diluted samples, a biotinylated ladder and primary and secondary antibodies were loaded into a ProteinSimple® Western plate. The plate was then loaded into the ProteinSimple Wes machine and automated Western blotting started. A diagrammatic representation of the immunoassay is detailed in Figure 8-3. Results were analysed using Compass software following the guidelines given by the manufacturer.

For groups with small sample sizes, Shapiro-Wilk normality test was used and power calculations performed to ensure results presented had sufficient statistical power; an alpha value equal to or greater than 0.8 was deemed as sufficient.

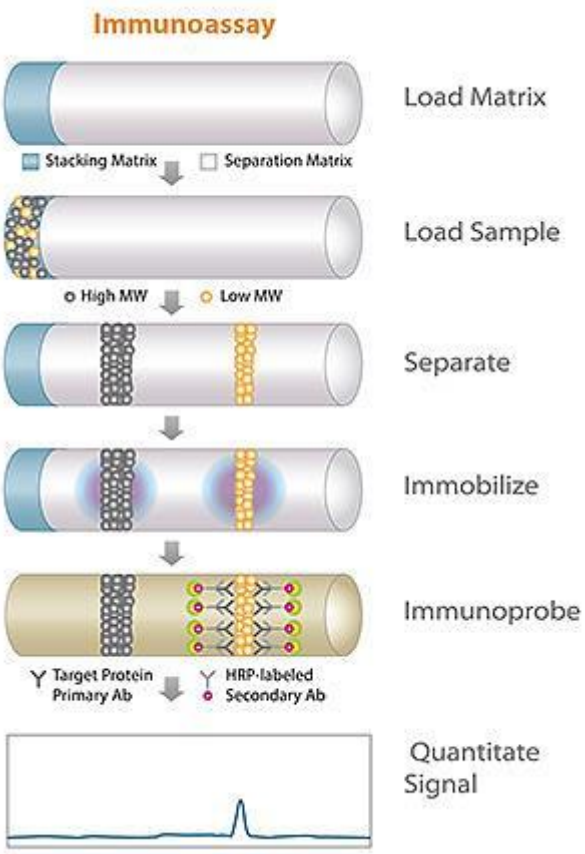

Figure 8-3 Diagrammatic representation of Simple Western immuno assay

(Diagram from ProteinSimple®) Sample is loaded from the plate automatically into the capillary tubes. Samples are separated by size through the stacking and separation matrix which fills in the capillary tube. Proprietary, photoactivated capture chemistry then immobilises proteins to the capillary wall. Primary antibodies are then used to detect target which are then visualised with a horseradish peroxidase-conjugate substrate. (http://www.proteinsimple.com/simple_western_assays.html)

8.2. Results

CavCAT standards were initially characterised by loading different concentrations of CavCAT with different dilutions of a sample of left ventricular homogenate to find the optimum CavCAT standard range with sample dilution (data not shown). Final runs of CavCAT standards and sample signal are plotted in Figure 8-4. CavCAT standards for Cav 3, cavin 1 and cavin 4 all have good expression (high signal to noise ratio) and antibody recognition. Unfortunately one of the CavCAT standards in the Cav 1 plates was undetectable (10 fmol), and another (500 fmol) did not appear to have worked, as the signal detected was very low, in the Cav 1 Western blot plate 1. A standard curve was still constructed, but the lower number of standards was taken into consideration when applying weighting to the results. The absolute concentration of protein in the samples was then calculated from this standard curve.

8.2.1. Cardiac myocytes vs. Myocardium

The caveolar protein quantification summary data is presented in Figure 8-5. Cav 1 protein concentration was significantly higher (by ≈100%) in myocardial samples compared to myocyte samples ($P<0.01$). There was no difference ($P=0.25$) in the protein concentration of Cav 3 in the myocardium compared to the myocyte samples. Cavin 1 protein concentration was significantly higher (by ≈300%) in myocardium compared to myocyte samples ($P<0.001$). Cavin 4 protein expression was also significantly higher (by ≈100%) in the myocardium compared to myocyte samples ($P<0.001$). Post hoc power calculations for cav1, cavin 1 and cavin 4 all result in an alpha value above 0.8. It was predicted there would be a slight decrease in the Cav 3 protein concentration within the myocardial samples compared to the cardiac myocyte samples, although any very small changes in Cav 3 may be too small to detect at this sample size (alpha =0.26).

In summary, the ubiquitously expressed isoforms of caveolin (Cav 1) and cavin (cavin 1) are the most highly expressed caveolar proteins in myocardial samples, whereas in myocyte samples, the muscle-specific caveolin, Cav 3, is the most highly expressed caveolar protein, closely followed by Cav 1.

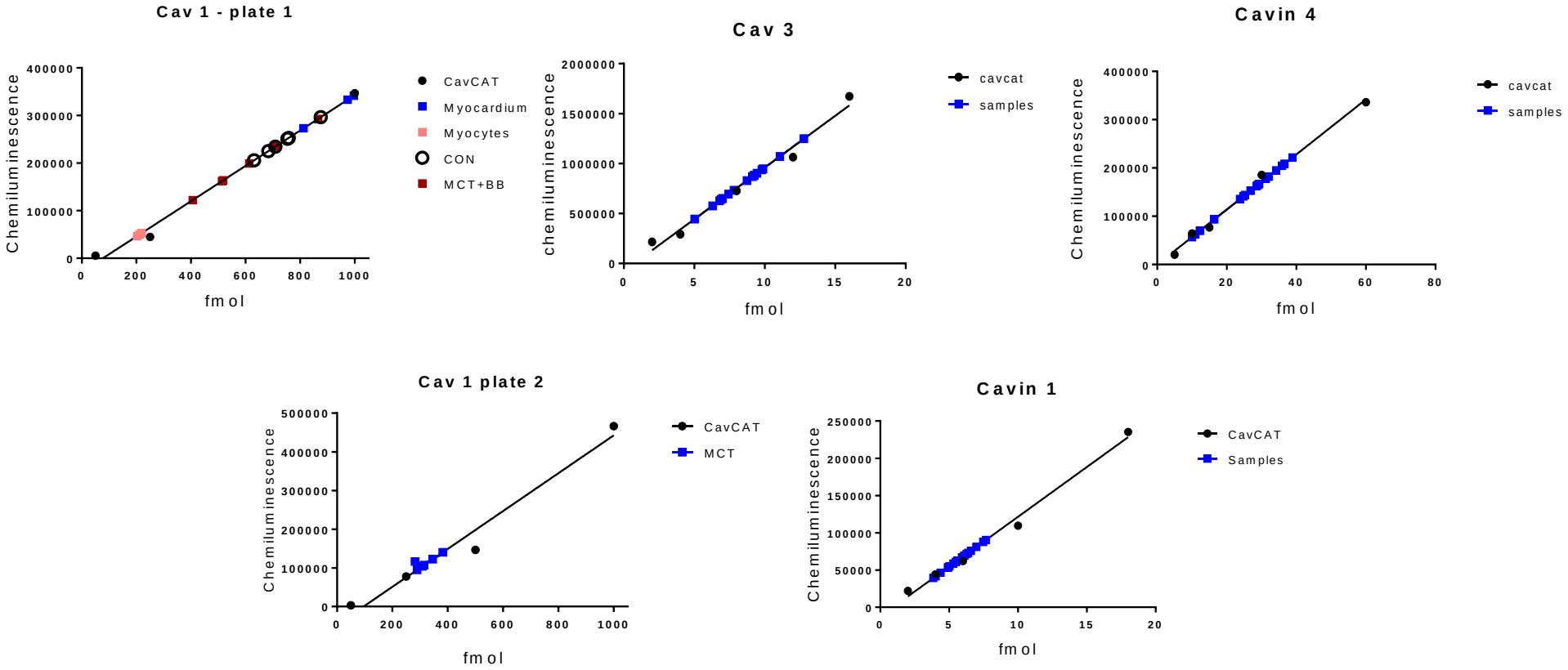

Figure 8-4 CavCAT standards and samples protein expression

Individual plate results of CavCAT and sample detected signal. Sample concentration calculated from standard curve produced from CavCAT signals.

8.2.2. Quantitative protein changes in the right ventricle of MCT animals

Myocardial homogenates which were previously used for analysis in Chapter 6 were tested with the CavCAT standards on the Simple Western system (Figure 8-6). Cav 1 protein concentration was significantly decreased by almost 50% in MCT animals compared to CON ($P<0.05$). MCT+BB samples showed a range of concentrations and there was no significant difference from CON or MCT. This differs from what was seen using traditional Western blotting in which both MCT and MCT+BB were significantly decreased compared to CON. Cav 3 protein concentration was significantly decreased in MCT compared to CON ($P<0.001$), with Cav 3 concentration in MCT almost half of that in CON. There was also a significant decrease in MCT+BB compared to CON ($P<0.01$). Again this was different to what was seen using traditional Western blotting in which there was a significant decrease in MCT expression compared to CON ($P<0.01$) and MCT+BB ($P<0.05$). Cavin 1 protein concentration was not different between the three groups, although there was a trend for a decrease in protein concentration in the MCT animals compared to CON ($P=0.14$), which mimics the significant decrease ($P<0.05$) in protein expression seen in the traditional Western blot. There was also no change in protein concentration of cavin 4 between the three groups, which corresponds to what was seen using traditional Western blot. Differences between the CavCAT and traditional Western blotting may also be down to reduced sample size measured in the CavCAT experiments, which resulted in some of the protein comparisons in the CavCAT being under powered.

The protein concentration of the caveolar proteins in CON animals was similar to the protein concentration seen in the myocardial homogenate sample (Figure 8-7). Cavin 4 protein expression is the only one which is significantly different between the two. CON, which is homogenised right ventricle from saline injected animals has a significantly higher protein concentration compared to the myocardial homogenate ($P<0.01$), which are left ventricular homogenates from saline injected animals. This could be an interesting difference between RV and LV cavin 4 protein concentrations, but as the RV and LV come from different animals at different times, the differences in these data points do not hold any significant meaning.

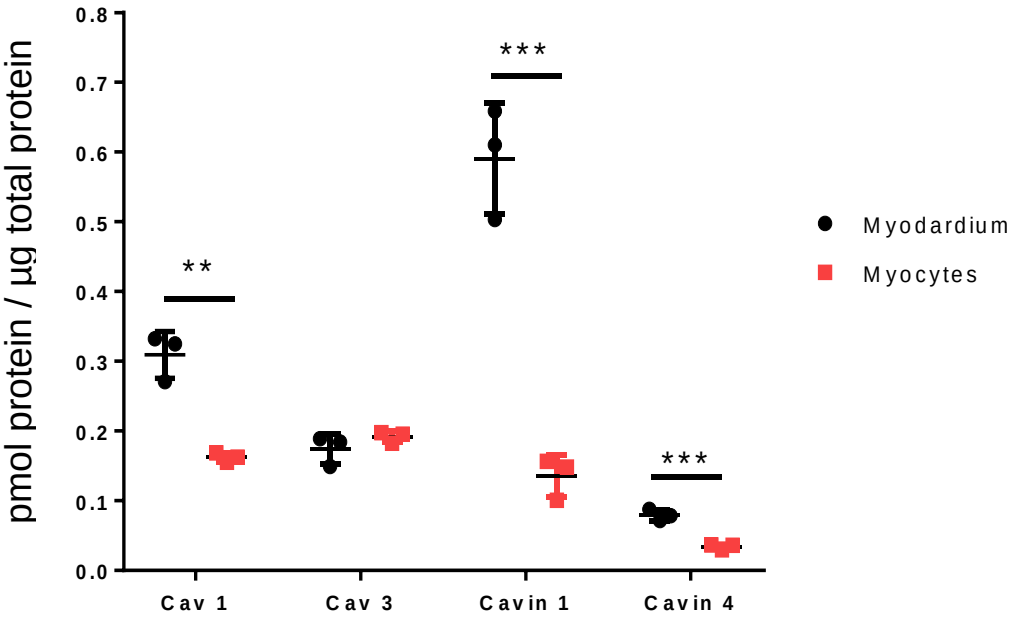

	Myocardium		Myocytes	
	Mean	SEM	Mean	SEM
Cav 1	0.309	0.019	0.162	0.004
Cav 3	0.174	0.013	0.192	0.005
Cavin 1	0.591	0.046	0.135	0.017
Cavin 4	0.079	0.005	0.034	0.002

Figure 8-5 Caveolar protein concentrations in myocyte and myocardial samples

Protein concentration was calculated from the standard curve from each CavCAT standard run on the same Western blot. Protein concentration was then corrected for the loading concentration of the sample so that the final protein concentration could be calculated. Myocardial homogenate samples (myocardium) n=3, myocyte homogenate samples (myocytes) n=3. Student's t-test, **P<0.01, ***P<0.001

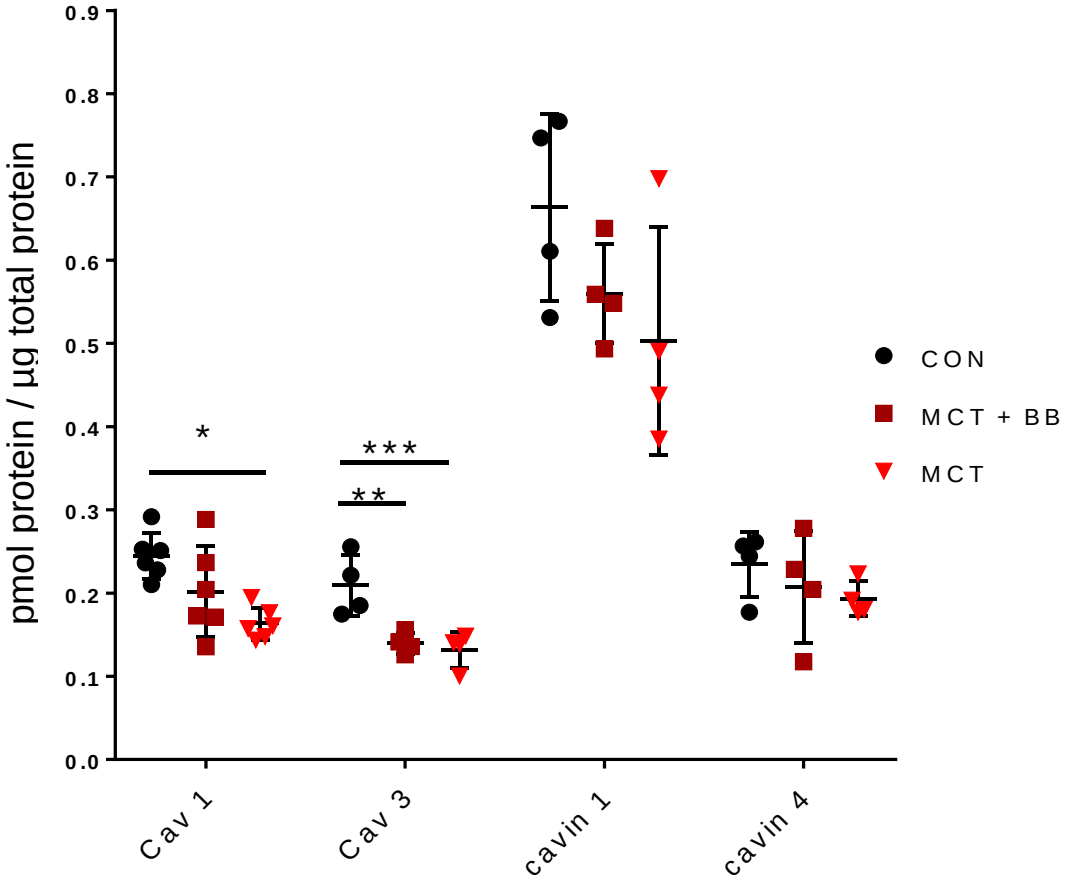

	CON		MCT+BB		MCT	
	Mean	SEM	Mean	SEM	Mean	SEM
Cav 1	0.245	0.011	0.201	0.022	0.163	0.008
Cav 3	0.209	0.018	0.140	0.006	0.132	0.011
Cavin 1	0.664	0.056	0.560	0.030	0.503	0.068
Cavin 4	0.235	0.020	0.207	0.034	0.193	0.010

Figure 8-6 Caveolar protein concentrations in right ventricular myocardial homogenate from MCT animals

Protein concentration was calculated from standard curve for each CavCAT standard run on the same Western blot. Protein concentration was then corrected for the loading concentration of the sample so that the final protein concentration could be calculated. Cav 1 CON n=6, MCT+BB n=6 MCT n=6.Cav 3, cavin 1, cavin 4, CON n=4, MCT+BB n=4 MCT n=4, One-Way ANOVA *P<0.05, **P<0.01, ***P<0.001

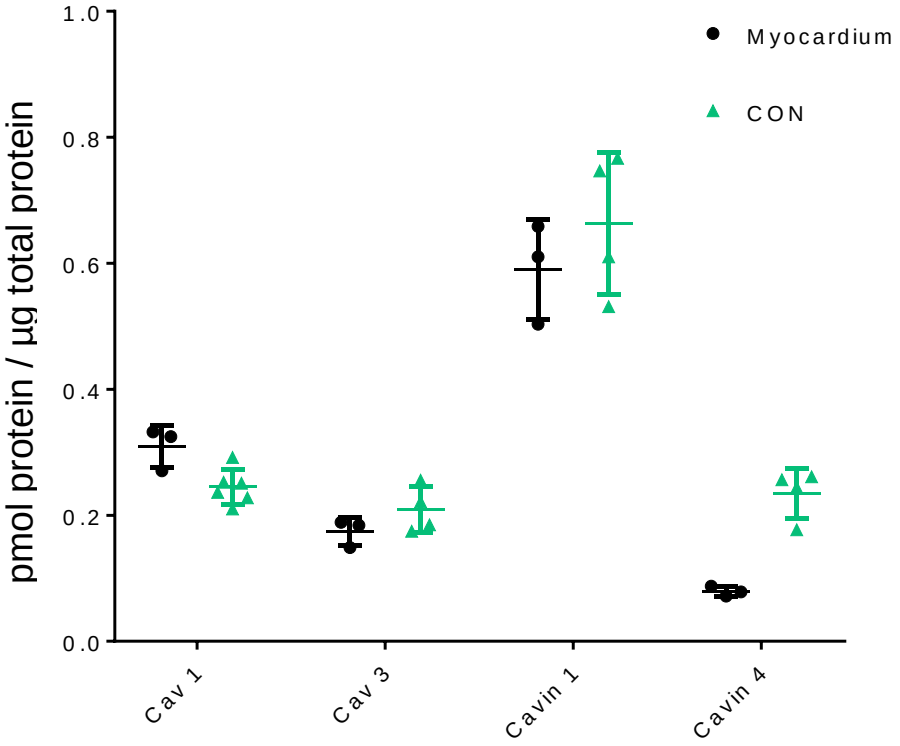

	Myocardium		CON	
	Mean	SEM	Mean	SEM
Cav 1	0.309	0.019	0.258	0.012
Cav 3	0.174	0.013	0.209	0.018
Cavin 1	0.591	0.046	0.664	0.056
Cavin 4	0.079	0.005	0.235	0.020

Figure 8-7 Caveolar protein concentrations in right ventricular muscle homogenate (CON) and left ventricular muscle homogenate (myocardium)

Protein concentration was calculated from standard curve for each CavCAT standard run on the same Western blot. Protein concentration was then corrected for the loading concentration of the sample so that the final protein concentration could be calculated. Myocaridum n=3, CON Cav 1 n=6, CON Cav 3, cavin 1 and caivin 4 n=4.

8.3. Limitations

When designing experiments for the Simple Western, Western blotting system, a number of limitations were evident which restricted the results which could be achieved. The automated Simple Western loads a set volume (4-5 µL) into the capillary tubes, which was identical for each of the samples within the plate. In accordance with manufacturer's notes, the sample volume loaded into the capillaries can vary from plate to plate. This meant that samples had to be diluted to equal protein concentrations, and this therefore limited the amount of protein that could be loaded for each sample. This was a problem when trying to measure protein concentrations in samples from myocyte sucrose gradient fractionation. Sample concentration was too low in many of the samples and caused issues with protein detection, and for this reason the results were unmeasurable. Ensuring the samples were diluted enough to fit within the linear range of the CavCAT standard was also another issue. Antibodies have a linear detectable range within which they should be used (Taylor et al., 2013). Several optimisation runs were performed to calculate the dilution needed for the samples to fall within the linear range of the CavCAT standards, and a limited number of Western blots fell within the measurable range. The Simple Western plate design and final loading volumes of samples and can be found in Appendix 1. Due to the length of time spent optimising sample and CavCAT concentrations and time limitations only a small number of samples were run through the Simple Wester process. This meant that some of the comparisons were underpowered and small changes or changes in samples with large amounts of variation may not be detected.

8.4. Discussion

The results from the quantitative measurements of the caveolar proteins in the muscle and myocyte samples were unexpected, in the context of current views of the expression of caveolar proteins between cell types. Two observations were particularly surprising: Firstly that the protein concentration of Cav 1 in myocyte samples is half that in myocardium, and second how close Cav 1 expresison levels are to that of Cav 3 (Cav 1 mean 0.162 pmols/µg sample, Cav 3 mean 0.192 pmols/µg sample). In the literature Cav 3 is considered as the most important caveolar protein within cardiac myocytes, and as mentioned previously (in Chapter 7), the role of Cav 1 within the cardiac myocyte has been all but dismissed. Within the myocardial sample however the Cav 1 protein concentration is almost twice as that in the myocyte sample, suggesting that around half of the cav 1 expression within the myocardial sample is from non-myocyte cells.

It was noted in the results that there was a problem with the CavCAT standards in plate 1, but despite this both the myocyte samples and myocardial samples chemiluminescence were close to a CavCAT standard, which were shown to run as a linear range up to 2 pmol/μL. Ideally this plate would have been re-run to confirm this result but due to time restrictions this was not possible. This result along with the results from Chapter 7, and the recent publication (Bai et al., 2016), will hopefully cause the scientific community to take a closer look as the possible role of Cav 1 within the cardiac myocyte.

One expected result was the similarity between Cav 3 protein concentration in myocyte and muscle samples. Although myocytes do not make up 100% of the protein content in the myocardial sample, they are predicted to make up the majority. Vascular smooth muscle cells are also present in the myocardial sample, although in very small quantities, which could contribute to the Cav 3 expression within the myocardial sample. Cav 3 is a predominantly muscle specific caveolin known to be highly expressed within cardiac myocytes (Song et al., 1996b). Cav 3 is also the most highly expressed of the caveolar proteins within the myocyte samples, consistent with its functional importance within the cardiac myocyte (Woodman et al., 2002; Tsutsumi et al., 2008; Parton et al., 1997).

8.4.1. Cavins

A large difference between cavin 1 protein concentration in myocardium and myocyte preparations illustrates an important caveat in interpreting cavin 1 protein expression results in myocardial samples. Cavin 1 is ubiquitously expressed in all the of cells types within the heart and within the vasculature supplying the heart (Hansen et al., 2013; Bastiani et al., 2009; Liu et al., 2008). What is surprising is the four fold difference in protein concentration in myocyte samples compared to myocardium, suggesting a large part of the cavin 1 protein expression in a myocardial homogenate comes from non-myocyte cells. This should be taken into consideration especially in disease models in which other cells within the heart can also undergo remodelling and increase the contribution the extracellular matrix makes to the myocardial structure (Fan et al., 2012; Vliegen et al., 1991; Schwab et al., 2013). This result may also go some way in explaining the discrepancies in changes to cavin 1 protein expression seen in different models of heart failure (Liu and Pilch, 2016; Mohamed et al., 2016). Cavin 1 was not originally discovered for its role in caveolae (Jansa et al., 1998), and there are still many aspects of its function which remain unclear. The precise role of cavin 1 in the cardiac myocyte is also not fully understood. Knock-out or mutations of Cavin 1 lead to a vast array of cardiac dysfunctions including cardiac

hypertrophy, fibrosis, and arrhythmias, and results in an almost complete loss of Cav 1 and Cav 3 protein expression within the heart (Liu et al., 2008; Rajab et al., 2010; Taniguchi et al., 2016). Cavin 1 is also shown to be a highly dynamic protein; after the selective β_1AR or β_2AR stimulation of cardiac myocytes cavin 1 is recruited to caveolae (Wypijewski et al., 2015). The dynamic capability is something to consider when studying the membrane location of cavin 1, and the potential benefit that the reduced processing time for myocardial samples confers. However, these data raise the question when studying the fractions from a sucrose gradient fractionation of how much of each fraction comes from the cardiac myocyte.

The significant reduction in cavin 4 protein concentration in cardiac myocytes compared with the myocardial samples is also unexpected. Cavin 4 is thought be a muscle specific cavin (Bastiani et al., 2009). One possibility is that the reduction in cavin 4 in myocyte preparations is from ubiqitination and degradation of the protein, which contains multiple proline, glutamic acid, serine, and threonine-rich (PEST) domains, as a result of the longer processing time for the myocyte samples (Bastiani et al., 2009). This may also affect Cavin 1 (which also contains multiple PEST domains) and may contribute in part to the dramatically lower protein concentrations of cavin 1 in the mycocyte sample compared to the myocardial sample (Bastiani et al., 2009; Wei et al., 2015).

8.4.2. Implications for measuring protein expression within the heart

There are a handful of studies to date which have addressed possible discrepancies within the literature because of the use of myocyte or myocardial sample (Leineweber et al., 2003; Yoshida et al., 2001). These two studies were looking at the differences in protein expression of the β-AR and their Gα subunits in heart disease models. Leineweber et al. showed a decrease in β_1AR expression (as measured with (+/-)[^{125}Iodo] cyanopindolol (ICYP)) in both the RV and LV in myocardial homogenates from MCT animals compared to control animals, whereas they only observed a decrease in β_1AR expression in the RV in myocyte homogenates (discussed in Chapter 5). In a myocardial infarction rat model Yoshida et al. reported no change in $G\alpha_s$ protein expression in myocardial homogenates but a significant decrease in myocyte samples compared to controls. This highlights the possible false positive and false negative interpretations from these kinds of data. The quantitative measurements of the caveolar proteins within this study highlight the differences in the Cav 1 and cavin 1 between myocyte and myocardial samples, which should be taken into

consideration when drawing conclusions from changes expression of these proteins in disease models.

Chapter 9. General discussion

9.1. Introduction

Cardiac myocytes are unlike any other cell in the body; they are highly specialised to allow for continuous and synchronous contractions throughout life. The membrane of the cell is the sole pathway for communication with the surroundings and vital for effective transport in and out of the cell. Caveolae are specialised microdomains of this membrane that organise proteins responsible for this transport. In this study we aimed to address how caveolar proteins change in heart failure and their putative influences on β-adrenergic (β-AR) signalling. By studying in vivo heart function and cellular responses to β-AR as well as protein expression and membrane location we can begin to theorise how function is influenced by changes in caveolar organisation.

The muscle-specific isoform, caveolin 3 (Cav 3), was originally thought to be the only caveolin protein present in cardiac myocytes, but a number of studies have shown evidence of both caveolin 1 (Cav 1) and caveolin 2 (Cav 2) expression in cardiac myocytes from a range of species (Head et al., 2006; Robenek et al., 2008)(Discussed in Chapter 7 and 8). Despite this, the presence of Cav 1 in ventricular myocytes is not widely accepted as many papers continue to state (lacking any citation or robust evidence) that Cav 1 is not present in the cardiac myocyte (Schwencke et al., 2006; Taniguchi et al., 2016). With only a few exceptions, Cav 3 is the main target in the study of cardiac myocytes, with demonstrated involvement in the regulation of many signalling elements, from localisation of the NCX and L-type Ca^{2+} channels to aiding in compartmentalisation of β_2AR cAMP signalling (Barbagallo et al., 2016; Bryant et al., 2014; Liu et al., 2003).

Caveolae and caveolar proteins are instrumental in orchestrating membrane location and function of many of the proteins involved in excitation contraction coupling and β-AR signalling. The way in which the spatial characteristics of β_2AR signalling are achieved in normal physiology is still not fully understood, although many mechanisms of cAMP compartmentalisation have been shown to play a role including the coupling of Cav 3 and PDE, and dual coupling of the receptor with $G\alpha s$ and $G\alpha_i$. Conflicting reports still remain within the literature, suggesting that a full understanding of the signalling of these receptors has not being reached (Wright et al., 2014; Rybin et al., 2000).

By characterising two models of heart failure, one of right ventricular (RV) failure and one of left ventricular (LV) failure, we have gathered a breadth of functional measurements from

the heart, cardiac muscle and myocytes and can relate these to changes in protein. This body of work aims to add to the current information within the literature and to support the idea of the dynamic regulation of caveolae in the myocyte.

9.2. Characterisation of heart failure

The characterisation of the LV failure model was achieved by in vivo hemodynamic measurements, post mortem organ weights and collagen staining of the heart. All heart failure animals developed increased heart weight, normalised to body weight, with reduced function (ejection fraction 33.9 ± 3.6% vs 76.9 ± 2.6% in the Sham group). Dilation of the left ventricle, and reduced ejection fraction and cardiac output were also observed with echocardiography and hemodynamic measurements (Chapter 3.). Increased lung and liver weight suggest systemic failure and fluid retention in these animals. All these features have clinical translation, as discussed in Houser et al., which is important for the use of small animal models of heart failure in relation to the clinical presentation (Houser et al., 2012). With reference to these guidelines, the phenotype presented in this model of pressure-overload heart failure has clinical relevance to dilated cardiomyopathy and hypertensive heart disease. The observed increase in collagen and fibrosis within the heart suggests an increase in extracellular matrix and possible stiffening of the myocardium (Jalil et al., 1989).

The RV model, induced by monocrotaline (MCT), and treated with the selective β_1AR blocker metoprolol, has previously been extensively characterised within the group (Benoist et al., 2011; Benoist et al., 2012; Stones et al., 2013; Fowler and 2016). In vivo hemodynamic measurements, post mortem organ weight and collagen staining of the heart have all been reported previously. In MCT animals, an increase heart weight normalised to body weight (which comes specifically from an increase in right ventricular weight), reduced ejection fraction (MCT 49.2 ± 2.8% vs CON 73.1 ± 3.6%) and cardiac output, and increased systolic and diastolic pressures were observed compared to the CON group (Fowler and 2016). Unlike the LV heart failure model there was no increase in fibrosis in the RV model, which may in part be due to the time progression to heart failure. The MCT model causes rapid onset of heart failure, from around 21 days post MCT injection, while in the LV model, onset of heart failure ranged from 12-28 weeks. The increased time in which the failing heart is under mechanical stress would produce more advanced remodelling within the heart and synthesis of the extracellular matrix. Of the functional and

haemodynamic measurements made, metoprolol treatment showed significant improvements in survival and a reduced wall thickness compared to MCT animals.

9.3. β-adrenergic signalling in heart failure

Hyperactivity of the sympathetic nervous system and increased sympathetic drive to the heart, with resultant β-AR desensitisation, are characteristic of heart failure. Increased levels of circulating plasma noradrenaline and tissue adrenaline and noradrenaline have been reported in both the MCT RV failure model (Kögler et al., 2003; Ishikawa et al., 1991) and the aortic banding LV failure model (Siri, 1988). This sympathetic drive is thought to cause desensitisation of the β-AR, uncoupling it from G protein subunits and promoting internalisation.

9.3.1. β-adrenergic responsiveness

β-adrenergic responsiveness, as measured by single myocyte contraction and $[Ca^{2+}]_i$, has not been studied in MCT animals to date. There are previous reports of decreased β_1AR density in isolated RV cardiac myocytes from MCT animals compared to controls, with a reduced cAMP production in response to stimulation (Leineweber et al., 2003).

In this study we showed a blunted response to selective β_1AR stimulation in terms of contraction amplitude, relaxation time and $[Ca^{2+}]_i$ transient amplitude in MCT animals compared to CON. This was partially recovered with β-blocker treatment. In multicellular trabeculae preparations from MCT animals, no significant increase in force in response to selective β_1AR stimulation was seen, which contrasts with the increase in force seen in muscle from CON animals. Metoprolol dosing had no effect on the response in MCT animals, perhaps because the dosing with metoprolol commenced too late after MCT injection (discussed in Section 5.4.4). In response to selective β_2AR stimulation in single myocytes, a proportion of cells showed a small increase in contraction amplitude in all three groups (CON, MCT+BB, MCT), with no difference between the groups. Only the CON animals showed a reduced time to 50% relaxation with selective β_2AR stimulation. This is similar to other reports that β_2AR stimulation only produces a small inotropic and lusitropic effect (Kuschel et al., 1999b), because of strong $G\alpha_i$ coupling in the rat (Kuschel et al., 1999a). Around one third of the cells in each group did not shown a positive inotropic response as indexed by fractional shortening. Taken together, these data suggest that there is a

reduction in the β_1AR functional response to stimulation in the RV heart failure, which is partially recovered with metoprolol treatment.

Selective stimulation of β-ARs was not performed in muscle or myocytes from the AB animals, as characterisation of the animal model took priority; it was not possible to isolate cells after hemodynamic recordings were performed. It is possible to measure β-AR responsiveness in vivo in tandem with hemodynamic measurements; previous studies have recorded the response to isoprenaline injection in vivo after recording stable pressure volume loops (Udelson et al., 1989). Although these experiments make it possible to measure β-AR responsiveness as well as hemodynamic measurements, it would not be appropriate for the present investigation as cardiac tissue from these animals could not be used for protein chemistry as β-AR stimulation has been shown to cause changes in the membrane location of key proteins of interest (cavin 1 and β_2AR) (Rybin et al., 2000; Wypijewski et al., 2015). The responses may also differ in the disease model compared to controls, giving misleading results.

9.3.2. β-adrenergic protein expression and membrane location

Changes in protein expression and membrane distribution are summarised in Table 9-1. In both the LV and RV model of heart failure there was a reduction in β_1AR and AC protein expression and an increase in G-protein receptor kinase (GRK)2 expression. In the RV model there was also an increase in $G\alpha_i$ protein expression which was not evident in the LV model. For all proteins whose expression changed in the RV model, metoprolol treatment partially recovered these changes in expression towards CON levels. These data suggest that, for both models, GRK2 internalisation contributes to the reduced β_1AR density on the plasma membrane. The reduction in β_1AR in the MCT animals fits with the reduction in response to β_1AR stimulation, with restoration of β_1AR expression in MCT+BB animals mimicking the restoration in β_1AR function. There was no change in β_2AR expression in either the RV or LV model compared to their respective controls. This again rationalises the lack of change in β_2AR function, measured by contraction amplitude, in the MCT animals compared to CON.

		RV heart failure	+ BB	LV heart failure
Protein expression	β1AR	↓	-	↓
	β2AR	-	↓	-
	AC 5/6	↓↓↓	-	↓
	Gαi3	↑↑↑	-	-
	GRK2	↑↑↑	-	↑
Protein membrane distribution	β1AR %	↓↓ BF ↑↑↑ HvF	-	n/a
	β2AR %	-	-	↑↑↑ BF ↓↓↓ HvF
	AC 5/6	↓ BF	↓ BF	n/a
	Gαi3	↑↑ HvF	↑ HvF	n/a
	GRK2	↑ HvF (0.06)	↑↑HvF	n/a
Protein expression	Cav 1	↓↓↓	↓↓	↓↓
	Cav 3	↓↓	-	-
	Cavin 1	↓	-	↓
	Cavin 4	-	-	↑
Protein membrane distribution	Cav 3	↓↓ BF	-	-
	Cav 3 %	↓ BF ↑ HvF	-	-
	Cav 1	-	-	-

Table 9-1 Summary data from Western blotting in heart failure models

Changes in protein expression of: β_1-adrenergic (β_1AR), β_2-adrenergic (β_2AR), adenylyl cycles (AC)5/6, Gα-inhibitor ($G\alpha_i$)3, G-protein receptor kinase (GRK)2, caveolin 1 (Cav 1), caveolin 3 (Cav 3), cavin 1 and cavin 4 in myocardial homogenate and in fractionated samples, buoyant fractions (BF), heavy fractions (HvF), as measured by Western blotting
Arrow represent significant changes in Western blotting, ↑/↓ $P<0.05$, ↑↑/↓↓ $P<0.01$, ↑↑↑/↓↓↓ $P<0.001$

The effect of LV and RV failure on the membrane distribution of the β-AR signalling proteins was also investigated. In the LV model when studying the β_2AR it was noted that an extra, higher molecular weight, band was present which was not apparent in Sham animals. This higher molecular weight band was present solely within the buoyant/caveolar fractions. A previous report has shown that the β_2AR is glycosylated and that this affected the membrane location (Rybin et al., 2003). However neither band within the buoyant fraction was shown to have an N-linked glycosylation, as tested with PNG-ase F (Chapter 4 .3.2.3). Other explanations for this higher molecular weight band include phosphorylation or palmitoylation (Liu et al., 2012; Adam et al., 1999), although these post-translational modifications were not tested within this study. It was noted there was a negative correlation between β_2AR located within the buoyant fraction and function, as measured by ejection fractions. Although this does not show a causative link, it is possible to speculate that this post-translational modification of the β_2AR within the lipid rich fractions, could have a negative influence on cardiac function.

Membrane protein organisation was more extensively studied within the RV model of failure. AC 5/6 expression was predominantly located within the buoyant/caveolae fractions, in agreement with previous studies (Head et al., 2006; Rybin et al., 2000; MacDougall et al., 2012). By contrast, β_1AR and β_2AR expression was predominantly located within the heavy/non-caveolar membrane fractions and $G\alpha_i$ 3 expression was equally distributed between caveolar and heavy fractions. In the MCT animals there was a reduction of AC 5/6 in the caveolar fractions as well as a reduction in the proportion of total β_1AR expression located here. This was coupled with an increase in expression of $G\alpha_i3$ and GRK2 within the heavy fractions. The MCT animals treated with β-blockers showed similar trends in expression of different membrane compartments (buoyant fractions/heavy fractions) as the MCT animals. The membrane distribution of β_2AR differs from previous reports, which was discussed in Chapter 4 and 6 (Section 4.3.2.3 and 6.4.2).

In the RV model, the membrane distribution data taken together with total protein expression suggests that there is a reduction in AC 5/6 which is predominantly caused by a reduction in AC 5/6 in the caveolar membrane fractions. This, in concert with reduced expression of β_1AR and its redistribution into non-caveolar membranes, suggests an uncoupling of β_1AR from AC 5/6. MCT animals treated with metoprolol improve the pattern of protein distributions in the membrane compared to the MCT animals. Together these data show that treatment with β-blockers acts to reverse remodelling of the myocardium by altering β-AR signalling protein expression, and to normalise altered protein

distribution. However specific membrane compartments in the β-blockers treated animals still showed altered protein expression levels similar to MCT (AC 5/6 and GRK2). Changes in protein expression may serve to promote increase survival and β-AR responsiveness, but it is not enough to completely rescue the failing phenotype.

9.4. Caveolae in remodelling in the RV and LV models

This is the first study to look at the array of caveolar protein changes in heart failure; these changes are summarised in Figure 9-1 and Figure 9-2. The overall trend was for a reduction in caveolar protein expression in the failing heart. Cav 1 and cavin 1 protein expression were both reduced in the LV and RV model of heart failure compared to their respective controls. Cav 3 expression was reduced in the RV model compared to CON, and was partially recovered with metoprolol treatment. Cavin 4 expression was increased in the LV model, but not the RV model, compared to the respective control groups. The increase in cavin 4 could be linked with the increased cellular hypertrophy and fibrosis seen in the AB animals (Ogata et al., 2014) (Chapter 4.4.1.3). The difference between LV and RV models may again reflect the difference in time of progression to heart failure.

As seen in Chapter 8, only a proportion of the Cav 1, cavin 1 and cavin 4 measured in myocardial samples originate in cardiac myocytes. Furthermore, the degree of change in caveolar protein concentration in RV samples (vs. CON) measured using the CavCAT standards and SimpleWestern system did not directly correlate with the degree of change in protein expression in the same model measured using traditional Western blotting. Although caveolar protein expression changes in both models of heart failure, consideration of other cellular changes in heart failure, such as an increase in fibrosis in the LV model, should be taken into consideration. A proliferation of fibroblasts or a reduction in vascular smooth muscle may alter the proportion of myocyte protein in a myocardial sample and mask or exacerbate changes in caveolar protein expression.

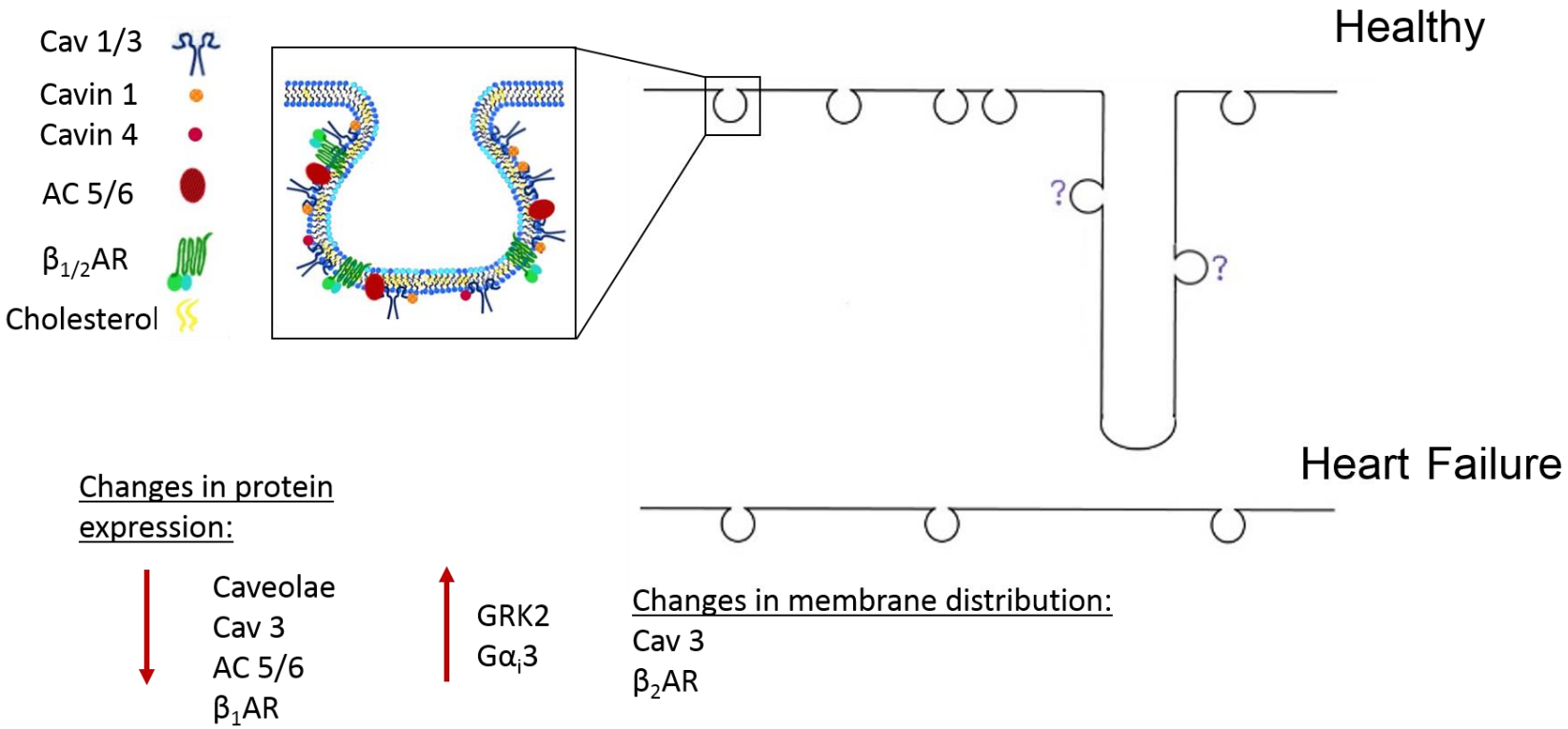

Figure 9-1 Summary of reported changes to caveolar and β-AR signalling proteins in heart failure

A number of key β-AR signalling proteins lie within the caveolar domain in a healthy cardiac myocyte including β_1AR, β_2AR, AC 5/6, $G\alpha_s$ (Head et al., 2006; Head et al., 2005; Calaghan and White, 2006; MacDougall et al., 2012; Rybin et al., 2000; Agarwal et al., 2011; Wypijewski et al., 2015). Currently the presence on caveolae in t-tubules is debated, although there are EM and super-resolution images that suggest they are present (Hong and Shaw, 2017; Fawcett and McNutt, 1969). In animal models and human patients with heart failure cardiac myocytes show a reduction in the number of t-tubules and morphological caveolae present, which in animals models is coupled with a reduction in cav 3 and other β-AR signalling proteins (Zhu et al., 2012; Gorelik et al., 2013; Feiner et al., 2011). Cav 3 and β_2AR proteins have also shown to be re-distributed from t-tubules to the surface sarcomere (Wright et al., 2014; Barbagallo et al., 2016).

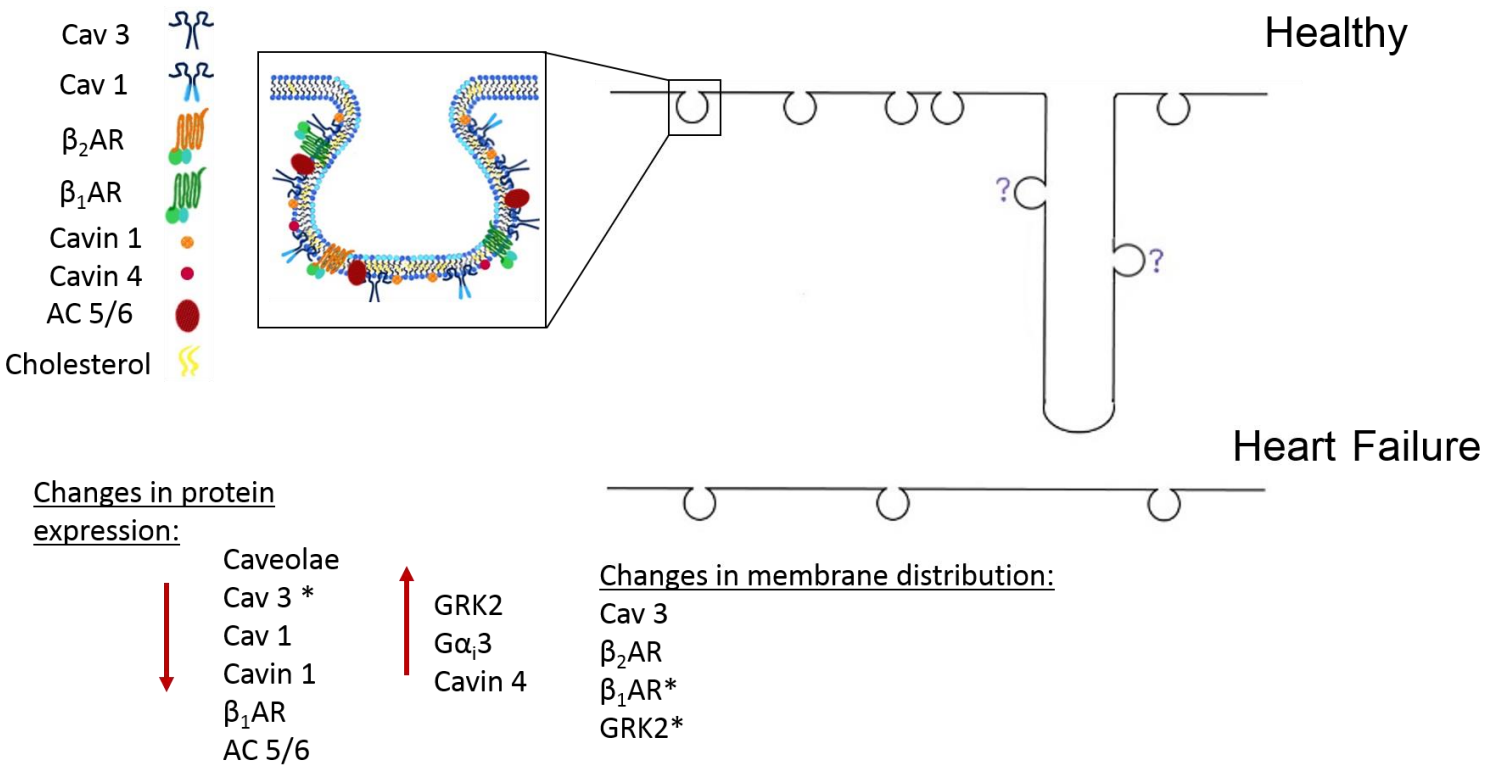

Figure 9-2 Summary of what the present study has added to our current knowledge of caveolae and β-AR signalling changes in heart failure:

The work from this thesis suggest that Cav 1 is vital for recruitment of the β_2AR to the caveolar domain, as well as supporting previous evidence of an array of different β-AR signalling proteins being present within this domain in healthy cardiac myocytes. In heart failure there was a reduction in Cav 3*, Cav 1 and cavin 1 suggesting a disruption to caveolar domain. Protein expression and membrane distribution was altered in key β-AR signalling proteins listed. * Changes only seen in the RV heart failure model.

It is interesting to note that there was no change in either Cav 3 expression or membrane distribution in the LV model. This may suggest that there is no change in Cav 3 function or morphologically-identifiable caveolae within the heart in this model. However, the reduction in cavin 1 (which is required for caveolar formation in all tissues (Park et al., 2002) could impact on caveolar density. Due to time restrictions, the visualisation of caveolae with election microscopy (EM) was not possible. EM is the only approach currently available to validate changes in morphological caveolae in the membrane. By contrast to the LV model, in RV failure there was a reduction in Cav 3 expression and a redistribution of Cav 3 from caveolar fractions. Taken in the context of the impact of Cav3 KO on caveolae in the cardiac cell (Galbiati et al., 2001), these data suggest a reduction in caveolae and disruption to their functional role within the heart. The changes in Cav 3 observed in the RV model and potential effects on caveolae may, in turn, explain some of the changes in expression and distribution of β-AR signalling proteins in MCT animals.

9.5. Caveolae in heart failure

Within the literature there are isolated reports of a reduction in Cav 3 expression and a reduction in caveolae in animal models of heart failure, as well as in samples from human patients (Feiner et al., 2011; Wright et al., 2014). Cav 3 is assumed to be the key protein within caveolae which is instrumental for β-AR signalling, and this is often the sole protein studied in relation to caveolar changes in heart failure. Cav 3 has been highlighted as potential target for treating heart failure, as cardiac-specific over-expression of Cav 3 has been shown to be cardio protective, and re-introduction of Cav 3 helps rescue some of the parameters of the failing phenotype (Song et al., 1996b; Barbagallo et al., 2016; Horikawa et al., 2011). Interestingly in our model of aortic banding we do not see any changes in Cav 3 expression or distribution across the membrane. Our data have shown for the first time that most of the myocardial Cav 3 expression comes from cardiac myocytes, as seen in the results of the quantitative blotting (Chapter 8.). The study of caveolae and Cav 3 in heart failure has been approached in many different ways including: EM, immunocytochemistry, cholesterol depletion, mutation of Cav 3, Western blotting of muscle homogenates (expression) and sucrose gradient fractions (distribution). The results of different approaches give slightly different conclusions which do not all fit neatly together into a cohesive model of caveolae changes in the failing heart. Taken together the current

literature of changes in caveolar protein and the results from the present study, we propose that sub-populations of caveolar exist which contain different caveolar proteins and related components and that, in a disease state such as heart failure, these populations may be differentially affected. The heterogeneity of caveolar protein content is not surprising considering the 249 proteins found to be high-confidence caveolar residents in the cardiac myocyte (Wypijewski et al., 2015). There would simply not be enough space within each individual caveola for this number of proteins. Other reports within the literature have also speculated on non-homogenous caveolar populations in the cardiac myocyte (Sampson et al., 2007; Shibata et al., 2006).

KO models may over-simplify the complex and dynamic micro-domains created by caveolae. Studies focusing on Cav 3 in heart failure may, in the process, discover new roles for caveolae in regulation of cardiac function. However, our quantitative analysis of caveolin isoform expression in the cardiac cell has highlighted the importance of studying the Cav 1 alongside Cav 3 in the cardiac cell. Cav 1 protein concentration in normal cardiac myocyte preparations was almost equal that of Cav 3 (Chapter 8). In the heart, Cav 1 has been shown to have a vital role in the heart's ability to protect against ischemic reperfusion injury by ischemic preconditioning (Patel et al., 2007). Cav 1 KO has also revealed a role for Cav 1 in regulation of the N^+/K^+-ATPase in the heart by facilitating interactions with other signalling proteins (Bai et al., 2016). Complexes of Cav 1/Cav 3 form with the ligand gated ion channel P2X7R in murine atrial cells (Pfleger et al., 2012). In the present study a reduction in Cav 1 and cavin 1 expression was seen in both models of heart failure, with a close correlation of Cav 1 expression with function in the LV failure model. It is therefore speculated that the reduction in Cav 1 and cavin 1 expression is linked with the reduced function of the heart. Further study of heart and myocyte function using mutated Cav 1 and cavin 1 (introduced by viral transfection) may help prove this link.

9.6. Caveolar interaction with β-adrenergic signalling

There are discrepancies in the literature regarding the location and compartmentalisation of β-AR signalling within the heart. It is generally agreed that β_1AR stimulation produces a robust cAMP response, which results in an increased inotropic and lusitropic effect, which is reduced in heart failure. On the other hand, data regarding the response to β_2AR are slightly more complex. It has previously been suggested that compartmentalised β_2AR signalling arises as a result of β_2AR coupling with $G\alpha_i$ in caveolae (MacDougall et al., 2012).

When interventions which disrupt caveolae are applied (disruption of Cav 3 binding via its scaffolding domain or cholesterol depletion), a more robust cAMP signal is achieved in response to selective β_2AR stimulation (MacDougall et al., 2012; Nikolaev et al., 2006). Interestingly in our RV heart failure model, although Cav 3 expression and caveolar localisation are reduced, the response to selective β_2AR stimulation (indexed by contraction) does not differ from CON animals. This again highlights different approaches to studying changes in heart failure; an increase in cAMP production may not directly translate to an increase in contraction. For the β_2AR, Barbagallo et al found that PDE4 was involved in compartmentalisation of the signal at caveolae and PDE3 in preventing myofilament (TnI) phosphorylation in normal myocytes, whereas in heart failure (rabbit) compartmentalisation by both PDEs was reduced with a consequent increase in TnI phosphorylation in response to selective β_2AR stimulation (Barbagallo et al., 2016). This was thought to be due to a decrease of PDE4 activity at the plasma membrane and a decrease in PDE3 influence at the myofilaments. In this model of heart failure, there was an increase in β_2AR signalling at the plasma membrane β-AR stimulation, promoting cAMP production and increasing phosphorylation of the myofilament protein TnI. However, the enhanced cAMP signals did not target SR proteins (PLB). Interestingly, the loss of normal compartmentalisation of the β_2AR signal in the failing myocyte could be restored by over expression of Cav 3, highlighting the essential role for Cav 3 in compartmentalisation of the β_2AR signal. This study also demonstrated disparities in compartmentalisation of β_2AR signalling in heart failure, possibly due to heterogeneous populations of caveolae being differentially affected.

9.6.1. Caveolin 1 and the β-adrenergic receptors

KO of Cav 1 has been shown to have many consequences for the cardiac myocyte and heart including: changes to the distribution of the β_2AR (as seen in this study using sucrose density gradient fractionation); reduced expression and altered distribution of MMP (as seen with immunocytochemistry (Cho et al., 2007)); reduced β-AR plasma membrane density, cardiac function and survival in a mouse model of myocardial infarction (Jasmin et al., 2006); impaired cardiac protection from ischemic reperfusion injury (Patel et al., 2007). No change in the density or morphology of caveolae has been reported in the cardiac myocyte of Cav 1 null mice, however this has only been assessed in surface sarcolemmal caveolae. It is possible that Cav 1 KO impacts on t-tubular caveolae. However, the presence of caveolae within the t-tubules remains a controversial topic due to their size (50-100 nm) and the distance between sarcolemmal and sarcoplasmic membrane in the dyads (10-15

nm). Caveolae in t-tubular membranes must lie outside the dyadic couplings. EM imaging of t-tubular structures along their entire longitudinal length is extremely difficult due to the nature of sectioning of EM. New cryo-EM techniques allowing 3D reconstruction of cells may reveal more details of microstructures within the t-tubules in the near future. Jasmin et al. propose that Cav 1 is involved in recruiting β-AR signalling proteins to the plasma membrane (Jasmin et al., 2006). Cav 1 may aid in recruiting a different population of proteins to the caveolae (compared with Cav 3) which results in a different form of compartmentalisation. In mouse ventricular myocytes (Cho et al., 2007) and rat ventricular myocytes (data not shown) immunocytochemisty reveals punctate staining for Cav 1 along the z-lines of the cardiac cell which may represent a population of caveolae/lipid rafts co-ordinating different signalling to that on the surface sarcolemma.

9.7. Future work

Post-translational modifications are important for regulation of protein membrane location as well as function. A possible post-translational modification was noted for β_2AR subpopulations contained in the buoyant fraction of heart homogenates prepared from LV heart failure animals. Although previously thought to be essential for membrane location, data in the present study strongly suggest that N-linked glycosylation cannot explain the observed shift in molecular weight band. However, the extent to which N-linked glycosylation is vital for the β_2AR location or function could be further investigated with mutation studies of the β_2AR and how mutation of the site of glycosylation would affect membrane location. Phosphorylation and, separately, palmitoylation – candidate forms of β_2AR post-translational modification – could be tested using with Phos-tag gels TM acrylamide gel electrophoresis and commercially available palmitoylation kits, respectively.

Gene KO mouse models are useful tools for confirming that the specific protein is involved in a mechanism or process being studied, although many of the KO models used are KO from birth and adaptive or compensatory mechanisms to the absence of the target protein are not known. This technique may also inappropriately simplify the conclusion(s) drawn, causing conflicting reports from different research groups. Heart-specific KO of Cav 1 could answer many questions regarding cardiomyopathies seen in the general Cav 1 KO model and reveal to what extent the observed cardiac dysfunction is due to lack of Cav 1 in cardiac myocytes. Responses to (non-selective) β-AR simulation are enhanced in hearts from Cav 1 KO mice compared to those of wild-type mice (Chow et al., 2010). One possible

explanation for this is that the loss of normal β_2AR-Gα_i coupling due to mislocalisation of the β_2AR (as we observed) enhances the β_2AR component of this response. It would be interesting to examine responses to selective β-AR stimulation in myocytes from Cav1 null animals compared to wild type mice for similarities in cholesterol depletion or competition for binding in caveolae with the Cav scaffolding domain peptide. It is reasonable to speculate that disruption of Cav 3 interactions at the scaffolding domain does not change the location of the β_2AR but disrupts recruitment of proteins involved in compartmentalisation, whereas cholesterol depletion, disrupting both Cav 1 and Cav 3, causes changes in membrane location of both β_2AR and regulatory proteins. Imaging of these proteins could help tease apart these differences.

Recent advances in super resolution microscopy may aid in revealing heterogenous populations of caveolae. Imaging of caveolar and caveolar proteins has previously only been achieved through EM and immunogold staining. Techniques such as single molecule location microscopy (SMLM) now allow for resolutions of 5-10 nm during immunofluorescent imaging, which would be high enough to begin to resolve collections of different caveolar proteins (Jayasinghe et al., 2015). Using SMLM to study the membrane location of different caveolar proteins could provide an experimental scenario in which heterogenous caveolae could be visualised. It would be very interesting to additionally address the possibility of disparities in caveolae subpopulations between the surface sarcolemma and t-tubule membranes. SMLM could also determine the extent to which βARs localise with caveolar proteins, thereby furthering the understanding of putative functional links between them.

Appendix 1

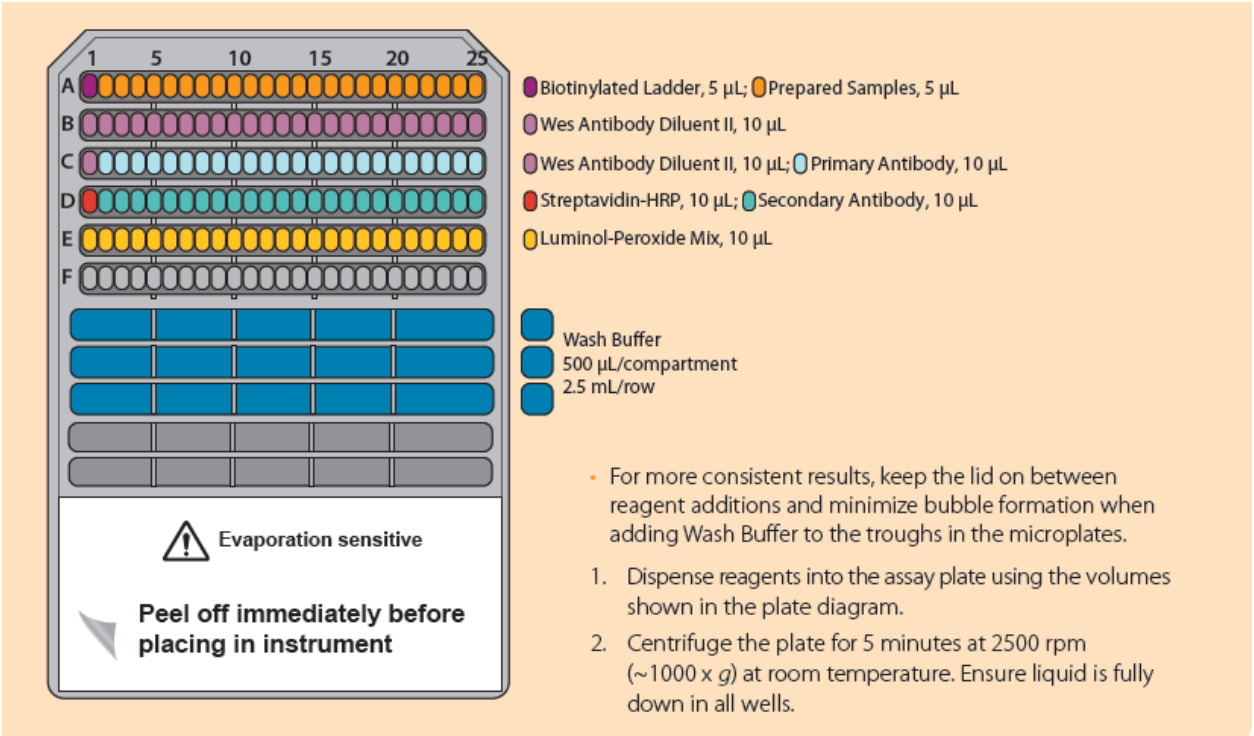

Example of plate used in SimpleWester Western blotting system (Chapter 8)

(ProteinSimple, 2016)

	1	2	3	4	5	6	7	8	9	10	11	12	13	14	15	16	17	18	19	20	21	22	23	24	25
Cav 3	Biot. Ladder	Blank 0.1 X SB	Cavcat1.2 2 fmol/ul	Cavcat1.2 4 fmol/ul	Cavcat1.2 8 fmol/ul	Cavcat1.2 12 fmol/ul	Cavcat1.2 16 ffol/ul	Saline 1 0.05ug/ul	Saline 2 0.05ug/ul	Saline 3 0.05ug/ul	Saline 4 0.05ug/ul	MCT 1 0.05ug/ul	MCT 2 0.05ug/ul	MCT 3 0.05ug/ul	MCT 4 0.05ug/ul	BB 1 0.05ug/ul	BB 2 0.05ug/ul	BB 3 0.05ug/ul	BB 4 0.05ug/ul	LV hom 1 0.05ug/ul	LV hom 2 0.05ug/ul	LV hom 3 0.05ug/ul	Myocyte hom 1 0.05ug/ul	Myocyte hom 2 0.05ug/ul	Myocyte hom 3 0.05ug/ul

	1	2	3	4	5	6	7	8	9	10	11	12	13	14	15	16	17	18	19	20	21	22	23	24	25
Cav 1.(1)	Biot. Ladder	Blank 0.1 X SB	Cavcat1.1 10fmol/ul	Cavcat1.1 50fmol/ul	Cavcat1.1 250fmol/ul	Cavcat1.1 500fmol/ul	Cavcat1.1 1000fmol/ul	AB 18 3ug/ul	AB 13 3ug/ul	AB 8 3ug/ul	AB 2 3ug/ul	AB 3 3ug/ul	AB 10 3ug/ul	Sham 20 3ug/ul	Sham 19 3ug/ul	Sham 1 3ug/ul	Sham 4 3ug/ul	Sham 6 3ug/ul	Sham 8 3ug/ul	MCT 1 1.4ug/ul	MCT 2 1.4ug/ul	MCT 3 1.4ug/ul	MCT 4 1.4ug/ul	MCT 5 1.4ug/ul	MCT 6 1.4ug/ul

	1	2	3	4	5	6	7	8	9	10	11	12	13	14	15	16	17	18	19	20	21	22	23	24	25
Cav 1.(2)	Biot. Ladder	Blank 0.1 X SB	Cavcat1.1 10fmol/ul	Cavcat1.1 50fmol/ul	Cavcat1.1 250fmol/ul	Cavcat1.1 500fmol/ul	Cavcat1.1 1000fmol/ul	BB1 1.4ug/ul	BB2 1.4ug/ul	BB3 1.4ug/ul	BB4 1.4ug/ul	BB5 1.4ug/ul	BB6 1.4ug/ul	Saline 1 1.4ug/ul	Saline 2 1.4ug/ul	Saline 3 1.4ug/ul	Saline 4 1.4ug/ul	Saline 5 1.4ug/ul	Saline 6 1.4ug/ul	LV 1 3ug/ul	LV 2 3ug/ul	LV 3 3ug/ul	My 1 1.3ug/ul	My 2 1.3ug/ul	My 3 1.3ug/ul

	1	2	3	4	5	6	7	8	9	10	11	12	13	14	15	16	17	18	19	20	21	22	23	24	25
Cavin 1	Biot. Ladder	Blank 0.1 X SB	Cavcat1.2 2 fmol/ul	Cavcat1.2 4 fmol/ul	Cavcat1.2 6 fmol/ul	Cavcat1.2 10 fmol/ul	Cavcat1.2 18 ffol/ul	Saline 1 0.01ug/ul	Saline 2 0.01ug/ul	Saline 3 0.01ug/ul	Saline 4 0.01ug/ul	MCT 1 0.01ug/ul	MCT 2 0.01ug/ul	MCT 3 0.01ug/ul	MCT 4 0.01ug/ul	BB 1 0.01ug/ul	BB 2 0.01ug/ul	BB 3 0.01ug/ul	BB 4 0.01ug/ul	LV hom 1 0.01ug/ul	LV hom 2 0.01ug/ul	LV hom 3 0.01ug/ul	Myocyte hom 1 0.04ug/ul	Myocyte hom 2 0.04ug/ul	Myocyte hom 3 0.04ug/ul

	1	2	3	4	5	6	7	8	9	10	11	12	13	14	15	16	17	18	19	20	21	22	23	24	25
Cavin 4	Biot. Ladder	Blank 0.1 X SB	Cavcat1.1 5 fmol/ul	Cavcat1.1 10 fmol/ul	Cavcat1.1 15 fmol/ul	Cavcat1.1 30 fmol/ul	Cavcat1.1 60 fmol/ul	Saline 1 0.14ug/ul	Saline 2 0.14ug/ul	Saline 3 0.14ug/ul	Saline 4 0.14ug/ul	MCT 1 0.14ug/ul	MCT 2 0.14ug/ul	MCT 3 0.14ug/ul	MCT 4 0.14ug/ul	BB 1 0.14ug/ul	BB 2 0.14ug/ul	BB 3 0.14ug/ul	BB 4 0.14ug/ul	LV hom 1 0.14ug/ul	LV hom 2 0.14ug/ul	LV hom 3 0.14ug/ul	Myocyte hom 1 0.8ug/ul	Myocyte hom 2 0.8ug/ul	Myocyte hom 3 0.8ug/ul

Plate loading template for quantitative Western blotting in SimpleWestern system (Chapter 8)

Each plate contains 25 wells for loading. Antibody used listed in each plate template. Biotiylated ladder is loaded in the first well followed by a black well with 0.1 x sample buffer (SB). The chosen dilution range of CavCAT was loaded in wells 2-7 and samples loaded in wells 8-25. Samples included right ventricular (RV) homogenate from CON (Saline), MCT (MCT) and MCT+BB (BB) animals (Chapter 6), as well as left ventricular homogenate (LV hom) and myocyte homogenate (myocyte hom) (Chapter 8). Samples from AB and Sham animals were tested in original runs, but due to time limitations were not included in subsequent runs.

References

Aboulaich, N., Chui, P.C., Asara, J.M., Flier, J.S. and Maratos-Flier, E. 2011. Polymerase I and transcript release factor regulates lipolysis via a phosphorylation-dependent mechanism. *Diabetes.* **60**(3), pp.757-765.

Adam, L., Bouvier, M. and Jones, T.L.Z. 1999. Nitric Oxide Modulates β2-Adrenergic Receptor Palmitoylation and Signaling. *Journal of Biological Chemistry.* **274**(37), pp.26337-26343.

Agarwal, S.R., MacDougall, D.A., Tyser, R., Pugh, S.D., Calaghan, S.C. and Harvey, R.D. 2011. Effects of cholesterol depletion on compartmentalized cAMP responses in adult cardiac myocytes. *Journal of Molecular and Cellular Cardiology.* **50**(3), pp.500-509.

Allan, D. 1996. Mapping the lipid distribution in the membranes of BHK cells (mini-review). *Molecular Membrane Biology.* **13**(2), pp.81-84.

Anand, I., McMurray, J., Cohn, J.N., Konstam, M.A., Notter, T., Quitzau, K., Ruschitzka, F. and Lüscher, T.F. 2004. Long-term effects of darusentan on left-ventricular remodelling and clinical outcomes in the EndothelinA Receptor Antagonist Trial in Heart Failure (EARTH): randomised, double-blind, placebo-controlled trial. *The Lancet.* **364**(9431), pp.347-354.

Ariotti, N., Rae, J., Leneva, N., Ferguson, C., Loo, D., Okano, S., Hill, M.M., Walser, P., Collins, B.M. and Parton, R.G. 2015. Molecular Characterization of Caveolin-induced Membrane Curvature. *Journal of Biological Chemistry.* **290**(41), pp.24875-24890.

Association, T.C.C.o.t.N.Y.H. 1964. Nomenclature and criteria for diagnosis of diseases of the heart and blood vessels. *Circulation.* **30**(3), pp.321-325.

Bai, L., Deng, X., Li, J., Wang, M., Li, Q., An, W., A, D. and Cong, Y.-S. 2011. Regulation of cellular senescence by the essential caveolar component PTRF/Cavin-1. *Cell Research.* **21**(7), pp.1088-1101.

Bai, Y., Wu, J., Li, D., Morgan, E.E., Liu, J., Zhao, X., Walsh, A., Saikumar, J., Tinkel, J., Joe, B., Gupta, R. and Liu, L. 2016. Differential roles of caveolin-1 in ouabain-induced Na^+/K^+-ATPase cardiac signaling and contractility. *Physiological Genomics.* **48**(10), pp.739-748.

Balijepalli, R.C., Foell, J.D., Hall, D.D., Hell, J.W. and Kamp, T.J. 2006. Localization of cardiac L-type Ca^{2+} channels to a caveolar macromolecular signaling complex is required for β_2-adrenergic regulation. *Proceedings of the National Academy of Sciences.* **103**(19), pp.7500-7505.

Ballard-Croft, C., Locklar, A.C., Kristo, G. and Lasley, R.D. 2006. Regional myocardial ischemia-induced activation of MAPKs is associated with subcellular redistribution of caveolin and cholesterol. *American Journal of Physiology - Heart and Circulatory Physiology.* **291**(2), pp.H658-H667.

Balycheva, M., Faggian, G., Glukhov, A.V. and Gorelik, J. 2015. Microdomain–specific localization of functional ion channels in cardiomyocytes: an emerging concept of local regulation and remodelling. *Biophysical Reviews.* **7**(1), pp.43-62.

Bandyopadhyay, D., Bajaj, N.S., Zein, J., Minai, O.A. and Dweik, R.A. 2015. Outcomes of β-blocker use in pulmonary arterial hypertension: a propensity-matched analysis. *European Respiratory Journal.* **46**(3), pp.750-760.

Barbagallo, F., Xu, B., Reddy, G.R., West, T., Wang, Q., Fu, Q., Li, M., Shi, Q., Ginsburg, K.S., Ferrier, W., Isidori, A.M., Naro, F., Patel, H.H., Bossuyt, J., Bers, D. and Xiang, Y.K. 2016. Genetically Encoded Biosensors Reveal PKA Hyperphosphorylation on the Myofilaments in Rabbit Heart Failure. *Circulation Research.* **119**(8), pp.931-943.

Bartel, S., Stein, B., Eschenhagen, T., Mende, U., Neumann, J., Schmitz, W., Krause, E.-G., Karczewski, P. and Scholz, H. 1996. Protein phosphorylation in isolated trabeculae from nonfailing and failing human hearts. *Molecular and Cellular Biochemistry.* **157**(1), pp.171-179.

Bartholomeu, J.B., Vanzelli, A.S., Rolim, N.P.L., Ferreira, J.C.B., Bechara, L.R.G., Tanaka, L.Y., Rosa, K.T., Alves, M.M., Medeiros, A., Mattos, K.C., Coelho, M.A., Irigoyen, M.C., Krieger, E.M., Krieger, J.E., Negrão, C.E., Ramires, P.R., Guatimosim, S. and Brum, P.C. 2008. Intracellular mechanisms of specific β-adrenoceptor antagonists involved in improved cardiac function and survival in a genetic model of heart failure. *Journal of Molecular and Cellular Cardiology.* **45**(2), pp.240-249.

Bastiani, M., Liu, L., Hill, M.M., Jedrychowski, M.P., Nixon, S.J., Lo, H.P., Abankwa, D., Luetterforst, R., Fernandez-Rojo, M., Breen, M.R., Gygi, S.P., Vinten, J., Walser, P.J., North, K.N., Hancock, J.F., Pilch, P.F. and Parton, R.G. 2009. MURC/Cavin-4 and cavin family members form tissue-specific caveolar complexes. *The Journal of Cell Biology.* **185**(7), pp.1259-1273.

Beavers, D.L., Landstrom, A.P., Chiang, D.Y. and Wehrens, X.H.T. 2014. Emerging roles of junctophilin-2 in the heart and implications for cardiac diseases. *Cardiovascular Research.* **103**(2), pp.198-205.

Beavo, J.A. 1995. Cyclic nucleotide phosphodiesterases: functional implications of multiple isoforms. *Physiological Reviews.* **75**(4), pp.725-748.

Beisiegel, U. 1986. Protein blotting. *ELECTROPHORESIS.* **7**(1), pp.1-18.

Belge, C., Hammond, J., Dubois-Deruy, E., Manoury, B., Hamelet, J., Beauloye, C., Markl, A., Pouleur, A.-C., Bertrand, L., Esfahani, H., Jnaoui, K., Götz, K.R., Nikolaev, V.O., Vanderper, A., Herijgers, P., Lobysheva, I., Iaccarino, G., Hilfiker-Kleiner, D., Tavernier, G., Langin, D., Dessy, C. and Balligand, J.-L. 2014. Enhanced Expression of β3-Adrenoceptors in Cardiac Myocytes Attenuates Neurohormone-Induced Hypertrophic Remodeling Through Nitric Oxide Synthase. *Circulation.* **129**(4), pp.451-462.

Bellenger, N.G., Burgess, M.I., Ray, S.G., Lahiri, A., Coats, A.J.S., Cleland, J.G.F. and Pennell, D.J. 2000. Comparison of left ventricular ejection fraction and volumes in heart failure by echocardiography, radionuclide ventriculography and cardiovascular magnetic resonance. Are they interchangeable? *Eur Heart J.* **21**(16), pp.1387-1396.

Benoist, D., Stones, R., Benson, A.P., Fowler, E.D., Drinkhill, M.J., Hardy, M.E.L., Saint, D.A., Cazorla, O., Bernus, O. and White, E. 2014. Systems approach to the study of stretch and arrhythmias in right ventricular failure induced in rats by monocrotaline. *Progress in Biophysics and Molecular Biology.* **115**(2–3), pp.162-172.

Benoist, D., Stones, R., Drinkhill, M., Bernus, O. and White, E. 2011. Arrhythmogenic substrate in hearts of rats with monocrotaline-induced pulmonary hypertension and right ventricular hypertrophy. *American Journal of Physiology - Heart and Circulatory Physiology.* **300**(6), pp.H2230-H2237.

Benoist, D., Stones, R., Drinkhill, M.J., Benson, A.P., Yang, Z., Cassan, C., Gilbert, S.H., Saint, D.A., Cazorla, O., Steele, D.S., Bernus, O. and White, E. 2012. Cardiac arrhythmia mechanisms in rats with heart failure induced by pulmonary hypertension. *American Journal of Physiology - Heart and Circulatory Physiology.* **302**(11), pp.H2381-H2395.

Bers, D.M. 2001. *Excitation-Contraction Coupling and Cardiac Contractile Force.* Springer Netherlands.

Bers, D.M. 2002. Cardiac excitation-contraction coupling. *Nature.* **415**(6868), pp.198-205.

Bers, D.M. 2008. Calcium Cycling and Signaling in Cardiac Myocytes. *Annual Review of Physiology.* **70**(1), pp.23-49.

Bers, D.M. 2016. Stabilizing ryanodine receptor gating quiets arrhythmogenic events in human heart failure and atrial fibrillation. *Heart Rhythm.*

Bogaard, H.J., Abe, K., Vonk Noordegraaf, A. and Voelkel, N.F. 2009. The Right Ventricle Under Pressure: Cellular and Molecular Mechanisms of Right-Heart Failure in Pulmonary Hypertension. *Chest.* **135**(3), pp.794-804.

Bogaard, H.J., Natarajan, R., Mizuno, S., Abbate, A., Chang, P.J., Chau, V.Q., Hoke, N.N., Kraskauskas, D., Kasper, M., Salloum, F.N. and Voelkel, N.F. 2010. Adrenergic Receptor Blockade Reverses Right Heart Remodeling and Dysfunction in Pulmonary Hypertensive Rats. *American Journal of Respiratory and Critical Care Medicine.* **182**(5), pp.652-660.

Bogoyevitch, M.A., Andersson, M.B., Gillespie-Brown, J., Clerk, A., Glennon, P.E., Fuller, S.J. and Sugden, P.H. 1996. Adrenergic receptor stimulation of the mitogen-activated protein kinase cascade and cardiac hypertrophy. *Biochemical Journal.* **314**(Pt 1), pp.115-121.

Böhm, M., Deutsch, H.J., Hartmann, D., La Rosée, K. and Stäblein, A. 1997. Improvement of Postreceptor Events by Metoprolol Treatment in Patients With Chronic Heart Failure. *Journal of the American College of Cardiology.* **30**(4), pp.992-996.

Brandl, C.J., deLeon, S., Martin, D.R. and MacLennan, D.H. 1987. Adult forms of the Ca2+ATPase of sarcoplasmic reticulum. Expression in developing skeletal muscle. *Journal Biological Chemistry.* **262**(8), pp.3768-3774.

Braz, J.C., Gregory, K., Pathak, A., Zhao, W., Sahin, B., Klevitsky, R., Kimball, T.F., Lorenz, J.N., Nairn, A.C., Liggett, S.B., Bodi, I., Wang, S., Schwartz, A., Lakatta, E.G., DePaoli-Roach, A.A., Robbins, J., Hewett, T.E., Bibb, J.A., Westfall, M.V., Kranias, E.G. and Molkentin, J.D. 2004. PKC-alpha regulates cardiac contractility and propensity toward heart failure. *Nature Medicine.* **10**(3), pp.248-254.

Brette, F. and Orchard, C. 2003. T-Tubule Function in Mammalian Cardiac Myocytes. *Circulation Research.* **92**(11), pp.1182-1192.

Brette, F., Sallé, L. and Orchard, C.H. 2004. Differential Modulation of L-type Ca^{2+} Current by SR Ca^{2+} Release at the T-Tubules and Surface Membrane of Rat Ventricular Myocytes. *Circulation Research.* **95**(1), pp.e1-e7.

Briand, N., Dugail, I. and Le Lay, S. 2011. Cavin proteins: New players in the caveolae field. *Biochimie.* **93**(1), pp.71-77.

Bristow, M.R., Ginsburg, R., Minobe, W., Cubicciotti, R.S., Sageman, W.S., Lurie, K., Billingham, M.E., Harrison, D.C. and Stinson, E.B. 1982. Decreased Catecholamine Sensitivity and β-Adrenergic-Receptor Density in Failing Human Hearts. *New England Journal of Medicine.* **307**(4), pp.205-211.

Bristow, M.R., Hershberger, R.E., Port, J.D., Minobe, W. and Rasmussen, R. 1989. Beta 1- and beta 2-adrenergic receptor-mediated adenylate cyclase stimulation in nonfailing and failing human ventricular myocardium. *Molecular Pharmacology.* **35**(3), pp.295-303.

Bristow, M.R., Minobe, W., Rasmussen, R., Larrabee, P., Skerl, L., Klein, J.W., Anderson, F.L., Murray, J., Mestroni, L. and Karwande, S.V. 1992. Beta-adrenergic neuroeffector abnormalities in the failing human heart are produced by local rather than systemic mechanisms. *The Journal of Clinical Investigation.* **89**(3), pp.803-815.

Bristow, M.R. and Quaife, R.A. 2015. The adrenergic system in pulmonary arterial hypertension: bench to bedside (2013 Grover Conference series). *Pulmonary Circulation.* **5**(3), pp.415-423.

Brodde, O.E., Engel, G., Hoyer, D., Bock, K.D. and Weber, F. 1981. The beta-adrenergic receptor in human lymphocytes: subclassification by the use of a new radio-ligand, $(+/-)^{-125}$ Iodocyanopindolol. *Life Sciences.* **29**(21), pp.2189-2198.

Brouri, F., Hanoun, N., Mediani, O., Saurini, F., Hamon, M., Vanhoutte, P.M. and Lechat, P. 2004. Blockade of β_1- and desensitization of β_2-adrenoceptors reduce isoprenaline-induced cardiac fibrosis. *European Journal of Pharmacology.* **485**(1–3), pp.227-234.

Brownridge, P., Lawless, C., Payapilly, A.B., Lanthaler, K., Holman, S.W., Harman, V.M., Grant, C.M., Beynon, R.J. and Hubbard, S.J. 2013. Quantitative analysis of chaperone network throughput in budding yeast. *Proteomics.* **13**(8), pp.1276-1291.

Brownridge, P.J., Harman, V.M., Simpson, D.M. and Beynon, R.J. 2012. Absolute multiplexed protein quantification using QconCAT technology. *Methods Mol Biol.* **893**, pp.267-293.

Bryant, S., Kimura, T.E., Kong, C.H.T., Watson, J.J., Chase, A., Suleiman, M.S., James, A.F. and Orchard, C.H. 2014. Stimulation of ICa by basal PKA activity is facilitated by caveolin-3 in cardiac ventricular myocytes. *Journal of Molecular and Cellular Cardiology.* **68**, pp.47-55.

Bundgaard, H., Liu, C.-C., Garcia, A., Hamilton, E.J., Huang, Y., Chia, K.K.M., Hunyor, S.N., Figtree, G.A. and Rasmussen, H.H. 2010. β_3 Adrenergic Stimulation of the Cardiac Na^+/K^+ Pump by Reversal of an Inhibitory Oxidative Modification. *Circulation.* **122**(25), pp.2699-2708.

Bylund, D.B. and Snyder, S.H. 1976. Beta adrenergic receptor binding in membrane preparations from mammalian brain. *Mol Pharmacol.* **12**(4), pp.568-580.

Byrne, D.P., Dart, C. and Rigden, D.J. 2012. Evaluating Caveolin Interactions: Do Proteins Interact with the Caveolin Scaffolding Domain through a Widespread Aromatic Residue-Rich Motif? *PLoS ONE.* **7**(9), pe44879.

Calaghan, S., Kozera, L. and White, E. 2008. Compartmentalisation of cAMP-dependent signalling by caveolae in the adult cardiac myocyte. *Journal of Molecular and Cellular Cardiology.* **45**(1), pp.88-92.

Calaghan, S. and White, E. 2006. Caveolae modulate excitation–contraction coupling and β_2-adrenergic signalling in adult rat ventricular myocytes. *Cardiovascular Research.* **69**(4), pp.816-824.

Cerbai, E., Guerra, L., Varani, K., Barbieri, M., Borea, P.A. and Mugelli, A. 1995. β-Adrenoceptor subtypes in young and old rat ventricular myocytes: a combined patch-clamp and binding study. *British Journal of Pharmacology.* **116**(2), pp.1835-1842.

Chen-Izu, Y., McCulle, S.L., Ward, C.W., Soeller, C., Allen, B.M., Rabang, C., Cannell, M.B., Balke, C.W. and Izu, L.T. 2006. Three-Dimensional Distribution of Ryanodine Receptor Clusters in Cardiac Myocytes. *Biophysical Journal.* **91**(1), pp.1-13.

Chen, J.-Q., Heldman, M.R., Herrmann, M.A., Kedei, N., Woo, W., Blumberg, P.M. and Goldsmith, P.K. 2013. Absolute quantitation of endogenous proteins with precision and accuracy using a capillary Western system. *Analytical Biochemistry.* **442**(1), pp.97-103.

Chen, J.Q., Wakefield, L.M. and Goldstein, D.J. 2015. Capillary nano-immunoassays: advancing quantitative proteomics analysis, biomarker assessment, and molecular diagnostics. *Journal of Translational Medicine.* **13**(182), pp.015-0537.

Cheng, J.P.X. and Nichols, B.J. 2016. Caveolae: One Function or Many? *Trends in Cell Biology.* **26**(3), pp.177-189.

Chesley, A., Lundberg, M.S., Asai, T., Xiao, R.-P., Ohtani, S., Lakatta, E.G. and Crow, M.T. 2000. The β_2-Adrenergic Receptor Delivers an Antiapoptotic Signal to Cardiac Myocytes Through G_i-Dependent Coupling to Phosphatidylinositol 3'-Kinase. *Circulation Research.* **87**(12), pp.1172-1179.

Cho, W.J., Chow, A.K., Schulz, R. and Daniel, E.E. 2007. Matrix metalloproteinase-2, caveolins, focal adhesion kinase and c-Kit in cells of the mouse myocardium. *Journal of Cellular and Molecular Medicine.* **11**(5), pp.1069-1086.

Chow, A.K., Daniel, E.E. and Schulz, R. 2010. Cardiac function is not significantly diminished in hearts isolated from young caveolin-1 knockout mice. *American Journal of Physiology - Heart and Circulatory Physiology.* **299**(4), pp.H1183-H1189.

Chu, L., Greenstein, J.L. and Winslow, R.L. 2016. Modeling Na^+-Ca^{2+} exchange in the heart: Allosteric activation, spatial localization, sparks and excitation-contraction coupling. *Journal of Molecular and Cellular Cardiology.* **99**, pp.174-187.

Ciarka, A., Doan, V., Velez-Roa, S., Naeije, R. and van de Borne, P. 2010. Prognostic Significance of Sympathetic Nervous System Activation in Pulmonary Arterial Hypertension. *American Journal of Respiratory and Critical Care Medicine.* **181**(11), pp.1269-1275.

Ciccarelli, M., Santulli, G., Pascale, V., Trimarco, B. and Iaccarino, G. 2013. Adrenergic receptors and metabolism: role in development of cardiovascular disease. *Front Physiol.* **4**(265), p00265.

Clarke, D.M., Loo, T.W., Inesi, G. and MacLennan, D.H. 1989. Location of high affinity Ca^{2+}-binding sites within the predicted transmembrahe domain of the sarco-plasmic reticulum Ca^{2+}-ATPase. *Nature.* **339**(6224), pp.476-478.

Collins, H.E. and Rodrigo, G.C. 2010. Inotropic Response of Cardiac Ventricular Myocytes to β-Adrenergic Stimulation With Isoproterenol Exhibits Diurnal Variation: Involvement of Nitric Oxide. *Circulation Research.* **106**(7), pp.1244-1252.

Colucci, W.S., Denniss, A.R., Leatherman, G.F., Quigg, R.J., Ludmer, P.L., Marsh, J.D. and Gauthier, D.F. 1988. Intracoronary infusion of dobutamine to patients with and without severe congestive heart failure. Dose-response relationships, correlation with circulating catecholamines, and effect of phosphodiesterase inhibition. *The Journal of Clinical Investigation.* **81**(4), pp.1103-1110.

Conti, M. and Beavo, J. 2007. Biochemistry and Physiology of Cyclic Nucleotide Phosphodiesterases: Essential Components in Cyclic Nucleotide Signaling. *Annual Review of Biochemistry.* **76**(1), pp.481-511.

Conti, M., Richter, W., Mehats, C., Livera, G., Park, J.-Y. and Jin, C. 2003. Cyclic AMP-specific PDE4 Phosphodiesterases as Critical Components of Cyclic AMP Signaling. *Journal of Biological Chemistry.* **278**(8), pp.5493-5496.

Couet, J., Li, S., Okamoto, T., Ikezu, T. and Lisanti, M.P. 1997. Identification of Peptide and Protein Ligands for the Caveolin-scaffolding Domain: Implications for the interaction of caveolin with caveolae-associated proteins. *Journal of Biological Chemistry.* **272**(10), pp.6525-6533.

Crossman, D.J., Young, A.A., Ruygrok, P.N., Nason, G.P., Baddelely, D., Soeller, C. and Cannell, M.B. 2015. t-tubule disease: Relationship between t-tubule organization and regional contractile performance in human dilated cardiomyopathy. *Journal of Molecular and Cellular Cardiology.* **84**, pp.170-178.

Dadson, K., Kovacevic, V., Rengasamy, P., Kim, G.H.E., Boo, S., Li, R.-K., George, I., Schulze, P.C., Hinz, B. and Sweeney, G. 2016. Cellular, structural and functional cardiac remodelling following pressure overload and unloading. *International Journal of Cardiology.* **216**, pp.32-42.

Dávila-Román, V.G., Vedala, G., Herrero, P., de las Fuentes, L., Rogers, J.G., Kelly, D.P. and Gropler, R.J. 2002. Altered myocardial fatty acid and glucose metabolism in idiopathic dilated cardiomyopathy. *Journal of the American College of Cardiology.* **40**(2), pp.271-277.

de Man, F.S., Handoko, M.L., van Ballegoij, J.J.M., Schalij, I., Bogaards, S.J.P., Postmus, P.E., van der Velden, J., Westerhof, N., Paulus, W.J. and Vonk-Noordegraaf, A. 2012. Bisoprolol Delays Progression Towards Right Heart Failure in Experimental Pulmonary Hypertension. *Circulation: Heart Failure.* **5**(1), pp.97-105.

De Souza, A.P., Cohen, A.W., Park, D.S., Woodman, S.E., Tang, B., Gutstein, D.E., Factor, S.M., Tanowitz, H.B., Lisanti, M.P. and Jelicks, L.A. 2005. MR imaging of caveolin gene-specific alterations in right ventricular wall thickness. *Magnetic Resonance Imaging.* **23**(1), pp.61-68.

Defer, N., Best-Belpomme, M. and Hanoune, J. 2000. Tissue specificity and physiological relevance of various isoforms of adenylyl cyclase. *American Journal of Physiology - Renal Physiology.* **279**(3), pp.F400-F416.

Despa, S., Brette, F., Orchard, C.H. and Bers, D.M. 2003. Na/Ca exchange and Na/K-ATPase function are equally concentrated in transverse tubules of rat ventricular myocytes. *Biophysical Journal.* **85**(5), pp.3388-3396.

Díaz, M.E., O'Neill, S.C. and Eisner, D.A. 2004. Sarcoplasmic Reticulum Calcium Content Fluctuation Is the Key to Cardiac Alternans. *Circulation Research.* **94**(5), pp.650-656.

Dibb, K.M., Clarke, J.D., Horn, M.A., Richards, M.A., Graham, H.K., Eisner, D.A. and Trafford, A.W. 2009. Characterization of an Extensive Transverse Tubular Network in Sheep Atrial Myocytes and its Depletion in Heart Failure. *Circulation: Heart Failure.* **2**(5), pp.482-489.

Díez, J. 2007. Mechanisms of Cardiac Fibrosis in Hypertension. *The Journal of Clinical Hypertension.* **9**(7), pp.546-550.

duBell, W.H., Gigena, M.S., Guatimosim, S., Long, X., Lederer, W.J. and Rogers, T.B. 2002. Effects of PP1/PP2A inhibitor calyculin A on the E-C coupling cascade in murine ventricular myocytes. *American Journal of Physiology - Heart and Circulatory Physiology.* **282**(1), pp.H38-H48.

Dupree, P., Parton, R., Raposo, G., Kurzchalia, T. and Simons, K. 1993. Caveolae and sorting in the trans-Golgi network of epithelial cells. *The EMBO Journal.* **12**(4), p1597.

Eghbali, M. 1992. Cardiac fibroblasts: function, regulation of gene expression, and phenotypic modulation. *Cardiac Adaptation in Heart Failure.* Springer, pp.183-189.

Eisner, D.A., Choi, H.S., Díaz, M.E., O'Neill, S.C. and Trafford, A.W. 2000. Integrative Analysis of Calcium Cycling in Cardiac Muscle. *Circulation Research.* **87**(12), pp.1087-1094.

Engelhardt, S., Böhm, M., Erdmann, E. and Lohse, M.J. 1996. Analysis of beta-adrenergic receptor mRNA levels in human ventricular biopsy specimens by quantitative polymerase chain reactions: Progressive reduction of beta1-adrenergic receptor mRNA in heart failure. *Journal of the American College of Cardiology.* **27**(1), pp.146-154.

Eschenhagen, T. 2008. β-adrenergic signaling in heart failure - adapt or die. *Nature Medicine.* **14**(5), pp.485-487.

Fabiato, A. and Fabiato, F. 1975. Contractions induced by a calcium-triggered release of calcium from the sarcoplasmic reticulum of single skinned cardiac cells. *Journal of Physiology.* **249**(3), pp.469-495.

Fan, D., Takawale, A., Lee, J. and Kassiri, Z. 2012. Cardiac fibroblasts, fibrosis and extracellular matrix remodeling in heart disease. *Fibrogenesis & Tissue Repair.* **5**, pp.15-15.

Fawcett, D.W. and McNutt, N.S. 1969. The Ultrastructure Of The Cat Myocardium. *I. Ventricular Papillary Muscle.* **42**(1), pp.1-45.

Feiner, E.C., Chung, P., Jasmin, J.F., Zhang, J., Whitaker-Menezes, D., Myers, V., Song, J., Feldman, E.W., Funakoshi, H., Degeorge Jr, B.R., Yelamarty, R.V., Koch, W.J., Lisanti, M.P., McTiernan, C.F., Cheung, J.Y., Bristow, M.R., Chan, T.O. and Feldman, A.M. 2011. Left Ventricular Dysfunction in Murine Models of Heart Failure and in Failing Human Heart is Associated With a Selective Decrease in the Expression of Caveolin-3. *Journal of Cardiac Failure.* **17**(3), pp.253-263.

Feldman, A.M., Weinberg, E.O., Ray, P.E. and Lorell, B.H. 1993. Selective changes in cardiac gene expression during compensated hypertrophy and the transition to cardiac decompensation in rats with chronic aortic banding. *Circulation Research.* **73**(1), pp.184-192.

Fillmore, N. and Lopaschuk, G.D. 2013. Targeting mitochondrial oxidative metabolism as an approach to treat heart failure. *Biochimica et Biophysica Acta (BBA) - Molecular Cell Research.* **1833**(4), pp.857-865.

Flesch, M., Ettelbrück, S., Rosenkranz, S., Maack, C., Cremers, B., Schlüter, K.-D., Zolk, O. and Böhm, M. 2001. Differential effects of carvedilol and metoprolol on isoprenaline-induced changes in β-adrenoceptor density and systolic function in rat cardiac myocytes. *Cardiovascular Research.* **49**(2), pp.371-380.

Floras, J.S. 2009. Sympathetic Nervous System Activation in Human Heart Failure: Clinical Implications of an Updated Model. *Journal of the American College of Cardiology.* **54**(5), pp.375-385.

Fowler, E.D. and 2016. *β1-adrenoceptor blockade treatment of right ventricular dysfunction caused by pulmonary hypertension*. thesis, University of Leeds.

Fowler, E.D., Benoist, D., Drinkhill, M.J., Stones, R., Helmes, M., Wüst, R.C.I., Stienen, G.J.M., Steele, D.S. and White, E. 2015. Decreased creatine kinase is linked to diastolic dysfunction in rats with right heart failure induced by pulmonary artery hypertension. *Journal of Molecular and Cellular Cardiology.* **86**, pp.1-8.

Fra, A.M., Williamson, E., Simons, K. and Parton, R.G. 1995. De novo formation of caveolae in lymphocytes by expression of VIP21-caveolin. *Proceedings of the National Academy of Sciences.* **92**(19), pp.8655-8659.

Franzini-Armstrong, C. 1975. Membrane particles and transmission at the triad. In: Moore, J.W. ed. *Membranes, Ions, and Impulses.* Boston, MA: Springer US, pp.141-154.

Freedman, N.J., Liggett, S.B., Drachman, D.E., Pei, G., Caron, M.G. and Lefkowitz, R.J. 1995. Phosphorylation and Desensitization of the Human -Adrenergic Receptor: Involvement Of G Protein-Coupled Receptor Kinases And Camp-Dependent Protein Kinase. *Journal of Biological Chemistry.* **270**(30), pp.17953-17961.

Fridolfsson, H.N. and Patel, H.H. 2013. Caveolin and caveolae in age associated cardiovascular disease. *Journal of Geriatric Cardiology : JGC.* **10**(1), pp.66-74.

Friedberg, M.K. and Redington, A.N. 2014. Right Versus Left Ventricular Failure. *Differences, Similarities, and Interactions.* **129**(9), pp.1033-1044.

Frohlich , E.D., Apstein , C., Chobanian , A.V., Devereux , R.B., Dustan , H.P., Dzau , V., Fauad-Tarazi , F., Horan , M.J., Marcus , M., Massie , B., Pfeffer , M.A., Re , R.N., Roccella , E.J., Savage , D. and Shub , C. 1992. The Heart in Hypertension. *New England Journal of Medicine.* **327**(14), pp.998-1008.

Fuchs, F. and Smith, S.H. 2001. Calcium, Cross-Bridges, and the Frank-Starling Relationship. *Physiology.* **16**(1), pp.5-10.

Fuhs, S.R. and Insel, P.A. 2011. Caveolin-3 Undergoes SUMOylation by the SUMO E3 Ligase PIASy: Sumoylation Affects G-Protein-Coupled Receptor Desensitization. *Journal of Biological Chemistry.* **286**(17), pp.14830-14841.

Fujii, J., Ueno, A., Kitano, K., Tanaka, S., Kadoma, M. and Tada, M. 1987. Complete complementary DNA-derived amino acid sequence of canine cardiac phospholamban. *Journal of Clinical Investigation.* **79**(1), pp.301-304.

Fujioka, Y., Komeda, M. and Matsuoka, S. 2000. Stoichiometry of Na^+-Ca^{2+} exchange in inside-out patches excised from guinea-pig ventricular myocytes. *The Journal of Physiology.* **523**(Pt 2), pp.339-351.

Galbiati, F., Engelman, J.A., Volonte, D., Zhang, X.L., Minetti, C., Li, M., Hou, H., Kneitz, B., Edelmann, W. and Lisanti, M.P. 2001. Caveolin-3 Null Mice Show a Loss of Caveolae, Changes in the Microdomain Distribution of the Dystrophin-Glycoprotein Complex, and T-tubule Abnormalities. *Journal of Biological Chemistry.* **276**(24), pp.21425-21433.

Gambin, Y., Ariotti, N., McMahon, K.-A., Bastiani, M., Sierecki, E., Kovtun, O., Polinkovsky, M.E., Magenau, A., Jung, W., Okano, S., Zhou, Y., Leneva, N., Mureev, S., Johnston, W., Gaus, K., Hancock, J.F., Collins, B.M., Alexandrov, K. and Parton, R.G. 2014. Single-molecule analysis reveals self assembly and nanoscale segregation of two distinct cavin subcomplexes on caveolae. *eLife.* **3**, pe01434.

García-Cardeña, G., Martasek, P., Masters, B.S.S., Skidd, P.M., Couet, J., Li, S., Lisanti, M.P. and Sessa, W.C. 1997. Dissecting the Interaction between Nitric Oxide Synthase (NOS) and Caveolin: Functional Significance Of The Nos Caveolin Binding Domainin Vivo. *Journal of Biological Chemistry.* **272**(41), pp.25437-25440.

Garg, V., Jiao, J. and Hu, K. 2009. Regulation of ATP-sensitive K^+ channels by caveolin-enriched microdomains in cardiac myocytes. *Cardiovascular Research.* **82**(1), pp.51-58.

Gauthier, C., Leblais, V., Kobzik, L., Trochu, J.N., Khandoudi, N., Bril, A., Balligand, J.L. and Le Marec, H. 1998. The negative inotropic effect of beta3-adrenoceptor stimulation is mediated by activation of a nitric oxide synthase pathway in human ventricle. *Journal of Clinical Investigation.* **102**(7), pp.1377-1384.

Gilbert, E.M., Abraham, W.T., Olsen, S., Hattler, B., White, M., Mealy, P., Larrabee, P. and Bristow, M.R. 1996. Comparative Hemodynamic, Left Ventricular Functional, and Antiadrenergic Effects of Chronic Treatment With Metoprolol Versus Carvedilol in the Failing Heart. *Circulation.* **94**(11), pp.2817-2825.

Goldman, Y.E. and Brenner, B. 1987. Special Topic: Molecular Mechanism of Muscle Contraction. *Annual Review of Physiology.* **49**(1), pp.629-636.

Goo, S., Joshi, P., Sands, G., Gerneke, D., Taberner, A., Dollie, Q., LeGrice, I. and Loiselle, D. 2009. Trabeculae carneae as models of the ventricular walls: implications for the delivery of oxygen. *The Journal of General Physiology.* **134**(4), pp.339-350.

Gordon, A.M., Homsher, E. and Regnier, M. 2000. Regulation of contraction in striated muscle. *Physiological Reviews.* **80**(2), pp.853-924.

Gorelik, J., Wright, P.T., Lyon, A.R. and Harding, S.E. 2013. Spatial control of βAR system in heart failure: the transverse tubule and beyond. *Cardiovascular Research.*

Grimm, M., Ling, H., Willeford, A., Pereira, L., Gray, C.B.B., Erickson, J.R., Sarma, S., Respress, J.L., Wehrens, X.H.T., Bers, D.M. and Brown, J.H. 2015. CaMKIIδ mediates β-adrenergic effects on RyR2 phosphorylation and SR Ca2 + leak and the pathophysiological response to chronic β-adrenergic stimulation. *Journal of Molecular and Cellular Cardiology.* **85**, pp.282-291.

Group, M.-H.S. 1999. Effect of metoprolol CR/XL in chronic heart failure: Metoprolol CR/XL Randomised Intervention Trial in-Congestive Heart Failure (MERIT-HF). *The Lancet.* **353**(9169), pp.2001-2007.

Grynkiewicz, G., Poenie, M. and Tsien, R.Y. 1985. A new generation of Ca2+ indicators with greatly improved fluorescence properties. *Journal of Biological Chemistry.* **260**(6), pp.3440-3450.

Guo, A., Zhang, C., Wei, S., Chen, B. and Song, L.-S. 2013. Emerging mechanisms of T-tubule remodelling in heart failure. *Cardiovascular Research.* **98**(2), pp.204-215.

Guo, T., Zhang, T., Mestril, R. and Bers, D.M. 2006. Ca^{2+}/Calmodulin-Dependent Protein Kinase II Phosphorylation of Ryanodine Receptor Does Affect Calcium Sparks in Mouse Ventricular Myocytes. *Circulation Research.* **99**(4), pp.398-406.

Gurtu, V. and Michelakis, E.D. 2015. Emerging Therapies and Future Directions in Pulmonary Arterial Hypertension. *Canadian Journal of Cardiology.* **31**(4), pp.489-501.

Gutierrez-Pajares, J.L., Iturrieta, J., Dulam, V., Wang, Y., Pavlides, S., Malacari, G., Lisanti, M.P. and Frank, P.G. 2015. Caveolin-3 Promotes a Vascular Smooth Muscle Contractile Phenotype. *Frontiers in Cardiovascular Medicine.* **2**(27).

Hagiwara, Y., Nishina, Y., Yorifuji, H. and Kikuchi, T. 2002. Immunolocalization of Caveolin-1 and Caveolin-3 in Monkey Skeletal, Cardiac and Uterine Smooth Muscles. *Cell Structure and Function.* **27**(5), pp.375-382.

Hall, D.D., Davare, M.A., Shi, M., Allen, M.L., Weisenhaus, M., McKnight, G.S. and Hell, J.W. 2007. Critical Role of cAMP-Dependent Protein Kinase Anchoring to the L-Type Calcium Channel Cav1.2 via A-Kinase Anchor Protein 150 in Neurons. *Biochemistry.* **46**(6), pp.1635-1646.

Hansen, C.G., Bright, N.A., Howard, G. and Nichols, B.J. 2009. SDPR induces membrane curvature and functions in the formation of caveolae. *Nature Cell Biology.* **11**(7), pp.807-814.

Hansen, C.G., Shvets, E., Howard, G., Riento, K. and Nichols, B.J. 2013. Deletion of cavin genes reveals tissue-specific mechanisms for morphogenesis of endothelial caveolae. *Nature Communications.* **4**, p1831.

Haque, M.Z., McIntosh, V.J., Abou Samra, A.B., Mohammad, R.M. and Lasley, R.D. 2016. Cholesterol Depletion Alters Cardiomyocyte Subcellular Signaling and Increases Contractility. *PLoS ONE.* **11**(7), pe0154151.

Hata, J.A., Williams, M.L. and Koch, W.J. 2004. Genetic manipulation of myocardial β-adrenergic receptor activation and desensitization. *Journal of Molecular and Cellular Cardiology.* **37**(1), pp.11-21.

Hayashi, T., Arimura, T., Ueda, K., Shibata, H., Hohda, S., Takahashi, M., Hori, H., Koga, Y., Oka, N., Imaizumi, T., Yasunami, M. and Kimura, A. 2004. Identification and functional analysis of a caveolin-3 mutation associated with familial hypertrophic cardiomyopathy. *Biochemical and Biophysical Research Communications.* **313**(1), pp.178-184.

Hayer, A., Stoeber, M., Bissig, C. and Helenius, A. 2010. Biogenesis of caveolae: stepwise assembly of large caveolin and cavin complexes. *Traffic.* **11**(3), pp.361-382.

Head, B.P., Patel, H.H., Roth, D.M., Lai, N.C., Niesman, I.R., Farquhar, M.G. and Insel, P.A. 2005. G-protein-coupled Receptor Signaling Components Localize in Both Sarcolemmal and Intracellular Caveolin-3-associated Microdomains in Adult Cardiac Myocytes. *Journal of Biological Chemistry.* **280**(35), pp.31036-31044.

Head, B.P., Patel, H.H., Roth, D.M., Murray, F., Swaney, J.S., Niesman, I.R., Farquhar, M.G. and Insel, P.A. 2006. Microtubules and Actin Microfilaments Regulate Lipid Raft/Caveolae Localization of Adenylyl Cyclase Signaling Components. *Journal of Biological Chemistry.* **281**(36), pp.26391-26399.

Heerdt, P.M., Holmes, J.W., Cai, B., Barbone, A., Madigan, J.D., Reiken, S., Lee, D.L., Oz, M.C., Marks, A.R. and Burkhoff, D. 2000. Chronic Unloading by Left Ventricular Assist Device Reverses Contractile Dysfunction and Alters Gene Expression in End-Stage Heart Failure. *Circulation.* **102**(22), pp.2713-2719.

Heilbrunn, S.M., Shah, P., Bristow, M.R., Valantine, H.A., Ginsburg, R. and Fowler, M.B. 1989. Increased beta-receptor density and improved hemodynamic response to catecholamine stimulation during long-term metoprolol therapy in heart failure from dilated cardiomyopathy. *Circulation.* **79**(3), pp.483-490.

Herzig, S., Raemy, E., Montessuit, S., Veuthey, J.-L., Zamboni, N., Westermann, B., Kunji, E.R.S. and Martinou, J.-C. 2012. Identification and Functional Expression of the Mitochondrial Pyruvate Carrier. *Science.* **337**(6090), pp.93-96.

Hibbs, R.G., Burch, G.E. and Phillips, J.H. 1958. The fine structure of the small blood vessels of normal human dermis and subcutis. *American Heart Journal.* **56**(5), pp.662-670.

Hill, M.M., Bastiani, M., Luetterforst, R., Kirkham, M., Kirkham, A., Nixon, S.J., Walser, P., Abankwa, D., Oorschot, V.M.J., Martin, S., Hancock, J.F. and Parton, R.G. 2008. PTRF-Cavin, a Conserved Cytoplasmic Protein Required for Caveola Formation and Function. *Cell.* **132**(1), pp.113-124.

Hill, M.M., Daud, N.H., Aung, C.S., Loo, D., Martin, S., Murphy, S., Black, D.M., Barry, R., Simpson, F., Liu, L., Pilch, P.F., Hancock, J.F., Parat, M.-O. and Parton, R.G. 2012. Co-Regulation of Cell Polarization and Migration by Caveolar Proteins PTRF/Cavin-1 and Caveolin-1. *PLoS ONE.* **7**(8), pe43041.

Hjalmarson, Å., Goldstein, S., Fagerberg, B. and et al. 2000. Effects of controlled-release metoprolol on total mortality, hospitalizations, and well-being in patients with heart failure: The metoprolol cr/xl randomized intervention trial in congestive heart failure (merit-hf). *JAMA.* **283**(10), pp.1295-1302.

Hong, T. and Shaw, R.M. 2017. Cardiac T-Tubule Microanatomy and Function. *Physiological Reviews.* **97**(1), pp.227-252.

Hopkins, W.E., Ochoa, L.L., Richardson, G.W. and Trulock, E.P. 1996. Comparison of the hemodynamics and survival of adults with severe primary pulmonary hypertension or Eisenmenger syndrome. *The Journal of heart and lung transplantation: the official*

publication of the International Society for Heart Transplantation. **15**(1 Pt 1), pp.100-105.

Horikawa, Y.T., Panneerselvam, M., Kawaraguchi, Y., Tsutsumi, Y.M., Ali, S.S., Balijepalli, R.C., Murray, F., Head, B.P., Niesman, I.R., Rieg, T., Vallon, V., Insel, P.A., Patel, H.H. and Roth, D.M. 2011. Cardiac-Specific Overexpression of Caveolin-3 Attenuates Cardiac Hypertrophy and Increases Natriuretic Peptide Expression and Signaling. *Journal of the American College of Cardiology.* **57**(22), pp.2273-2283.

Houser, S.R., Margulies, K.B., Murphy, A.M., Spinale, F.G., Francis, G.S., Prabhu, S.D., Rockman, H.A., Kass, D.A., Molkentin, J.D., Sussman, M.A. and Koch, W.J. 2012. Animal Models of Heart Failure: A Scientific Statement From the American Heart Association. *Circulation Research.* **111**(1), pp.131-150.

Humbert, M., Sitbon, O., Chaouat, A., Bertocchi, M., Habib, G., Gressin, V., Yaïci, A., Weitzenblum, E., Cordier, J.-F., Chabot, F., Dromer, C., Pison, C., Reynaud-Gaubert, M., Haloun, A., Laurent, M., Hachulla, E., Cottin, V., Degano, B., Jaïs, X., Montani, D., Souza, R. and Simonneau, G. 2010. Survival in Patients With Idiopathic, Familial, and Anorexigen-Associated Pulmonary Arterial Hypertension in the Modern Management Era. *Circulation.* **122**(2), pp.156-163.

Hunter, P.J., McCulloch, A.D. and ter Keurs, H.E.D.J. 1998. Modelling the mechanical properties of cardiac muscle. *Progress in Biophysics and Molecular Biology.* **69**(2–3), pp.289-331.

Huxley, A.F. and Simmons, R.M. 1971. Proposed Mechanism of Force Generation in Striated Muscle. *Nature.* **233**(5321), pp.533-538.

Huxtable, R.J. 1990. Activation and pulmonary toxicity of pyrrolizidine alkaloids. *Pharmacology & Therapeutics.* **47**(3), pp.371-389.

Hwang, H.S., Nitu, F.R., Yang, Y., Walweel, K., Pereira, L., Johnson, C.N., Faggioni, M., Chazin, W.J., Laver, D., George, A.L., Cornea, R.L., Bers, D.M. and Knollmann, B.C. 2014. Divergent Regulation of Ryanodine Receptor 2 Calcium Release Channels by Arrhythmogenic Human Calmodulin Missense Mutants: Novelty and Significance. *Circulation Research.* **114**(7), pp.1114-1124.

Iaccarino, G., Tomhave, E.D., Lefkowitz, R.J. and Koch, W.J. 1998. Reciprocal In Vivo Regulation of Myocardial G Protein–Coupled Receptor Kinase Expression by β-Adrenergic Receptor Stimulation and Blockade. *Circulation.* **98**(17), pp.1783-1789.

Ikonnikov, G. and Yelle, D. 2016. *Physiology Of Cardiac Conduction And Contractility.* [Online]. Available from: http://www.pathophys.org/physiology-of-cardiac-conduction-and-contractility/

Ilangumaran, S. and Hoessli, D.C. 1998. Effects of cholesterol depletion by cyclodextrin on the sphingolipid microdomains of the plasma membrane. *Biochemical Journal.* **335**(Pt 2), pp.433-440.

Insel, P.A., Head, B.P., Patel, H.H., Roth, D.M., Bundey, R.A. and Swaney, J.S. 2005. Compartmentation of G-protein-coupled receptors and their signalling components in lipid rafts and caveolae. *Biochemical Society Transactions.* **33**, pp.1131-1134.

Ishikawa, S., Honda, M., Yamada, S., Morioka, S. and Moriyama, K. 1991. Biventricular down-regulation of beta-adrenergic receptors in right ventricular hypertrophy induced by monocrotaline. *Japanese circulation journal.* **55**(11), pp.1077-1085.

Isidori, A.M., Cornacchione, M., Barbagallo, F., Di Grazia, A., Barrios, F., Fassina, L., Monaco, L., Giannetta, E., Gianfrilli, D., Garofalo, S., Zhang, X., Chen, X., Xiang, Y.K., Lenzi, A., Pellegrini, M. and Naro, F. 2015. Inhibition of type 5 phosphodiesterase counteracts β2-adrenergic signalling in beating cardiomyocytes. *Cardiovascular Research.* **106**(3), pp.408-420.

Jaber, M., Koch, W.J., Rockman, H., Smith, B., Bond, R.A., Sulik, K.K., Ross, J., Lefkowitz, R.J., Caron, M.G. and Giros, B. 1996. Essential role of β-adrenergic receptor kinase 1 in

cardiac development and function. *Proceedings of the National Academy of Sciences.* **93**(23), pp.12974-12979.

Jalil, J.E., Doering, C.W., Janicki, J.S., Pick, R., Shroff, S.G. and Weber, K.T. 1989. Fibrillar collagen and myocardial stiffness in the intact hypertrophied rat left ventricle. *Circulation Research.* **64**(6), pp.1041-1050.

Jansa, P., Mason, S.W., Hoffmann-Rohrer, U. and Grummt, I. 1998. Cloning and functional characterization of PTRF, a novel protein which induces dissociation of paused ternary transcription complexes. *The EMBO Journal.* **17**(10), pp.2855-2864.

Jasmin, J.-F., Mercier, I., Dupuis, J., Tanowitz, H.B. and Lisanti, M.P. 2006. Short-Term Administration of a Cell-Permeable Caveolin-1 Peptide Prevents the Development of Monocrotaline-Induced Pulmonary Hypertension and Right Ventricular Hypertrophy. *Circulation.* **114**(9), pp.912-920.

Jayasinghe, I.D., Cannell, M.B. and Soeller, C. 2009. Organization of Ryanodine Receptors, Transverse Tubules, and Sodium-Calcium Exchanger in Rat Myocytes. *Biophysical Journal.* **97**(10), pp.2664-2673.

Jayasinghe, I.D., Clowsley, A.H., Munro, M., Hou, Y., Crossman, D.J. and Soeller, C. 2015. Revealing T-Tubules in Striated Muscle with New Optical Super-Resolution Microscopy Techniquess. *European journal of translational myology.* **25**(1).

Kasahara, Y., Kiyatake, K., Tatsumi, K., Sugito, K., Kakusaka, I., Yamagata, S.-i., Ohmori, S., Kitada, M. and Kuriyama, T. 1997. Bioactivation of Monocrotaline by P-450 3A in Rat Liver. *Journal of Cardiovascular Pharmacology.* **30**(1), pp.124-129.

Kassner, A., Toischer, K., Bohms, B., Kolkhof, P., Abraham, G., Hasenfuβ, G., Morshuis, M., Schulte Eistrup, S., El-Banayosy, A., Gummert, J. and Milting, H. 2012. Regulation of cyclic adenosine monophosphate release by selective β2-adrenergic receptor stimulation in human terminal failing myocardium before and after ventricular assist device support. *The Journal of Heart and Lung Transplantation.* **31**(10), pp.1127-1135.

Kaumann, A., Bartel, S., Molenaar, P., Sanders, L., Burrell, K., Vetter, D., Hempel, P., Karczewski, P. and Krause, E.-G. 1999. Activation of β_2-Adrenergic Receptors Hastens Relaxation and Mediates Phosphorylation of Phospholamban, Troponin I, and C-Protein in Ventricular Myocardium From Patients With Terminal Heart Failure. *Circulation.* **99**(1), pp.65-72.

Kaur, S., Kong, C.H.T., Cannell, M.B. and Ward, M.-L. 2016. Depotentiation of intact rat cardiac muscle unmasks an Epac-dependent increase in myofilament Ca2+ sensitivity. *Clinical and Experimental Pharmacology and Physiology.* **43**(1), pp.88-94.

Keen, E.N. 1955. The postnatal development of the human cardiac ventricles. *Journal of Anatomy.* **89**(Pt 4), pp.484-502.

Kikuchi, T., Oka, N., Koga, A., Miyazaki, H., Ohmura, H. and Imaizumi, T. 2005. Behavior of Caveolae and Caveolin-3 During the Development of Myocyte Hypertrophy. *Journal of Cardiovascular Pharmacology.* **45**(3), pp.204-210.

Kim, J.-H., Peng, D., Schlebach, J.P., Hadziselimovic, A. and Sanders, C.R. 2014. Modest Effects of Lipid Modifications on the Structure of Caveolin-3. *Biochemistry.* **53**(27), pp.4320-4322.

Knoebel, S.B. and Weber, K.T. 1989. ACC Anniversary SeminarCardiac interstitium in health and disease: The fibrillar collagen network. *Journal of the American College of Cardiology.* **13**(7), pp.1637-1652.

Kobayashi, T. and Solaro, R.J. 2005. Calcium, think filaments, and the integrative biology of cardiac contractility. *Annual Review of Physiology.* **67**(1), pp.39-67.

Kögler, H., Hartmann, O., Leineweber, K., Nguyen van, P., Schott, P., Brodde, O.-E. and Hasenfuss, G. 2003. Mechanical Load-Dependent Regulation of Gene Expression in Monocrotaline-Induced Right Ventricular Hypertrophy in the Rat. *Circulation Research.* **93**(3), pp.230-237.

Koitabashi, N. and Kass, D.A. 2012. Reverse remodeling in heart failure - mechanisms and therapeutic opportunities. *Nat Rev Cardiol.* **9**(3), pp.147-157.

Komarova, Y. and Malik, A.B. 2010. Regulation of endothelial permeability via paracellular and transcellular transport pathways. *Annual Review of Physiology.* **72**, pp.463-493.

Korecky, B. and Rakusan, K. 1978. Normal and hypertrophic growth of the rat heart: changes in cell dimensions and number. *American Journal of Physiology - Heart and Circulatory Physiology.* **234**(2), pp.H123-H128.

Kostin, S., Scholz, D., Shimada, T., Maeno, Y., Mollnau, H., Hein, S. and Schaper, J. 1998. The internal and external protein scaffold of the T-tubular system in cardiomyocytes. *Cell and Tissue Research.* **294**(3), pp.449-460.

Kovtun, O., Tillu, V.A., Ariotti, N., Parton, R.G. and Collins, B.M. 2015. Cavin family proteins and the assembly of caveolae. *Journal of Cell Science.* **128**(7), pp.1269-1278.

Kozera, L., White, E. and Calaghan, S. 2009. Caveolae Act as Membrane Reserves Which Limit Mechanosensitive $I_{Cl,swell}$ Channel Activation during Swelling in the Rat Ventricular Myocyte. *PLoS ONE.* **4**(12), pe8312.

Kramer, T.C. 1942. The partitioning of the truncus and conus and the formation of the membranous portion of the interventricular septum in the human heart. *American Journal of Anatomy.* **71**(3), pp.343-370.

Kritzer, M.D., Li, J., Dodge-Kafka, K. and Kapiloff, M.S. 2012. AKAPs: The architectural underpinnings of local cAMP signaling. *Journal of Molecular and Cellular Cardiology.* **52**(2), pp.351-358.

Kuschel, M., Zhou, Y.-Y., Cheng, H., Zhang, S.-J., Chen, Y., Lakatta, E.G. and Xiao, R.-P. 1999a. G_i Protein-mediated Functional Compartmentalization of Cardiac β_2-Adrenergic Signaling. *Journal of Biological Chemistry.* **274**(31), pp.22048-22052.

Kuschel, M., Zhou, Y.-Y., Spurgeon, H.A., Bartel, S., Karczewski, P., Zhang, S.-J., Krause, E.-G., Lakatta, E.G. and Xiao, R.-P. 1999b. β_2-Adrenergic cAMP Signaling Is Uncoupled From Phosphorylation of Cytoplasmic Proteins in Canine Heart. *Circulation.* **99**(18), pp.2458-2465.

Larsen, W.J., Sherman, L.S., Potter, S.S. and Scott., W.J. 2001. *Human embryology.* 3rd ed. ed. New York ; Edinburgh : Churchill Livingstone, c2001.: Churchill Livingstone.

Lattion, A.-L., Abuin, L., Nenniger-Tosato, M. and Cotecchia, S. 1999. Constitutively active mutants of the β1-adrenergic receptor. *FEBS Letters.* **457**(3), pp.302-306.

Leblais, V., Delannoy, E., Fresquet, F., Bégueret, H., Bellance, N., Banquet, S., Allières, C., Leroux, L., Desgranges, C., Gadeau, A. and Muller, B. 2008. β-adrenergic relaxation in pulmonary arteries: preservation of the endothelial nitric oxide-dependent β2 component in pulmonary hypertension. *Cardiovascular Research.* **77**(1), pp.202-210.

Lee, E., Marcucci, M., Daniell, L., Pypaert, M., Weisz, O.A., Ochoa, G.-C., Farsad, K., Wenk, M.R. and De Camilli, P. 2002. Amphiphysin 2 (Bin1) and T-Tubule Biogenesis in Muscle. *Science.* **297**(5584), pp.1193-1196.

Lee, J.K., Kodama, I., Honjo, H., Anno, T., Kamiya, K. and Toyama, J. 1997. *Stage-dependent changes in membrane currents in rats with monocrotaline-induced right ventricular hypertrophy.*

Lefkowitz, R.J. 1998. G protein-coupled receptors. III. New roles for receptor kinases and beta-arrestins in receptor signaling and desensitization. *Journal of Biological Chemistry.* **273**(30), pp.18677-18680.

Lehrer, S.S., Golitsina, N.L. and Geeves, M.A. 1997. Actin-tropomyosin activation of myosin subfragment 1 ATPase and thin filament cooperativity. The role of tropomyosin flexibility and end-to-end interactions. *Biochemistry.* **36**(44), pp.13449-13454.

Leineweber, K., Seyfarth, T., Abraham, G., Gerbershagen, H.-P., Heinroth-Hoffmann, I., Pönicke, K. and Brodde, O.-E. 2003. Cardiac β-Adrenoceptor Changes in Monocrotaline-Treated

Rats: Differences Between Membrane Preparations From Whole Ventricles and Isolated Ventricular Cardiomyocytes. *Journal of Cardiovascular Pharmacology.* **41**(3), pp.333-342.

Leroy, J., Abi-Gerges, A., Nikolaev, V.O., Richter, W., Lechêne, P., Mazet, J.-L., Conti, M., Fischmeister, R. and Vandecasteele, G. 2008. Spatiotemporal Dynamics of β-Adrenergic cAMP Signals and L-Type Ca^{2+} Channel Regulation in Adult Rat Ventricular Myocytes. *Role of Phosphodiesterases.* **102**(9), pp.1091-1100.

Levin, K.R. and Page, E. 1980. Quantitative studies on plasmalemmal folds and caveolae of rabbit ventricular myocardial cells. *Circulation Research.* **46**(2), pp.244-255.

Li, W., Wang, K., Lin, G., Peng, Y. and Zheng, J. 2016. Lysine Adduction by Reactive Metabolite(s) of Monocrotaline. *Chemical Research in Toxicology.* **29**(3), pp.333-341.

LiDCO Group, p. *Normal Hemodynamic Parameters.* [Online]. Available from: http://www.lidco.com/clinical/hemodynamic.php

Lisanti, M.P., Scherer, P.E., Vidugiriene, J., Tang, Z., Hermanowski-Vosatka, A., Tu, Y.H., Cook, R.F. and Sargiacomo, M. 1994. Characterization of caveolin-rich membrane domains isolated from an endothelial-rich source: implications for human disease. *Journal of Cell Biology.* **126**(1), pp.111-126.

Litwin, S.E., Katz, S.E., Weinberg, E.O., Lorell, B.H., Aurigemma, G.P. and Douglas, P.S. 1995. Serial Echocardiographic-Doppler Assessment of Left Ventricular Geometry and Function in Rats With Pressure-Overload Hypertrophy: Chronic Angiotensin-Converting Enzyme Inhibition Attenuates the Transition to Heart Failure. *Circulation.* **91**(10), pp.2642-2654.

Liu, L., Brown, D., McKee, M., LeBrasseur, N.K., Yang, D., Albrecht, K.H., Ravid, K. and Pilch, P.F. 2008. Deletion of Cavin/PTRF Causes Global Loss of Caveolae, Dyslipidemia, and Glucose Intolerance. *Cell Metabolism.* **8**(4), pp.310-317.

Liu, L., Mohammadi, K., Aynafshar, B., Wang, H., Li, D., Liu, J., Ivanov, A.V., Xie, Z. and Askari, A. 2003. Role of caveolae in signal-transducing function of cardiac Na^+/K^+-ATPase. *American Journal of Physiology - Cell Physiology.* **284**(6), pp.C1550-C1560.

Liu, L. and Pilch, P.F. 2008. A Critical Role of Cavin (Polymerase I and Transcript Release Factor) in Caveolae Formation and Organization. *Journal of Biological Chemistry.* **283**(7), pp.4314-4322.

Liu, L. and Pilch, P.F. 2016. PTRF/Cavin-1 promotes efficient ribosomal RNA transcription in response to metabolic challenges. *eLife.* **5**, pe17508.

Liu, R., Wang, D., Shi, Q., Fu, Q., Hizon, S. and Xiang, Y.K. 2012. Palmitoylation Regulates Intracellular Trafficking of β_2 Adrenergic Receptor/Arrestin/Phosphodiesterase 4D Complexes in Cardiomyocytes. *PLoS ONE.* **7**(8), pe42658.

Lohse, M.J., Benovic, J.L., Codina, J., Caron, M.G. and Lefkowitz, R.J. 1990. beta-Arrestin: a protein that regulates beta-adrenergic receptor function. *Science.* **248**(4962), pp.1547-1550.

Lopaschuk, G.D., Ussher, J.R., Folmes, C.D., Jaswal, J.S. and Stanley, W.C. 2010. Myocardial fatty acid metabolism in health and disease. *Physiol Rev.* **90**(1), pp.207-258.

Lowes, B.D., Minobe, W., Abraham, W.T., Rizeq, M.N., Bohlmeyer, T.J., Quaife, R.A., Roden, R.L., Dutcher, D.L., Robertson, A.D., Voelkel, N.F., Badesch, D.B., Groves, B.M., Gilbert, E.M. and Bristow, M.R. 1997. Changes in gene expression in the intact human heart. Downregulation of alpha-myosin heavy chain in hypertrophied, failing ventricular myocardium. *The Journal of Clinical Investigation.* **100**(9), pp.2315-2324.

Ludwig, A., Howard, G., Mendoza-Topaz, C., Deerinck, T., Mackey, M., Sandin, S., Ellisman, M.H. and Nichols, B.J. 2013. Molecular Composition and Ultrastructure of the Caveolar Coat Complex. *PLoS Biology.* **11**(8), pe1001640.

Ludwig, A., Nichols, B.J. and Sandin, S. 2016. Architecture of the caveolar coat complex. *Journal of Cell Science.* **129**(16), pp.3077-3083.

Luo, W., Grupp, I.L., Harrer, J., Ponniah, S., Grupp, G., Duffy, J.J., Doetschman, T. and Kranias, E.G. 1994. Targeted ablation of the phospholamban gene is associated with markedly enhanced myocardial contractility and loss of beta-agonist stimulation. *Circulation Research.* **75**(3), pp.401-409.

Lygate, C. 2006. Surgical models of hypertrophy and heart failure: Myocardial infarction and transverse aortic constriction. *Drug Discovery Today: Disease Models.* **3**(3), pp.283-290.

Maack, C., Cremers, B., Flesch, M., Höper, A., Südkamp, M. and Böhm, M. 2000. Different intrinsic activities of bucindolol, carvedilol and metoprolol in human failing myocardium. *British Journal of Pharmacology.* **130**(5), pp.1131-1139.

Macdonald, J.L. and Pike, L.J. 2005. A simplified method for the preparation of detergent-free lipid rafts. *Journal of Lipid Research.* **46**(5), pp.1061-1067.

MacDougall, D.A., Agarwal, S.R., Stopford, E.A., Chu, H., Collins, J.A., Longster, A.L., Colyer, J., Harvey, R.D. and Calaghan, S. 2012. Caveolae compartmentalise β2-adrenoceptor signals by curtailing cAMP production and maintaining phosphatase activity in the sarcoplasmic reticulum of the adult ventricular myocyte. *Journal of Molecular and Cellular Cardiology.* **52**(2), pp.388-400.

MacDougall, D.A. and Calaghan, S. 2013. A novel approach to the Langendorff technique: preparation of isolated cardiomyocytes and myocardial samples from the same rat heart. *Experimental Physiology.* **98**(8), pp.1295-1300.

Macdougall, L.K., Jones, L.R. and Cohen, P. 1991. Identification of the major protein phosphatases in mammalian cardiac muscle which dephosphorylate phospholamban. *European Journal of Biochemistry.* **196**(3), pp.725-734.

Mackenzie, R.J., Lawless, C., Holman, S.W., Lanthaler, K., Beynon, R.J., Grant, C.M., Hubbard, S.J. and Eyers, C.E. 2016. Absolute protein quantification of the yeast chaperome under conditions of heat shock. *Proteomics.* **16**(15-16), pp.2128-2140.

MacLennan, D.H. 1970. Purification and Properties of an Adenosine Triphosphatase from Sarcoplasmic Reticulum. *Journal of Biological Chemistry.* **245**(17), pp.4508-4518.

MacLennan, D.H. and Kranias, E.G. 2003. Phospholamban: a crucial regulator of cardiac contractility. *Nature Reviews of Molecular and Cellular Biology.* **4**(7), pp.566-577.

MacNee, W. 1994. Pathophysiology of cor pulmonale in chronic obstructive pulmonary disease. Part One. *American Journal of Respiratory and Critical Care Medicine.* **150**(3), pp.833-852.

Mak, S., Witte, K.K., Al-Hesayen, A., Granton, J.J. and Parker, J.D. 2012. Cardiac sympathetic activation in patients with pulmonary arterial hypertension. *American Journal of Physiology - Regulatory, Integrative and Comparative Physiology.* **302**(10), pp.R1153-R1157.

Makarewich, C.A., Correll, R.N., Gao, H., Zhang, H., Yang, B., Berretta, R.M., Rizzo, V., Molkentin, J.D. and Houser, S.R. 2012. A Caveolae Targeted L-type Ca^{2+} Channel Antagonist Inhibits Hypertrophic Signaling Without Reducing Cardiac Contractility. *Circulation Research.* **110**(5), pp.669-674.

Malenfant, S. and Perros, F. 2016. β-blockers in pulmonary arterial hypertension: generation might matter. *European Respiratory Journal.* **47**(2), pp.682-684.

Maley, F., Trimble, R.B., Tarentino, A.L. and Plummer, T.H. 1989. Characterization of glycoproteins and their associated oligosaccharides through the use of endoglycosidases. *Analytical Biochemistry.* **180**(2), pp.195-204.

Markandeya, Y.S., Phelan, L.J., Woon, M.T., Keefe, A.M., Reynolds, C.R., August, B.K., Hacker, T.A., Roth, D.M., Patel, H.H. and Balijepalli, R.C. 2015. Caveolin-3 Overexpression Attenuates Cardiac Hypertrophy via Inhibition of T-type Ca^{2+} Current Modulated by

Protein Kinase Cα in Cardiomyocytes. *Journal of Biological Chemistry.* **290**(36), pp.22085-22100.

Marx, S.O., Reiken, S., Hisamatsu, Y., Jayaraman, T., Burkhoff, D., Rosemblit, N. and Marks, A.R. 2000. PKA phosphorylation dissociates FKBP12. 6 from the calcium release channel (ryanodine receptor): defective regulation in failing hearts. *Cell.* **101**(4), pp.365-376.

Marzo, K.P., Frey, M.J., Wilson, J.R., Liang, B.T., Manning, D.R., Lanoce, V. and Molinoff, P.B. 1991. Beta-adrenergic receptor-G protein-adenylate cyclase complex in experimental canine congestive heart failure produced by rapid ventricular pacing. *Circulation Research.* **69**(6), pp.1546-1556.

McMahon, K.A., Zajicek, H., Li, W.P., Peyton, M.J., Minna, J.D., Hernandez, V.J., Luby-Phelps, K. and Anderson, R.G.W. 2009. SRBC/cavin-3 is a caveolin adapter protein that regulates caveolae function. *The EMBO Journal.* **28**(8), pp.1001-1015.

McMartin, L. and Summers, R.J. 1999. Functional analysis of desensitization of the β-adrenoceptor signalling pathway in rat cardiac tissues following chronic isoprenaline infusion. *British Journal of Pharmacology.* **127**(4), pp.1012-1020.

McMurray, J.J.V., Adamopoulos, S., Anker, S.D., Auricchio, A., Böhm, M., Dickstein, K., Falk, V., Filippatos, G., Fonseca, C., Gomez-Sanchez, M.A., Jaarsma, T., Køber, L., Lip, G.Y.H., Maggioni, A.P., Parkhomenko, A., Pieske, B.M., Popescu, B.A., Rønnevik, P.K., Rutten, F.H., Schwitter, J., Seferovic, P., Stepinska, J., Trindade, P.T., Voors, A.A., Zannad, F., Zeiher, A., Bax, J.J., Baumgartner, H., Ceconi, C., Dean, V., Deaton, C., Fagard, R., Funck-Brentano, C., Hasdai, D., Hoes, A., Kirchhof, P., Knuuti, J., Kolh, P., McDonagh, T., Moulin, C., Popescu, B.A., Reiner, Ž., Sechtem, U., Sirnes, P.A., Tendera, M., Torbicki, A., Vahanian, A., Windecker, S., McDonagh, T., Sechtem, U., Bonet, L.A., Avraamides, P., Ben Lamin, H.A., Brignole, M., Coca, A., Cowburn, P., Dargie, H., Elliott, P., Flachskampf, F.A., Guida, G.F., Hardman, S., Iung, B., Merkely, B., Mueller, C., Nanas, J.N., Nielsen, O.W., Ørn, S., Parissis, J.T. and Ponikowski, P. 2012. ESC Guidelines for the diagnosis and treatment of acute and chronic heart failure 2012. *The Task Force for the Diagnosis and Treatment of Acute and Chronic Heart Failure 2012 of the European Society of Cardiology. Developed in collaboration with the Heart Failure Association (HFA) of the ESC.* **33**(14), pp.1787-1847.

Meder, D. and Simons, K. 2006. Lipid Rafts, Caveolae, and Membrane Traffic. *Lipid Rafts and Caveolae.* Wiley-VCH Verlag GmbH & Co. KGaA, pp.1-23.

Messer, A.E., Jacques, A.M. and Marston, S.B. 2007. Troponin phosphorylation and regulatory function in human heart muscle: Dephosphorylation of Ser23/24 on troponin I could account for the contractile defect in end-stage heart failure. *Journal of Molecular and Cellular Cardiology.* **42**(1), pp.247-259.

Michel, J.B., Salzmann, J.L., Ossondo Nlom, M., Bruneval, P., Barres, D. and Camilleri, J.P. 1986. Morphometric analysis of collagen network and plasma perfused capillary bed in the myocardium of rats during evolution of cardiac hypertrophy. *Basic Res Cardiol.* **81**(2), pp.142-154.

Mika, D., Bobin, P., Pomérance, M., Lechêne, P., Westenbroek, R.E., Catterall, W.A., Vandecasteele, G., Leroy, J. and Fischmeister, R. 2013. Differential regulation of cardiac excitation–contraction coupling by cAMP phosphodiesterase subtypes. *Cardiovascular Research.* **100**(2), pp.336-346.

Miura, M., Hirose, M., Endoh, H., Wakayama, Y., Sugai, Y., Nakano, M., Fukuda, K., Shindoh, C., Shirato, K. and Shimokawa, H. 2011. Acceleration of Ca^{2+} Waves in Monocrotaline-Induced Right Ventricular Hypertrophy in the Rat. *Circulation Journal.* **75**(6), pp.1343-1349.

Miyamoto, M.I., del Monte, F., Schmidt, U., DiSalvo, T.S., Kang, Z.B., Matsui, T., Guerrero, J.L., Gwathmey, J.K., Rosenzweig, A. and Hajjar, R.J. 2000. Adenoviral gene transfer of

SERCA2a improves left-ventricular function in aortic-banded rats in transition to heart failure. *Proceedings of the National Academy of Sciences.* **97**(2), pp.793-798.

Mohamed, B.A., Asif, A.R., Schnelle, M., Qasim, M., Khadjeh, S., Lbik, D., Schott, P., Hasenfuss, G. and Toischer, K. 2016. Proteomic analysis of short-term preload-induced eccentric cardiac hypertrophy. *Journal of Translational Medicine.* **14**(1), p149.

Molina, C.E., Johnson, D.M., Mehel, H., Spätjens, R.L.H.M.G., Mika, D., Algalarrondo, V., Slimane, Z.H., Lechêne, P., Abi-Gerges, N., van der Linde, H.J., Leroy, J., Volders, P.G.A., Fischmeister, R. and Vandecasteele, G. 2014. Interventricular Differences in β-Adrenergic Responses in the Canine Heart: Role of Phosphodiesterases. *Journal of the American Heart Association.* **3**(3).

Monier, S., Dietzen, D.J., Hastings, W.R., Lublin, D.M. and Kurzchalia, T.V. 1996. Oligomerization of VIP21-caveolin in vitro is stabilized by long chain fatty acylation or cholesterol. *FEBS Letters.* **388**(2-3), pp.143-149.

Monier, S., Parton, R.G., Vogel, F., Behlke, J., Henske, A. and Kurzchalia, T.V. 1995. VIP21-caveolin, a membrane protein constituent of the caveolar coat, oligomerizes in vivo and in vitro. *Mol Biol Cell.* **6**(7), pp.911-927.

Moss, R.L. 2016. Cardiac myosin-binding protein C: A protein once at loose ends finds its regulatory groove. *Proceedings of the National Academy of Sciences.* **113**(12), pp.3133-3135.

Mozaffarian, D., Benjamin, E.J., Go, A.S., Arnett, D.K., Blaha, M.J., Cushman, M., Das, S.R., de Ferranti, S., Després, J.-P., Fullerton, H.J., Howard, V.J., Huffman, M.D., Isasi, C.R., Jiménez, M.C., Judd, S.E., Kissela, B.M., Lichtman, J.H., Lisabeth, L.D., Liu, S., Mackey, R.H., Magid, D.J., McGuire, D.K., Mohler, E.R., Moy, C.S., Muntner, P., Mussolino, M.E., Nasir, K., Neumar, R.W., Nichol, G., Palaniappan, L., Pandey, D.K., Reeves, M.J., Rodriguez, C.J., Rosamond, W., Sorlie, P.D., Stein, J., Towfighi, A., Turan, T.N., Virani, S.S., Woo, D., Yeh, R.W. and Turner, M.B. 2016. Heart Disease and Stroke Statistics—2016 Update. *A Report From the American Heart Association.* **133**(4), pp.e38-e360.

Murata, T., Lin, M.I., Huang, Y., Yu, J., Bauer, P.M., Giordano, F.J. and Sessa, W.C. 2007. Reexpression of caveolin-1 in endothelium rescues the vascular, cardiac, and pulmonary defects in global caveolin-1 knockout mice. *The Journal of Experimental Medicine.* **204**(10), pp.2373-2382.

Nagaya, N., Nishikimi, T., Uematsu, M., Satoh, T., Kyotani, S., Sakamaki, F., Kakishita, M., Fukushima, K., Okano, Y., Nakanishi, N., Miyatake, K. and Kangawa, K. 2000. Plasma Brain Natriuretic Peptide as a Prognostic Indicator in Patients With Primary Pulmonary Hypertension. *Circulation.* **102**(8), pp.865-870.

Naito, D., Ogata, T., Hamaoka, T., Nakanishi, N., Miyagawa, K., Maruyama, N., Kasahara, T., Taniguchi, T., Nishi, M., Matoba, S. and Ueyama, T. 2015. The coiled-coil domain of MURC/cavin-4 is involved in membrane trafficking of caveolin-3 in cardiomyocytes. *American Journal of Physiology - Heart and Circulatory Physiology.* **309**(12), pp.H2127-H2136.

Napp, A., Brixius, K., Pott, C., Ziskoven, C., Boelck, B., Mehlhorn, U., Schwinger, R.H.G. and Bloch, W. 2009. Effects of the β3-Adrenergic Agonist BRL 37344 on Endothelial Nitric Oxide Synthase Phosphorylation and Force of Contraction in Human Failing Myocardium. *Journal of Cardiac Failure.* **15**(1), pp.57-67.

Neely, J.R. and Morgan, H.E. 1974. Relationship between carbohydrate and lipid metabolism and the energy balance of heart muscle. *Annual Review Physiology.* **36**, pp.413-459.

Nerbonne, J.M. 2000. Molecular basis of functional voltage-gated K+ channel diversity in the mammalian myocardium. *Journal of Physiology.* **2**, pp.285-298.

Nerbonne, J.M. and Kass, R.S. 2005. Molecular Physiology of Cardiac Repolarization. *Physiological Reviews.* **85**(4), pp.1205-1253.

NICE, N.I.f.H.a.C.E. 2010. *Chronic heart failure in adults: management.* [Online]. [Accessed November]. Available from: https://www.nice.org.uk/guidance/cg108/chapter/Introduction

Nichols, C.B., Rossow, C.F., Navedo, M.F., Westenbroek, R.E., Catterall, W.A., Santana, L.F. and McKnight, G.S. 2010. Sympathetic Stimulation of Adult Cardiomyocytes Requires Association of AKAP5 With a Subpopulation of L-Type Calcium Channels. *Circulation Research.* **107**(6), pp.747-756.

Nieminen, M.S., Brutsaert, D., Dickstein, K., Drexler, H., Follath, F., Harjola, V.-P., Hochadel, M., Komajda, M., Lassus, J., Lopez-Sendon, J.L., Ponikowski, P. and Tavazzi, L. 2006. EuroHeart Failure Survey II (EHFS II): a survey on hospitalized acute heart failure patients: description of population. *Eur Heart J.* **27**(22), pp.2725-2736.

Nikolaev, V.O., Bünemann, M., Schmitteckert, E., Lohse, M.J. and Engelhardt, S. 2006. Cyclic AMP Imaging in Adult Cardiac Myocytes Reveals Far-Reaching β_1-Adrenergic but Locally Confined β_2-Adrenergic Receptor–Mediated Signaling. *Circulation Research.* **99**(10), pp.1084-1091.

Nikolaev, V.O., Moshkov, A., Lyon, A.R., Miragoli, M., Novak, P., Paur, H., Lohse, M.J., Korchev, Y.E., Harding, S.E. and Gorelik, J. 2010. β_2-Adrenergic Receptor Redistribution in Heart Failure Changes cAMP Compartmentation. *Science.* **327**(5973), pp.1653-1657.

Noble, A. 2005. *The cardiovascular system.* Edinburg: Churchill Livingstone.

Noble, A., Johnson, R., Thomas, A. and Bass, P. 2013. *The Cardiovascular System: Systems of the Body Series.* Elsevier Health Sciences UK.

Nootens, M., Kaufmann, E., Rector, T., Toher, C., Judd, D., Francis, G.S. and Rich, S. 1995. Neurohormonal activation in patients with right ventricular failure from pulmonary hypertension: Relation to hemodynamic variables and endothelin levels. *Journal of the American College of Cardiology.* **26**(7), pp.1581-1585.

O'Neill, R.A., Bhamidipati, A., Bi, X., Deb-Basu, D., Cahill, L., Ferrante, J., Gentalen, E., Glazer, M., Gossett, J., Hacker, K., Kirby, C., Knittle, J., Loder, R., Mastroieni, C., Maclaren, M., Mills, T., Nguyen, U., Parker, N., Rice, A., Roach, D., Suich, D., Voehringer, D., Voss, K., Yang, J., Yang, T. and Vander Horn, P.B. 2006. Isoelectric focusing technology quantifies protein signaling in 25 cells. *Proc Natl Acad Sci U S A.* **103**(44), pp.16153-16158.

Ogata, T., Naito, D., Nakanishi, N., Hayashi, Y.K., Taniguchi, T., Miyagawa, K., Hamaoka, T., Maruyama, N., Matoba, S., Ikeda, K., Yamada, H., Oh, H. and Ueyama, T. 2014. MURC/Cavin-4 facilitates recruitment of ERK to caveolae and concentric cardiac hypertrophy induced by α1-adrenergic receptors. *Proceedings of the National Academy of Sciences of the United States of America.* **111**(10), pp.3811-3816.

Opie, L.H. and Knuuti, J. 2009. The Adrenergic-Fatty Acid Load in Heart Failure. *Journal of the American College of Cardiology.* **54**(18), pp.1637-1646.

Ostrom, R.S., Gregorian, C., Drenan, R.M., Xiang, Y., Regan, J.W. and Insel, P.A. 2001. Receptor Number and Caveolar Co-localization Determine Receptor Coupling Efficiency to Adenylyl Cyclase. *Journal of Biological Chemistry.* **276**(45), pp.42063-42069.

Pacher, P., Mabley, J.G., Liaudet, L., Evgenov, O.V., Marton, A., Haskó, G., Kollai, M. and Szabó, C. 2004. Left ventricular pressure-volume relationship in a rat model of advanced aging-associated heart failure. *American Journal of Physiology - Heart and Circulatory Physiology.* **287**(5), pp.H2132-H2137.

Pacher, P., Nagayama, T., Mukhopadhyay, P., Batkai, S. and Kass, D.A. 2008. Measurement of cardiac function using pressure-volume conductance catheter technique in mice and rats. *Nature Protocols.* **3**(9), pp.1422-1434.

Page, E. 1978. Quantitative ultrastructural analysis in cardiac membrane physiology. *American Journal of Physiology.* **235**(5), pp.C147-158.

Page, E., McCallister, L.P. and Power, B. 1971. Stereological Measurements of Cardiac Ultrastructures Implicated in Excitation-Contraction Coupling. *Proceedings of the National Academy of Sciences.* **68**(7), pp.1465-1466.

Palade, G.E. 1953. Fine structure of blood capillaries. *Journal of Applied physics.* **24**(1), pp.1424-1436.

Pankey, E.A., Edward, J.A., Swan, K.W., Bourgeois, C.R.T., Bartow, M.J., Yoo, D., Peak, T.A., Song, B.M., Chan, R.A., Murthy, S.N., Prieto, M.C., Giles, T.D. and Kadowitz, P.J. 2016. Nebivolol has a beneficial effect in monocrotaline-induced pulmonary hypertension. *Canadian Journal of Physiology and Pharmacology.* **94**(7), pp.758-768.

Park, D.S., Woodman, S.E., Schubert, W., Cohen, A.W., Frank, P.G., Chandra, M., Shirani, J., Razani, B., Tang, B., Jelicks, L.A., Factor, S.M., Weiss, L.M., Tanowitz, H.B. and Lisanti, M.P. 2002. Caveolin-1/3 double-knockout mice are viable, but lack both muscle and non-muscle caveolae, and develop a severe cardiomyopathic phenotype. *The American journal of pathology.* **160**(6), pp.2207-2217.

Park, S.Y., Trinity, J.D., Gifford, J.R., Diakos, N.A., McCreath, L., Drakos, S. and Richardson, R.S. 2016. Mitochondrial function in heart failure: The impact of ischemic and non-ischemic etiology. *International Journal of Cardiology.* **220**, pp.711-717.

Parton, R.G. 2003. Caveolae - from ultrastructure to molecular mechanisms. *Nature Reviews of Molecular and Cellular Biology.* **4**(2), pp.162-167.

Parton, R.G. and Simons, K. 2007. The multiple faces of caveolae. *Nature Reviews of Molecular and Cellular Biology.* **8**(3), pp.185-194.

Parton, R.G., Way, M., Zorzi, N. and Stang, E. 1997. Caveolin-3 associates with developing T-tubules during muscle differentiation. *Journal of Cell Biology.* **136**(1), pp.137-154.

Patel, H.H. and Insel, P.A. 2009. Lipid Rafts and Caveolae and Their Role in Compartmentation of Redox Signaling. *Antioxidants & Redox Signaling.* **11**(6), pp.1357-1372.

Patel, H.H., Tsutsumi, Y.M., Head, B.P., Niesman, I.R., Jennings, M., Horikawa, Y., Huang, D., Moreno, A.L., Patel, P.M., Insel, P.A. and Roth, D.M. 2007. Mechanisms of cardiac protection from ischemia/reperfusion injury: a role for caveolae and caveolin-1. *Faseb J.* **21**(7), pp.1565-1574.

Patrucco, E., Albergine, M.S., Santana, L.F. and Beavo, J.A. 2010. Phosphodiesterase 8A (PDE8A) regulates excitation–contraction coupling in ventricular myocytes. *Journal of Molecular and Cellular Cardiology.* **49**(2), pp.330-333.

Patten, R.D. and Hall-Porter, M.R. 2009. Small Animal Models of Heart Failure: Development of Novel Therapies, Past and Present. *Circulation: Heart Failure.* **2**(2), pp.138-144.

Pelkmans, L. and Zerial, M. 2005. Kinase-regulated quantal assemblies and kiss-and-run recycling of caveolae. *Nature.* **436**(7047), pp.128-133.

Penela, P., Murga, C., Ribas, C., Tutor, A.S., Peregrín, S. and Mayor, F. 2006. Mechanisms of regulation of G protein-coupled receptor kinases (GRKs) and cardiovascular disease. *Cardiovascular Research.* **69**(1), pp.46-56.

Peterson, B.Z., DeMaria, C.D., Adelman, J.P. and Yue, D.T. 1999. Calmodulin is the Ca2+ sensor for Ca2+ -dependent inactivation of L-type calcium channels. *Neuron.* **22**(3), pp.549-558.

Pfleger, C., Ebeling, G., Bläsche, R., Patton, M., Patel, H.H., Kasper, M. and Barth, K. 2012. Detection of caveolin-3/caveolin-1/P2X7R complexes in mice atrial cardiomyocytes in vivo and in vitro. *Histochemistry and Cell Biology.* **138**(2), pp.231-241.

Piao, L., Fang, Y.-H., Parikh, K.S., Ryan, J.J., D'Souza, K.M., Theccanat, T., Toth, P.T., Pogoriler, J., Paul, J., Blaxall, B.C., Akhter, S.A. and Archer, S.L. 2012. GRK2-Mediated Inhibition of Adrenergic and Dopaminergic Signaling in Right Ventricular HypertrophyClinical Perspective. *Therapeutic Implications in Pulmonary Hypertension.* **126**(24), pp.2859-2869.

Pilch, P.F. and Liu, L. 2011. Fat caves: caveolae, lipid trafficking and lipid metabolism in adipocytes. *Trends in Endocrinology & Metabolism.* **22**(8), pp.318-324.

Pinali, C., Bennett, H., Davenport, J.B., Trafford, A.W. and Kitmitto, A. 2013. Three-Dimensional Reconstruction of Cardiac Sarcoplasmic Reticulum Reveals a Continuous Network Linking Transverse-Tubules. *This Organization Is Perturbed in Heart Failure.* **113**(11), pp.1219-1230.

Platonova, E., Winterflood, C.M., Junemann, A., Albrecht, D., Faix, J. and Ewers, H. 2015. Single-molecule microscopy of molecules tagged with GFP or RFP derivatives in mammalian cells using nanobody binders. *Methods.* **88**, pp.89-97.

ProteinSimple. 2016. *http://www.proteinsimple.com/wes.html.* [Online]. Available from: http://www.proteinsimple.com/wes.html

Rajab, A., Straub, V., McCann, L.J., Seelow, D., Varon, R. and Barresi, R. 2010. Fatal cardiac arrhythmia and long-QT syndrome in a new form of congenital generalized lipodystrophy with muscle rippling (CGL4) due to PTRF-CAVIN mutations. *PLoS Genet.* **6**.

Raman, S., Kelley, M.A. and Janssen, P.M.L. 2006. Effect of muscle dimensions on trabecular contractile performance under physiological conditions. *Pflügers Archiv.* **451**(5), pp.625-630.

Rapundalo, S.T. 1998. Cardiac protein phosphorylation: functional and pathophysiological correlates. *Cardiovascular Research.* **38**(3), pp.559-588.

Ratajczak, P., Damy, T., Heymes, C., Oliviéro, P., Marotte, F., Robidel, E., Sercombe, R., Boczkowski, J., Rappaport, L. and Samuel, J.-L. 2003. Caveolin-1 and -3 dissociations from caveolae to cytosol in the heart during aging and after myocardial infarction in rat. *Cardiovascular Research.* **57**(2), pp.358-369.

Razani, B., Wang, X.B., Engelman, J.A., Battista, M., Lagaud, G., Zhang, X.L., Kneitz, B., Hou, H., Christ, G.J., Edelmann, W. and Lisanti, M.P. 2002. Caveolin-2-Deficient Mice Show Evidence of Severe Pulmonary Dysfunction without Disruption of Caveolae. *Molecular and Cellular Biology.* **22**(7), pp.2329-2344.

Reddy, Y. 1976. Phosphorylation of cardiac regulatory proteins by cyclic AMP-dependent protein kinase. *American Journal of Physiology -- Legacy Content.* **231**(5), pp.1330-1336.

Reiken, S., Wehrens, X.H.T., Vest, J.A., Barbone, A., Klotz, S., Mancini, D., Burkhoff, D. and Marks, A.R. 2003. β-Blockers Restore Calcium Release Channel Function and Improve Cardiac Muscle Performance in Human Heart Failure. *Circulation.* **107**(19), pp.2459-2466.

Richards, M.A., Clarke, J.D., Saravanan, P., Voigt, N., Dobrev, D., Eisner, D.A., Trafford, A.W. and Dibb, K.M. 2011. Transverse tubules are a common feature in large mammalian atrial myocytes including human. *American journal of physiology - Heart and circulatory physiology.* **301**(5), p12.

Richardson, D.W., Kontos, H.A., Raper, A.J. and Patterson, J.L., Jr. 1967. Modification by Beta-Adrenergic Blockade of the Circulatory Responses to Acute Hypoxia in Man*. *The Journal of Clinical Investigation.* **46**(1), pp.77-85.

Robenek, H., Weissen-Plenz, G. and Severs, N.J. 2008. Freeze-fracture replica immunolabelling reveals caveolin-1 in the human cardiomyocyte plasma membrane. *Journal of Cellular and Molecular Medicine.* **12**(6a), pp.2519-2521.

Rockman, H.A., Koch, W.J. and Lefkowitz, R.J. 2002. Seven-transmembrane-spanning receptors and heart function. *Nature.* **415**(6868), pp.206-212.

Rog-Zielinska, E.A., Johnston, C.M., O'Toole, E.T., Morphew, M., Hoenger, A. and Kohl, P. 2016. Electron tomography of rabbit cardiomyocyte three-dimensional ultrastructure. *Progress in Biophysics and Molecular Biology.* **121**(2), pp.77-84.

Rondelet, B., Dewachter, C., Kerbaul, F., Kang, X., Fesler, P., Brimioulle, S., Naeije, R. and Dewachter, L. 2012. Prolonged overcirculation-induced pulmonary arterial

hypertension as a cause of right ventricular failure. *European Heart Journal* **33**(8), pp.1017-1026.

Rothberg, K.G., Heuser, J.E., Donzell, W.C., Ying, Y.-S., Glenney, J.R. and Anderson, R.G.W. 1992. Caveolin, a protein component of caveolae membrane coats. *Cell.* **68**(4), pp.673-682.

Rybin, V.O., Pak, E., Alcott, S. and Steinberg, S.F. 2003. Developmental Changes in β_2-Adrenergic Receptor Signaling in Ventricular Myocytes: the Role of G_i proteins and Caveolae Microdomains. *Molecular Pharmacology.* **63**(6), pp.1338-1348.

Rybin, V.O., Xu, X., Lisanti, M.P. and Steinberg, S.F. 2000. Differential Targeting of β-Adrenergic Receptor Subtypes and Adenylyl Cyclase to Cardiomyocyte Caveolae: A Mechanism To Functionally Regulate The Camp Signaling Pathway. *Journal of Biological Chemistry.* **275**(52), pp.41447-41457.

Sadler, T.W. and Langman, J. 2014. *Langman's medical embryology.* Philadelphia: Lippincott Williams & Wilkins.

Salazar, N.C., Chen, J. and Rockman, H.A. 2007. Cardiac GPCRs: GPCR signaling in healthy and failing hearts. *Biochimica et Biophysica Acta (BBA) - Biomembranes.* **1768**(4), pp.1006-1018.

Sampson, L.J., Davies, L.M., Barrett-Jolley, R., Standen, N.B. and Dart, C. 2007. Angiotensin II-activated protein kinase C targets caveolae to inhibit aortic ATP-sensitive potassium channels. *Cardiovascular Research.* **76**(1), pp.61-70.

Sandow, A. 1952. Excitation-Contraction Coupling in Muscular Response. *The Yale Journal of Biology and Medicine.* **25**(3), pp.176-201.

Sanguinetti, M.C. and Jurkiewicz, N.K. 1990. Two components of cardiac delayed rectifier K+ current. Differential sensitivity to block by class III antiarrhythmic agents. *The Journal of General Physiology.* **96**(1), pp.195-215.

Scheffler, I.E. 2007. Mitochondrial Electron Transfer and Oxidative Phosphorylation. *Mitochondria.* John Wiley & Sons, Inc., pp.168-297.

Schoenwolf, G.C., Bleyl, S.B., Brauer, P.R. and Francis-West, P.H. 2015. *Larsen's human embryology.* Philadelphia, PA: Churchill Livingstone.

Schröder, F., Handrock, R., Beuckelmann, D.J., Hirt, S., Hullin, R., Priebe, L., Schwinger, R.H.G., Weil, J. and Herzig, S. 1998. Increased Availability and Open Probability of Single L-Type Calcium Channels From Failing Compared With Nonfailing Human Ventricle. *Circulation.* **98**(10), pp.969-976.

Schwab, B.C., Seemann, G., Lasher, R.A., Torres, N.S., E. M, W., x00Fc, lfers, Arp, M., Carruth, E.D., Bridge, J.H.B. and Sachse, F.B. 2013. Quantitative Analysis of Cardiac Tissue Including Fibroblasts Using Three-Dimensional Confocal Microscopy and Image Reconstruction: Towards a Basis for Electrophysiological Modeling. *IEEE Transactions on Medical Imaging.* **32**(5), pp.862-872.

Schwencke, C., Braun-Dullaeus, R.C., Wunderlich, C. and Strasser, R.H. 2006. Caveolae and caveolin in transmembrane signaling: Implications for human disease. *Cardiovascular Research.* **70**(1), pp.42-49.

Sedarat, F., Xu, L., Moore, E.D.W. and Tibbits, G.F. 2000. Colocalization of dihydropyridine and ryanodine receptors in neonate rabbit heart using confocal microscopy. *American Journal of Physiology - Heart and Circulatory Physiology.* **279**(1), pp.H202-H209.

Segura, A.M., Frazier, O.H. and Buja, L.M. 2014. Fibrosis and heart failure. *Heart Failure Reviews.* **19**(2), pp.173-185.

Selvam, B., Wereszczynski, J. and Tikhonova, I.G. 2012. Comparison of Dynamics of Extracellular Accesses to the β1 and β2 Adrenoceptors Binding Sites Uncovers the Potential of Kinetic Basis of Antagonist Selectivity. *Chemical Biology & Drug Design.* **80**(2), pp.215-226.

Seyfarth, T., Gerbershagen, H.-P., Giessler, C., Leineweber, K., Heinroth-Hoffmann, I., Pönicke, K. and Brodde, O.-E. 2000. The Cardiac β -Adrenoceptor-G-protein(s)-adenylyl Cyclase

System in Monocrotaline-treated Rats. *Journal of Molecular and Cellular Cardiology.* **32**(12), pp.2315-2326.

Sharma, V. and McNeill, J.H. 2011. Parallel effects of β-adrenoceptor blockade on cardiac function and fatty acid oxidation in the diabetic heart: Confronting the maze. *World Journal of Cardiology.* **3**(9), pp.281-302.

Sharma, V., Sharma, A., Saran, V., Bernatchez, P.N., Allard, M.F. and McNeill, J.H. 2011. beta-receptor antagonist treatment prevents activation of cell death signaling in the diabetic heart independent of its metabolic actions. *Eur J Pharmacol.* **657**(1-3), pp.117-125.

Shen, X., Kaur, S., Power, A., Williams, L.Z.J. and Ward, M.-L. 2016. Positive Inotropic Effect of Prostaglandin F2α in Rat Ventricular Trabeculae. *Journal of Cardiovascular Pharmacology.* **68**(1), pp.81-88.

Shibata, E.F., Brown, T.L.Y., Washburn, Z.W., Bai, J., Revak, T.J. and Butters, C.A. 2006. Autonomic Regulation of Voltage-Gated Cardiac Ion Channels. *Journal of Cardiovascular Electrophysiology.* **17**, pp.S34-S42.

Siddiqui, M.R., Komarova, Y.A., Vogel, S.M., Gao, X., Bonini, M.G., Rajasingh, J., Zhao, Y.-Y., Brovkovych, V. and Malik, A.B. 2011. Caveolin-1–eNOS signaling promotes p190RhoGAP-A nitration and endothelial permeability. *The Journal of Cell Biology.* **193**(5), pp.841-850.

Sinha, B., Köster, D., Ruez, R., Gonnord, P., Bastiani, M., Abankwa, D., Stan, R.V., Butler-Browne, G., Vedie, B. and Johannes, L. 2011. Cells respond to mechanical stress by rapid disassembly of caveolae. *Cell.* **144**(3), pp.402-413.

Siri, F.M. 1988. Sympathetic changes during development of cardiac hypertrophy in aortic-constricted rats. *American Journal of Physiology - Heart and Circulatory Physiology.* **255**(3), pp.H452-H457.

Smart, E.J., Ying, Y.S., Mineo, C. and Anderson, R.G. 1995. A detergent-free method for purifying caveolae membrane from tissue culture cells. *Proceedings of the National Academy of Sciences.* **92**(22), pp.10104-10108.

Song, K.S., Li, S., Okamoto, T., Quilliam, L.A., Sargiacomo, M. and Lisanti, M.P. 1996a. Co-purification and Direct Interaction of Ras with Caveolin, an Integral Membrane Protein of Caveolae Microdomains: Detergent-Free Purification Of Caveolae Membranes. *Journal of Biological Chemistry.* **271**(16), pp.9690-9697.

Song, K.S., Scherer, P.E., Tang, Z., Okamoto, T., Li, S., Chafel, M., Chu, C., Kohtz, D.S. and Lisanti, M.P. 1996b. Expression of Caveolin-3 in Skeletal, Cardiac, and Smooth Muscle Cells: Caveolin-3 Is A Component Of The Sarcolemma And Co-Fractionates With Dystrophin And Dystrophin-Associated Glycoproteins. *Journal of Biological Chemistry.* **271**(25), pp.15160-15165.

Stanley, W.C., Recchia, F.A. and Lopaschuk, G.D. 2005. Myocardial Substrate Metabolism in the Normal and Failing Heart. *Physiological Reviews.* **85**(3), pp.1093-1129.

Staus, D.P., Strachan, R.T., Manglik, A., Pani, B., Kahsai, A.W., Kim, T.H., Wingler, L.M., Ahn, S., Chatterjee, A., Masoudi, A., Kruse, A.C., Pardon, E., Steyaert, J., Weis, W.I., Prosser, R.S., Kobilka, B.K., Costa, T. and Lefkowitz, R.J. 2016. Allosteric nanobodies reveal the dynamic range and diverse mechanisms of G-protein-coupled receptor activation. *Nature.* **535**(7612), pp.448-452.

Steinfath, M., Lavicky, J., Schmitz, W., Scholz, H., Döring, V. and Kalmár, P. 1992. Regional distribution of β1- and β2-adrenoceptors in the failing and nonfailing human heart. *European Journal of Clinical Pharmacology.* **42**(6), pp.607-611.

Stoeber, M., Schellenberger, P., Siebert, C.A., Leyrat, C., Helenius, A. and Grünewald, K. 2016. Model for the architecture of caveolae based on a flexible, net-like assembly of Cavin1 and Caveolin discs. *Proceedings of the National Academy of Sciences.*

Stones, R., Benoist, D., Peckham, M. and White, E. 2013. Microtubule proliferation in right ventricular myocytes of rats with monocrotaline-induced pulmonary hypertension. *Journal of Molecular and Cellular Cardiology.* **56**, pp.91-96.

Swynghedauw, B. 1999. Molecular Mechanisms of Myocardial Remodeling. *Physiological Reviews.* **79**(1), pp.215-262.

Tada, M. and Katz, A.M. 1982. Phosphorylation of the sarcoplasmic reticulum and sarcolemma. *Annual Reviews of Physiology.* **44**, pp.401-423.

Takemoto, Y., Yoshiyama, M., Takeuchi, K., Omura, T., Komatsu, R., Izumi, Y., Kim, S. and Yoshikawa, J. 1999. Increased JNK, AP-1 and NF-kappa B DNA binding activities in isoproterenol-induced cardiac remodeling. *J Mol Cell Cardiol.* **31**(11), pp.2017-2030.

Tamada, A., Hattori, Y., Houzen, H., Yamada, Y., Sakuma, I., Kitabatake, A. and Kanno, M. 1998. Effects of β-adrenoceptor stimulation on contractility, $[Ca^{2+}]_i$, and Ca^{2+} current in diabetic rat cardiomyocytes. *American Journal of Physiology - Heart and Circulatory Physiology.* **274**(6), pp.H1849-H1857.

Tanaka, M., Fujiwara, H., Onodera, T., Wu, D.J., Hamashima, Y. and Kawai, C. 1986. Quantitative analysis of myocardial fibrosis in normals, hypertensive hearts, and hypertrophic cardiomyopathy. *British Heart Journal.* **55**(6), pp.575-581.

Taniguchi, T., Maruyama, N., Ogata, T., Kasahara, T., Nakanishi, N., Miyagawa, K., Naito, D., Hamaoka, T., Nishi, M., Matoba, S. and Ueyama, T. 2016. PTRF/Cavin-1 Deficiency Causes Cardiac Dysfunction Accompanied by Cardiomyocyte Hypertrophy and Cardiac Fibrosis. *PLoS ONE.* **11**(9), pe0162513.

Taylor, S.C., Berkelman, T., Yadav, G. and Hammond, M. 2013. A Defined Methodology for Reliable Quantification of Western Blot Data. *Molecular Biotechnology.* **55**(3), pp.217-226.

Teerlink, J.R., Pfeffer, J.M. and Pfeffer, M.A. 1994. Progressive ventricular remodeling in response to diffuse isoproterenol-induced myocardial necrosis in rats. *Circulation Research.* **75**(1), pp.105-113.

Teichholz, L.E., Kreulen, T., Herman, M.V. and Gorlin, R. 1976. Problems in echocardiographic volume determinations: Echocardiographic-angiographic correlations in the presence or absence of asynergy. *The American Journal of Cardiology.* **37**(1), pp.7-11.

Telser, A. 2002. Molecular Biology of the Cell, 4th Edition. *Shock.* **18**(3), p289.

Timofeyev, V., Myers, R.E., Kim, H.J., Woltz, R., Sirish, P., Heiserman, J., Li, N., Singapuri, A., Tang, T., Yarov-Yarovoy, V., Yamoah, E.N., Hammond, K. and Chiamvimonvat, N. 2013. Adenylyl Cyclase Subtype-Specific Compartmentalization: Differential Regulation of L-type Ca2+ Current in Ventricular Myocytes. *Circulation Research.*

Touchnet, R.U.a. 2016. *Anatomy & Physiology.* [Online]. Available from: http://cnx.org/contents/FPtK1zmh@6.27:raNQgZ7E@3/Overview-of-Anatomy-and-Physio

Traill, T.A., Gibson, D.G. and Brown, D.J. 1978. Study of left ventricular wall thickness and dimension changes using echocardiography. *British Heart Journal.* **40**(2), pp.162-169.

Triposkiadis, F., Karayannis, G., Giamouzis, G., Skoularigis, J., Louridas, G. and Butler, J. 2009. The Sympathetic Nervous System in Heart Failure: Physiology, Pathophysiology, and Clinical Implications. *Journal of the American College of Cardiology.* **54**(19), pp.1747-1762.

Tsien, R.Y., Rink, T.J. and Poenie, M. 1985. Measurement of cytosolic free Ca2+ in individual small cells using fluorescence microscopy with dual excitation wavelengths. *Cell Calcium.* **6**(1), pp.145-157.

Tsuchihashi, H., Nakashima, Y., Kinami, J. and Nagatomo, T. 1990. Characteristics of ^{125}I-Iodocyanopindolol Binding to β-Adrenergic and Serotonin-1B Receptors of Rat Brain: Selectivity of β-Adrenergic Agents. *The Japanese Journal of Pharmacology.* **52**(2), pp.195-200.

Tsutsui, H., Ishihara, K. and Cooper, G. 1993. Cytoskeletal role in the contractile dysfunction of hypertrophied myocardium. *Science.* **260**(5108), pp.682-687.

Tsutsumi, Y.M., Horikawa, Y.T., Jennings, M.M., Kidd, M.W., Niesman, I.R., Yokoyama, U., Head, B.P., Hagiwara, Y., Ishikawa, Y., Miyanohara, A., Patel, P.M., Insel, P.A., Patel, H.H. and Roth, D.M. 2008. Cardiac-Specific Overexpression of Caveolin-3 Induces Endogenous Cardiac Protection by Mimicking Ischemic Preconditioning. *Circulation.* **118**(19), pp.1979-1988.

Tyska, M.J., Dupuis, D.E., Guilford, W.H., Patlak, J.B., Waller, G.S., Trybus, K.M., Warshaw, D.M. and Lowey, S. 1999. Two heads of myosin are better than one for generating force and motion. *Proceedings of the National Academy of Sciences.* **96**(8), pp.4402-4407.

Udelson, J.E., Cannon, R.O., Bacharach, S.L., Rumble, T.F. and Bonow, R.O. 1989. Beta-adrenergic stimulation with isoproterenol enhances left ventricular diastolic performance in hypertrophic cardiomyopathy despite potentiation of myocardial ischemia. Comparison to rapid atrial pacing. *Circulation.* **79**(2), pp.371-382.

Ungerer, M., Böhm, M., Elce, J., Erdmann, E. and Lohse, M. 1993a. Altered expression of beta-adrenergic receptor kinase and beta 1-adrenergic receptors in the failing human heart. *Circulation.* **87**(2), pp.454-463.

Ungerer, M., Böhm, M., Elce, J.S., Erdmann, E. and Lohse, M.J. 1993b. Altered expression of beta-adrenergic receptor kinase and beta 1-adrenergic receptors in the failing human heart. *Circulation.* **87**(2), pp.454-463.

Uray, I.P., Connelly, J.H., Frazier, O.H., Taegtmeyer, H. and Davies, P.J.A. 2003. Mechanical unloading increases caveolin expression in the failing human heart. *Cardiovascular Research.* **59**(1), pp.57-66.

Uray, I.P., Connelly, J.H., Thomázy, V., Shipley, G.L., Vaughn, W.K., Frazier, O.H., Taegtmeyer, H. and Davies, P.J.A. 2002. Left ventricular unloading alters receptor tyrosine kinase expression in the failing human heart. *The Journal of Heart and Lung Transplantation.* **21**(7), pp.771-782.

Valdivia, H.H., Kaplan, J.H., Ellis-Davies, G.C.R. and Lederer, W.J. 1995. Rapid Adaptation of Cardiac Ryanodine Receptors: Modulation by Mg^{2+} and Phosphorylation. *Science (New York, N.Y.).* **267**(5206), pp.1997-2000.

van der Heyden, M.A.G., Wijnhoven, T.J.M. and Opthof, T. 2005. Molecular aspects of adrenergic modulation of cardiac L-type Ca²⁺ channels. *Cardiovascular Research.* **65**(1), pp.28-39.

Vatner, D.E., Homcy, C.J., Sit, S.P., Manders, W.T. and Vatner, S.F. 1984. Effects of pressure overload, left ventricular hypertrophy on beta-adrenergic receptors, and responsiveness to catecholamines. *Journal of Clinical Investigation.* **73**(5), pp.1473-1482.

Vatta, M., Ackerman, M.J., Ye, B., Makielski, J.C., Ughanze, E.E., Taylor, E.W., Tester, D.J., Balijepalli, R.C., Foell, J.D., Li, Z., Kamp, T.J. and Towbin, J.A. 2006. Mutant Caveolin-3 Induces Persistent Late Sodium Current and Is Associated With Long-QT Syndrome. *Circulation.* **114**(20), pp.2104-2112.

Velez-Roa, S., Ciarka, A., Najem, B., Vachiery, J.-L., Naeije, R. and van de Borne, P. 2004. Increased Sympathetic Nerve Activity in Pulmonary Artery Hypertension. *Circulation.* **110**(10), pp.1308-1312.

Verde, I., Vandecasteele, G., Lezoualc'h, F. and Fischmeister, R. 1999. Characterization of the cyclic nucleotide phosphodiesterase subtypes involved in the regulation of the L-type Ca^{2+} current in rat ventricular myocytes. *British Journal of Pharmacology.* **127**(1), pp.65-74.

Versluis, J.P., Heslinga, J.W., Sipkema, P. and Westerhof, N. 2004. Contractile reserve but not tension is reduced in monocrotaline-induced right ventricular hypertrophy. *American Journal of Physiology - Heart and Circulatory Physiology.* **286**(3), pp.H979-H984.

Villarreal, F.J., Kim, N.N., Ungab, G.D., Printz, M.P. and Dillmann, W.H. 1993. Identification of functional angiotensin II receptors on rat cardiac fibroblasts. *Circulation.* **88**(6), pp.2849-2861.

Vliegen, H.W., Van Der Laarse, A., Cornelisse, C.J. and Eulderink, F. 1991. Myocardial changes in pressure overload-induced left ventricular hypertrophy. *A study on tissue composition, polyploidization and multinucleation.* **12**(4), pp.488-494.

Vonk-Noordegraaf, A., Haddad, F., Chin, K.M., Forfia, P.R., Kawut, S.M., Lumens, J., Naeije, R., Newman, J., Oudiz, R.J., Provencher, S., Torbicki, A., Voelkel, N.F. and Hassoun, P.M. 2013. Right heart adaptation to pulmonary arterial hypertension: physiology and pathobiology. *J Am Coll Cardiol.* **62**(25 Suppl), pp.D22-33.

Wagenknecht, T., Radermacher, M., Grassucci, R., Berkowitz, J., Xin, H.-B. and Fleischer, S. 1997. Locations of Calmodulin and FK506-binding Protein on the Three-dimensional Architecture of the Skeletal Muscle Ryanodine Receptor. *Journal of Biological Chemistry.* **272**(51), pp.32463-32471.

Wandt, B., Bojö, L., Tolagen, K. and Wranne, B. 1999. Echocardiographic assessment of ejection fraction in left ventricular hypertrophy. *Heart.* **82**(2), pp.192-198.

Wang, G.-Y., McCloskey, D.T., Turcato, S., Swigart, P.M., Simpson, P.C. and Baker, A.J. 2006. Contrasting inotropic responses to α_1-adrenergic receptor stimulation in left versus right ventricular myocardium. *American Journal of Physiology - Heart and Circulatory Physiology.* **291**(4), pp.H2013-H2017.

Wang, Y., De Arcangelis, V., Gao, X., Ramani, B., Jung, Y.-s. and Xiang, Y. 2008. Norepinephrine- and Epinephrine-induced Distinct β2-Adrenoceptor Signaling Is Dictated by GRK2 Phosphorylation in Cardiomyocytes. *Journal of Biological Chemistry.* **283**(4), pp.1799-1807.

Ward, M.-L., Pope, A.J., Loiselle, D.S. and Cannell, M.B. 2003. Reduced contraction strength with increased intracellular [Ca2+] in left ventricular trabeculae from failing rat hearts. *The Journal of Physiology.* **546**(2), pp.537-550.

Waugh, M.G., Chu, K.M.E., Clayton, E.L., Minogue, S. and Hsuan, J.J. 2011. Detergent-free isolation and characterization of cholesterol-rich membrane domains from trans-Golgi network vesicles. *Journal of Lipid Research.* **52**(3), pp.582-589.

Wei, Z., Zou, X., Wang, H., Lei, J., Wu, Y. and Liao, K. 2015. The N-terminal leucine-zipper motif in PTRF/cavin-1 is essential and sufficient for its caveolae-association. *Biochemical and Biophysical Research Communications.* **456**(3), pp.750-756.

Wier, W., Cannell, M., Berlin, Marban, E. and Lederer, W. 1987. Cellular and subcellular heterogeneity of [Ca2+]i in single heart cells revealed by fura-2. *Science.* **235**(4786), pp.325-328.

Williams, Jamie J.L. and Palmer, Timothy M. 2014. Cavin-1: caveolae-dependent signalling and cardiovascular disease. *Biochemical Society Transactions.* **42**(2), pp.284-288.

Witcher, D.R., Kovacs, R.J., Schulman, H., Cefali, D.C. and Jones, L.R. 1991. Unique phosphorylation site on the cardiac ryanodine receptor regulates calcium channel activity. *Journal of Biological Chemistry.* **266**(17), pp.11144-11152.

Wong, J., Baddeley, D., Bushong, Eric A., Yu, Z., Ellisman, Mark H., Hoshijima, M. and Soeller, C. 2013. Nanoscale Distribution of Ryanodine Receptors and Caveolin-3 in Mouse Ventricular Myocytes: Dilation of T-Tubules near Junctions. *Biophysical Journal.* **104**(11), pp.L22-L24.

Woodman, S.E., Park, D.S., Cohen, A.W., Cheung, M.W.-C., Chandra, M., Shirani, J., Tang, B., Jelicks, L.A., Kitsis, R.N., Christ, G.J., Factor, S.M., Tanowitz, H.B. and Lisanti, M.P. 2002.

Caveolin-3 Knock-out Mice Develop a Progressive Cardiomyopathy and Show Hyperactivation of the p42/44 MAPK Cascade. *Journal of Biological Chemistry.* **277**(41), pp.38988-38997.

Wright, P.T., Nikolaev, V.O., O'Hara, T., Diakonov, I., Bhargava, A., Tokar, S., Schobesberger, S., Shevchuk, A.I., Sikkel, M.B., Wilkinson, R., Trayanova, N.A., Lyon, A.R., Harding, S.E. and Gorelik, J. 2014. Caveolin-3 regulates compartmentation of cardiomyocyte beta2-adrenergic receptor-mediated cAMP signaling. *Journal of Molecular and Cellular Cardiology.* **67**, pp.38-48.

Wunderlich, C., Schmeisser, A., Heerwagen, C., Ebner, B., Schober, K., Braun-Dullaeus, R.C., Schwencke, C., Kasper, M., Morawietz, H. and Strasser, R.H. 2008. Chronic NOS inhibition prevents adverse lung remodeling and pulmonary arterial hypertension in caveolin-1 knockout mice. *Pulmonary Pharmacology & Therapeutics.* **21**(3), pp.507-515.

Wunderlich, C., Schober, K., Lange, S.A., Drab, M., Braun-Dullaeus, R.C., Kasper, M., Schwencke, C., Schmeisser, A. and Strasser, R.H. 2006. Disruption of caveolin-1 leads to enhanced nitrosative stress and severe systolic and diastolic heart failure. *Biochemical and Biophysical Research Communications.* **340**(2), pp.702-708.

Wypijewski, K.J., Tinti, M., Chen, W., Lamont, D., Ashford, M.L.J., Calaghan, S.C. and Fuller, W. 2015. Identification of Caveolar Resident Proteins in Ventricular Myocytes Using a Quantitative Proteomic Approach: Dynamic Changes in Caveolar Composition Following Adrenoceptor Activation. *Molecular & Cellular Proteomics.* **14**(3), pp.596-608.

Xiang, Y. and Kobilka, B.K. 2003. Myocyte adrenoceptor signaling pathways. *Science.* **300**(5625), pp.1530-1532.

Xiang, Y., Rybin, V.O., Steinberg, S.F. and Kobilka, B. 2002. Caveolar Localization Dictates Physiologic Signaling of β2-Adrenoceptors in Neonatal Cardiac Myocytes. *Journal of Biological Chemistry.* **277**(37), pp.34280-34286.

Xiao, R.-P. 2001. β-Adrenergic Signaling in the Heart: Dual Coupling of the β2-Adrenergic Receptor to Gs and Gi Proteins. *Science Signaling.* **2001**(104), pp.re15-re15.

Xiao, R.-P., Avdonin, P., Zhou, Y.-Y., Cheng, H., Akhter, S.A., Eschenhagen, T., Lefkowitz, R.J., Koch, W.J. and Lakatta, E.G. 1999a. Coupling of β2-Adrenoceptor to Gi Proteins and Its Physiological Relevance in Murine Cardiac Myocytes. *Circulation Research.* **84**(1), pp.43-52.

Xiao, R.-P., Cheng, H., Zhou, Y.-Y., Kuschel, M. and Lakatta, E.G. 1999b. Recent Advances in Cardiac β2-Adrenergic Signal Transduction. *Circulation Research.* **85**(11), pp.1092-1100.

Xie, Y.P., Chen, B., Sanders, P., Guo, A., Li, Y., Zimmerman, K., Wang, L.C., Weiss, R.M., Grumbach, I.M., Anderson, M.E. and Song, L.S. 2012. Sildenafil prevents and reverses transverse-tubule remodeling and Ca(2+) handling dysfunction in right ventricle failure induced by pulmonary artery hypertension. *Hypertension.* **59**(2), pp.355-362.

Xu, L. and Meissner, G. 2004. Mechanism of calmodulin inhibition of cardiac sarcoplasmic reticulum Ca 2+ release channel (ryanodine receptor). *Biophysical Journal.* **86**(2), pp.797-804.

Xu, Y.-J., Shao, Q. and Dhalla, N.S. 1997. Fura-2 fluorescent technique for the assessment of Ca^{2+} homeostasis in cardiomyocytes. *Molecular and Cellular Biochemistry.* **172**(1), pp.149-157.

Yamamoto, M., Toya, Y., Schwencke, C., Lisanti, M.P., Myers, M.G. and Ishikawa, Y. 1998. Caveolin Is an Activator of Insulin Receptor Signaling. *Journal of Biological Chemistry.* **273**(41), pp.26962-26968.

Yang, G., Xu, H., Li, Z. and Li, F. 2014. Interactions of caveolin-1 scaffolding and intramembrane regions containing a CRAC motif with cholesterol in lipid bilayers. *Biochimica et Biophysica Acta (BBA) - Biomembranes.* **1838**(10), pp.2588-2599.

Yang, P.-C., Boras, B.W., Jeng, M.-T., Docken, S.S., Lewis, T.J., McCulloch, A.D., Harvey, R.D. and Clancy, C.E. 2016. A Computational Modeling and Simulation Approach to Investigate Mechanisms of Subcellular cAMP Compartmentation. *PLOS Computational Biology* **12**(7), pe1005005.

Yang, X., Cohen, M.V. and Downey, J.M. 2010. Mechanism of Cardioprotection by Early Ischemic Preconditioning. *Cardiovascular Drugs and Therapy.* **24**(3), pp.225-234.

Yao, Y., Hong, S., Zhou, H., Yuan, T., Zeng, R. and Liao, K. 2009. The differential protein and lipid compositions of noncaveolar lipid microdomains and caveolae. *Cell Research.* **19**(4), pp.497-506.

Yoshida, H., Tanonaka, K., Miyamoto, Y., Abe, T., Takahashi, M., Anand-Srivastava, M.B. and Takeo, S. 2001. Characterization of cardiac myocyte and tissue β-adrenergic signal transduction in rats with heart failure. *Cardiovascular Research.* **50**(1), pp.34-45.

Yu, J., Bergaya, S., Murata, T., Alp, I.F., Bauer, M.P., Lin, M.I., Drab, M., Kurzchalia, T.V., Stan, R.V. and Sessa, W.C. 2006. Direct evidence for the role of caveolin-1 and caveolae in mechanotransduction and remodeling of blood vessels. *The Journal of Clinical Investigation.* **116**(5), pp.1284-1291.

Zakhary, D.R., Moravec, C.S. and Bond, M. 2000. Regulation of PKA Binding to AKAPs in the Heart: Alterations in Human Heart Failure. *Circulation.* **101**(12), pp.1459-1464.

Zamah, A.M., Delahunty, M., Luttrell, L.M. and Lefkowitz, R.J. 2002. Protein Kinase A-mediated Phosphorylation of the β2-Adrenergic Receptor Regulates Its Coupling to Gs and Gi : Demonstration In A Reconstituted System. *Journal of Biological Chemistry.* **277**(34), pp.31249-31256.

Zhang, G.X., Kimura, S., Nishiyama, A., Shokoji, T., Rahman, M., Yao, L., Nagai, Y., Fujisawa, Y., Miyatake, A. and Abe, Y. 2005. Cardiac oxidative stress in acute and chronic isoproterenol-infused rats. *Cardiovasc Res.* **65**(1), pp.230-238.

Zhao, Y.-Y., Liu, Y., Stan, R.-V., Fan, L., Gu, Y., Dalton, N., Chu, P.-H., Peterson, K., Ross, J. and Chien, K.R. 2002. Defects in caveolin-1 cause dilated cardiomyopathy and pulmonary hypertension in knockout mice. *Proceedings of the National Academy of Sciences of the United States of America.* **99**(17), pp.11375-11380.

Zhu, W.-Z., Wang, S.-Q., Chakir, K., Yang, D., Zhang, T., Brown, J.H., Devic, E., Kobilka, B.K., Cheng, H. and Xiao, R.-P. 2003. Linkage of β1-adrenergic stimulation to apoptotic heart cell death through protein kinase A–independent activation of Ca^{2+}/calmodulin kinase II. *The Journal of Clinical Investigation.* **111**(5), pp.617-625.

Zhu, W., Petrashevskaya, N., Ren, S., Zhao, A., Chakir, K., Gao, E., Chuprun, J.K., Wang, Y., Talan, M., Dorn, G.W., Lakatta, E.G., Koch, W.J., Feldman, A.M. and Xiao, R.-P. 2012. Gi-Biased β2AR Signaling Links GRK2 Upregulation to Heart Failure. *Circulation Research.* **110**(2), pp.265-274.